Novel Diiron Dichalcogenolato Complexes:

Models for Active Site of [FeFe]-Hydrogenase

Dissertation

Zur Erlangung des akademischen Grades doctor rerum naturalium

(Dr. rer. nat.)

vorgelegt dem Rat der Chemisch-Geowissenschaftlichen Fakultät

der Friedrich-Schiller-Universität Jena

von
Mohammad Harb, MSc
geboren am 28.07.1980
in Dair Abi Said/Jordan

1. Gutachter: .....

2. Gutachter: .....

Tag der öffentlichen Verteidigung: .....

Contents

List of Publications ..... **I**

1 Introduction **1**

1.1 General Aspects

1.2 Hydrogenases Definition

1.3 Hydrogenases Classification

1.3.1 **[NiFe]-Hydrogenase** .....

1.3.2 **[Fe]-Hydrogenase** .....

1.3.3 **[FeFe]-Hydrogenase** .....

2 Structural Models of [FeFe]-Hydrogenase **12**

2.1 $Fe_2(\mu\text{-}SCH_2XCH_2S\text{-}\mu)(CO)_6$ with Different Bridgeheads (X)

2.2 $Fe_2(\mu\text{-}S(CH_2)_nS\text{-}\mu)$ with Different Length Linkers (n = 2, 3, 4, 5)

2.3 The Substitution Reactions of CO Groups

2.3.1 **Substitution by Phosphine or Phosphite Ligands** .....

2.3.2 **Substitution by Bidentate Ligands** .....

2.3.3 **Substitution by Cyanide Ligand** .....

2.3.4 **Substitution by N-heterocyclic Carbenes (NHCs) Ligands**.....

2.4 [2Fe3S] Model Complexes

2.5 [4Fe4S] Model Complexes

2.6 Oxidation of Model Complexes

2.7 Mixed S (Se and Te) Model Complexes

3 Publications **23**

3.1 [MK1] Synthesis and Characterization of Diiron Diselenolato Complexes Including Iron Hydrogenase Models.

3.2 [MK2] Phosphane- and Phosphite-Substituted Diiron Diselenolato Complexes as Models for [FeFe]-Hydrogenases.

3.3 [MK3] Preparation and Characterization of Diiron-Dichalcogenolato Complexes Containing an Oxetane Ring: [FeFe]-Hydrogenase Models.

3.4 [MK4] Synthesis and Characterization of [FeFe]-Hydrogenase Models with Bridging Moieties Containing (S, Se) and (S, Te).
3.5 [MK5] [FeFe]-Hydrogenase Models Containing Different Length Diselenolato Bridging Moieties.
3.6 [MK6] Substitution Reactions at [FeFe]-Hydrogenase Models Containing [2Fe3S] Cluster by Phosphine or Phosphite Ligands.
3.7 [MK7] Synthesis and Characterization of Novel [FeFe]-Hydrogenase Models Containing Mixed S and Se Bridging Moieties.

4 Documentation of Authorship 83

5 Summary 87

6 References 95

7 Acknowledgements 107

Declaration of Authorship 109

Curriculum Vitae 110

List of Publications

Published/accepted Articles

[MK1] M. K. Harb, T. Niksch, J. Windhager, H. Görls, R. Holze, L. T. Lockett, N. Okumura, D. H. Evans, R. S. Glass, D. L. Lichtenberger, M. El-khateeb, W. Weigand. ***Synthesis and Characterization of Diiron Diselenolato Complexes Including Iron Hydrogenase Models.*** *Organometallics* **2009**, *28*, 1039-1048.

[MK2] M. K. Harb, J. Windhager, A. Daraosheh, H. Görls, L. T. Lockett, N. Okumura, D. H. Evans, R. S. Glass, D. L. Lichtenberger, M. El-khateeb, W. Weigand. ***Phosphane- and Phosphite-Substituted Diiron Diselenolato Complexes as Models for [FeFe]-Hydrogenases.*** *Eur. J. Inorg. Chem.* **2009**, 3414-3420.

[MK3] A. Q. Daraosheh, M. K. Harb, J. Windhager, H. Görls, M. El-khateeb, W. Weigand. ***Substitution Reactions at [FeFe]-Hydrogenase Models Containing [2Fe3S] Cluster by Phosphine or Phosphite Ligands.*** *Organometallics* **2009**, *28*, 6275-6280.

[MK4] M. K. Harb, U.-P. Apfel, J. Kübel, H. Görls, G. A. N. Felton, T. Sakamoto, D. H. Evans, R. S. Glass, D. L. Lichtenberger, M. El-khateeb, W. Weigand. ***Preparation and Characterization of Homologous Diiron Dithiolato, Diselenato, and Ditellurato Complexes: [FeFe]-Hydrogenase Models.*** *Organometallics* **2009**, *28*, 6666-6675.

[MK5] M. K. Harb, H. Görls, L. T. Lockett, G. A. N. Felton, D. H. Evans, R. S. Glass, D. L. Lichtenberger, M. El-khateeb, W. Weigand. ***Synthesis and Characterization of [FeFe]-Hydrogenases Models with Bridging Moieties Containing (S, Se) and (S, Te).*** *Eur. J. Inorg. Chem.* **2010**, Accepted.

Non-Published Articles

[MK6] M. K. Harb, A. Daraosheh, H. Görls, R. S. Glass, D. L. Lichtenberger, M. El-khateeb, W. Weigand. ***[FeFe]-Hydrogenase Models Containing Different Length Diselenolato Bridging Moieties.*** *In preparation*.

[MK7] M. K. Harb, A. Daraosheh, T. Niksch, H. Görls, R. S. Glass, D. L. Lichtenberger, M. El-khateeb, W. Weigand. ***Synthesis and Characterization of Novel [FeFe]-Hydrogenase Models Containing Mixed S and Se Bridging Moieties.*** *In preparation*.

1. Introduction

Explanatory note: This cumulative thesis comprises five full papers. The author of this thesis is the first author of four papers and co-author of one paper. Three articles have been published in the *Organometallics* and the others in *European Journal of Inorganic Chemistry*. The sixth as well as seventh article will be submitted soon. All journals are peer reviewed.

All articles deal with the structural and electrochemical investigations of the [FeFe]-hydrogenase active site. The author papers are assigned as **[MK1 – MK7]** in the text.

1.1 General Aspects

The most commonly used fossil fuels for the energy production purpose are non-renewable natural energy resources. Over 85% of the energy used in the world is from non-renewable supplies, due to their relatively cheap price and ease to get. Coal, petroleum and natural gas are all considered non-renewable because they can't be replenished (made again) in a short period of time. These resources will be diminishes in the coming few decades and becomes more harmful to the environment (raising carbon dioxide (CO_2) into the atmosphere). Therefore, the search for cleaner and environmentally friendly alternative energy recourses becomes a major challenge for the scientific community. Ethanol, bio-diesel and hydrogen gas are the main renewable fuels which could be used instead of fossil fuels. Hydrogen received more attention as alternative future fuel[1-8] than the others. This is explained by the fact that combustion of hydrogen gas results in the formation of water as the only product. Moreover, hydrogen gas can be directly converted to electricity with high conversion efficiencies.[9,10] Therefore, hydrogen production process in good yield became a very important process and many research reports appear every year concerning this process.[11-17] In nature, green plants, algae and some bacteria generate hydrogen from water using sunlight as an energy source.[18-20] In order to enrol the hydrogen production in industrial scale for using as energy resource, two main ways are developing nowadays:

- Biological hydrogen production: Hydrogen production with the help of microorganisms such as, fermentative bacteria, photosynthetic bacteria, cyanobacterium, algae and heterotrophic bacteria.[21-34] To date, however, no

microorganism with suitably, high and sustainable hydrogen gas productivity has been reported that would allow industrial scale generation of biohydrogen energy. Therefore the method shown below is taking more attention.

- Chemical hydrogen production: This involves the preparation and characterization of model complexes of the active site of the hydrogenase enzyme, which are able to catalyze the molecular hydrogen production process; this point will discuss intensively in this work.

These two ways have several advantages over hydrogen production using photoelectrochemical or thermochemical processes such as low energy requirement, cost effectiveness and low environmental impact.

1.2 Hydrogenases Definition

Hydrogenases are a group of natural metalloenzymes which are capable to catalyze the hydrogen production process from water by a reversible two-electron transfer between protons and molecular hydrogen (Eq. 1).[35-38]

$$2H^+ + 2e^- \underset{}{\overset{\text{Hydrogenase}}{\rightleftharpoons}} H_2 \qquad \textbf{Eq. 1}$$

Bact. E. coli,[39,40] has been shown to catalyze the above reaction in completely reversible way. The hydrogenase system is the most negative reversible oxidation-reduction as yet described in living cells. This hydrogenase system has two important functions:

1. Balance of the redox potential in the cell.
2. Evolution of hydrogen or provision of energy by oxidation of molecular hydrogen.

The enzyme hydrogenase is found in many microorganisms such as bacteria, archaea and eukaryotes. It was first discovered more than 75 years ago by Stephenson and Stickland in colon bacteria.[41]

An important representative example of these enzymes was isolated from *Desulfovibrio desulfuricans*.[42,43] This enzyme can produce 9000 molecules of hydrogen per second at 30 °C (hypothetically 1 mol of this enzyme could fill an airship of 13000 m^3 volume in about 10 min).[44] Nearly all hydrogenases contain several Fe-S clusters of different types and further redox active species, which may be involved in the electron transfer reactions.

1.3 Hydrogenases Classification

Hydrogenases are subdivided into three major kinds on the basis of the metal content of the active site. These enzymes, which have been reviewed by several groups, are: [NiFe]-, [FeFe]- and [Fe]-hydrogenases.[36,37,43,45-58] Moreover, the [NiFeSe]-hydrogenase is a subgroup of the [NiFe]-hydrogenase, in which one of the cysteine ligands bonded to the nickel atom is replaced by a selenocysteine.[59] The three hydrogenases types differ functionally from each other, for example [NiFe]-hydrogenase tend to be more involved in hydrogen oxidation and are less sensitive to inhibition by oxygen and carbon monoxide. Whereas, [FeFe]-hydrogenase have higher hydrogen production activity compared to other types and suffer less of product inhibition.[35,45,46]

1.3.1 [NiFe]-Hydrogenase

The [NiFe]-hydrogenase is heterodimeric proteins consisting of small and large subunits. The small subunit contains three Fe-S clusters, while the large subunit containing the active nickel-iron centre. [NiFe]-hydrogenase was first crystallized in 1987 from *Desulfovibrio* (D.) *vulgaris Miyazaki* by Higuchi et al.,[60] and in the same year from *D. gigas* by Niviere et al.[61] The first crystal structure of [NiFe]-hydrogenase was reported for the *D. gigas* enzyme in 1995 (Figure 1).[62] The structure revealed the presence of a nickel atom in the active site and eleven iron atoms arranged in a chain of three iron-sulfur clusters: two of cubane type and the middle one a [3Fe4S] cluster (Figure 2). Till the time of the preparation of this thesis, only five crystal structures of [NiFe]-hydrogenase are known. These are the enzymes from *D. gigas*,[62-65] *D. vulgaris Miyazaki F.*,[66-69] *D. desulfuricans,*[70] *D. fructosovorans*[71,72] *and Desulfomicrobium (Dm.) baculatum.*[59] These structures, together with spectroscopic data, show that the active site of [NiFe]-hydrogenase can be reviewed as {Ni(μ-S-Cys)$_2$Fe}-butterfly arrangement formed by the bridging cysteinyl ligands and the geometry around the Ni centre is distorted square-planar (Figure 2).[73,74] [NiFe]-hydrogenase show a preference for H_2 oxidation rather than its production, therefore, they are classeified as H_2-oxidizers.

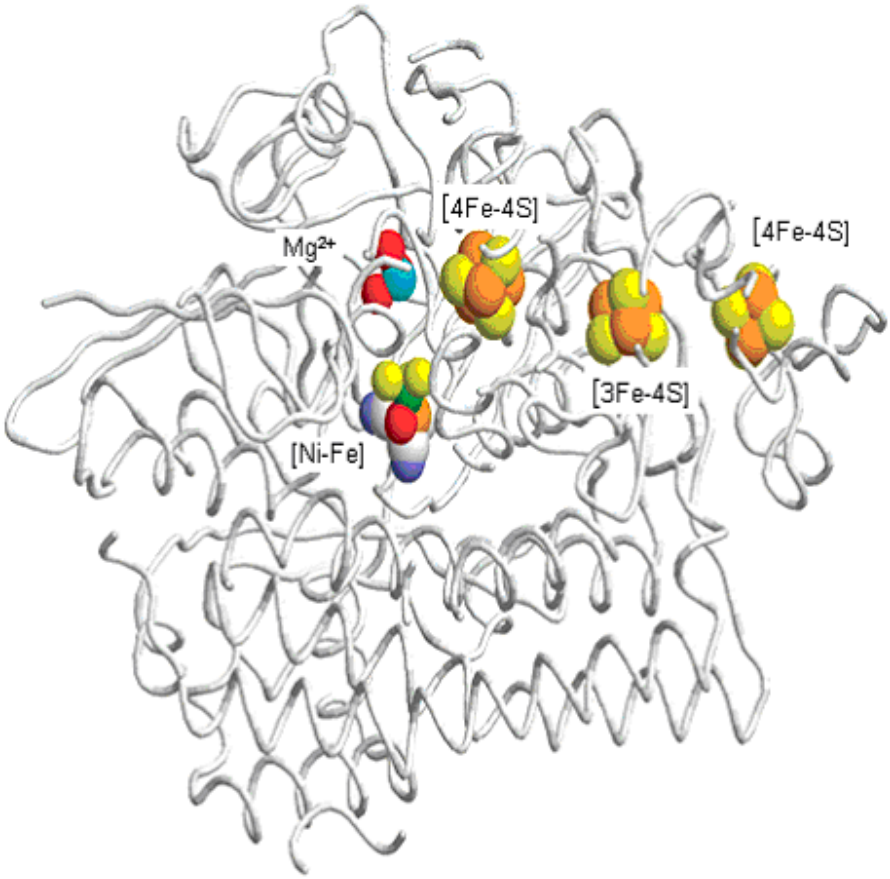

Figure 1: Crystal structure of [NiFe]-hydrogenase from *D. gigas* [ref. 62].

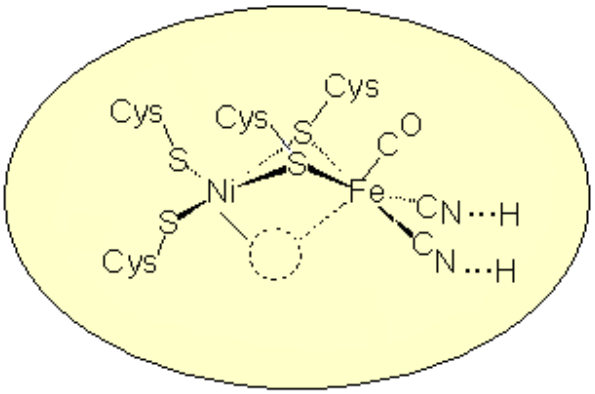

Figure 2: General structure of the active site of [NiFe]-hydrogenase

A subfamily, indicated as [NiFeSe]-hydrogenase, has a cysteine sulfur replaced by a selenium atom in the form of selenocysteine.[75] The first crystal structure determination of a [NiFeSe]-hydrogenase isolated from *Desulfomicrobium baculatum* has been published in 1999.[59]

The catalytic activity of [NiFe]-hydrogenase enzymes toward the oxidation of dihydrogen is discussed intensively in the literature.[76] Based on DFT calculations, the acceptable mechanism of the hydrogen oxidation catalytic process by the active site of these enzymes [NiFe]-hydrogenase is presented in Scheme 1.1.[76]

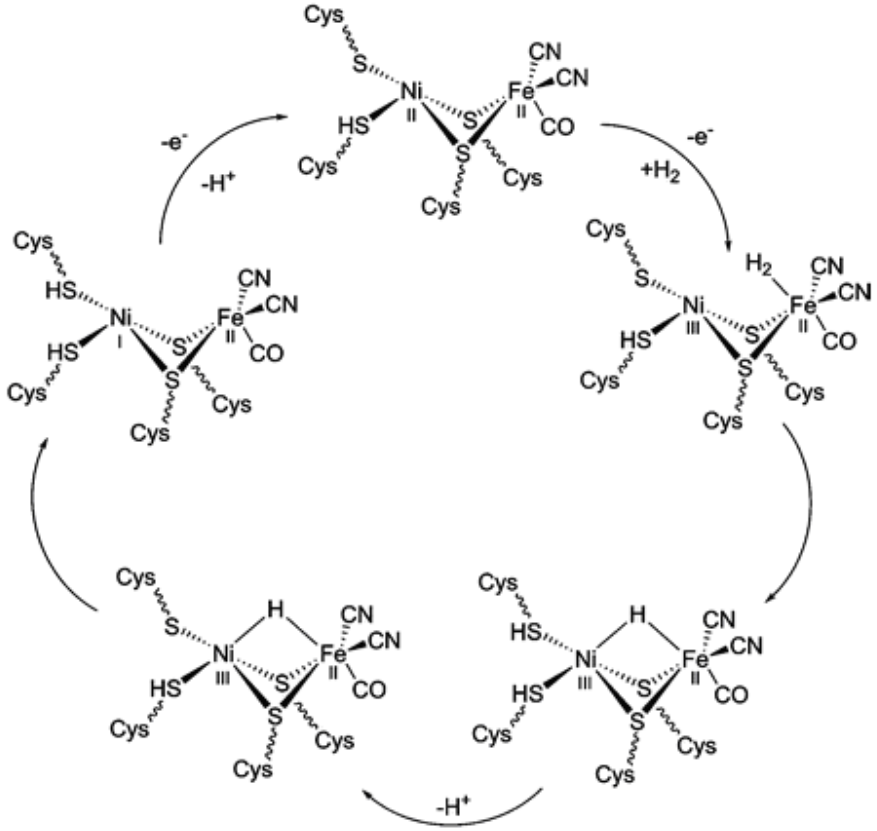

Scheme 1.1: Proposed catalytic cycle for H_2 oxidation by the active site of [NiFe]-hydrogenase adopted from reference [75].

1.3.2 [Fe]-Hydrogenase

This type of hydrogenases does not contain nickel atom or any iron sulfur cluster and has been recently found only in methanogens.[47,56] Shima *et al.* has been characterized the active site of the enzyme by X-ray crystallography.[50] In this structure, the iron centre has a square pyramidal geometry, in which the sp^2-hybridized N of the pyridinol derivative binds apically to iron, two cis-CO ligands, a cysteinyl thiolato and an unknown ligand occupying the equatorial positions. In Figure 3 show the X-ray and active site structure of the [Fe]-hydrogenase.

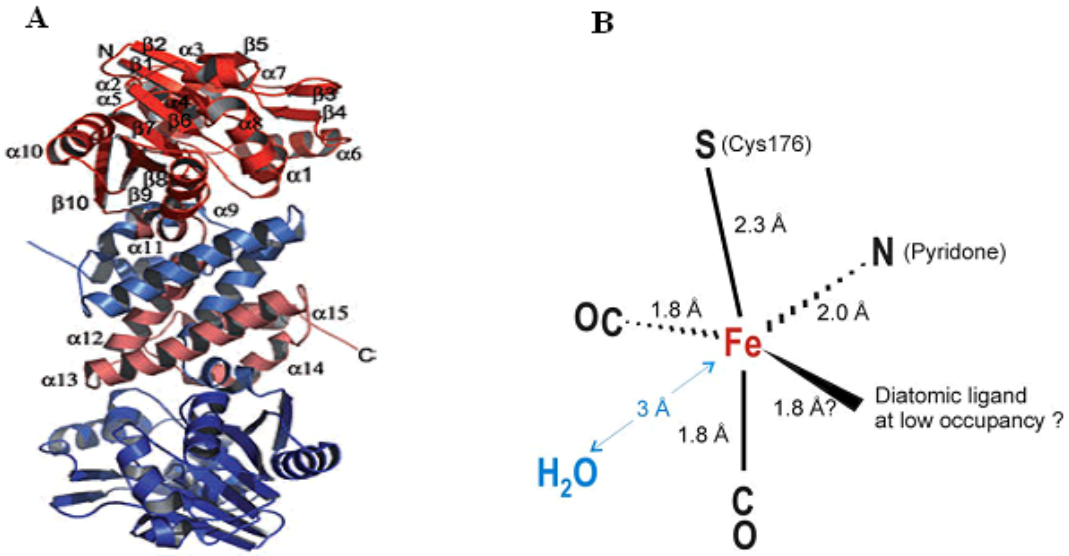

Figure 3: A) Crystal structure of [Fe]-hydrogenase from methanogens [ref. 47a]. **B)** The active site structure of [Fe]-hydrogenase [ref. 47b].

In principle, the H_2 is splitted at a mononuclear iron-carbonyl centre to release a proton and transfer a hydride to a carrier (methenyltetrahydromethanopterin), which catalizes the reversible reduction of methenyltetrahydromethanopterin (sub^+) with dihydrogen to methylenetetrahydromethanopterin (Sub-H) and proton (Eq. 2).[56]

$$Sub^+ + H_2 \longrightarrow Sub\text{-}H + H^+ \qquad \textbf{Eq. 2}$$

1.3.3 [FeFe]-Hydrogenase

[FeFe]-hydrogenase was first found in the gram positive bacterium *Clostridium (C.) pasteurianum,* this was the first organism containing no nickel but only iron atoms in the hydrogenase.[77] This was followed by the work of several groups, which involves the characterized of the [FeFe]-hydrogenase from different organisms.[42,54,78-93] Molecular masses of [FeFe]-hydrogenase can vary from 45 to 130 kDa.[56] The enzymes whose active sites have been elucidated by X-ray diffraction were isolated from *C. pasteurianum* (Figure 4A) and *D. desulfuricans* (Figure 4B).[94,95,98]

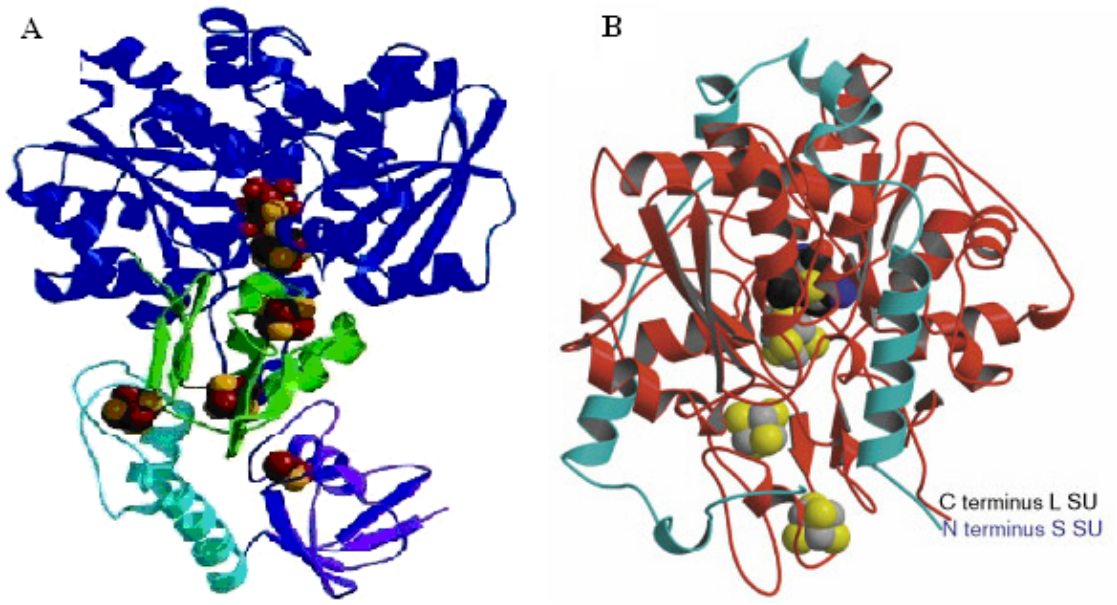

Figure 4: Three-dimensional structures of [FeFe]-hydrogenase from: (**A**) C. *pasteurianum* I (CpI) [ref 94] and (**B**) *D. desulphuricans* (Dd) [ref. 95].

The structure determination results from X-ray diffraction studies and spectroscopic data for [FeFe]-hydrogenase from *D. vulgaris*,[96-98] show that the active sites of these hydrogenases are formed by a {4Fe4S}- and {2Fe2S}-cluster, respectively, as shown in Figure 5. At the subsite a terminal carbon monoxide, a bridging carbon monoxide and a cyanide ligand are bound at each iron atom. Moreover, the two iron atoms share two bridging sulfur atoms within the linker (SCH_2XCH_2S). Currently, it remains undecided experimentally whether X is CH_2, NH or O. The active site of [FeFe]-hydrogenase is buried deeply within the protein and the H_2 migrates to or from the active site passes through hydrophobic channels.

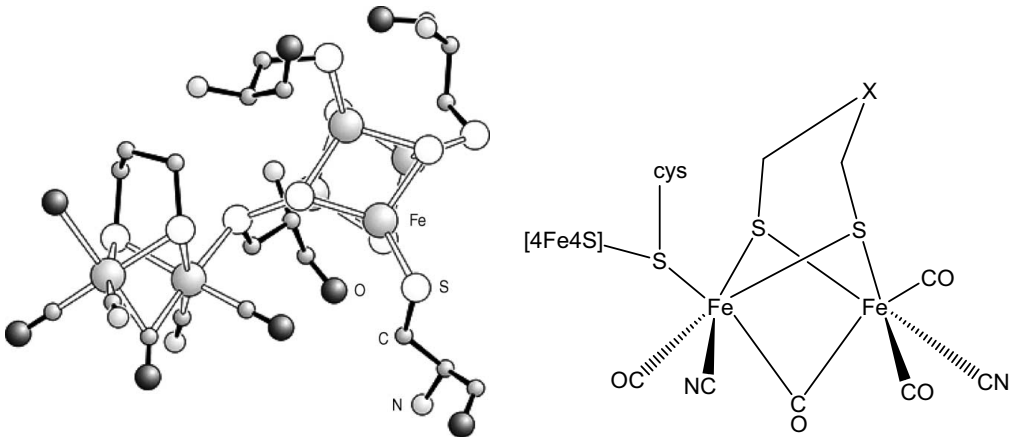

Figure 5: Composite structure of the H-cluster constructed from the crystal structures of [FeFe]-hydrogenase, X = CH_2, NH or O [ref. 98b].

The proposed catalytic cycle of [FeFe]-hydrogenase model complexes

The redox potential-controlled spectroscopic studies[91,99,100] guide to proposal of the catalytic cycle for the active site of [FeFe]-hydrogenase and show that these enzymes are able to catalyze the consumption and production of H_2.[93,101,102] Crystallographic and FT-IR studies recommend that the main structural change in the active site during the catalytic cycle is the movement of the bridging CO ligand toward the distal Fe atom of the active site and lead to a terminal coordination.[72] The generated vacant site has been proposed to be the site for substrate binding which could receive the hydrogen atom and forming H_2 (Scheme 1.2).

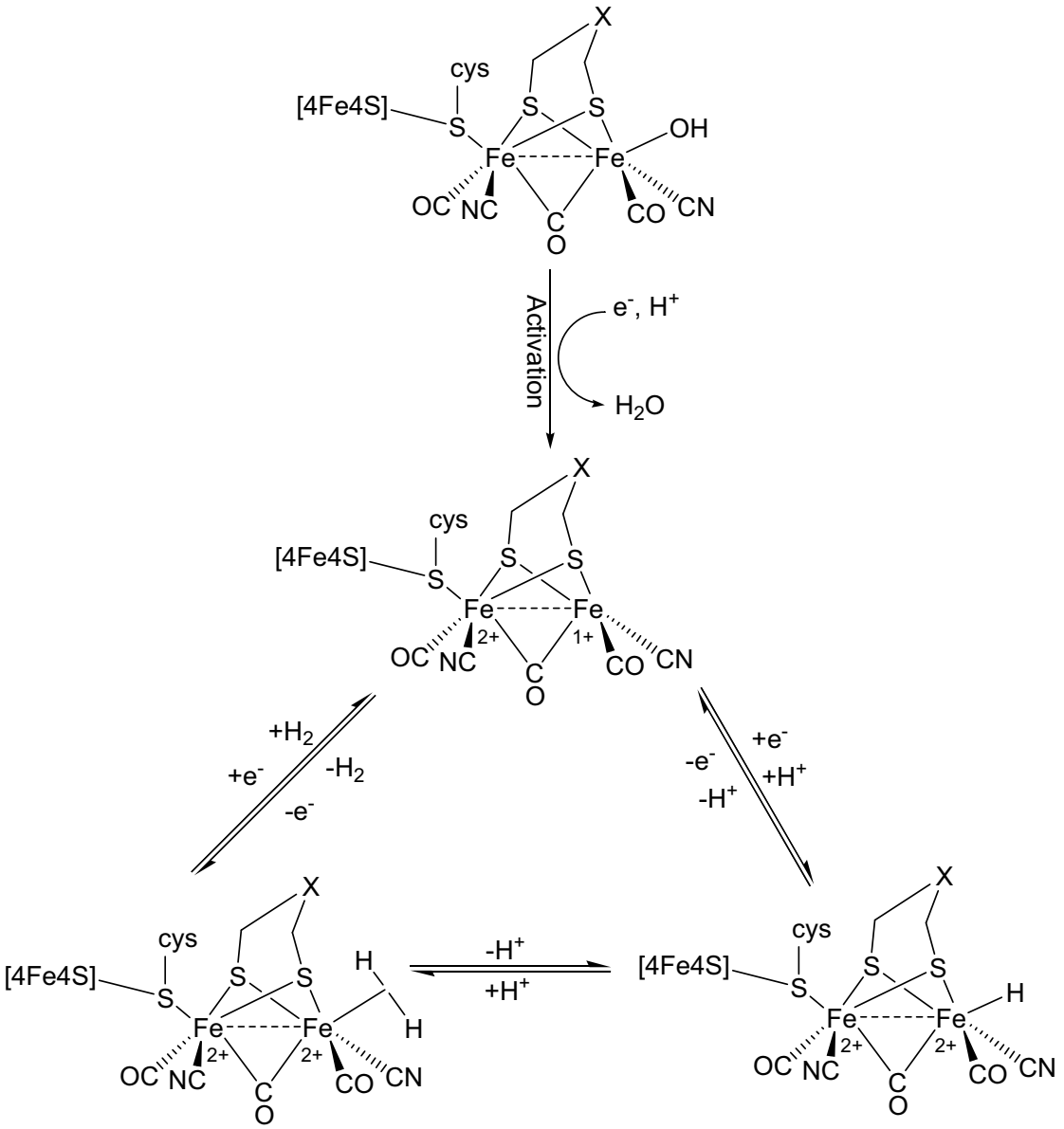

Scheme 1.2: Possible catalytic cycle for H_2 evolution by the active site of [FeFe]-hydrogenase.

The (proposed) catalytic cycle for model complexes

Diiron propanedithiolate (PTD)[103] is one of the simplest models of [FeFe]-hydrogenase, therefore, several theoretical and electrochemical efforts are reported in order to investigate the mechanism for hydrogen production by this complex.[47,104-106] Greco *et al*. studied the H_2 evolving path catalyzed by PDT model complex using density functional theory (Scheme 1.3).[106]

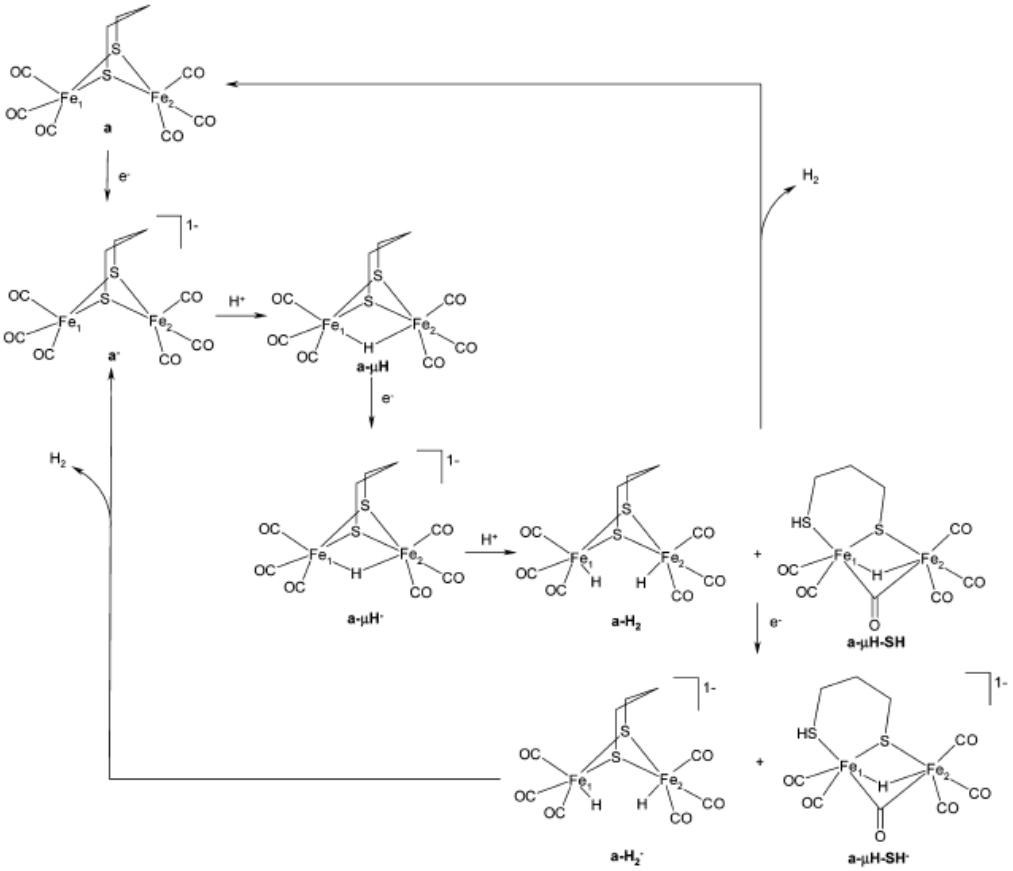

Scheme. 1.3: Possible catalytic cycle for H_2 evolution by PDT model complex adapted from reference [105].

Moreover, the electrochemical studies proved that $Fe_2(\mu\text{-}SCH_2NHCH_2S\text{-}\mu)(CO)_6$, which has a NH-group in the bridgehead unit, is the most active toward the catalytic hydrogen production compared to other model complexes.[43,107] Therefore, the catalytic activity of this compound has been investigated and presented in Scheme 1.4.[107]

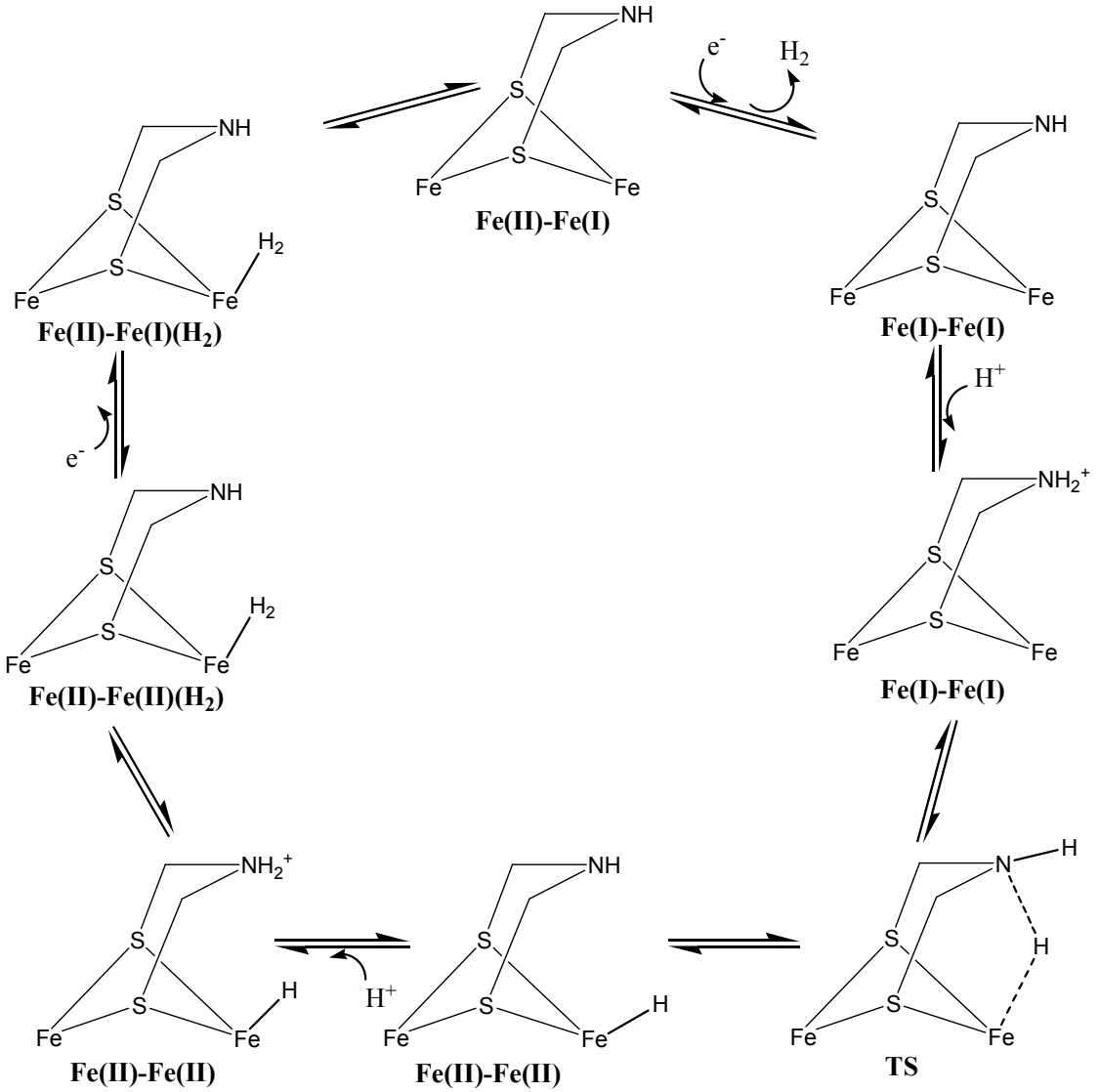

Scheme 1.4: Possible catalytic cycle for the hydrogen-generation at the active site of $Fe_2(\mu\text{-}S_2C_2H_4NH)(CO)_6$ model complex [ref. 98a].

Similar to the [FeNi]-hydrogenase, the [FeFe]-hydrogenase can catalyze the consumption and production of H_2, however, [FeFe]-hydrogenase has been considered mainly to be H_2-producers. They have higher hydrogen production activity and suffer less product-inhibition. Because of these facts, [FeFe]-hydrogenase received more attention in biomimetic studies and several model complexes have been made, characterized and their catalytic activity towards hydrogen production are well documented. A brief discussion of the [FeFe]-hydrogenase model complexes are shown below.

2. Structural Models of [FeFe]-Hydrogenase

Since the first diiron propanedithiolate (PDT)[103] complex was prepared as [FeFe]-hydrogenase model complex, several efforts to prepare and characterize analogous model compounds have been reported. The number of these model complexes which ascribed as active site of the [FeFe]-hydrogenase has grown progressively during the last several years.

2.1 $Fe_2(\mu\text{-}SCH_2XCH_2S\text{-}\mu)(CO)_6$ with Different Bridgeheads (X).

Diiron propanedithiolate (PDT) hexacarbonyl (**1**) was the first synthetic model complex of [FeFe]-hydrogenase active site, which was first described by the work of Seyferth[103] and later by others (Figure 6).[44,108-110] Rauchfuss and others show that the bridgehead CH_2 group could be formally replaced by NH (**2**) or O (**3**) (Figure 6).[111-115] In Jena, the replacement of bridgehead group by S atom was recently investigated (**4**) (Figure 6).[116] In this research work, the model analogues with selenium bridgehead (X = Se (**5**)) was achieved (Figure 6).[MK1]

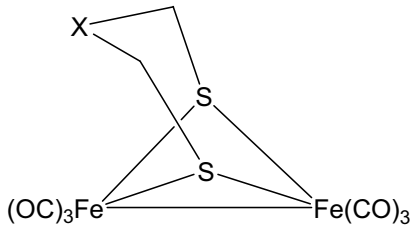

1: X = CH_2 **2**: X = O
3: X = NH **4**: X = S
5: X = Se

Figure 6: Model complexes of [FeFe]-hydrogenase active site with different bridgehead moieties.

Substituted methylene groups in the brdgehead (X = CHR [R = C(O)OH, C(O)NHEt, C(O)NHGly, O(Sugar), OH and CRR' (R, R') = (Me, Me), (Et, Et) (Et, Bu) of **1** have been reported in literature.[117-119] Moreover the bridgehead analogous of **3** X = NR [R = THF, Ph and substituted phenyls, Me, $C(O)CH_2Cl$, CH_2(thiophene), CH_2(furan), $C(O)CH_2S(O)Me$] have been also reported.[111-113,120-126]

2.2 $Fe_2(\mu\text{-}S(CH_2)_XS\text{-}\mu)$ with Different Length Linkers (x = 2, 3, 4, 5).

Ethane diiron dithiolate model complex (**6**) and butane analogues (**7**) were described by Seyferth and co-workers (Figure 7).[103,127] The geometry of unprepared pentyl analogues (**8**) and the known complexes **1**, **6** and **7** have been optimized by Darensbourg and co-workers, in order to determine the role of the length of the dithiolate linker in the stabilization or destabilization of the rotated structure.[128]

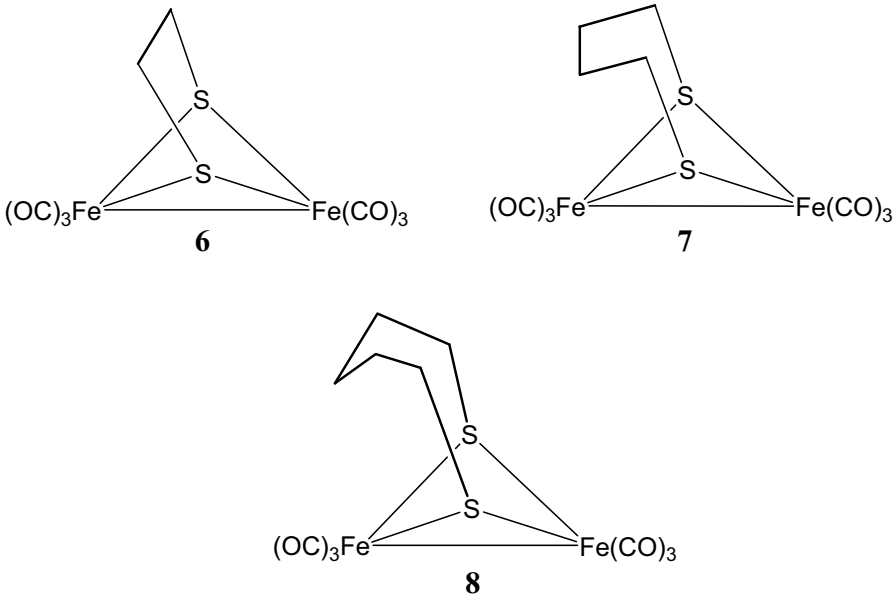

Figure 7: Model complexes of [FeFe]-hydrogenase active site with different dithiolato length linkers.

In the present work, we set out to prepare the analogues diiron diselenolate model complexes with different length linker [x = 3 (**9**), 4 (**10**), 5 (**11**)], in order to determine the role of the length of the diselenolato linker on the [FeFe] model complexes and to elucidate the influence of the length linker on the hydrogenase activity (Figure 8).[MK1,MK6]

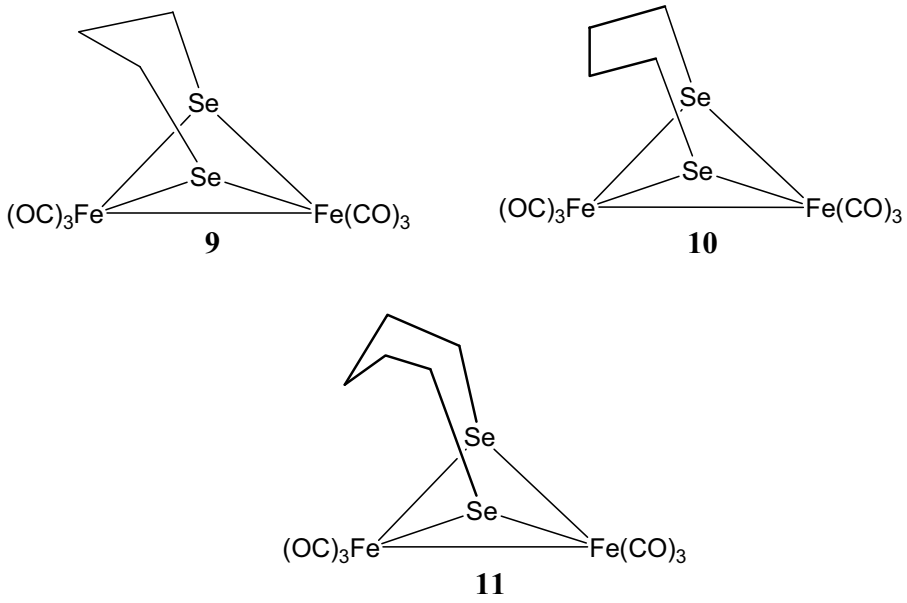

Figure 8: Model complexes of [FeFe]-hydrogenase active site with different diselenolato length linkers.

2.3 The Substitution Reactions of CO Groups.

The replacement of one or more carbonyl ligands from [FeFe]-hydrogenase model complexes by good donor ligands, such as cyanide, phosphite, carbene and isonitrile ligands has been reported in order to modify the catalytic properties for hydrogen generation. The substitution reactions of [FeFe]-hydrogenase with bidentate ligands such as bisphosphines ($Ph_2P(CH_2)_nPPh_2$) and diamines were also investigated. Some of these substituted model complexes are discussed below.

2.3.1 Substitution by Phosphine or Phosphite Ligands

In order to get complexes with high electron density at the iron atoms to inhance their reduction ability, substitution of CO ligands of propane dithiolate complex **1** was investigated. The first substituted model complex (**12**) of [FeFe]-hydrogenase was reported by Hasan *et. al* and is shown in Figure 9.[129] In the same year, Darensbourg and coworkers investigate the displacement of two CO ligands from **1** by two PMe_3 ligands to form **13** as shown in Figure 9.[44] Sun and coworkers prepared a series of mono- and disubstituted diiron complexes [(μ-PDT)-$Fe_2(CO)_5L$] [L = PPh_3 (**12**), $P(OEt)_3$ (**13**), PMe_3

(**14**), PMe_2Ph (**15**) and [(μ-PDT)$Fe_2(CO)_4L_2$] [L = PPh_3 (**16**), $P(OEt)_3$ (**17**), PMe_2Ph (**18**)] (Scheme 1.6).[130, 131] The mono- (**19**) and di-substituted (**20**) complexes were also prepared by the electrochemical reduction of **1** (Figure 9).[132] Moreover, a series of propanedithiolate iron complexes containing pendant nitrogen bases on the phosphine ligands with general formula [(μ-PDT)$Fe_2(CO)_5L$] {L = $PPh_2NH(CH_2)_2N(CH_3)_2$ (**21**), PPh_2NH-(2-$NH_2C_6H_4$) (**22**), PPh_2[2-$N(CH_3)_2CH_2C_6H_4$] (**23**)}, were investigated (Figure 9).[133] Three diiron PDT complexes with mono-phosphine ligands namely, (l-PDT)$Fe_2(CO)_5$[Ph_2PNH(t-Bu)] (**24**), (l-PDT)$Fe_2(CO)_5(Ph_2PH)$ (**25**) and (l-PDT)$Fe_2(CO)_5$[$Ph_2PFe(CO)_2Cp$] (**26**) were prepared and structurally characterized (Figure 9).[134] Additionally, the replacement of terminal CO groups from [FeFe]-hydrogenase model complexes by a number of mono and di substituted phosphine and phosphite ligands were reported.[104,125,135-154]

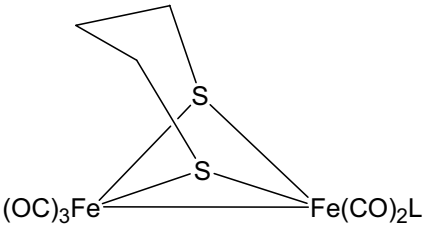

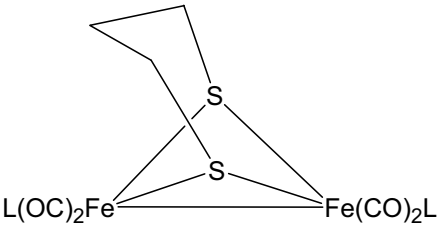

12: L = PPh_3 **14**: L = $P(OEt)_3$
15: L = PMe_3 **16**: L = PMe_2Ph
20: L = $P(OMe)_3$
22: L = $PPh_2NH(CH_2)_2N(CH_3)_2$
23: L = PPh_2NH-($2NH_2C_6H_4$)
24: L = PPh_2[2-$N(CH_3)_2CH_2C_6H_4$
25: L = Ph_2PNH(t-Bu)
26: L = Ph_2PH **27**: L = $Ph_2PFe(CO)_2Cp$

13: L = PMe_3
17: L = PPh_3
18: L = $P(OEt)_3$
19: L = PMe_2Ph
21: L = $P(OMe)_3$

Figure 9: Some examples of substituted model complexes of **1** by phosphine or phosphite ligands.

Proceeding from this idea and with the aim of increase the electron density at the iron atoms and to enhance its basicity, we carried out a substitution study of carbonyl groups of $Fe_2(\mu$-$Se_2C_3H_5CH_3)(CO)_6$ (**27**) by PPh_3 or $P(OMe)_3$ (Figure 10).[MK2]

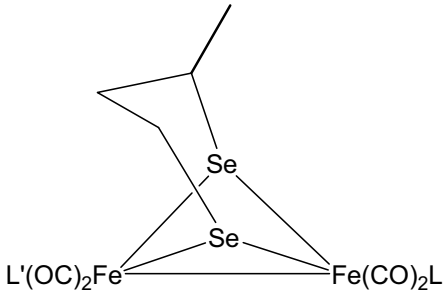

27: L = L' = CO
28: L = PPh_3, L' = CO
29: L = $P(OMe)_3$, L' = CO
30: L = L' = $P(OMe)_3$

Figure 10: Substituted model complexes of one or two carbonyl groups [ref. MK2].

2.3.2 Substitution by Bidentate Ligands

In general, bidentate ligands should be capable to form three structural types of complexes with the [2Fe2S] unit, one in which the ligand coordinates to both of the iron atoms (Figure 11A) in a bridging mode, the other in which the ligand chelates to one iron atoms (Figure 11B) and the last in which the ligand coordinates to the metal through one phosphorus atom and leaving the other free (dangling mode) (Figure 11C). The other P-atom could coordinate to a photosensitizer. In addition, bidentate ligands could give a complex where the phosphine ligand coordinates to two 2Fe2S units (Figure 11D). Talarmin and others developed this chemistry and set the scene for the synthesis of these complexes where the bidentate ligands are bisphosphanes or diamines.[155-169]

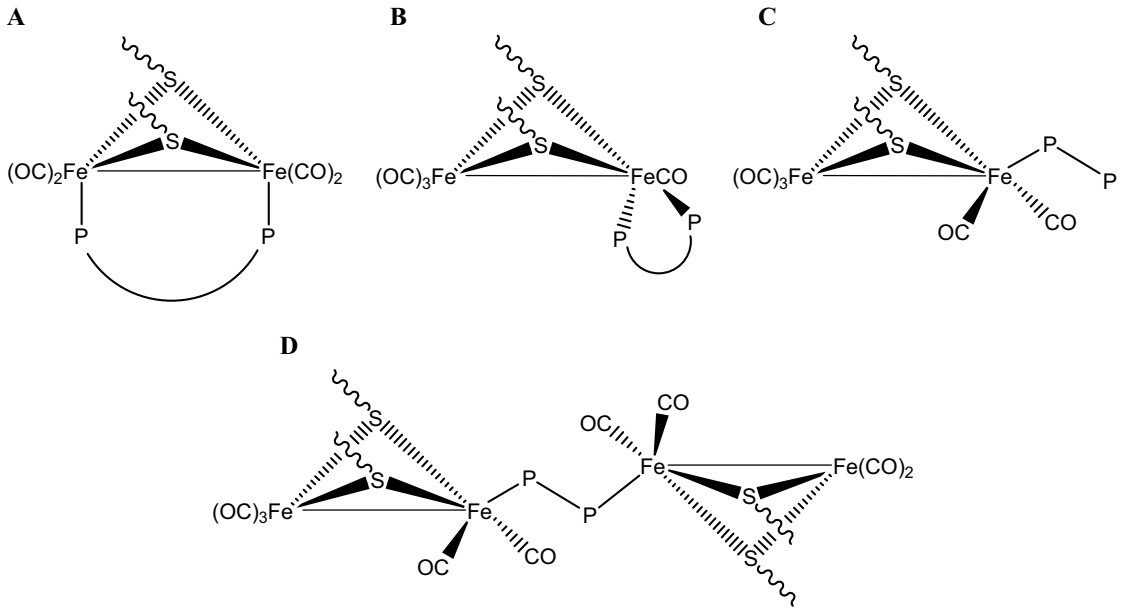

Figure 11: The possible coordination structural types of complexes containing a bidentate phosphine ligand.

In this work, the replacement of carbonyl ligands of **27** by bis(diphenylphosphanyl)ethane (dppe) afforded the chelate diiron complex **31** and the bridged tetrairon complex **32** (Scheme 1.7).[MK2]

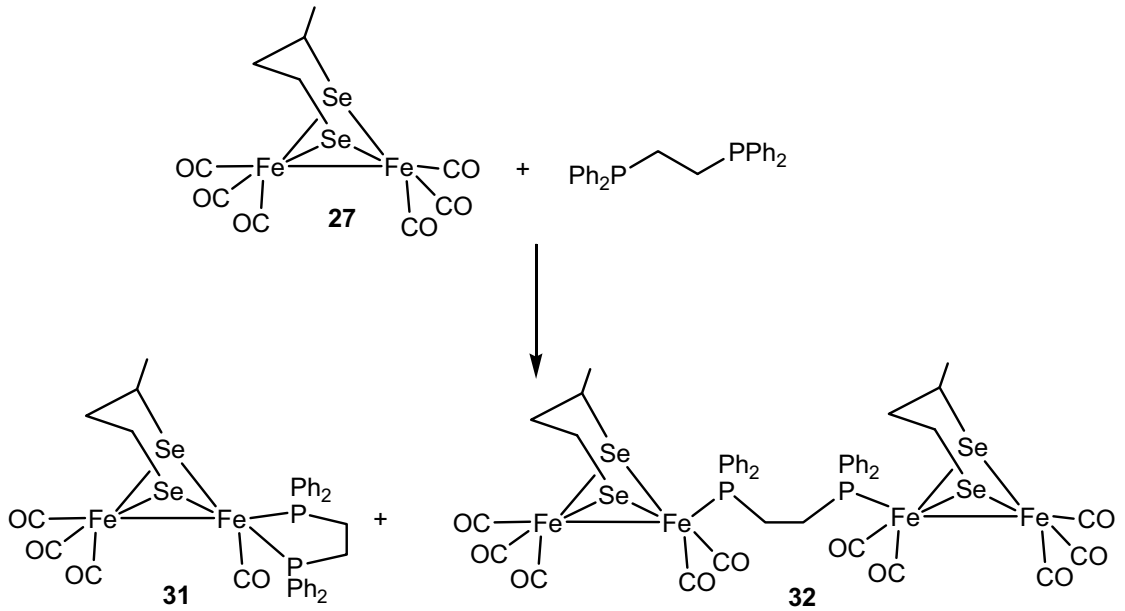

Scheme 1.7: Models of [FeFe]-hydrogenase containing a chelate (**31**) or bridged dppe ligand (**32**)

2.3.3 Substitution by Cyanide Ligand

X-ray crystal structures of [FeFe]-hydrogenase isolated from *Clostridium pasteurianum* and *Desulfovibrio desulfuricans* suggest that the active site contains CN ligands. In order to make model complexes resamble the active site closely, the substitution of CO groups by CN^- or iso-cyanide ligands received special attention. Therefore, several CN^- and iso-CN^- containing model complexes were reported as [FeFe]-hydrogenase.[108,170-181] Rauchfuss,[170] followed in the same year by Pickett[171] and their respective co-workers reported the synthesis and characterization of the first dinuclear iron–sulfur complex **33** bearing both CO and CN^- ligands (Figure12). This complex was followed by a number of model complexes containing both CO and CN^- ligands. In our laboratory, $(Et_4N)[Fe_2(\mu\text{-}SCH_2SCH_2S\text{-}\mu)(CO)_5CN]$ (**34**) was successfully isolated (Figure12).[182]

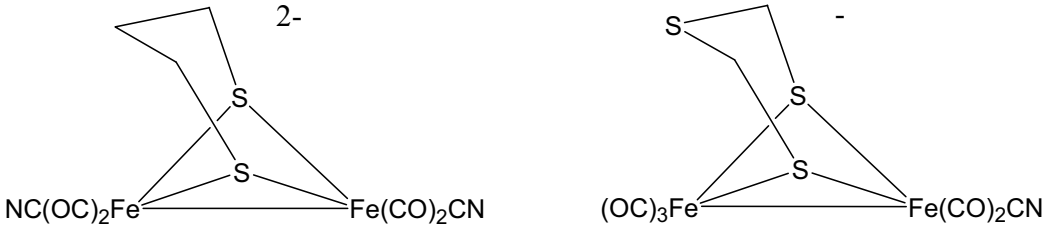

33 **34**

Figure 12: Examples of [FeFe]-hydrogenase models bearing both CO and CN ligands.

2.3.4 Substitution by N-heterocyclic Carbenes (NHCs) Ligands.

N-heterocyclic carbenes (NHCs) have received considerable attention as ligands in organometallic chemistry,[183-186] because their great electron-donating power compared to phosphine ligands as example. NHCs are strong σ-donor ligands having little or moderate π-accepting ability and are tuneable both electronically and structurally.[187-191] Therefore, the substitution reactions of [FeFe]-hydrogenase with NHCs were investigated, and gained a lot of interest by several working groups.[118,192-200]

2.4 [2Fe3S] Model Complexes.

The X-ray structures of natural [FeFe]-hydrogenase isolated from *Desulfovibrio desulfuricans*, show that the active centre of these enzymes possesses a [2Fe3S]-subsite. The first model compound $Fe_2[MeSCH_2C(Me)(CH_2S)_2](CO)_5$ (**35**) which contain this subsite and its cyano substituted compound $Fe_2[MeSCH_2C(Me)(CH_2S)_2](CO)_4(CN)_2$ (**36**) were investigated (Figure 13).[110,201,202] Only few examples of [2Fe3S] model complexes are known:[46,173,203-205] $Fe_2[PhCH_2SCH_2C(Me)(CH_2S)_2](CO)_5$ (**37**), $Fe_2[PhSCH_2C(Me)(CH_2S)_2](CO)_4(CN)_2$ (**38**), $Fe_2[CH_3C(CH_2S)_2(CH_2S\{CH_2\}_2$-N-pyrrole)$](CO)_5$ (**39**), $Fe_2[CH_3C(CH_2S)_2(CH_2S\{CH_2\}_2OH)](CO)_5$ (**40**), $Fe_2[(SCH_2)_2NCH_2CH_2SMe](CO)_5$ (**41**) (Figure 13). In our laboratory, the reaction of 1,2,6-trithionane with $Fe_2(CO)_9$ has been investigated and proved to yield [2Fe3S] model complex $Fe_2(\mu$-$S_2(C_3H_6)_2S$-$\mu)(CO)_5$ (**42**) (Figure 13).[116]

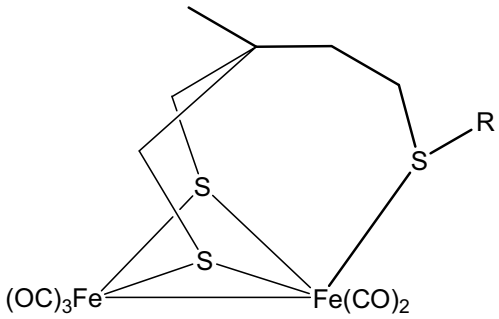

35: R = CH_3
36: R = Ph
37: R = CH_2CH_2N-Pyrrole
38: R = CH_2CH_2OH

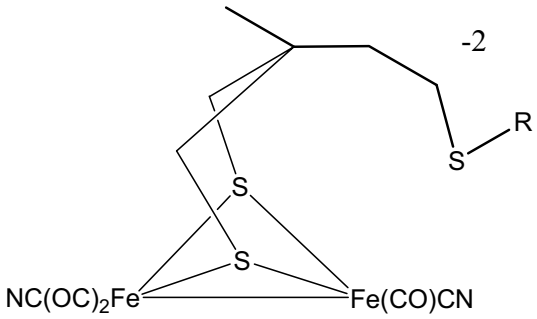

39: R = CH_3
40: R = Ph

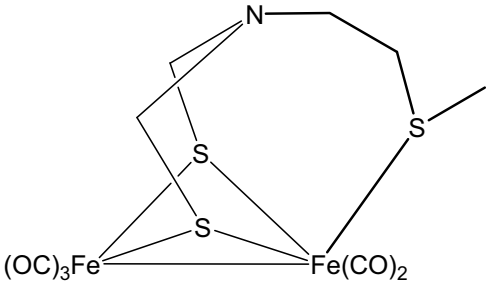

41

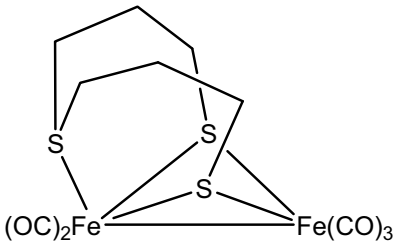

42

Figure 13: Model complexes of [FeFe]-hydrogenase active site containing [2Fe3S]-subsite.

In order to elucidate the role of the "on-off" coordination mode of the thioether group in the [2Fe3S] complex **43** which is related to the active site of [FeFe]-hydrogenase, the replacement of CO ligands of **43** by phosphite or phosphine ligands are described (Figure 14) and yielded the mono (**43**, **44**) and disubstituted (**45**, **46**) model complexes.[MK3]

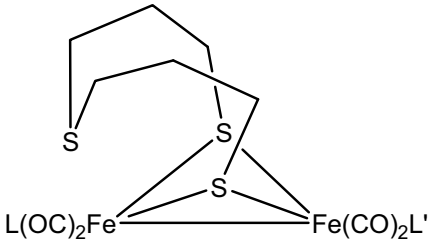

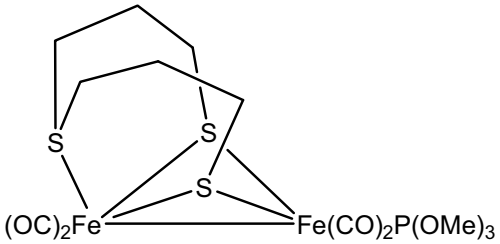

44

43: L = CO, L' = $P(OMe)_3$
45: L = L' = $P(OMe)_3$
46: L = L' = $P(OMe)_3$

Figure 14: Model complexes of [FeFe]-hydrogenase active site containing [2Fe3S]-subsite prepared in our laboratory.

2.5 [4Fe4S] Model Complexes.

Tetrairon model complexes can be formed by linking of two $Fe_2S_2(CO)_6$ subcluster cores.[206-209] In 2007, Zhang *et al*. reported [4Fe4S] model complexes, namely $[Fe_4(C_4H_8S_2)_2(CO)_{12}]$ (**47**) which was formed by linking of two fragments through two dithiolate bridging linkers (Figure 15A).[210]

My research aimed to prepare a series of tetrairon $[Fe_2(\mu\text{-}Se(CH_2)_nSe\text{-}\mu)(CO)_6]_2$ model complexes containing selenolato ligands with different length linkers (**48**: n = 5, **49**: n = 6) (Figure 15B).[MK6] The role of the length of the diselenolato linker in the [FeFe] model complexes on the hydrogenases activity are discussed.

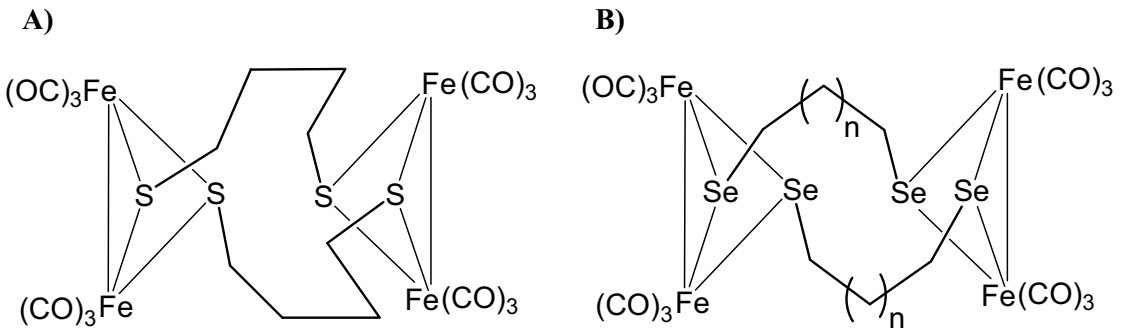

47

48:n = 3
49:n = 4

Figure 15: Tetrairon model complexes as active site of [FeFe]-hydrogenase.

2.6 Oxidation of Model Complexes.

The [FeFe]-hydrogenase model complexes with sulfenato bridging ligands could enhance the stability of the model complexes and offer a new approach towards the syntheses of functionalized models of the active site. The ethane-1,2-sulfenatothiolato complex **50** was the first complex which can be considered as oxidized [FeFe]-hydrogenases model.[211] Weigand and co-workers have shown the preparation of sulfenatothiolato (**51**) and disulfenato (**52**) compounds by the reaction of $Fe_2(CO)_9$ with dimethyldioxirane (DMD) (Figure 16).[116] Moreover, they were systematically studied the oxidation of thiolato and thioether of $[Fe_2(SDT)(CO)_6]$ compound. The oxidation of $[Fe_2(SDT)(CO)_6]$, $[Fe_2(CO)_6(SC((CH_2)_5)\text{-}SC((CH_2)_5)S)]$ and $[Fe_2(CO)_6(SC(Me)_2SC(Me)_2S)]$ with varying amounts of dimethyldioxirane (DMD) lead to the formation of several oxidized [FeFe]-hydrogenase model complexes.[212] The influence of the oxidized ligands on the electrochemical properties of complexes was also investigated.[212] Very recently, also Darensboug investigated the oxygenation of [2Fe2S] model complexes.[213]

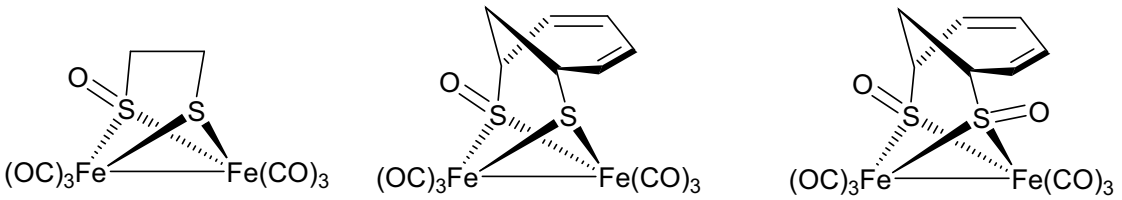

50 **51** **52**

Figure 16: Oxidized [FeFe]-hydrogenase model complexes.

2.7 Mixed S (Se and Te) Model Complexes.

In the present work, I have prepared and characterized for the first time diiron complexes containing mixed dichalcogenolato ligands (S, Se or S, Te) (Figure 17).[MK5, MK7]

The purposes for launching such a study are:

(i) To elucidate the influence of the bridged iron cores containing mixed dichalcogenolato ligands on the structure and electrochemical ability of hydrogenases model complexes.

(ii) To make a comparison of biomimetic chemistry between these mixed dichalcogenolato-containing models and their sulfur or selenium analogous.

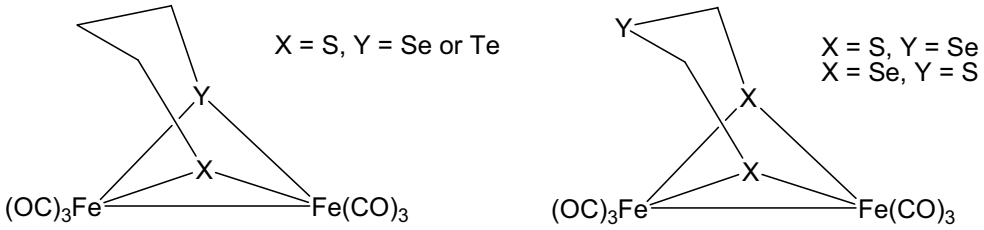

53: X = S, Y = Se
54: X = S, Y = Te

55: X = S, Y = Se
56: X = Se, Y = S

Figure 17: Models of [FeFe]-hydrogenase containing mixed dichalcogenolato ligands prepared in our laboratory.

Moreover, oxetane-containing dithiolato, diselenolato and ditellurolato diiron complexes have been prepared and characterized during my PhD work (Figure 18). The objective of this work was to determine the basis for the difference in reorganization energy of [2Fe2Y] (Y=S, Se, and Te) cores. We have chosen the oxetane ring because it allows the five-membered ring to which it is attached to be stable for all three 1,2-dichalcogenolane.[MK4]

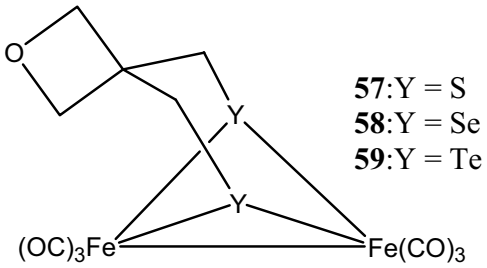

57:Y = S
58:Y = Se
59:Y = Te

Figure 18: Oxetane-containing dithiolato, diselenolato and ditellurolato diiron complexes

Publications

2.1 [MK1] Synthesis and Characterization of Diiron Diselenolato Complexes Including Iron Hydrogenase Models.

M. K. Harb, T. Niksch, J. Windhager, H. Görls, R. Holze, L. T. Lockett, N. Okumura, D. H. Evans, R. S. Glass, D. L. Lichtenberger, M. El-khateeb, W. Weigand.

***Organometallics* 2009, *28*, 1039-1048.**

Synthesis and Characterization of Diiron Diselenolato Complexes Including Iron Hydrogenase Models

Mohammad K. Harb,[†] Tobias Niksch,[†] Jochen Windhager,[†] Helmar Görls,[†] Rudolf Holze,[§] L. Tori Lockett,[⊥] Noriko Okumura,[⊥] Dennis H. Evans,*[,⊥] Richard S. Glass,*[,⊥] Dennis L. Lichtenberger,*[,⊥] Mohammad El-khateeb,*[,‡] and Wolfgang Weigand*[,†]

Institut für Anorganische and Analytische Chemie, Friedrich-Schiller-Universität Jena, August-Bebel-Strasse 2, 07743 Jena, Germany, Chemistry Department, Jordan University of Science and Technology, 22110 Irbid, Jordan, Institut für Chemie, Technische Universität Chemnitz, Strasse der Nationen 62, 09111 Chemnitz, Germany, and Department of Chemistry, The University of Arizona, Tucson, Arizona 85721

Received August 1, 2008

Diiron diselenolato complexes have been prepared as models of the active site of [FeFe]-hydrogenases. Treatment of $Fe_3(CO)_{12}$ with 1 equiv of 1,3-diselenocyanatopropane (**1**) in THF at reflux afforded the model compound $Fe_2(\mu\text{-}Se_2C_3H_6)(CO)_6$ (**2**) in 68% yield. The analogous methyl-substituted complex, $Fe_2(\mu\text{-}Se_2C_3H_5CH_3)(CO)_6$ (**3**), was obtained from the reaction of $Fe_3(CO)_{12}$ with the in situ generated compound 3-methyl-1,2-diselenolane (**4**). In contrast, the reaction of $Fe_3(CO)_{12}$ with 1,3,5-triselenacyclohexane (**5**) produced a mixture of $Fe_2(\mu^2,\kappa\text{-Se,C-}SeCH_2SeCH_2)(CO)_6$ (**6**), $Fe_2[(\mu\text{-}SeCH_2)_2Se](CO)_6$ (**7**), and $Fe_2(\mu\text{-}Se_2CH_2)(CO)_6$ (**8**). Compounds **2**, **3**, **6**, and **7** were characterized by IR, ^1H, ^{13}C, and ^{77}Se NMR spectroscopy, mass spectrometry, elemental analysis, and X-ray single-crystal structure analysis. The He I and He II photoelectron spectra for **3** are reported, and the electronic structure is further analyzed with the aid of DFT computations. The calculated reorganization energy of the cation of **3** to the "rotated" structure, which has a semibridging carbonyl ligand, is less than that of the analogous complexes with sulfur instead of selenium. Complexes **2** and **3** have been proved to be catalysts for electrochemical reduction of protons from the weak acids pivalic and acetic acid, respectively, to give hydrogen.

Introduction

Extensive research is taking place to synthesize hydrogenase model complexes to catalyze the production of hydrogen for use as an alternative fuel.[1−12] Hydrogenases are enzymes that catalyze the reversible two-electron transfer between protons and molecular hydrogen. Hydrogenases are subdivided into two major kinds: [NiFe]- and [FeFe]-hydrogenases.[13−18] The structure of the active site of [FeFe]-hydrogenases has been established by high-resolution X-ray crystallographic and spectroscopic studies.[19−25] The [FeFe]-hydrogenases are efficient catalysts for H_2 production;[2,26] therefore many efforts to characterize the structure of the active site of this enzyme are reported.[27−33]

Investigations of model complexes of the active sites of [FeFe]-hydrogenases (some examples of minimal models are shown in Scheme 1a) have also been reported.[29−33] These complexes contain two dithiolato-bridged iron cores. In Jena,

* Corresponding author. E-mail: c8wewo@uni-jena.de.
[†] Friedrich-Schiller-Universität Jena.
[‡] Jordan University of Science and Technology.
[§] Technische Universität Chemnitz.
[⊥] The University of Arizona.

(1) Nicolet, Y.; Cavazza, C.; Camps, J. C. F. *J. Inorg. Biochem.* **2002**, *91*, 1.
(2) Coontz, R. H. B. *Science* **2004**, *305*, 957.
(3) Melis, A.; Zhang, L.; Forestier, M.; Ghirardi, M. L.; Seibert, M. *Plant Physiol.* **2000**, *122*, 127.
(4) Woodward, J.; Orr, M.; Cordray, K.; Greenbaum, E. *Nature* **2000**, *405*, 1014.
(5) Ghirardi, M. L.; Zhang, L.; Lee, J. W.; Flynn, T.; Seibert, M.; Greenbaum, E.; Melis, A. *Trends Biotechnol.* **2000**, *18*, 506.
(6) Greenbaum, E.; Blankinship, S. L.; Lee, J. W.; Ford, R. M. *J. Phys. Chem. B* **2001**, *105*, 3605.
(7) Melis, A.; Happe, T. *Plant Physiol.* **2001**, *127*, 740.
(8) Chornet, E.; Czernik, S. *Nature* **2002**, *418*, 928.
(9) Tamagnini, P.; Axelsson, R.; Lindberg, P.; Oxelfelt, F.; Wünschiers, R.; Lindblad, P. *Microbiol. Mol. Biol. Rev.* **2002**, *66*, 1.
(10) Happe, T.; Hemschemeier, A.; Winkler, M.; Kaminski, A. *Trends Plant Sci.* **2002**, *7*, 246.
(11) Hallenbeck, P. C.; Benemann, J. R. *Int. J. Hydrogen Energy* **2002**, *27*, 1185.
(12) Tsygankov, A. A.; Fedorov, A. S.; Kosourov, S. N.; Rao, K. K. *Biotechnol. Bioeng.* **2002**, *80*, 777.
(13) Albracht, S. P. J. *Biochim. Biophys. Acta Bioenerg.* **1994**, *1188*, 167.
(14) Graf, E. G.; Thauer, R. K. *FEBS Lett.* **1981**, *136*, 165.
(15) Cammack, R.; Patil, D.; Aguirre, R.; Hatchikian, E. C. *FEBS Lett.* **1982**, *142*, 289.
(16) Adams, M. W. W.; Mortenson, L. E. *J. Biol. Chem.* **1984**, *259*, 7045.
(17) Wang, G.; Benecky, M. J.; Huynh, B. H.; Cline, J. F.; Adams, M. W. W.; Mortenson, L. E.; Hoffman, B. M.; Münck, E. *J. Biol. Chem.* **1984**, *259*, 14328.
(18) Hatchikian, E. C.; Forget, N.; Fernandez, V. M.; Williams, R.; Cammack, R. *Eur. J. Biochem.* **1992**, *209*, 357.
(19) Peters, J. W.; Lanzilotta, W. N.; Lemon, B. J.; Seefeldt, L. C. *Science* **1998**, *282*, 1853.
(20) Nicolet, Y.; Piras, C.; Legrand, P.; Hatchikian, C. E.; Camps, J. C. F. *Structure* **1999**, *7*, 13.
(21) Adams, M. W. W.; Johnson, M. K.; Zambrano, I. C.; Mortenson, L. E. *Biochimie* **1986**, *68*, 35.
(22) Adams, M. W. W. *Biochim. Biophys. Acta Bioenerg.* **1990**, *1020*, 115.
(23) Chen, J. S.; Mortenson, L. E. *Biochim. Biophys. Acta Protein Struct.* **1974**, *371*, 283.
(24) Chen, J. S.; Blanchard, D. K. *Biochem. Biophys. Res. Commun.* **1978**, *84*, 1144.
(25) Adams, M. W. W.; Mortenson, L. E. *Biochim. Biophys. Acta Bioenerg.* **1984**, *766*, 51.
(26) Cammack, R. *Nature* **1999**, *397*, 214.

10.1021/om800748p CCC: $40.75 © 2009 American Chemical Society
Publication on Web 01/29/2009

Scheme 1

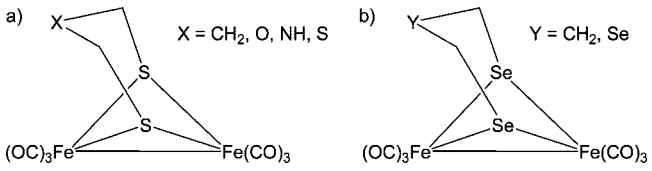

the reactions of sulfur-containing heterocycles with $Fe_2(CO)_9$ have been investigated and proved to yield dithiolato diiron complexes.[33,34] The substitution of carbonyl groups by CN^- or phosphines and their oxidation reactions were also investigated.[30−32,34−41] As an extension of our efforts in this area, we launched a study concerning the preparation and characterization of butterfly diiron complexes containing diselenolato-ligands (Scheme 1b). Only a very small number of $[Fe_2Se_2]$ complexes are known.[42] The ability of these complexes to act as models of the [FeFe]-hydrogenases will be presented. These complexes may also provide insight into the role of selenium in the [NiFeSe]-hydrogenases.[43]

Results and Discussion

Reaction of 1,3-Diselenocyanatopropane (1) with $Fe_3(CO)_{12}$. Treatment of $Fe_3(CO)_{12}$ with **1** in THF under reflux conditions for 2 h resulted in the formation of the diiron diselenolato complex $Fe_2(\mu\text{-}Se_2C_3H_6)(CO)_6$ (**2**) (eq 1).

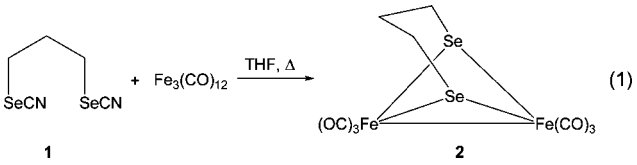

Complex **2**, which has been fully characterized by IR, multinuclear NMR spectroscopy, mass spectrometry, elemental analysis, and X-ray crystallography, is air-stable in the solid state and for several hours in hexane solution. The ^1H NMR spectrum of **2** exhibits two signals in a 1:2 ratio for the two different CH_2 moieties at 1.62 (CH_2CH_2Se) and 2.18 ppm (CH_2Se). These resonances are shifted downfield compared to the analogous sulfur-containing complex.[38] Its $^{13}C\{^1H\}$ NMR spectrum displays two resonances at 14.5 ppm for the C2 and 30.1 ppm for C1/C3. These resonances are also shifted downfield compared to those reported for the sulfur analogues.[38] One signal was observed at 145 ppm in the $^1H^{77}Se$ HMBC NMR spectrum of **2**, indicating equivalent Se atoms. This value is shifted to higher field than those reported for $Fe_2(\mu\text{-}Se_2CH_2)(CO)_6$ (**8**) and $[Fe(\mu\text{-}CH_2)Se(CO)_3]_2$.[42d] The mass spectrum of **2** showed the molecular ion peak at $m/z = 482$ and subsequent stepwise loss of six CO groups.

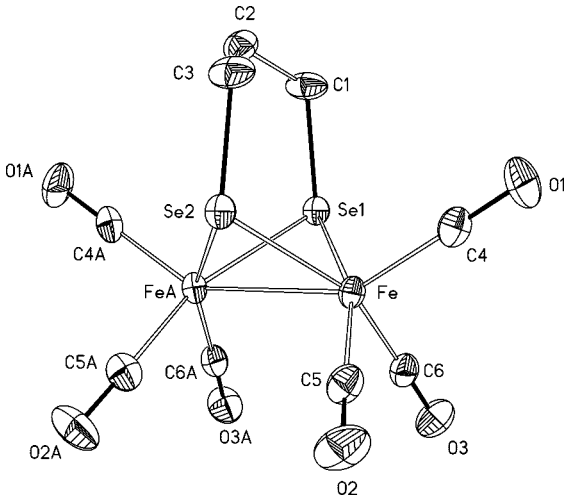

Figure 1. ORTEP drawing of $Fe_2(\mu\text{-}Se_2C_3H_6)(CO)_6$ (**2**) with thermal ellipsoids set at the 50% probability level (hydrogen atoms and the disordered C2A were omitted for clarity). Selected distances [Å] and angles [deg]: Fe−FeA 2.5610(8), Fe−Se1 2.3724(6), Fe−Se2 2.3673(6), Fe−Se1−FeA 65.33(2), Fe−Se2−FeA 65.49(2).

The X-ray diffraction analysis reveals the proposed structure of **2** as shown in Figure 1. The coordination geometry around the iron cores in **2** is rather similar to that in its sulfur analogue $Fe_2(\mu\text{-}S_2C_3H_6)(CO)_6$.[44] The Fe−Fe bond distance in **2** is 2.5610(8) Å, which is longer than that in the sulfur analogue [2.5103(11) Å].[44] The elongation of the Fe−Fe bond could be due to the larger size of selenium atoms. The Fe−Fe bond in **2** is shorter than those reported for the oxidized state diiron subsite (2.62 and 2.60 Å)[19,20] and is comparable to that found in the reduced state diiron subsite of the enzyme structure (2.55 Å).[27] As observed in the sulfur analogues, the C2 methylene group is disordered over two positions with 50% probability. The Fe−Se bond lengths are comparable to those reported for **8** and for $Fe_2(\mu\text{-}SeCH_2CH_2Se)(CO)_6$.[42d]

Reaction of 3-Methyl-1,2-diselenolane (4) with $Fe_3(CO)_{12}$. Treatment of $Fe_3(CO)_{12}$ with **4** at reflux in THF gave complex **3** in 73% yield (eq 2).

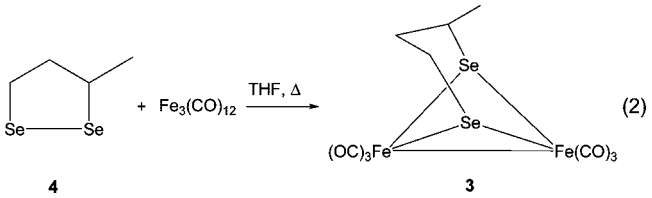

The stability of complex **3** is comparable to that of **2** in solution and in the solid state. The ^1H NMR spectrum of **3** exhibits a doublet at 1.34 ppm due to the methyl group. $^1H,^1H$

(27) Nicolet, Y.; Lacey, A. L. D.; Vernéde, X.; Fernandez, V. M.; Hatchikian, E. C.; Camps, J. C. F. *J. Am. Chem. Soc.* **2001**, *123*, 1596.
(28) Lawrence, J. D.; Li, H.; Rauchfuss, T. B. *Chem. Commun.* **2001**, 1482.
(29) Seyferth, D.; Womack, G. B.; Gallagher, M. K.; Cowie, M.; Hames, B. W.; Fackler, J. P.; Mazany, A. M. *Organometallics* **1987**, *6*, 283.
(30) Lawrence, J. D.; Li, H.; Rauchfuss, T. B.; Bénard, M.; Rohmer, M. M. *Angew. Chem., Int. Ed.* **2001**, *40*, 1768.
(31) Song, L. C.; Yang, Z. Y.; Bian, H. Z.; Liu, Y.; Wang, H. T.; Liu, X. F.; Hu, Q. M. *Organometallics* **2005**, *24*, 6126.
(32) Song, L. C.; Yang, Z. Y.; Hua, Y. J.; Wang, H. T.; Liu, Y.; Hu, Q. M. *Organometallics* **2007**, *26*, 2106.
(33) Windhager, J.; Rudolph, M.; Bräutigam, S.; Görls, H.; Weigand, W. *Eur. J. Inorg. Chem.* **2007**, 2748.
(34) Windhager, J.; Görls, H.; Petzold, H.; Mloston, G.; Linti, G.; Weigand, W. *Eur. J. Inorg. Chem.* **2007**, 4462.
(35) Gao, W.; Ekström, J.; Liu, J.; Chen, C.; Eriksson, L.; Weng, L.; Akermark, B.; Sun, L. *Inorg. Chem.* **2007**, *46*, 1981.
(36) Li, P.; Wang, M.; He, C.; Li, G.; Liu, X.; Chen, C.; Akermark, B.; Sun, L. *Eur. J. Inorg. Chem.* **2005**, 2506.
(37) Ezzaher, S.; Capon, J. F.; Gloaguen, F.; Pétillon, F. Y.; Schollhammer, P.; Talarmin, J. *Inorg. Chem.* **2007**, *46*, 3426.
(38) Lyon, E. J.; Georgakaki, I. P.; Reibenspies, J. H.; Darensbourg, M. Y. *J. Am. Chem. Soc.* **2001**, *123*, 3268.
(39) Gloaguen, F.; Lawrence, J. D.; Schmidt, M.; Wilson, S. R.; Rauchfuss, T. B. *J. Am. Chem. Soc.* **2001**, *123*, 12518.
(40) Cloirec, A. L.; Best, S. P.; Borg, S.; Davies, S. C.; Evans, D. J.; Hughes, D. L.; Pickett, C. J. *Chem. Commun.* **1999**, 2285.
(41) Song, L. C.; Yang, Z. Y.; Bian, H. Z.; Hu, Q. M. *Organometallics* **2004**, *23*, 3082.

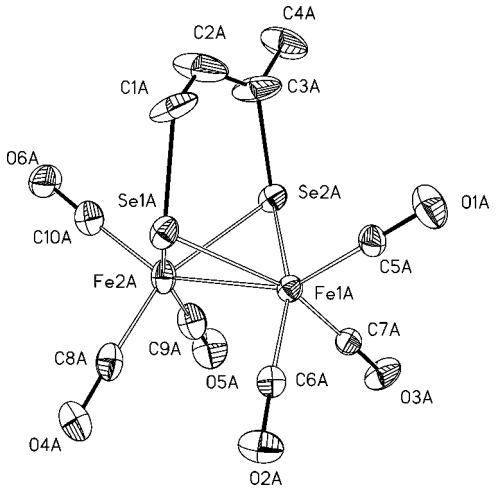

Figure 2. ORTEP drawing of $Fe_2(\mu\text{-}Se_2C_3H_5CH_3)(CO)_6$ (**3**). Selected bond distances [Å] and angles [deg]: Fe1A−Fe2A 2.5471(15), Fe1A−Se1A 2.3664(12), Fe1A−Se2A 2.3656(12), Fe2A−Se1A 2.3745(13), Fe2A−Se2A 2.3643(13), Fe1A−Se1A−Fe2A 65.05(4), Fe1A−Se2A−Fe2A 65.22(4).

COSY, $^1H,^{13}C$ HSQC, and $^1H,^{13}C$ HMBC NMR experiments allowed the assignment of the other five chemically nonequivalent different protons. The $^{13}C\{^1H\}$ NMR spectrum exhibits four resonances at 16.6 (C1), 25.3 (C4), 26.9 (C3), and 38.8 (C2) ppm, while the CO signals are observed at 208.6 and 209.0 ppm. Two signals at 157 and 248 ppm are obtained in the ^{77}Se NMR spectrum of **3** due to the presence of two different Se atoms. The mass spectrum of **3** shows the molecular ion peak at $m/z = 494$ followed by several peaks obtained by loss of CO groups. The structure of **3** was examined by X-ray diffraction analysis (see Figure 2). The Fe−Fe bond lengths of the two symmetrically independent molecules of **3** are 2.5492(14) and 2.5471(15) Å and, thus, similar to the analogous bond lengths in the reduced state diiron subsite of the enzyme structure.[27] The Fe−Se bond distances are comparable to those observed for **2**.

Reaction of 1,3,5-Triselenacyclohexane (5) with $Fe_3(CO)_{12}$. The reaction of $Fe_3(CO)_{12}$ with **5** in THF at reflux for 1 h leads to interesting fragmentation of the heterocyclic ring, yielding products **6**, **7**, and the known complex **8**[42d] (Scheme 2). These products were characterized by IR spectroscopy, multinuclear NMR spectroscopy, mass spectrometry, elemental analysis, and X-ray crystallography. The ^1H NMR spectrum of **6** displays two AB spin systems for the two methylene groups with the following resonances: 1.91 and 3.09 ppm for $SeCH_2Fe$ and 3.09 and 5.68 ppm for $SeCH_2Se$. However, the ^1H NMR spectrum of **7** displays one resonance at 3.31 ppm for the methylene groups. Based on $^1H,^{13}C$ HSQC and $^1H,^{13}C$ HMBC NMR experiments of **6**, the resonances at 18.8 and 31.3 ppm were assigned to $SeCH_2Fe$ and $SeCH_2Se$, respectively, while the spectrum of **7** displays one resonance at 30.2 ppm for the methylene groups. Additionally the carbonyl groups showed a resonance at 209.4 ppm. On the basis of the $^1H^{77}Se$ HMBC NMR spectrum of **6**, the ^{77}Se resonances at 220 and 315 ppm can be assigned to the selenolato and the iron-coordinated seleno ether group, respectively. The resonances of the Se atoms of complex **7** appear at 123 and 209 ppm. In a formal sense, formation of complex **6** might be explained by a fragmentation of the trimer $(H_2CSe)_3$ into selenoformaldehyde H_2CSe and the dimer $(H_2CSe)_2$. The dimer was trapped by $Fe_3(CO)_{12}$, yielding complex **6**, which is stable in solution for several hours and highly stable in the solid state. Compounds containing selenoformaldehyde as a ligand were not detected. The homologous 1,3,5-trithiane was reported to react with $Fe(CO)_5$ by insertion into a C−S bond, affording a complex with a structure similar to that of **6**, but with an additional H_2CS moiety, $[Fe_2(\mu^2,\kappa\text{-}S,C\text{-}SCH_2SCH_2SCH_2)(CO)_6]$.[45] Broader studies are needed to elucidate the fragmentation mechanism of the trimer in the presence of metal complexes.

The molecular structures of **6** and **7** were determined and are shown in Figures 3 and 4, respectively. The Fe−Fe distance in **7** of 2.5555(10) Å is comparable to those of **2** and **3**. In contrast, the analogous distance in **6** of 2.6592(14) Å is longer than those of **2**, **3**, and **7**. These differences might be attributed to the bridging ligands. While **2**, **3**, and **7** have bridging diselenolato ligands bonded to the iron atoms through both selenium atoms, complex **6** has two different types of Se−Fe bond. The selenolato group is bonded to the two iron atoms, and the seleno ether moiety is coordinated to one iron atom. The Fe−Se bond lengths of **7** are within the range observed for **2** and **3**. In complex **6**, the Fe1−Se1 and Fe2−Se1 bond lengths (2.359(1), 2.374(1) Å) are comparable to those in **2**, **3**, and **7**, while the Fe2−Se2 distance at 2.436(1) Å is significantly longer. In all complexes the geometry around the iron atoms is distorted octahedral as observed from the bond angles.

The IR spectra of complexes **2**, **3**, and **7** (KBr disk) show three strong absorption bands in the regions of 1988−1992, 2026−2030, and 2064−2069 cm^{-1}. These data are within the same ranges as those observed for sulfur analogues.[30−33] The IR spectrum of **6** (KBr disk) shows a medium band at 1918 cm^{-1} and two strong absorption bands at 1975 and 2037 cm^{-1}.

Photoelectron Ionizations. The He I and He II photoelectron spectra of **3** are shown in Figure 5. The assignment of the general character of the ionizations is based on analogous sulfur compounds previously reported.[46−48] This region of the photoelectron spectrum is expected to contain contributions from the Fe metal d-based ionizations, which includes the formal metal−metal bond of the diiron molecule and the three occupied d orbitals of each Fe center that back-bond to the carbonyls.

Ionization of the selenium nonbonding 4p orbital electrons is expected to occur in this region also, based on the photoelectron spectra of alkynyl selenols[49] and selenadiazoles[50] and comparison with the photoelectron spectra of other organome-

(42) (a) Hieber, W.; Gruber, J. *Z. Anorg. Allg. Chem.* **1958**, *296*, 91–103. (b) Gao, S.; Fan, J.; Sun, S.; Peng, X.; Zhao, X.; Hou, J. *Dalton Trans.* **2008**, *16*, 2128–2135. (c) Seyferth, D.; Henderson, R. S. *J. Organomet. Chem.* **1981**, *204*, 333–343. (d) Mathur, P.; Manimaran, B.; Trivedi, R.; Hossain, M. M.; Arabatti, M. *J. Organomet. Chem.* **1996**, *515*, 155–162. (e) Apfel, U.-P.; Halpin, Y.; Gottschaldt, M.; Görls, H.; Vos, J. G.; Weigand, W. *Eur. J. Inorg. Chem.* **2008**, 5112–5118.

(43) (a) Garcin, E.; Vernède, X.; Hatchikian, E. C.; Volbeda, A.; Frey, M.; Fontecilla-Camps, J. C. *Structure (London)* **1999**, *7*, 557–566. (b) Stein, M.; Lubitz, W. *Phys. Chem. Chem. Phys.* **2001**, *3*, 5115–5120.

(44) Lyon, E. J.; Georgakaki, I. P.; Reibenspies, J. H.; Darensbourg, M. Y. *Angew. Chem., Int. Ed.* **1999**, *38*, 3178.

(45) Raubenheimer, H. G.; Linford, L.; Lombard, A. van A. *Organometallics* **1989**, *8*, 2062–2063.

(46) (a) Andersen, E. L.; Fehlner, T. P.; Foti, A. E.; Salahub, D. R. *J. Am. Chem. Soc.* **1980**, *102*, 7422–7429. (b) van Dam, H.; Louwen, J. N.; Oskam, A.; Doran, M.; Hillier, I. H. *J. Electron Spectrosc. Relat. Phenom.* **1980**, *21*, 57–69.

(47) Yang, X.; Razavet, M.; Wang, X.; Pickett, C. J.; Wang, L. *J. Phys. Chem. A* **2003**, *107*, 4612–4618.

(48) Glass, R. S.; Gruhn, N. E.; Lorance, E.; Singh, M. S.; Stessman, N. Y. T.; Zakai, U. I. *Inorg. Chem.* **2005**, *44*, 5728–5737.

(49) Guillemin, J.; Bajor, G.; Riague, E.; Khater, B.; Veszpremi, T. *Organometallics* **2007**, *26*, 2507–2518.

(50) Cozzolino, A. F.; Gruhn, N. E.; Lichtenberger, D. L.; Vargas-Bacaa, I. *Inorg. Chem.* **2008**, in press.

Scheme 2

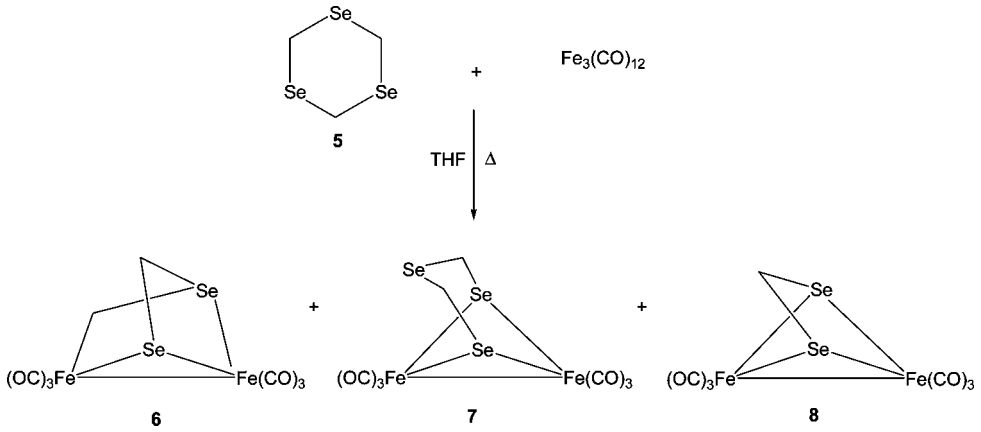

tallic Fe−S complexes.[51] Thus, at least nine orbital ionizations are expected in this region with mixing of iron, carbonyl, and selenium 4p character. The first ionization feature spans from about 7.3 to 8.9 eV. This broad feature shows a slight shoulder on the low ionization energy side, corresponding to the HOMO-based ionization, which is calculated to be primarily the Fe−Fe bond, as described below. Ionizations above 8.9 eV show substantially decreased intensity relative to those below 8.9 eV when He II excitation is used instead of He I excitation, indicating substantial selenium character associated with these ionizations. According to theoretical partial photoionization cross-sections,[52] the probability for ionization from a selenium 4p orbital drops by almost a factor of 15 from He I to He II excitation, while the probability of ionization from an iron 3d orbital increases by almost a factor of 2. The observed changes in the relative intensities of the ionizations are not that great, suggesting significant mixing of iron and selenium character in the ionizations in this region, with the larger selenium character in the ionizations above 8.9 eV.

Electronic Structure. Theoretical computations have been carried out on molecule **3** to assist understanding the electronic structure and properties of these molecules. A computational methodology has been developed previously for systems of this type and found to agree well with the properties of diiron systems.[53] The Fe−Fe bond distance, calculated to be 2.566 Å for **3**, is close to that of the crystal structure, 2.548 Å. To our knowledge calculated Fe−Se bond distances have not been compared to experiment previously. The average calculated gas-phase Fe−Se distance of 2.405 Å compares well with the average Fe−Se distance from the crystal structure of 2.368 Å. Frequency calculations were performed to further assess the validity of the theoretical analysis. The calculated values for the carbonyl stretching frequencies are 1994, 2022, and 2060 cm^{-1}, which are comparable to the experimental values of 1988, 2026, and 2065 cm^{-1}.

Theoretical calculations also account well for the experimental adiabatic and vertical lowest ionization energies measured by photoelectron spectroscopy and provide additional insight into the nature of the molecular orbitals and electronic structure. In Figure 5 the arrow at the low ionization energy, at 7.45 eV, corresponds to the calculated adiabatic ionization from the neutral to the cation with both structures fully optimized. It can be seen that the calculated adiabatic ionization energy is close to the experimental onset of the ionization band. The optimized cation geometry, shown in Figure 6, features a semibridging carbonyl ligand and little to no lengthening of the Fe−Fe bond compared with neutral **3**. The calculated geometries of the neutral and cationic molecules in the gas phase are given in the Supporting Information.

The arrow placed at higher ionization energy in the spectrum points to the calculated vertical ionization energy. The difference between the adiabatic and vertical ionization energies is the reorganization energy of the cation from the nonbridging structure to the semibridging "rotated" structure. This has been discussed in more detail previously[54] and is analogous to the reported structure of the active site for [FeFe]hydrogenase.[19−25] The calculated reorganization energy for this cation is 0.45 eV.

This reorganization energy to the semibridging carbonyl structure is less than the ∼0.65 eV reorganization energies found in a similar study for the related 1,2-benzenedithiolato, 2,3-pyridinedithiolato, and 1,3-propanedithiolato $Fe_2(CO)_6$ complexes and considerably less than the 0.82 eV reorganization energy of the norbornanedithiolato $Fe_2(CO)_6$ complex. This smaller reorganization energy suggests that these seleno complexes may be amenable to faster electron transfer processes than the corresponding thiolato complexes.

Also shown in Figure 5 are the calculated Kohn−Sham orbital energies shifted such that the HOMO energy aligns with the calculated vertical ionization energy. The Kohn−Sham orbitals for the HOMO and LUMO are shown in Figure 7, and for deeper valence orbitals are shown in the Supporting Information.

It can be seen, as noted previously, that the HOMO consists primarily of the metal−metal bonding contribution between the Fe d_{z^2} orbitals with some delocalization to the carbonyl ligands, due to back-bonding. The LUMO shows principally a metal−metal antibonding interaction between the Fe d_{z^2} orbitals along with a contribution of an Fe−Se antibonding combination of these orbitals with the Se 4p orbitals. The orbitals from 9 to 10 eV are calculated (as seen in SI-8−10 in the Supporting Information) to have substantial selenium 4p character, in agreement with the comparison of the He I and He II data, with the orbital closest to the peak at 9.13 eV (SI-8), being a combination of the predominantly selenium 4p lone pairs directed outward from the molecule. In addition, this orbital, as well as the two orbitals

(51) Cranswick, M. A.; Gruhn, N. E.; Oorhles-Steele, O.; Ruddick, K. R.; Burzlaff, N.; Schenk, W. A.; Lichtenberger, D. L. *Inorg. Chim. Acta* **2008**, *361*, 1122–1133.

(52) Yeh, J. J.; Lindau, I. *At. Data Nucl. Data Tables* **1985**, *32*, 1–155.

(53) (a) Felton, G. A. N.; Vannucci, A. K.; Chen, J.; Lockett, L. T.; Okumura, N.; Petro, B. J.; Zakai, U. I.; Evans, D. H.; Glass, R. S.; Lichtenberger, D. L. *J. Am. Chem. Soc.* **2007**, *129*, 12521. (b) Borg, S. J.; Ibrahim, S. K.; Pickett, C. J.; Best, S. P. *C. R. Chimie* **2008**, *11*, 852–860.

(54) Petro, B. J.; Vannucci, A. K.; Lockett, L. T.; Mebi, C.; Kottani, R.; Gruhn, N. E.; Nichol, G. S.; Goodyer, P. A. J.; Evans, D. H.; Glass, R. S.; Lichtenberger, D. L. *J. Mol. Struct.* **2008**, *890*, 281–288.

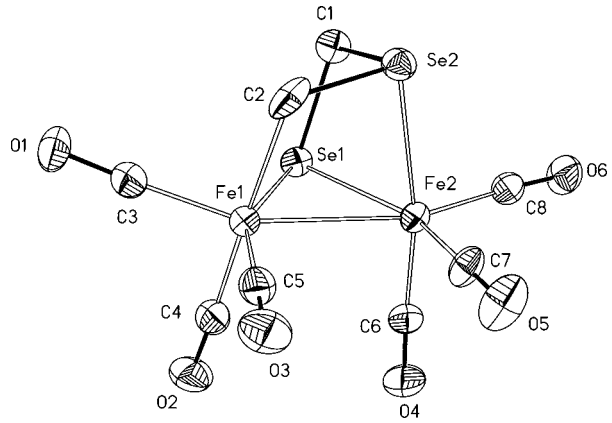

Figure 3. ORTEP drawing of $Fe_2(\mu^2,\kappa\text{-}Se,C\text{-}SeCH_2SeCH_2)(CO)_6$ (**6**). Selected bond distances [Å] and angles [deg]: Fe1−Fe2 2.6592(14), Fe1−Se1 2.3588(12), Fe2−Se1 2.3743(14), Fe2−Se2 2.4359(12), Fe1−Se1−Fe2 68.36(4), C2−Se2−Fe2 89.9(2), Se2−C2−Fe1 108.2(3).

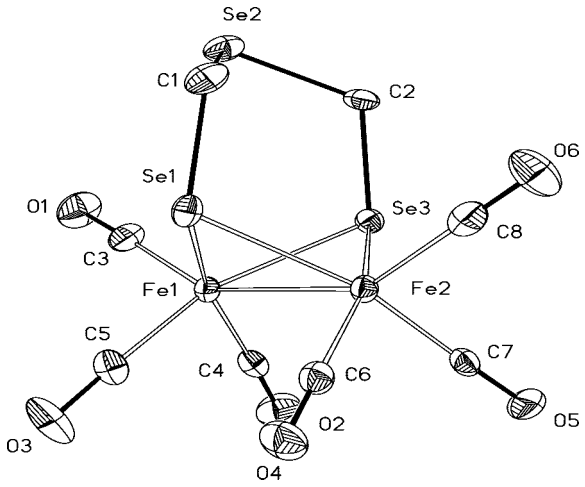

Figure 4. ORTEP drawing of $Fe_2[(\mu\text{-}SeCH_2)_2Se](CO)_6$ (**7**). Selected bond distances [Å] and angles [deg]: Fe1−Fe2 2.5555(10), Fe1−Se1 2.3840(10), Fe1−Se3 2.3703(10), Fe2−Se1A 2.3785(9), Fe2−Se3 2.3755(9), Fe1−Se1−Fe2 64.90(3), Fe1−Se3−Fe2 65.16(3).

near the peaks at 9.60 and 9.79 eV, are calculated to contain Fe character in addition to Se character. The next calculated orbital energy is in the vicinity of 10.5 eV, which falls outside of the energy range of the figure. It is also noted that the HOMO−1 and HOMO−2 orbitals have significant selenium character, consistent with the mixing that is suggested by the He I/He II comparison. Given the expected differences in electron relaxation energies with ionization, which are generally larger for metal-based ionizations in the region from 7.5 to 9 eV, the agreement between the pattern of the calculated orbital energies and the observed ionizations is very good and lends confidence to the assignments.

The measured gas-phase ionization energies and validation of the calculated structures and orbital characters provide a starting point for comparison to the electrochemical properties of these molecules presented in the next section.

Electrochemical Investigations. Cyclic voltammograms (CV) of **2** and **3** were recorded in order to identify the electrochemically induced oxidation and reduction processes and to test the ability of these complexes to catalyze the reduction of weak acids to form dihydrogen. Compound **2** was investigated in acetonitrile using a platinum working electrode. Voltammograms are shown in Figure 8. All scans were initiated from the open-circuit potential of 0.0 V vs the Ag/AgCl reference electrode.

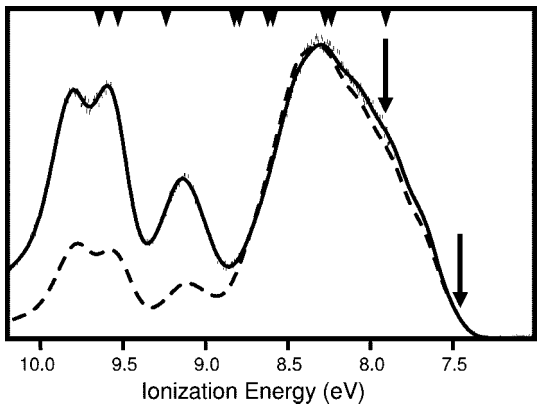

Figure 5. He I (solid line) and He II (dashed line) photoelectron spectra of complex **3**. The arrow at the lower ionization energy points to the calculated adiabatic ionization energy corresponding to the optimized structure of the cation (see Figure 6). The arrow at the higher ionization energy points to the calculated vertical ionization energy corresponding to the structure of the neutral molecule. Triangles at the top of the figure indicate the calculated energies of molecular orbitals of the neutral molecule with the HOMO energy aligned to the calculated vertical ionization energy.

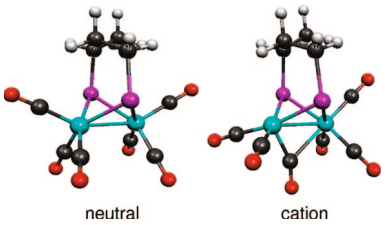

Figure 6. Calculated neutral and cation structures of compound **3**.

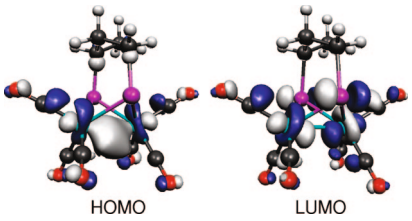

Figure 7. Highest occupied and lowest unoccupied orbitals of complex **3**.

Scans in the range 0.0 to +1.6 V revealed one main irreversible anodic peak, which occurred at +1.39 V (E_1) and whose height suggests an overall two-electron oxidation process. This peak can be assigned to the oxidation of both Fe(I) to Fe(II), followed by decomposition of the product. Small irreversible oxidation peaks at +0.66 (E_5) and +0.9 V were not assigned. Two scans probed reduction processes. The first, in the 0 to −1.4 V region, shows some very small and ill-defined reduction peaks and essentially no oxidative features. However, when the negative-going scan was extended to −1.7 V, a substantial reduction peak was observed at −1.46 V (E_2). On the return sweep, a small anodic peak at −1.35 V (E_3) suggests that some of the reduction product survives long enough to be detected. A follow-up product of the reduction is probably responsible for the anodic peak seen at −0.31 V (E_4). The preceding shoulder of the main reduction peak at −1.46 V

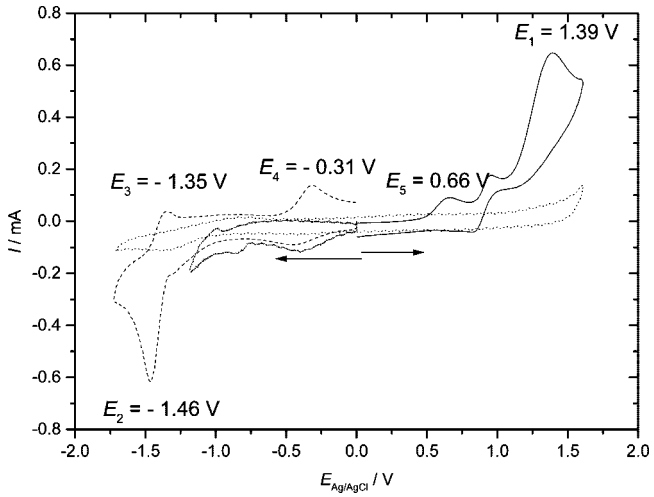

Figure 8. Cyclic voltammograms of **2** at a platinum electrode in a solution of 0.1 M *n*-Bu_4NPF_6 in acetonitrile ($dE/dt = 0.1\ V \cdot s^{-1}$, nitrogen purged; dotted line: supporting electrolyte only; for further assignments of scans see text).

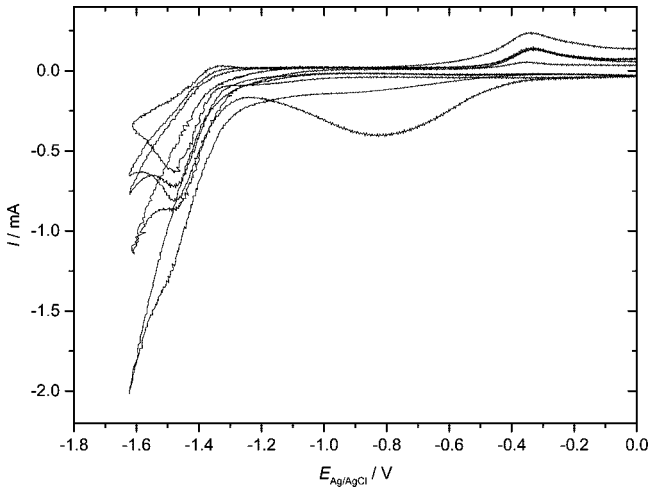

Figure 9. Cyclic voltammograms of **2** at a platinum electrode in a solution of 0.1 M *n*-Bu_4NPF_6 in acetonitrile ($dE/dt = 0.1\ V \cdot s^{-1}$, nitrogen purged, with added pivalic acid). Top trace: no addition. In subsequent traces in total 1, 2, 4, and 10 molar equiv of acid were present after addition.

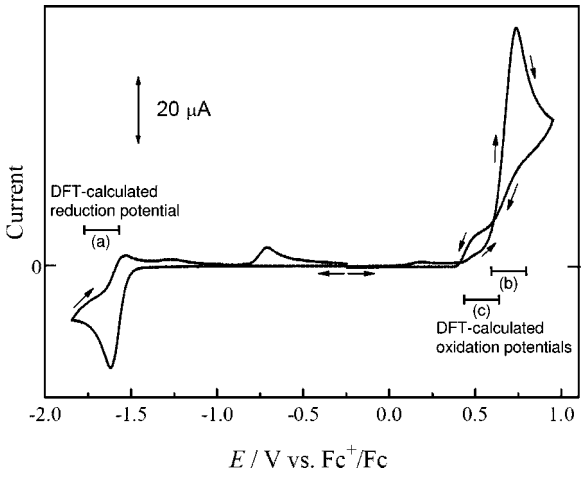

Figure 10. Background-corrected voltammograms of 1.02 mM **3** in acetonitrile with 0.10 M tetrabutylammonium hexafluorophosphate at glassy carbon (0.10 V/s, purged with argon). DFT-calculated potentials (±0.1 V) are indicated by horizontal bars: (a) reduction potential, (b) oxidation potential to cation structure without a bridging carbonyl similar to the neutral molecule, (c) oxidation potential to the cation structure with a bridging carbonyl as in Figure 6.

renders it difficult to evaluate the peak height. For the corresponding sulfur-containing complex (propanedithiolato ligand) and related molecules there is some controversy concerning the overall number of electrons required in the reduction, with some claiming a two-electron process and others only one.[33,55−58] It has recently been shown[58b] that at rapid scan rates the reduction peak splits into two peaks, each of which is interpreted to be a one-electron process. Pivalic acid was chosen as a proton source to test the ability of **2** to catalyze the reduction of protons. Figure 9 includes voltammograms of **2**, obtained under the same conditions as in Figure 8, but with addition of 0, 1, 2, 4, and 10 molar equiv of pivalic acid. The voltammogram with no added acid is identical to the corresponding curve in Figure 8. Addition of 1, 2, and 4 molar equiv causes a small but significant increase in the reduction peak at −1.46 V, which we attribute to the ability of **2** to catalyze the electroreduction of the acid. The other effect of added acid is to suppress the oxidation peak at −0.31 V. (The cause of the large, broad peak near −0.8 V that is seen in one of the voltammograms is unknown.) The voltammogram with addition of 10 molar equiv reveals a sharply increasing cathodic current at −1.5 to −1.6 V.

This current is due to the direct reduction of pivalic acid. It is known[59] that platinum surfaces are good catalysts for reduction of weak acids in acetonitrile, which constitutes a serious interference in the desired study of the catalytic reaction. Consequently, in the remainder of our studies, the glassy carbon working electrode was used. The overpotential for the direct reduction of weak acids is much larger on glassy carbon compared with platinum.[59]

Figure 10 contains voltammograms for **3** obtained in acetonitrile at the glassy carbon electrode. The exploration of positive potentials produces a voltammogram resembling that of **2**. There is a single irreversible oxidation peak with peak potential of +0.76 V vs ferrocene. The height of this peak corresponds to two or more electrons involved in the overall irreversible oxidation process. Only a very small preceding anodic peak is seen in this case. An unusual curve-crossing is observed on the return scan, but it was not further investigated. Also shown in Figure 10 are the DFT-calculated oxidation potentials for **3**. There are two choices for the structure of the cation, one similar to the structure of the neutral molecule and one in which there is a bridging carbonyl, as in the optimized structure of the cation in the gas phase shown in Figure 6, and corresponding to the measured adiabatic ionization energy. The calculated oxidation potentials coincide with the energy region at which oxidation processes are initiated in solution, but do not provide a definitive basis for the mechanism of the electrochemistry or structures of the intermediates.

(55) Apfel, U. P.; Halpin, Y.; Görls, H.; Vos, J. G.; Schweizer, B.; Linti, G.; Weigand, W. *Chem. Biodiversity* **2007**, *4*, 2138.
(56) Darchen, A.; Mousser, H.; Patin, H. *Chem. Commun.* **1988**, 968.
(57) Chong, D.; Georgakaki, I. P.; Meia-Rodriguez, R.; Sanabria-Chinchilla, J.; Soriaga, M. P.; Darensbourg, M. Y. *Dalton Trans.* **2003**, 4158.
(58) (a) Borg, S. J.; Behrsing, T.; Best, S. P.; Razavet, M.; Liu, X.; Pickett, C. J. *J. Am. Chem. Soc.* **2004**, *126*, 16988. (b) Capon, J.-F.; Ezzaher, S.; Gloaguen, F.; Pétillon, F. Y.; Schollhammer, P.; Talarmin, J.; Davin, T. J.; McGrady, J. E.; Muir, K. W. *New J. Chem.* **2007**, *31*, 2052.
(59) Felton, G. A. N.; Glass, R. S.; Lichtenberger, D. L.; Evans, D. H. *Inorg. Chem.* **2006**, *45*, 9181.

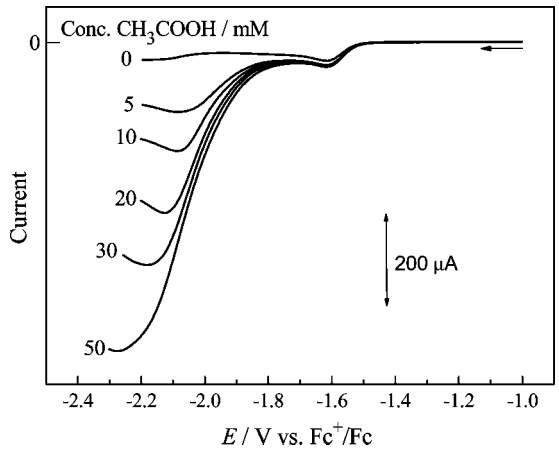

Figure 11. Voltammograms of 1.02 mM **3** in acetonitrile with 0.10 M tetrabutylammonium hexafluorophosphate at glassy carbon. Concentration of added acetic acid is as indicated in the figure (0.10 V/s, purged with argon). Background current has not been subtracted. Return sweeps are deleted for clarity.

The voltammogram in the negative potential range reveals a single reduction peak, at −1.62 V, which is accompanied by a small anodic peak indicating that the product of the reduction persists sufficiently to be detected on the reverse scan. There is also another anodic peak near −1.25 and a more prominent peak at −0.70 V. These are likely due to secondary products formed at the main reduction peak. Importantly, the height of the reduction peak is close to that expected for a one-electron reduction process, as judged by comparison with the known two-electron reduction of [(μ-1,2-benzenedithiolato)][Fe(CO)$_3$]$_2$.[53a] A clue to the chemistry that is occurring is found when the system is saturated with one atmosphere of CO. In this case, the height of the reduction peak at −1.6 V increases and there is a dramatic increase in the height of the corresponding oxidation peak, indicating that the reaction may be moving toward an overall two-electron reversible redox process. This suggests that the irreversibility seen in the absence of CO is associated with loss of CO in the anions. The mechanism for the reduction of **2** and **3** and their catalytic hydrogen production with weak acid has not been investigated in detail. However, such detailed studies of the mechanism for reduction and electrocatalytic hydrogen production with [μ-pdtFe$_2$(CO)$_6$], the sulfur analogue of **2**, have revealed interesting and complex behavior.[58b] Of particular note are the reversible cleavage of an Fe−S bond, dimer formation, CO loss, and CO complexation under a CO atmosphere on reduction. The effect of Se instead of S on these processes is of interest. As already indicated, CO loss on reduction of **3** may be occurring and provides a transition from a one- to two-electron reduction. The complex behavior of such systems will be investigated further in the future.

The potential calculated for the first reduction of **3** by density functional theory is in good agreement with the experimental observation shown in Figure 10. The second reduction is calculated to be almost 0.9 eV higher in potential, consistent with the observation of a one-electron reduction in the region shown in Figure 10. According to the calculations, the primary structural change that occurs with reduction is lengthening the Fe−Fe bond distance by about 0.3 A. This is consistent with the Fe−Fe antibonding nature of the LUMO of the molecule presented earlier.

Catalysis of the reduction of weak acids by **3** was tested with acetic acid in acetonitrile at the glassy carbon electrode. The results are displayed in Figure 11. Similar to the behavior of **2** with pivalic acid, the main reduction peak for **3** at −1.62 V grows slightly upon adding acetic acid but has reached its maximum height after the addition of 5 mM acid. Because of the higher overpotential for reduction of acid at glassy carbon, it is possible to extend the scans to about −2.3 V without significant interference from the direct reduction of acetic acid. What is seen is a new peak that appears near −2.1 to −2.2 V, which we assign to the reduction of acid to dihydrogen catalyzed by **3**, as has been indicated in recent work on dithiolate complexes.[53] This peak grows in height as the concentration of acetic acid is increased. The standard potential for reduction of acetic acid in acetonitrile is −1.46 V vs ferrocene,[59] so catalysis is occurring with about 0.5 V overpotential.

Complex **3** was also investigated in dichloromethane, and the behavior was analogous to that seen in acetonitrile. The anodic peak pattern was more complex than in acetonitrile, but there did appear to be more reductive current on the reverse scan.

Conclusions

Several new diiron selenium complexes have been synthesized and fully characterized including single-crystal X-ray analysis. The electrochemistry of two of these complexes, **2** and **3**, which serve as models for iron hydrogenase with Fe$_2$Se$_2$ substituting for the Fe$_2$S$_2$ core, reveal catalytic production of hydrogen in the presence of weak acid. The observed behavior is analogous to that found for related models with Fe$_2$S$_2$ cores. More insight into the effect of substituting Se for S was obtained from the photoelectron spectrum of **3** and theoretical calculations. This analysis revealed that the reorganization energy of **3** with an Fe$_2$Se$_2$ core is substantially lower than that for analogous complexes with Fe$_2$S$_2$ cores. The consequences of this unanticipated effect, which may lead to faster electron transfer with complexes containing Fe$_2$Se$_2$ rather than Fe$_2$S$_2$ cores, are under further investigation.

Experimental Section

Caution! All operations have to be carried out in a well-ventilated hood. All selenium-containing compounds are potentially highly toxic; aluminum selenide (Al_2Se_3) and hydrogen selenide (H_2Se) are known to be strong poisons.

For the preparation of aluminum selenide we strongly recommend not to use larger amounts of starting materials. Particular care must be taken, as the ceramic pot might break due to the high temperature and as some amount of gaseous selenium evolves. If necessary, Al_2Se_3 should be stored in a desiccator, not in a Schlenk flask; even after careful drying some hydrogen selenide evolved and led to overpressure.

All gases passing through the apparatus during the preparation of **5** should be bubbled through concentrated aqueous NaOH and lead nitrate solutions. All glassware was rinsed thoroughly with aqueous NaOH solution after use. Selenium-contaminated wastes must be collected and disposed of separately.

General Comments. All reactions were performed using standard Schlenk techniques under inert atmosphere. The ^{1}H, ^{13}C{^{1}H}, ^{77}Se{^{1}H}, and 2D NMR (^{1}H,^{1}H COSY, ^{1}H,^{13}C HSQC, ^{1}H,^{77}Se HMBC) spectra were recorded on a Bruker AVANCE 200 or 400 MHz spectrometer using the solvent residual peak or a concentrated solution of SeO_2 in D_2O as reference. The ^{77}Se chemical shifts are reported relative to neat Me_2Se [$\delta(Me_2Se) = \delta(SeO_2) + 1302.6$ ppm].[60] Mass spectra were recorded on a Finnigan MAT SSQ 710

(60) Burns, R. C.; Collins, M. J.; Gillespie, R. J.; Schrobilgen, G. J. *Inorg. Chem.* **1986**, *25*, 4465.

Table 1. Crystallographic Data and Refinement Details for $Fe_2(\mu\text{-}Se_2C_3H_6)(CO)_6$ (2), $Fe_2(\mu\text{-}Se_2C_3H_6)CH_3(CO)_6$ (3), $Fe_2(\mu^2,\kappa\text{-}Se,C\text{-}SeCH_2SeCH_2)(CO)_6$ (6), and $Fe_2[(\mu\text{-}SeCH_2)_2Se](CO)_6$ (7)

	2	3	6	7
empirical formula	$C_9H_6Fe_2O_6Se_2$	$C_{10}H_8Fe2O_6Se_2$	$C_8H_4Fe_2O_6Se_2$	$C_8H_4Fe_2O_6Se_3$
fw	479.76	493.78	465.73	544.69
cryst size (mm)	0.04 × 0.04 × 0.04	0.05 × 0.05 × 0.02	0.04 × 0.04 × 0.04	0.05 × 0.04 × 0.04
cryst syst	monoclinic	triclinic	monoclinic	monoclinic
space group	$P2_1/m$	$P1$	$P2_1/n$	$P2_1/n$
volume (Å^3)	699.78(4)	1525.0(2)	1304.0(4)	1420.46(10)
Z	2	4	4	4
unit cell dimensions				
a (Å)	6.9331(2)	9.3751(8)	8.1933(16)	8.2074(4)
b (Å)	13.3655(5)	11.3861(8)	17.580(4)	20.3782(9)
c (Å)	7.0981(1)	15.6552(12)	9.0947(18)	8.977(3)
α (deg)		78.426(5)		
β (deg)	108.879(2)	74.230(4)	95.49(3)	108.905(3)
γ (deg)		73.066(4)		
index ranges	$-8 \le h \le 8$	$-12 \le h \le 12$	$-9 \le h \le 10$	$-10 \le h \le 9$
	$-17 \le k \le 16$	$-13 \le k \le 14$	$-22 \le k \le 121$	$-25 \le k \le 26$
	$-10 \le l \le 9$	$-20 \le l \le 20$	$-9 \le l \le 11$	$-10 \le l \le 11$
data/params	1471/98	4105/363	2952/163	2508/172
F(000)	456	736	880	1016
D_{calc} (g/cm^3)	2.277	2.151	2.372	2.547
μ (mm^{-1})	7.289	6.692	7.819	9.743
λ (Å)	0.71073	0.71073	0.71073	0.71073
R1[a]	0.0375	0.0582	0.0501	0.0491
wR2[b]	0.0975	0.1234	0.1105	0.1066
GOF[c]	1.051	1.010	1.041	1.023
CCDC #	653752	653753	653754	653755

[a] $R1 = \sum||F_o| - |F_c||/\sum|F_o|$. [b] $wR2 = \{\sum[w(F_o^2 - F_c^2)^2]/\sum[w(F_o^2)^2]\}^{1/2}$. [c] $GOF = \{\sum[w(F_o^2 - F_c^2)^2]/(n - p)\}^{1/2}$, where n is the number of reflections and p is the total number of parameters refined.

instrument. IR spectra were measured on a Perkin-Elmer System 2000 FT-IR spectrometer. Elemental analyses were performed with a LECO CHNS-932 apparatus. Silica gel 60 (0.015−0.040 mm) was used for column chromatography; TLC was done using Merck TLC aluminum sheets (Silica gel 60 F_{254}). THF and hexane were distilled from sodium/benzophenone under Ar; CH_2Cl_2 was dried over calcium hydride and distilled prior to use. 1,3-Diselenocyanatopropane[61,62] and disodium diselenide[63] were prepared according to literature protocols. $Fe_3(CO)_{12}$ was purchased from Aldrich, aluminum, selenium, and potassium selenocyanate from Acros Organics, and sodium borohydride from Fisher Scientific and were used without further purification. Yield calculations were based on substoichiometric utilized chemicals or on $Fe_3(CO)_{12}$ for the diiron complexes.

Preparation of $Fe_2(\mu\text{-}Se_2C_3H_6)(CO)_6$ (2). A green solution of $Fe_3(CO)_{12}$ (0.55 g, 1.10 mmol) in THF (40 mL) was treated with **1** (0.40 g, 1.6 mmol) and heated at reflux for 2 h. The resulting brown-red mixture was evaporated to dryness in vacuo. The obtained solid was suspended in a minimum amount of hexane and column chromatographed (SiO_2/hexane). From the major red fraction, **2** was obtained as a red solid (0.36 g, 68%) and was recrystallized from hexane at 25 °C. Mp: 109−110 °C. Anal. Calcd for $C_9H_6Fe_2O_6Se_2$: C, 22.53; H, 1.26. Found: C, 22.39; H, 1.46. IR (KBr disk): $\nu_{C\equiv O}$ 2064 (s), 2026 (vs), 1988 (vs) cm^{-1}. ^{1}H NMR (200 MHz, $CDCl_3$): δ 1.62 (m, 2H, $SeCH_2CH_2$), 2.19 (t, $^3J_{H,H}$ = 5.8 Hz, 4H, $SeCH_2$) ppm. $^{13}C\{^1H\}$ NMR (50 MHz, $CDCl_3$): δ 14.5 ($SeCH_2CH_2$), 30.1 ($SeCH_2$), 208.7 (CO) ppm. ^{1}H,^{77}Se HMBC (76 MHz, $CDCl_3$): δ 145 (s, Se) ppm. DEI-MS (m/z): 482 (M^+), 454 ($M^+ - CO$), 426 ($M^+ - 2CO$) 398 ($M^+ - 3CO$), 368 ($M^+ - 4CO$), 342 ($M^+ - 5CO$).

Preparation of $Fe_2(\mu\text{-}Se_2C_3H_5CH_3)(CO)_6$ (3). A solution of **4** was prepared according to the procedure above using selenium (0.47 g, 6.00 mmol), sodium borohydride (0.15 g, 4.00 mmol), and 1,3-dibromobutane (0.24 mL, 2.00 mmol). The resulting solution was treated with $Fe_3(CO)_{12}$ (0.95 g, 1.89 mmol) in THF (40 mL) at reflux for 2 h. The resulting brown-red mixture was evaporated to dryness in vacuo. The obtained solid was suspended in a minimum amount of hexane and column chromatographed (SiO_2/hexane). The red fraction (0.90 g, 73%) was collected, dried, and recrystallized from pentane at 25 °C. Mp: 69−70 °C. Anal. Calcd for $C_{10}H_8Fe_2O_6Se_2$: C, 24.32; H, 1.63. Found: C, 24.35; H, 1.79. IR (KBr disk): $\nu_{C\equiv O}$ 2065 (s), 2026 (vs), 1988 (vs) cm^{-1}. ^{1}H NMR (200 MHz, $CDCl_3$): δ 1.13 (d, $^2J_{H,H}$ = 12.0 Hz, 1H, $SeCH_2CH_AH_B$), 1.34 (d, $^3J_{H,H}$ = 6.0 Hz, 3H, CH_3), 1.77 (d, $^2J_{H,H}$ = 12.0 Hz, 1H, $SeCH_2CH_AH_B$), 1.93 (m, 1H, $SeCH_CH_D$), 2.24 (m, 1H, SeCH), 2.62 (m, 1H, $SeCH_CH_D$) ppm. $^{13}C\{^1H\}$ NMR (50 MHz, $CDCl_3$): δ 16.5 ($SeCH_2$), 25.3 (CH_3), 26.9 (SeCH), 38.8 ($SeCH_2CH_2$), 208.6 (CO), 209.0 (CO) ppm. $^{77}Se\{^1H\}$ NMR (76 MHz, $CDCl_3$): δ 156, 249 ppm. DEI-MS (m/z): 494 (M^+), 468 ($M^+ - CO$), 440 ($M^+ - 2CO$) 410 ($M^+ - 3CO$), 384 ($M^+ - 4CO$), 354 ($M^+ - 5CO$), 326 ($M^+ - 6CO$).

Preparation of 3-Methyl-1,2-diselenolane (4). A solution of disodium diselenide, Na_2Se_2, was prepared in situ following a literature procedure.[63] Therefore selenium (2.37 g, 30 mmol) and sodium borohydride (0.81 g, 21 mmol) were reacted in ethanol (40 mL). After the mixture was heated to reflux for 1.5 h it was cooled to 0 °C, and 1,3-dibromobutane (2.16 g, 10 mmol) dissolved in ethanol (5 mL) was added within 15 min. The deep red reaction mixture was allowed to warm to room temperature and was stirred overnight before it was added to 100 mL of water. After stirring for 2 h the precipitated selenium was removed by filtration, and the filtrate was extracted with dichloromethane (3 × 30 mL), washed with water (2 × 30 mL), and dried with sodium sulfate. The solvent was removed in vacuo, and the residue was chromatographed (SiO_2/CH_2Cl_2), giving **4** as a deep red, viscous oil (1.47 g, 69%) that polymerized rapidly when neat. However, a solution might be stored in a refrigerator unpolymerized for several weeks. No reproducible boiling point could be determined due to the polymerization, while elemental analysis could not be performed because of the high volatility of the compound. ^{1}H NMR (400 MHz, $CDCl_3$): δ 1.51 (d with ^{77}Se satellites, $^3J_{H,H}$ = 6.8 Hz, $^3J_{H,Se}$ =

(61) Morgan, G. T.; Burstall, F. T. *J. Chem. Soc.* **1930**, *40*, 1497.
(62) Clarembeau, M.; Cravador, A.; Dumont, W.; Hevesi, L.; Krief, A.; Lucchetti, J.; Ende, D. V. *Tetrahedron* **1985**, *41*, 4793.
(63) Block, E.; Dikarev, E. V.; Glass, R. S.; Jin, J.; Li, B.; Li, X.; Zhang, S. Z. *J. Am. Chem. Soc.* **2006**, *128*, 14949.

20.0 Hz, 3H, CH_3), 2.51 (m, 1H, $SeCH_2CH_AHB$), 2.92 (m, 1H, $SeCH_2CH_AH_B$), 3.31 (t with ^{77}Se satellites, $^3J_{H,H} = 6.2$ Hz, ^2J(H,Se) = 14.8 Hz, 2H, $SeCH_2$), 4.05 (m, 1H, CH) ppm. $^{13}C\{^1H\}$ NMR (100 MHz, $CDCl_3$): δ 21.1 (s, CH3), 29.2 (s with ^{77}Se satellites, $^1J_{C,Se} = 61.9$ Hz, $SeCH_2$), 45.7 (s with ^{77}Se satellites, $^1J_{C,Se} = 62.3$ Hz, CH), 47.7 (s, $SeCH_2CH_2$) ppm. ^{77}Se NMR (76 MHz, $CDCl_3$): δ 310 (s with ^{77}Se satellites, $^1J_{Se,Se} = 373$ Hz, $CH_2SeSeCH$, 403 (s with ^{77}Se satellites, $^1J_{Se,Se} = 373$ Hz, $CH_2SeSeCH$) ppm. DEI-MS (*m*/*z*): 216 (M^+).

Preparation of 1,3,5-Triselenacyclohexane (5). The preparation of aluminum selenide and **5** is analogous to literature procedures.[64,65] As we modified the preparation of the latter considerably, a detailed synthesis is given. Aluminum selenide, Al_2Se_3, was prepared from the elements. Aluminum powder (4.05 g, 150 mmol) and finely ground selenium (8.29 g, 105 mmol) were mixed and placed in a ceramic pot, which was placed on a heat-resistant plate. The reaction was started by the addition of an ignited peace of magnesium, and the pot was immediately covered with a ceramic plate. After the mixture was cooled to room temperature (30 min), the brown mass was placed in a crucible and pulverized. Some pieces of elemental aluminum were separated, and the foul smelling brown powder was dried carefully in vacuo. For the preparation of **5** the following apparatus was used. A three-necked flask was equipped with a good working stirring bar, a dropping funnel, gas inlet, and outlet. The outlet, bearing a three-way stopcock, was connected with a safety bottle followed by a second three-necked flask, which was equipped with an inlet with a wide opening (to prevent the clogging from separated product), a stirring bar, and outlet. The third neck was closed with a stopper, which proved to be very useful for introducing the reagents. Following the reaction flask three washing bottles were arranged, with the first being empty, the second charged with concentrated sodium hydroxide solution, and the last being filled with concentrated lead nitrate solution. A tube was connected conducting all gases directly in the hood. The second channel of the three-way stopcock following the first flask was additionally connected with the sodium hydroxide washing bottle, thus bypassing the reaction flask. This proved useful for any manipulations or incidents. The crude Al_2Se_3 (34.90 g, 120 mmol) was placed in the first flask, and the whole apparatus was evacuated carefully (excluding the washing bottles) and purged with a stream of argon for 30 min. The reaction flask was charged with 10 M hydrochloric acid (150 mL, 1.5 mol) and formaldehyde solution (23 mL, 36%, 300 mmol) and was protected from light with aluminum foil. The argon stream was stopped, and 2 M hydrochloric acid was added dropwise (caution!) to the Al_2Se_3 with stirring. Because the evolution of hydrogen selenide was slow under these conditions, most of the gas was absorbed in the reaction flask. After 15 min the reaction mixture warmed to 35 °C and showed some white precipitate. From time to time it was necessary to apply a slight stream of argon due to some underpressure and to prevent the inlet from clogging. The passing-in of hydrogen selenide was continued until no more H_2Se evolved from the aluminum selenide, which took 12 to 16 h. The reaction mixture was stirred for another 24 h before the last traces of hydrogen selenide were removed with a stream of argon. The solution was filtered through a frit, and the remaining white solid was washed carefully with 200 mL of water, ethanol, and diethyl ether. The white powder was dried in vacuo and showed to be analytically pure (19.36 g, 69%). No decomposition was observed when stored under exclusion of light and air during several months. Mp: 220−222 °C (lit. 215 °C).[54] Anal. Calcd for $C_3H_6Se_3$: C, 12.92; H, 2.17. Found: C, 13.06; H, 2.21. ^{1}H NMR (200 MHz, DMSO-d_6): δ 4.26 (t with ^{77}Se satellites, $^2J_{H,Se} = 14.2$ Hz, 6H, CH_2) ppm. $^{13}C\{^1H\}$ NMR (50 MHz, DMSO-d_6): δ 14.2 (s, CH_2) ppm. ^{77}Se NMR (76 MHz, DMSO-d_6): δ 273 (t, $^2J_{Se,H} = 14.2$ Hz, Se) ppm. DEI-MS (*m*/*z*): 280 (M^+), 94 (CH_2Se^+).

Preparation of $Fe_2(\mu^2,\kappa$-Se,C-$SeCH_2SeCH_2)(CO)_6$ (6), $Fe_2[(\mu$-$SeCH_2)_2Se](CO)_6$ (7), and $Fe_2(\mu$-$Se_2CH_2)(CO)_6$ (8). $Fe_3(CO)_{12}$ (0.49 g, 0.97 mmol) and **5** (0.27 g, 0.97 mmol) were refluxed in THF (20 mL) for 1 h under argon. The color of the green solution changed to red-brown. The reaction mixture was cooled to room temperature, and the solvent was removed under reduced pressure. The crude brown product was purified by column chromatography (SiO_2/hexane). A dark orange fraction of complex **8** (0.11 g, 25%, mp 80−81 °C (79−81° [42d])), the orange main fraction containing complex **6** (0.077 g, 17%), and the third red fraction containing **7** (0.048 g, 9%) were isolated. Crystals of **6** and **7** suitable for X-ray diffraction analysis were obtained by slow evaporation of concentrated pentane solutions at 25 °C.

$Fe_2(\mu^2,\kappa$-Se,C-$SeCH_2SeCH_2)(CO)_6$ (6): mp 108−109 °C. Anal. Calcd for $C_8H_4Fe_2O_6Se_2$: C, 20.63; H, 0.87. Found: C, 21.12; H, 0.81. IR (KBr disk): $\nu_{C\equiv O}$ 2037 (vs), 1975 (vs, sh), 1918 (m) cm^{-1}. ^{1}H NMR (400 MHz, $CDCl_3$): δ 1.91 (d, $^2J_{H,H} = 9.6$ Hz, 1H, $SeCH_AH_BFe$), 3.09 (m, 2H, $SeCH_AH_BFe$ and $SeCH_CH_DSe$), 5.68 (d, $^2J_{H,H} = 8.8$ Hz, 1H, $SeCH_CH_DSe$) ppm. $^{13}C\{^1H\}$ NMR (100 MHz, $CDCl_3$): δ 18.8 ($SeCH_2Fe$), 31.3 ($SeCH_2Se$), 208.0 (CO), 210.5 (CO), 215.0 (CO) ppm. ^{1}H ^{77}Se HMBC (76 MHz, $CDCl_3$): δ 220 ($SeCH_2Se$), 315 ($SeCH_2Fe$) ppm. DEI-MS (*m*/*z*): 468 (M^+). 438 ($M^+ - CO$), 412 ($M^+ - 2CO$) 384 ($M^+ - 3CO$), 298 ($M^+ - 6CO$).

$Fe_2[(\mu$-$SeCH_2)_2Se](CO)_6$ (7). Mp: 150−151 °C. Anal. Calcd for $C_8H_4Fe_2O_6Se_2 \cdot 0.25$pentane: C, 19.76; H, 1.17. Found: C, 19.55; H, 1.04. IR (KBr disk): $\nu_{C\equiv O}$ 2069 (s), 2030 (vs), 1992 (vs) cm^{-1}. ^{1}H NMR (200 MHz, $CDCl_3$): δ 3.30 (s, 4H, CH_2). $^{13}C\{^1H\}$ NMR (100 MHz, $CDCl_3$): δ 30.2 (CH_2), 209.4 (CO) ppm. ^{1}H,^{77}Se HMBC NMR (76 MHz, $CDCl_3$): δ 124, 209 ppm. DEI-MS (*m*/*z*): 546 (M^+), 518 ($M^+ - CO$), 490 ($M^+ - 2CO$), 462 ($M^+ - 3CO$), 434 ($M^+ - 4CO$), 406 ($M^+ - 5CO$), 378 ($M^+ - 6CO$).

Crystal Structure Determination. The intensity data for the compounds were collected on a Nonius KappaCCD diffractometer, using graphite-monochromated Mo Kα radiation. Data were corrected for Lorentz and polarization effects, but not for absorption effects.[66,67]

The structures were solved by direct methods (SHELXS)[68] and refined by full-matrix least-squares techniques against F_o^2 (SHELXL-97).[69] All hydrogen atoms were included at calculated positions with fixed thermal parameters. All non-hydrogen atoms were refined anisotropically.[69] XP (SIEMENS Analytical X-ray Instruments, Inc.) was used for structure representations.

Electrochemical Measurements. In Chemnitz, cyclic voltammetry was performed in a small volume three-compartment cell with porous glass frits separating the counter and the reference electrode equipped with a Luggin capillary from the main cell volume. A nonaqueous silver chloride reference electrode was used in all experiments. Its potential versus the ferrocene/ferrocenium reference electrode was found to be $E_{Ag/AgCl} = -0.43$ V vs ferrocene; that is, for conversion into the ferrocene scale this value must be subtracted from all potential values reported here. A platinum sheet (apparent surface area 1.12 cm^2) and glassy carbon disk (apparent surface area 0.28 cm^2, HTW, Thierhaupten, embedded into a PTFE2 cylinder) working electrodes and a platinum sheet counter electrode were used. Electrolyte solutions were prepared from dried tetrabutylammonium hexafluorophosphate, n-Bu_4NPF_6 (Fluka, purissimum) 0.1 M in dried acetonitrile (Merck LiChroSolv). A custom-built potentiostat interfaced to a personal computer

(64) Waitkins, G. R.; Shutt, R. *Inorg. Synth.* **1946**, *2*, 183.
(65) Vanino, L.; Schinner, A. *J. Prakt. Chem.* **1915**, *91* (1−3), 116.
(66) *COLLECT, Data Collection Software*; Nonius, B. V.: The Netherlands, 1998.
(67) Otwinowski, Z.; Minor, W. Processing of X-Ray Diffraction Data Collected in Oscillation Mode. In *Methods in Enzymology. 276, Macromolecular Crystallography, Part A*; Carter, C. W.; Sweet, R. M., Eds.; pp 307−326.
(68) Sheldrick, G. M. *Acta Crystallogr., Sect. A* **1990**, *46*, 467.
(69) Sheldrick, G. M. *SHELXL-97 (Release 97-2)*; University of Göttingen: Germany, 1997.

running with custom-designed software for cyclic voltammetry was employed. All experiments were run with solutions purged with nitrogen saturated with acetonitrile at room temperature at a scan rate of $dE/dt = 0.1\ V \cdot s^{-1}$ if not stated otherwise. In Tucson, the electrochemical procedures and apparatus were almost identical to those employed in Chemnitz. These have been reported elsewhere.[70] Differences were that in Tucson solutions were purged with argon, the glassy carbon disk working electrode (0.0707 cm^2) was from Bioanalytical Systems, the instrument was a Princeton Applied Research model 2273 Parstat, and the experiments were conducted at room temperature. The laboratory reference electrode was a silver wire in contact with 0.010 M $AgNO_3$ in acetonitrile with 0.10 M tetrabutylammonium hexafluorophosphate. The potential of the ferrocenium ion/ferrocene couple was frequently measured with respect to this reference, and all potentials have been reported vs ferrocene.

Photoelectron Spectra. Photoelectron spectra were recorded using an instrument that features a 36 cm hemispherical analyzer (McPherson),[71] with custom-designed photon source, sample cells, detection and control electronics, calibration, and data analysis as described previously.[72,73] The sample sublimed cleanly, with no visible changes in the spectra during data collection. The sublimation temperature for photoelectron data collection of compound **3** was 62−123 C at $\sim 10^{-4}$ Torr pressure in the instrument sample cell. Instrument resolution ranged from 22 to 29 meV, as measured by the argon $^2P_{3/2}$ ionization peak.

In the figure of the He I and He II photoelectron spectra, the He I data points are represented by vertical dashes with the length of each dash representing the variance of the electron counts measured at that ionization energy. The solid line is the best fit of the He I data with a minimum number of Gaussian peaks to represent the contour of the ionization intensity. In many regions of the spectrum the signal-to-noise is so high that the width of the solid line is comparable to the variance of the data and overlays the vertical dashes. The dashed line is a similar representation of the contour of ionization intensity obtained with the He II photon source, scaled to match the low ionization energy intensity in the He I spectrum for visual comparison of the change in relative intensity at higher ionization energies.

Density Functional Theory Computations. All computations were performed using ADF2006.01d.[74−76] Computational details were as previously described[50] and are provided in the Supporting Information. For comparison of the calculated gas-phase CO stretching frequencies to the experimental solution phase IR spectra, the calculated frequencies were scaled by a factor of 1.002, which shifts the frequencies by approximately 4 cm^{-1} in the carbonyl stretching region.

Acknowledgment. Financial support for this work was provided by the Freistaat Thüringen (Landesgraduiertenstipendium to J.W.), the DAAD (Ph.D. grant to M.H.), and the U.S. National Science Foundation through its Collaborative Research in Chemistry program, Grant No. CHE 0527003.

Supporting Information Available: CIF files giving crystallographic data for $Fe_2(\mu\text{-}Se_2C_3H_6)(CO)_6$ (**2**), $Fe_2(\mu\text{-}Se_2C_3H_5\text{-}CH_3)(CO)_6$ (**3**), $Fe_2(\mu^2,\kappa\text{-}Se,C\text{-}SeCH_2SeCH_2)(CO)_6$ (**6**), and $Fe_2(\mu\text{-}Se_2CH_2)(CO)_6$ (**7**). Details of computational methodology, comparison of selected geometry features of **3** and $\mathbf{3}^+$, optimized atom coordinates of **3** and $\mathbf{3}^+$, orbital surface plots of the HOMO to HOMO−9 with calculated energies for molecule **3**. This material is available free of charge via the Internet at http://pubs.acs.org.

OM800748P

(70) Macías-Ruvalcaba, N. A.; Evans, D. H. *J. Phys. Chem. B* **2005**, *109*, 14642.

(71) Siegbahn, K.; Nordling, C.; Fahlman, A.; Nordberg, R.; Hamrin, K.; Hedman, J.; Johansson, G.; Bergmark, T.; Karlsson, S. E.; Lindgren, I.; Lindberg, B. *Nova Acta Regiae Soc. Sci. Upsaliensis* **1967**, *20*, 282.

(72) Lichtenberger, D. L.; Kellogg, G. E.; Kristofzski, J. G.; Page, D.; Turner, S.; Klinger, G.; Lorenzen, J. *Rev. Sci. Instrum.* **1986**, *57*, 2366.

(73) Cranswick, M. A.; Dawson, A.; Cooney, J. J. A.; Gruhn, N. E.; Lichtenberger, D. L.; Enemark, J. H. *Inorg. Chem.* **2007**, *46*, 10639–10646.

(74) *ADF2006.01d, SCM*; Theoretical Chemistry, Vrije Universiteit: Amsterdam, The Netherlands, 2006, http://www.scm.com.

(75) Guerra, C. F.; Handgraaf, J. -.; Baerends, E. J.; Bickelhaupt, F. M. *J. Comput. Chem.* **2004**, *25*, 189–210.

(76) Te Velde, G.; Bickelhaupt, F. M.; Baerends, E. J.; Fonseca Guerra, C.; Van Gisbergen, S. J. A.; Snijders, J. G.; Ziegler, T. *J. Comput. Chem.* **2001**, *22*, 931–967.

2.2 [MK2] Phosphane- and Phosphite-Substituted Diiron Diselenolato Complexes as Models for [FeFe]-Hydrogenases.

M. K. Harb, J. Windhager, A. Daraosheh, H. Görls, L. T. Lockett, N. Okumura, D. H. Evans, R. S. Glass, D. L. Lichtenberger, M. El-khateeb, W. Weigand.

Eur. J. Inorg. Chem. **2009, 3414-3420.**

DOI: 10.1002/ejic.200900252

Phosphane- and Phosphite-Substituted Diiron Diselenolato Complexes as Models for [FeFe]-Hydrogenases

Mohammad K. Harb,[a] Jochen Windhager,[a] Ahmad Daraosheh,[a] Helmar Görls,[a] L. Tori Lockett,[b] Noriko Okumura,[b] Dennis H. Evans,*[b] Richard S. Glass,*[b] Dennis L. Lichtenberger,*[b] Mohammad El-khateeb,[c] and Wolfgang Weigand*[a]

Dedicated to Professor Ingo-Peter Lorenz on the occasion of his 65th birthday

Keywords: Iron / Hydrogenases / Substitution / Electrocatalysis / Ligand effects / Enzyme catalysis / Selenium

The displacement of terminal CO ligands in $Fe_2(\mu\text{-}Se_2C_3H_5CH_3)(CO)_6$ (**1**) by triphenylphosphane, trimethyl phosphite, and bis(diphenylphosphanyl)ethane (dppe) ligands is investigated. Treatment of **1** with 1 equiv. of triphenylphosphane afforded $Fe_2(\mu\text{-}Se_2C_3H_5CH_3)(CO)_5(PPh_3)$ (**2**). The mono- and disubstituted phosphite complexes $Fe_2(\mu\text{-}Se_2C_3H_5CH_3)(CO)_5P(OMe)_3$(**3**)and$Fe_2(\mu\text{-}Se_2C_3H_5CH_3)(CO)_4[P(OMe)_3]_2$ (**4**) were obtained from the reaction of **1** with excess $P(OMe)_3$ at reflux in toluene. In contrast, the reaction of **1** with 1 equiv. of dppe in the presence of $Me_3NO{\cdot}2H_2O$ gave a mixture of $Fe_2(\mu\text{-}Se_2C_3H_5CH_3)(CO)_4(\kappa^2\text{-dppe})$ (**5**) and $[Fe_2(\mu\text{-}Se_2C_3H_5CH_3)(CO)_5]_2(\mu\text{-dppe})$ (**6**). The newly synthesized complexes **2**–**6** were fully characterized by IR, ^1H NMR, ^{13}C NMR, $^{77}Se\{^1H\}$ NMR, and $^{31}P\{^1H\}$ NMR spectroscopy, mass spectrometry, elemental analysis, and X-ray diffraction analysis. Complex **2** has proved to be a catalyst for the electrochemical reduction of the weak acid, acetic acid, to give molecular hydrogen.
(© Wiley-VCH Verlag GmbH & Co. KGaA, 69451 Weinheim, Germany, 2009)

Introduction

The search for alternative energy sources is a challenge for mankind. Hydrogen is one of these energy sources.[1–4] Hydrogenases are enzymes that produce dihydrogen from water. An important representative example of these enzymes was isolated from *Desulfovibrio desulfuricans*.[5,6] This enzyme can produce 9000 molecules of hydrogen per second at 30 °C (hypothetically 1 mol of this enzyme could fill an airship of 13000 m^3 in about 10 min).[6] Therefore several diiron dithiolato model compounds as biomimics for the active site of this enzyme have been described (Scheme 1a).[7–24] The catalytic properties for hydrogen generation by models of [FeFe]-hydrogenases can be modified by substitution of the CO ligands. The replacement of one or two carbonyl ligands from [FeFe]-hydrogenase model complexes by CN^-, phosphanes, phosphite, carbene, and isocyanide ligands have been reported in the literature.[9–11,23–30] These complexes also serve as models of the active site of [FeFe]-hydrogenases. The substitution reactions of [FeFe]-hydrogenases with bidentate ligands such as bis(phosphanes) $[Ph_2P(CH_2)_nPPh_2]$ and diamines were also investigated.[31–36] Recently, the preparation and characterization of diiron models containing diselenolato ligands have been reported (Scheme 1b).[37–40] The ability of these complexes to act as models for the [FeFe]-hydrogenases has also been investigated. In this paper, the substitution reactions of one or two carbonyl groups of $Fe_2(\mu\text{-}Se_2C_3H_5CH_3)(CO)_6$ (**1**) by PPh_3 or $P(OMe)_3$ are studied in order to increase the electron density at the iron atoms and to enhance its basicity. The replacement of carbonyl ligands of **1** by bis(diphenylphosphanyl)ethane (dppe) in order to obtain dissymmetrically disubstituted diiron systems is also described. In addition, the electrochemistry of the monophosphane complex **2** was investigated by cyclic voltammetry, in order to compare its electrochemistry with **1** as well as with its sulfur analogues.

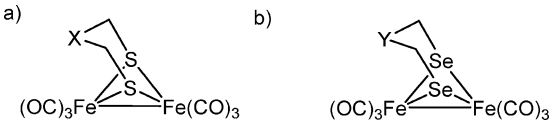

Scheme 1. (a) Models of [FeFe]-hydrogenases containing dithiolato ligands (X = CH_2, NH, O, S). (b) Models of [FeFe]-hydrogenases containing diselenolato ligands (Y = CH_2, Se, NPh).

[a] Institut für Anorganische und Analytische Chemie, Friedrich-Schiller-Universität Jena,
August-Bebel-Straße 2, 07743 Jena, Germany
[b] Department of Chemistry, The University of Arizona,
Tucson, AZ 85721, USA
[c] Chemistry Department, Jordan University of Science and Technology,
22110 Irbid, Jordan

© 2009 Wiley-VCH Verlag GmbH & Co. KGaA, Weinheim

Results and Discussion

Stirring of $Fe_2(\mu\text{-}Se_2C_3H_5CH_3)(CO)_6$ (**1**) at room temperature with 1 equiv. of triphenylphosphane in the presence of trimethylamine *N*-oxide dihydrate ($Me_3NO{\cdot}2H_2O$) gives the complex $Fe_2(\mu\text{-}Se_2C_3H_5CH_3)(CO)_5(PPh_3)$ (**2**) (Scheme 2). The $CH_2CH_2CH(CH_3)$ moiety bridging the selenium atoms desymmetrizes the iron atoms,[41] and the PPh_3 ligand may be *cis* or *trans* to the CH_3 group in the bridge. However, only one diastereomer has been found. In contrast, heating of **1** at reflux with an excess amount of $P(OMe)_3$ in toluene for 3 h gives two complexes, namely $Fe_2(\mu\text{-}Se_2C_3H_5CH_3)(CO)_5P(OMe)_3$ (**3**) and $Fe_2(\mu\text{-}Se_2C_3H_5CH_3)(CO)_4[P(OMe)_3]_2$ (**4**) (Scheme 2), in which one (**3**) or two (**4**) carbonyl ligands are substituted by $P(OMe)_3$.

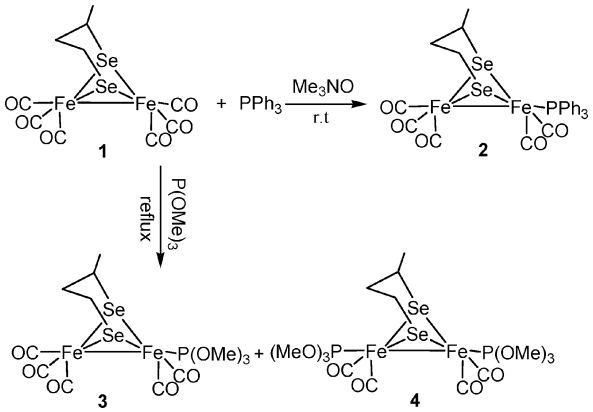

Scheme 2. Models of substituted [FeFe]-hydrogenase complexes $Fe_2(\mu\text{-}Se_2C_3H_5CH_3)(CO)_5(PPh_3)$ (**2**), $Fe_2(\mu\text{-}Se_2C_3H_5CH_3)(CO)_5P(OMe)_3$ (**3**), and $Fe_2(\mu\text{-}Se_2C_3H_5CH_3)(CO)_4[P(OMe)_3]_2$ (**4**) prepared in our laboratory.

The reaction of compound **1** with 1 equiv. of dppe in the presence of $Me_3NO{\cdot}2H_2O$ gives a mixture of the chelated diiron complex $Fe_2(\mu\text{-}Se_2C_3H_5CH_3)(CO)_4(\kappa^2\text{-dppe})$ (**5**) and the bridged tetrairon complex $[Fe_2(\mu\text{-}Se_2C_3H_5CH_3)(CO)_5]_2(\mu\text{-dppe})$ (**6**), which can be separated by column chromatography (Scheme 3). Compounds **2**–**6** have been characterized by IR and multinuclear NMR spectroscopy, mass spectrometry, elemental analysis, as well as by X-ray crystallography. These complexes are air-stable in the solid state and are stable for several hours in solution. The ^1H NMR spectra for **2**–**6** exhibit a doublet at δ = 1.09, 1.28, 1.24, 1.52, and 1.03 ppm, respectively, for the methyl group of the diselenolato ligand. $^1H,^1H$ COSY, $^1H,^{13}C$ HSQC, and $^1H,^{13}C$ HMBC NMR spectroscopic experiments allowed the assignment of the other five chemically nonequivalent protons of the diselenolato ligand. These resonances are comparable to those of the unsubstituted complex **1**.[38] The $^{13}C\{^1H\}$ NMR spectra for **2**–**6** exhibit four resonances for the bridging unit. These resonances are in the same range as those observed for **1**.[38] In addition, the expected resonance for the carbonyl groups and the phosphane ligands were observed. Two signals are obtained in the $^{77}Se\{^1H\}$ NMR spectra for complexes **2**–**6** because of the presence of two different Se atoms. The ^1H-^{77}Se HMBC spectrum allows the assignment of the two different Se atoms. The $^{31}P\{^1H\}$ NMR spectra of **2** and **3** show one signal at δ = 72.1 and 193.1 ppm, respectively, whereas for **4** two resonances are observed at δ = 186.5 and 189.2 ppm from the nonequivalent iron atoms.

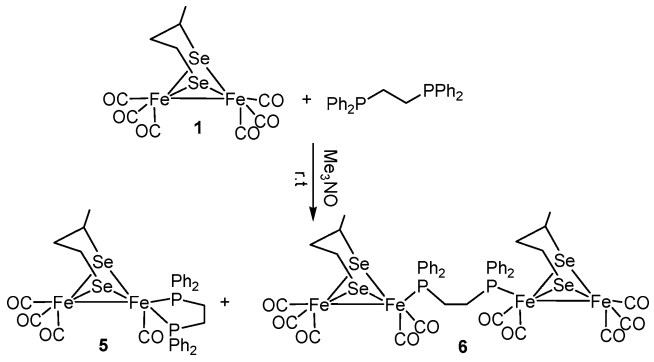

Scheme 3. Models of [FeFe]-hydrogenases containing a chelated dppe ligand (**5**) and bridged dppe ligand (**6**) prepared in our laboratory.

The $^{31}P\{^1H\}$ NMR spectrum of **5** displays signals at δ = 98.7 and 96.3 ppm ($^2J_{PP}$ = 20.3 Hz) representing an AB spin system, which indicates the presence of two nonequivalent phosphorus atoms. These resonances can be assigned to the basal-apical isomer of a diiron complex with a chelating dppe ligand.[32–34] Only one diastereoisomer has been observed. The mass spectra of **2**–**5** show the molecular ion peaks followed by the fragmentation of five CO groups in **2** and **3**, and four in **4** and **5**. Compound **6** exhibits two singlets in the $^{31}P\{^1H\}$ NMR spectrum at δ = 66.1 and 66.2 ppm. These resonances are shifted to higher fields compared to those reported for sulfur analogues.[31–34] The two signals (ratio 1:1) in the $^{31}P\{^1H\}$ NMR spectrum of **6** could be explained by the presence of two diastereoisomers in solution resulting from the flap pointing toward or away from the phosphane ligand. A temperature-dependent $^{31}P\{^1H\}$ NMR study (T = 273–333 K) shows that these two species are not in equilibrium. MS analysis shows the fragmentation of 10 CO groups and the molecular peak at m/z = 1330, which suggests the presence of a tetranuclear complex in which two diiron moieties are linked by a dppe ligand.

The IR spectra of **2**–**6** show three absorption bands in the regions of 1916–1955, 1972–1996, and 2033–2040 cm^{-1}. These data are within the same ranges observed for the unsubstituted[38] complex and for the sulfur analogues.[26,31–33]

The molecular structures of **2**–**6** were determined and are shown in Figures 1, 2, 3, 4, and 5, respectively. The coordination geometry around the iron cores in all complexes are similar to those in its sulfur analogues.[26,31–34] The central 2Fe2Se structures of all of the complexes are in the butterfly conformation, as was observed for the sulfur ana-

 © 2009 Wiley-VCH Verlag GmbH & Co. KGaA, Weinheim

logues.[26,31–34] The displacement of one or two carbonyl groups by phosphanes or phosphite has only a small effect on the Fe–Fe distances as compared to that of **1** [2.5471(15) Å].[38] The Fe–Fe bonds in **2**–**6** are longer than those in the sulfur derivatives {**2**: 2.5573(16) Å [sulfur derivative: 2.5247(6) Å[26]], **3**: 2.5881(12) Å [sulfur derivative: 2.5142(9) Å[26]], **4**: 2.5506(6) Å, **5**: 2.6180(7) Å [sulfur derivative: 2.547(7) Å[32]], **6**: 2.5506(13) Å [sulfur derivative: 2.5108(14) Å[31]]} because of the larger size of the selenium atoms.[26,31–34] The Fe–Se bonds in **2**–**6** are slightly longer (ca. 0.017 Å) than that in the unsubstituted compound **1** due to the stronger σ-donor properties of phosphanes or phosphite ligands compared to carbonyl groups.[38] The Fe–P bond lengths [**2**: 2.246(2) Å, **3**: 2.1596(17) Å, **4**: 2.1651(8) Å and 2.1601(9) Å, **5**: 2.2323(11) Å and 2.1913(9) Å, **6**: 2.2236(18) Å] are comparable to those observed for sulfur and selenium analogues.[26,31–34,40] In compounds **2**–**4** and **6** the P atoms are coordinated to Fe in an apical position, which has been proved by $^{31}P\{^{1}H\}$ NMR spectroscopy and X-ray crystallography (Figures 1, 2, 3, and 5), whereas the apical-basal isomer is observed in **5** (Figure 4). In principle, for the monosubstituted complexes **2** and **3** the phosphane ligand may occupy an apical or basal position. The X-ray crystal structure of **2** shows that the phosphane ligand occupies an apical position. In addition, the stereochemistry of **2** is complicated by the possibility of forming diastereomers. That is, one with the CH_3 group of the bridge and P moiety on the same side (*cis*) or the other with the CH_3 group of the bridge and P moiety on opposite sides (*trans*). Furthermore, each diastereomer may adopt either of two conformations obtained by inverting the flap of the $CH_2CH_2CH(CH_3)$ moiety resulting in an equatorial or axial CH_3 group and the flap pointing toward or away from the phosphane ligand. It can be seen from the X-ray structure of **2** that the CH_3 group is equatorial and *trans* to the phosphane ligand and the flap points away from the phosphane ligand. As pointed out above, the ^{31}P NMR spectrum of **2** shows only one resonance signal suggesting that only one diastereomer is present. In **3** the P ligand is basal. There are two different basal positions owing to the dissymmetry induced by the $CH_2CH_2CH(CH_3)$ bridge. In **3** the phosphite ligand occupies the basal position *syn* to the equatorial CH_3 group, and the flap points toward the phosphane ligand. In **4** the phosphane ligands are on different Fe atoms, and both occupy apical positions with the equatorial CH_3 group. Owing to the dissymmetry of the $CH_2CH_2CH(CH_3)$ moiety the two phosphane ligands are nonequivalent as already noted above in the ^{31}P NMR spectroscopic analysis. For **5**, both P atoms of the dppe are on one Fe atom with one P atom apical and the other basal. Surprisingly, the CH_3 group is *cis* and the flap points toward the apical P atom, and the CH_3 group is *syn* to the basal P atom of the dppe ligand. In **6** both P atoms of the bridging dppe ligand occupy apical positions. The CH_3 group occupies an equatorial position and is *cis* to the phosphane ligand, and the flap points toward the phosphane ligand. The stereochemistry for the two 2Fe2Se centers is the same.

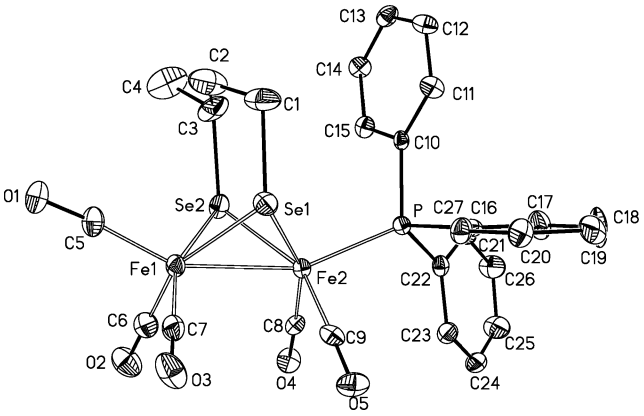

Figure 1. ORTEP drawing of $Fe_2(\mu\text{-}Se_2C_3H_5CH_3)(CO)_5(PPh_3)$ (**2**). Selected distances [Å] and angles [°]: Fe1–Fe2 2.5573(16), Fe1–Se1 2.3868(16), Fe1–Se2 2.3792(15), Fe2–Se1 2.3791(15), Fe2–Se2 2.3940(14); Fe1–Se1–Fe2 64.90(5), Fe1–Se2–Fe2 64.79(5).

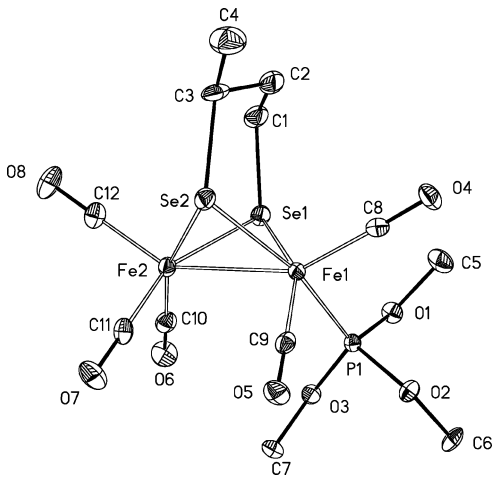

Figure 2. ORTEP drawing of $Fe_2(\mu\text{-}Se_2C_3H_5CH_3)(CO)_5P(OMe)_3$ (**3**). Selected distances [Å] and angles [°]: Fe1–Fe2 2.5881(12), Fe1–Se1 2.3723(10), Fe1–Se2 2.3723(10), Fe2–Se1 2.3792(11), Fe2–Se2 2.3814(11); Fe1–Se1–Fe2 66.01(3), Fe1–Se2–Fe2 65.97(3).

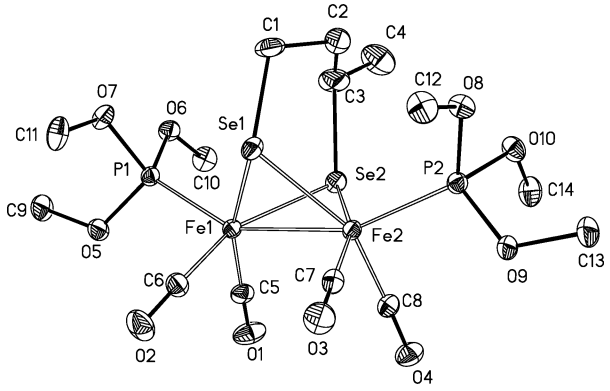

Figure 3. ORTEP drawing of $Fe_2(\mu\text{-}Se_2C_3H_5CH_3)(CO)_4[P(OMe)_3]_2$ (**4**). Selected distances [Å] and angles [°]: Fe1–Fe2 2.5506(6), Fe1–Se1 2.3787(5), Fe1–Se2 2.3828(5), Fe2–Se1 2.3818(5), Fe2–Se2 2.3817(5); Fe1–Se1–Fe2 64.794(16), Fe1–Se2–Fe2 64.733(16).

 © 2009 Wiley-VCH Verlag GmbH & Co. KGaA, Weinheim

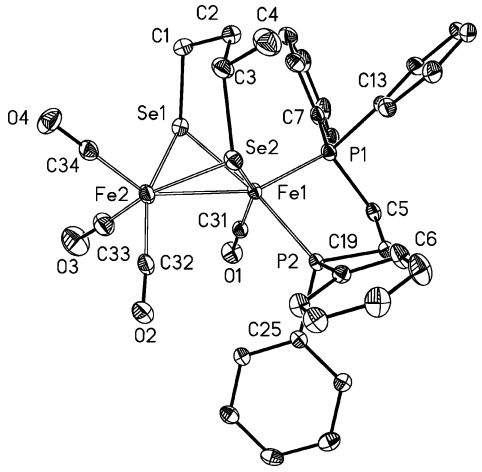

Figure 4. ORTEP drawing of $Fe_2(\mu\text{-}Se_2C_3H_5CH_3)(CO)_4(\kappa^2\text{-dppe})$ (**5**). Selected distances [Å] and angles [°]: Fe1–Fe2 2.6180(7), Fe1–Se1 2.3685(6), Fe1–Se2 2.3738(6), Fe2–Se1 2.3839(6), Fe2–Se2 2.3924(6); Fe1–Se1–Fe2 66.853(19), Fe1–Se2–Fe2 66.636(19).

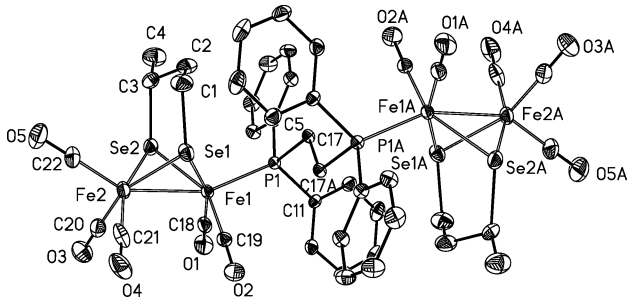

Figure 5. ORTEP drawing of $[Fe_2(\mu\text{-}Se_2C_3H_5CH_3)(CO)_5]_2(\mu\text{-dppe})$ (**6**). Selected distances [Å] and angles [°]: Fe1–Fe2 2.5506(13), Fe1–Se1 2.3871(12), Fe1–Se2 2.3743(12), Fe2–Se1 2.3904(13), Fe2–Se2 2.3774(13); Fe1–Se1–Fe2 64.54(4), Fe1–Se2–Fe2 64.93(4).

Electrochemical Investigations

Cyclic voltammograms of **2** were recorded in order to identify the electrochemical oxidation and reduction processes and to test the ability of these complexes to catalyze the reduction of weak acids to form dihydrogen. Complex **2** was studied in dichloromethane. As expected for the replacement of CO by a phosphane ligand, the phosphane complex **2** is more easily oxidized than the unsubstituted complex **1** with an anodic peak potential of +0.35 V vs. ferrocene compared to +0.76 V for **1**.[38] There is a reasonable degree of reversibility to the oxidation process. The reduction peak for **2**, whose height is also close to that expected for a one-electron process, appears at –2.00 V and is irreversible (Figure 6). As expected, the potential is more negative than that observed for **1** (–1.83 V).[38] As noted elsewhere,[42] replacement of CO by a phosphane ligand causes a shift of both the anodic and cathodic peaks in the negative direction. The shifts seen for **2**, 0.41 and 0.17 V, respectively, may be compared with shifts of 0.62 and 0.18 V seen upon replacing CO by PPh_3 in a sulfur analogue similar to **2**, $Fe_2[\mu\text{-}S(CH_2)_3S](CO)_6$.[26]

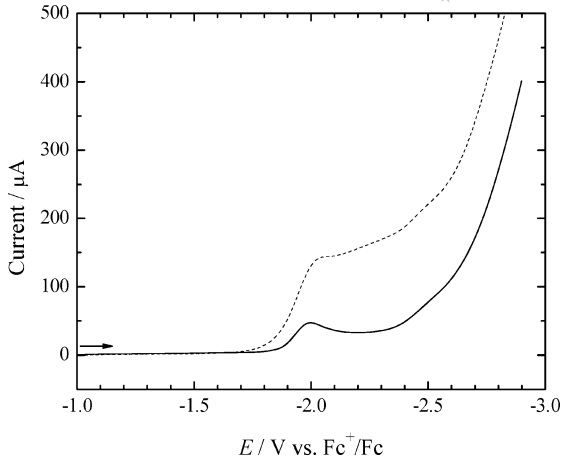

Figure 6. Cyclic voltammograms of 1.0 mM **2** in CH_2Cl_2 with 0.10 M Bu_4NPF_6 and a scan rate of 0.10 V s^{-1}. Solid: **2** alone. Dashed: **2** + 10.5 mM CH_3COOH. Return sweeps omitted for clarity.

Addition of acetic acid results in catalytic reduction at the main peak rather than a separate, more negative peak as seen with **1**[38] (dashed curve, Figure 6). Thus, **2** is capable of catalyzing the production of dihydrogen by the reduction of weak acids.

Conclusions

The present study showed that the desymmetrized $Fe_2(\mu\text{-}Se_2C_3H_5CH_3)(CO)_6$ (**1**) reacts with PPh_3 and $P(OMe)_3$ producing the mono- and disubstituted complexes **2**–**4**; only one diastereoisomer has been observed in complexes **2**–**4**. By using the bidentate ligand dppe, a mixture of the chelated diiron (**5**) and the bridged tetrairon (**6**) complexes were obtained as observed for the sulfur-PDT derivatives. For $Fe_2(\mu\text{-}Se_2C_3H_5CH_3)(CO)_4(\kappa^2\text{-dppe})$ (**5**) we have also obtained only one diastereoisomer with an apical-basal position of the dppe ligand, whereas two diastereoisomers have been detected for $[Fe_2(\mu\text{-}Se_2C_3H_5CH_3)(CO)_5]_2(\mu\text{-dppe})$ (**6**) as indicated by the ^{31}P NMR spectra. The results of the X-ray diffraction analysis show that the Fe–Fe distances in **2**–**6** are significantly longer than those in their sulfur analogues due to the larger size of the selenium atom. The stereochemistry is complicated by the fact that the phosphane ligand may occupy an apical or basal position (and there are two basal P diastereomers: one with the P and CH_3 group *syn* and the other *anti*), and for each of these (apical and two basal) there are two diastereomers (*cis* and *trans*), each of which can exist as two conformers with an axial or equatorial CH_3 group owing to the "flap" of the bridge, which can point toward or away from the P ligand. The electrochemical investigations of **2** showed oxidation and reduction behavior that is consistent with substitution of a CO group, as in **1** with a phosphane ligand. Catalytic reduction of acetic acid was seen at the first reduction peak of **2**.

 © 2009 Wiley-VCH Verlag GmbH & Co. KGaA, Weinheim

Experimental Section

General Comments: All reactions were performed by using standard Schlenk and vacuum-line techniques under an inert gas. The ^1H, $^{13}C\{^1H\}$, $^{77}Se\{^1H\}$ $^{31}P\{^1H\}$, and 2D NMR (^1H,^1H COSY, ^1H,^{13}C HSQC, ^1H,^{13}C HMBC, ^1H,^{77}Se HMBC) spectra were recorded with either a Bruker Avance 200 or 400 MHz spectrometer by using the solvent residual peak or a concentrated solution of SeO_2 in D_2O as the reference. The ^{77}Se chemical shifts are reported relative to neat Me_2Se [$\delta(Me_2Se) = \delta(SeO_2) + 1302.6$ ppm].[43] External standard 85% H_3PO_4 was used as a reference for $^{31}P\{^1H\}$ spectral measurements. The mass spectra were recorded with a Finnigan MAT SSQ 710 instrument. The IR spectra were measured with a Perkin–Elmer System 2000 FT-IR spectrometer. Elemental analyses were performed with a Leco CHNS-932 apparatus. Silica gel 60 (0.015–0.040 mm) was used for column chromatography, and TLC was performed by using Merck TLC aluminum sheets (Silica gel 60 F_{254}). $Fe_3(CO)_{12}$ was purchased from Aldrich, solvents from Fisher Scientific, and other chemicals from Acros, and were used without further purification. All of the solvents used were dried and distilled prior to use according to standard methods. $Fe_2(\mu\text{-}Se_2C_3H_5CH_3)(CO)_6$ (**1**) was prepared according to a literature procedure.[38]

Preparation of $Fe_2(\mu\text{-}Se_2C_3H_5CH_3)(CO)_5PPh_3$ (2): A solution of **1** (60 mg, 0.12 mmol) and $Me_3NO{\cdot}2H_2O$ (24 mg, 0.22 mmol) in MeCN was stirred at room temperature for 10 min. Then, triphenylphosphane (32 mg, 0.12 mmol) was added and the mixture stirred for 2 h. The resulting dark red mixture was concentrated to dryness under vacuum. The obtained solid was redissolved in a minimum amount of CH_2Cl_2 and the solution column-chromatographed (SiO_2/hexane). From the major red fraction, which was eluted with hexane/diethyl ether (2:1), **2** was obtained as a red solid, and was recrystallized from pentane at –25 °C. Yield 67 mg (77%). M.p. 193–194 °C. $C_{27}H_{23}Fe_2O_5PSe_2$ (728.05): calcd. C 44.54, H 3.18; found C 44.49, H 3.35. ^1H NMR (400 MHz, $CDCl_3$, 25 °C): δ = 0.58 (m, 1 H, $SeCH_2CH_AH_B$), 1.09 (d, ^3J = 6.8 Hz, 3 H, CH_3), 1.27 (m, 1 H, $SeCH_2CH_AH_B$), 1.71 (m, 1 H, $SeCH_CH_D$), 2.00 (m, 1 H, SeCH), 2.03 (m, 1 H, $SeCH_CH_D$), 7.24–7.67 (m, 15 H, PPh_3) ppm. $^{13}C\{^1H\}$ NMR (50 MHz, $CDCl_3$): δ = 17.4 ($SeCH_2$), 25.7 (CH_3), 27.9 (SeCH), 38.5 ($SeCH_2CH_2$), 128.3, 130.1, 133.6, 136.0, 136.8 (PPh_3), 206.9, 210.3, 214.1, 214.3 (CO) ppm. $^{77}Se\{^1H\}$ NMR (76 MHz, $CDCl_3$): δ = 135 ($SeCH_2$), 467 (SeCH) ppm. $^{31}P\{^1H\}$ NMR (200 MHz, $CDCl_3$): δ = 72.1 (PPh_3) ppm. FTIR (KBr): $\tilde{\nu}$ = 2037 (vs), 1978 (vs), 1926 (w) cm^{-1}. MS (DEI = 70 eV): *m*/*z* (%) = 728 (1) [M^+], 672 (3) [M^+ – 56; 2 CO], 644 (3) [M^+ – 84; 3 CO], 588 (10) [M^+ – 140; 5 CO].

Preparation of $Fe_2(\mu\text{-}Se_2C_3H_5CH_3)(CO)_5P(OMe)_3$ (3) and $Fe_2(\mu\text{-}Se_2C_3H_5CH_3)(CO)_4[P(OMe)_3]_2$ (4): A solution of trimethyl phosphite [$P(OMe)_3$; 67 mg, 0.54 mmol] and **1** (90 mg, 0.18 mmol) in toluene (25 mL) was heated under reflux for 3 h. The resulting dark red mixture was concentrated to dryness under vacuum. The obtained solid was redissolved in a minimum amount of CH_2Cl_2 and the solution column-chromatographed (SiO_2/hexane). Products **3** and **4** were obtained from the first and the second fraction, respectively, by using hexane/CH_2Cl_2 (2:1) and then pure CH_2Cl_2 as eluents. Complex **3** was recrystallized from hexane at –25 °C and **4** from ethyl ether at 0 °C.

$Fe_2(\mu\text{-}Se_2C_3H_5CH_3)(CO)_5P(OMe)_3$ (3): Yield 38 mg (36%). M.p. 74–75 °C. $C_{12}H_{17}Fe_2O_8PSe_2$ (589.84): calcd. for $6C_{12}H_{17}Fe_2O_8PSe_2{\cdot}1$hexane C 25.84, H 3.24; found C 25.67, H 3.14. ^1H NMR (400 MHz, $CDCl_3$, 25 °C): δ = 1.06 (m, 1 H, $SeCH_2CH_AH_B$), 1.28 (d, ^3J = 8.4 Hz, 3 H, CH_3), 1.68 (m, 1 H, $SeCH_2CH_AH_B$), 2.06 (m, 1 H, $SeCH_CH_D$), 2.47 (m, 1 H, SeCH), 2.57 (m, 1 H, $SeCH_CH_D$), 3.72 [s, 9 H, $P(OMe)_3$] ppm. $^{13}C\{^1H\}$ NMR (50 MHz, $CDCl_3$): δ = 29.4 ($SeCH_2$), 32.8 (CH_3), 37.1 (SeCH), 38.6 ($SeCH_2CH_2$), 52.0, 52.4 $P(OMe)_3$, 210.4, 210.9 (CO) ppm. $^{77}Se\{^1H\}$ (76 MHz, $CDCl_3$): δ = 396 ($SeCH_2$), 403 (SeCH) ppm. $^{31}P\{^1H\}$ NMR (200 MHz, $CDCl_3$): δ = 193.9 $P(OMe)_3$ ppm. FTIR (KBr): $\tilde{\nu}$ = 2040 (s), 1985 (vs, sh), 1931 (w) cm^{-1}. MS (DEI = 70 eV): *m*/*z* (%) = 590 (60) [M^+], 562 (9) [M^+ – 28; CO], 534 (12) [M^+ – 56; 2 CO], 506 (7) [M^+ – 84; 3 CO], 450 (23) [M^+ – 140; 5 CO].

$Fe_2(\mu\text{-}Se_2C_3H_5CH_3)(CO)_4[P(OMe)_3]_2$ (4): Yield 57 mg (46%). M.p. 155–156 °C. $C_{14}H_{26}Fe_2O_{10}P_2Se_2$ (685.91): calcd. C 24.51, H 3.82; found C 24.69, H 3.86. ^1H NMR (400 MHz, $CDCl_3$, 25 °C): δ = 1.11 (m, 1 H, $SeCH_2CH_AH_B$), 1.24 (d, ^3J = 6.6 Hz, 3 H, CH_3), 1.53 (m, 1 H, $SeCH_2CH_AH_B$), 1.74 (m, 1 H, $SeCH_CH_D$), 1.89 (m, 1 H, SeCH), 2.39 (m, 1 H, $SeCH_CH_D$), 3.71, 3.77 [s, 18 H, 2 $P(OMe)_3$] ppm. $^{13}C\{^1H\}$ NMR (50 MHz, $CDCl_3$): δ = 16.1 ($SeCH_2$), 25.2 (CH_3), 26.1 (SeCH), 38.6 ($SeCH_2CH_2$), 51.4, 51.5, 51.8, 51.9 $P(OMe)_3$, 213.1, 213.4, 214.4, 214.7 (CO) ppm. $^{77}Se\{^1H\}$ NMR (76 MHz, $CDCl_3$): δ = 252 ($SeCH_2$), 402 (SeCH) ppm. $^{31}P\{^1H\}$ NMR (200 MHz, $CDCl_3$): δ = 186.5, 189.2 [$P(OMe)_3$] ppm. FTIR (KBr): $\tilde{\nu}$ = 2040 (m), 1996 (vs), 1955 (vs, sh) cm^{-1}. MS (DEI = 70 eV): *m*/*z* (%) = 686 (12) [M^+], 630 (9) [M^+ – 56; 2 CO], 602 (2) [M^+ – 84; 3 CO], 574 (16) [M^+ – 112; 4 CO].

Synthesis of $Fe_2(\mu\text{-}Se_2C_3H_5CH_3)(CO)_4(\kappa^2\text{-dppe})$ (5) and $[Fe_2(\mu\text{-}Se_2C_3H_5CH_3)(CO)_5]_2(\mu\text{-dppe})$ (6): A solution of **1** (98 mg, 0.20 mmol) and $Me_3NO{\cdot}2H_2O$ (45 mg, 0.40 mmol) dissolved in MeCN was stirred at room temperature for 10 min. A solution of dppe (80 mg, 0.20 mmol) dissolved in CH_2Cl_2 (2 mL) was added and the combined solutions were stirred for 1 h. Then the solvent was evaporated under reduced pressure. The crude product was purified by chromatography on silica gel using hexane/CH_2Cl_2 (1:2) as the eluent. Complex **5** was obtained from the first red fraction and recrystallized from hexane/CH_2Cl_2 at –25 °C. A second red brownish band provided complex **6**, which was also recrystallized from hexane/CH_2Cl_2 at –25 °C.

$Fe_2(\mu\text{-}Se_2C_3H_5CH_3)(CO)_4(\kappa^2\text{-dppe})$ (5): Yield 33 mg (20%). M.p. 208–209 °C. $C_{34}H_{32}Fe_2O_4P_2Se_2$ (836.17): calcd. C 48.84, H 3.86; found C 48.45, H 3.88. ^1H NMR: δ = 0.91 (m, 1 H, SeCH), 1.24 (m, 1 H, $SeCH_2CH_AH_B$), 1.52 (d, ^3J = 6.2 Hz, 3 H, CH_3), 1.69 (m, 1 H, $SeCH_CH_D$), 1.90 (m, 1 H, $SeCH_2CH_AH_B$), 2.15 (m, 1 H, $SeCH_CH_D$), 2.52, 2.93 (m, 4 H, PCH_2CH_2P), 7.24–7.46 (m, 20 H, 2 PPh_2) ppm. $^{13}C\{^1H\}$ NMR (50 MHz, $CDCl_3$): δ = 21.2 (SeCH), 27.5 ($SeCH_2$), 29.2 (CH_3), 29.7 ($SeCH_2CH_2$), 45.8, 47.8 (PCH_2CH_2P) 128.6, 130.3, 132.4 (2 PPh_2), 210.2 (CO) ppm. $^{77}Se\{^1H\}$NMR (76 MHz, $CDCl_3$): δ = 234 ($SeCH_2$), 402 (SeCH) ppm. $^{31}P\{^1H\}$ NMR (200 MHz, $CDCl_3$, 25 °C): δ = 96.3 (d, $^2J_{PP}$ = 20.3 Hz), 98.7 (d, $^2J_{PP}$ = 20.3 Hz) ppm. FTIR (KBr): $\tilde{\nu}$ = 2037 (s), 1975 (vs), 1919 (w) cm^{-1}. MS (DEI = 70 eV): *m*/*z* (%) = 836 (8) [M^+], 808 (2) [M^+ – 28; CO], 752 (9) [M^+ – 84; 3 CO], 724 (38) [M^+ – 112; 4 CO].

$[Fe_2(\mu\text{-}Se_2C_3H_5CH_3)(CO)_5]_2(\mu\text{-dppe})$ (6): Yield 101 mg (76%). M.p. 193–194 °C. $C_{44}H_{40}Fe_4O_{10}P_2Se_4$ (1329.95): calcd. for $3C_{44}H_{40}Fe_4O_{10}P_2Se_4{\cdot}2$hexane C 41.22, H 3.58; found C 41.61, H 3.58. ^1H NMR (400 MHz, $CDCl_3$, 25 °C): δ = 0.69 (m, 2 H, 2 SeCH), 0.85 (m, 2 H, 2 $SeCH_2CH_AH_B$), 1.03 (d, ^3J = 6.4 Hz, 6 H, 2 CH_3), 1.35 (m, 2 H, 2 $SeCH_CH_D$), 1.56 (m, 2 H, 2 $SeCH_2CH_AH_B$), 1.87 (m, 2 H, 2 $SeCH_CH_D$), 2.65, 2.81 (m, 4 H, PCH_2CH_2P), 7.03–7.51 (m, 20 H, 2 PPh_2) ppm. $^{13}C\{^1H\}$ NMR (50 MHz, $CDCl_3$): δ = 17.9 ($SeCH_2$), 25.5 (SeCH), 27.7 ($SeCH_2CH_2$), 30.3, 32.4 (PCH_2CH_2P), 39.1 (CH_3), 125.1, 127.9, 128.8, 137.4 (2 PPh_2), 210.8 (CO) ppm. $^{77}Se\{^1H\}$ NMR (76 MHz, $CDCl_3$): δ = 313 ($SeCH_2$), 409 (SeCH) ppm. $^{31}P\{^1H\}$ NMR

 © 2009 Wiley-VCH Verlag GmbH & Co. KGaA, Weinheim

Table 1. Crystal data and refinement details for the X-ray structure determinations.

	2	**3**	**4**	**5**	**6**
Empirical formula	$C_{27}H_{23}Fe_2O_5PSe_2$	$C_{12}H_{17}Fe_2O_8PSe_2$	$C_{14}H_{26}Fe_2O_{10}P_2Se_2$	$C_{34}H_{32}Fe_2O_4P_2Se_2$	$C_{44}H_{40}Fe_4O_{10}P_2Se_4{\cdot}2CH_2Cl_2$
M_r [g mol^{-1}]	728.04	589.85	685.91	836.16	1499.79
T [°C]	–90(2)	–90(2)	–90(2)	–90(2)	–90(2)
Crystal system	monoclinic	monoclinic	orthorhombic	monoclinic	monoclinic
Space group	$P2_1/n$	$P2_1/n$	$Pbca$	$P2_1/n$	$P2_1/n$
a [Å]	11.5652(5)	8.4457(2)	16.3859(5)	19.2256(5)	12.5031(7)
b [Å]	15.2712(8)	23.3951(9)	16.6265(4)	9.6723(3)	16.3825(9)
c [Å]	16.5167(8)	10.0243(4)	17.8597(4)	19.5069(6)	13.5152(6)
α [°]	90	90	90	90	90
β [°]	108.486(3)	103.832(2)	90	115.157(2)	98.663(3)
γ [°]	90	90	90	90	90
V [Å^3]	2766.6(2)	1923.24(12)	4865.7(2)	3283.35(17)	2736.8(2)
Z	4	4	8	4	2
ρ [g cm^{-3}]	1.748	2.037	1.873	1.692	1.820
μ [cm^{-1}]	37.73	54.11	43.61	32.36	40.06
Measured data	18398	12801	32744	22695	18250
Data with $I>2\sigma(I)$	3882	3307	4571	5446	3907
Unique data/R_{int}	6277/0.0819	4351/0.0701	5567/0.0585	7499/0.0638	6250/0.0755
wR_2 (all data, on F^2)[a]	0.1856	0.1259	0.0776	0.0889	0.1638
R_1 [$I>2\sigma(I)$][a]	0.0762	0.0544	0.0335	0.0422	0.0674
s[b]	1.094	1.092	1.023	1.026	1.019
Residual density [e Å^{-3}]	2.300/–1.889	2.370/–1.633	0.684/–0.786	0.911/–0.467	2.259/–1.956
Absorption method	none	none	none	none	none
CCDC no.	705054	705055	705056	705057	705058

[a] Definition of the R indices: $R_1 = (\Sigma||F_o| - |F_c||)/\Sigma|F_o|$; $wR_2 = \{\Sigma[w(F_o^2 - F_c^2)^2]/\Sigma[w(F_o^2)^2]\}^{1/2}$ with $w^{-1} = \sigma^2(F_o^2) + (aP)^2$. [b] $s = \{\Sigma[w(F_o^2 - F_c^2)^2]/(N_o - N_p)\}^{1/2}$.

(200 MHz, $CDCl_3$): δ = 66.1, 66.2 (2 PPh_2) ppm. FTIR (KBr): $\tilde{\nu}$ = 2033 (vs), 1972 (vs), 1916 (w) cm^{-1}. MS (DEI = 70 eV): m/z (%) = 1330 (2) [M$^+$], 1176 (7) [M$^+$ – 154; 2 Ph], 1120 (5) [M$^+$ – 210; 2 Ph + 2 CO], 1064 (10) [M$^+$ – 266; 2 Ph + 4 CO], 1036 (16) [M$^+$ – 294; 2 Ph + 5 CO], 931 (88) [M$^+$ – 399; 3 Ph + 6 CO], 903 (45) [M$^+$ – 427; 3 Ph + 7 CO].

Crystal Structure Determination: The intensity data for the compounds were collected with a Nonius KappaCCD diffractometer by using graphite-monochromated Mo-K_α radiation. Data were corrected for Lorentz and polarization effects, but not for absorption effects.[44,45] The structures were solved by direct methods (SHELXS)[46] and refined by full-matrix least-squares techniques against F_o^2 (SHELXL-97).[47] All hydrogen atoms were included at calculated positions with fixed thermal parameters. All non-hydrogen atoms were refined anisotropically. All non-disordered non-hydrogen atoms were refined anisotropically.[47] XP (SIEMENS Analytical X-ray Instruments, Inc.) was used for structure representations (Table 1). CCDC-705054 (for **2**), -705055 (for **3**), -705056 (for **4**), -705057 (for **5**), and -705058 (for **6**) contain the supplementary crystallographic data for this paper. These data can be obtained free of charge from The Cambridge Crystallographic Data Centre via www.ccdc.cam.ac.uk/data_request/cif.

Electrochemical Measurements: The electrochemical procedures, apparatus, and sources and treatment of solvent and electrolyte have been described.[38,48] Solutions were purged with argon, the glassy carbon disk working electrode (0.0707 cm^2) was from Bioanalytical Systems, the instrument was a Princeton Applied Research Model 2273 Parstat, and the experiments were conducted at room temperature. The laboratory reference electrode was a silver wire in contact with 0.010 M $AgNO_3$ in acetonitrile with 0.10 M tetrabutylammonium hexafluorophosphate. The potential of the ferrocenium ion/ferrocene couple was frequently measured with respect to this reference, and all potentials have been reported vs. ferrocene.

Acknowledgments

Financial support for this work was provided for M. H. by the Deutscher Akademischer Austausch Dienst (DAAD). D. H. E., R. S. G., and D. L. L. gratefully acknowledge support from the National Science Foundation through the Collaborative Research in Chemistry Program, Grant No. 0527003.

[1] S. Shima, O. Pilak, S. Vogt, M. Schick, M. S. Stagni, W. M. Klaucke, E. Warkentin, R. K. Thauer, U. Ermler, *Science* **2008**, *321*, 572–575.
[2] R. Cammack, M. Frey, R. Robson, *Hydrogen as a Fuel: Learning from Nature*, Taylor & Francis, London, **2001**.
[3] R. H. B. Coontz, *Science* **2004**, *305*, 957–975.
[4] A. Melis, L. Zhang, M. Forestier, M. L. Ghirardi, M. Seibert, *Plant Physiol.* **2000**, *122*, 127–136.
[5] B. R. Glick, W. G. Martin, S. M. Martin, *Can. J. Microbiol.* **1980**, *26*, 1214–1223.
[6] E. C. Hatchikian, N. Forget, V. M. Fernandez, R. Williams, R. Cammack, *Eur. J. Biochem.* **1992**, *209*, 357–365.
[7] X. Zhao, I. P. Georgakaki, M. L. Miller, J. C. Yarbrough, M. Y. Darensbourg, *J. Am. Chem. Soc.* **2001**, *123*, 9710–9711.
[8] X. Zhao, C. Y. Chiang, M. L. Miller, M. V. Rampersad, M. Y. Darensbourg, *J. Am. Chem. Soc.* **2003**, *125*, 518–524.
[9] F. Gloaguen, J. D. Lawrence, M. Schmidt, S. R. Wilson, T. B. Rauchfuss, *J. Am. Chem. Soc.* **2001**, *123*, 12518–12527.
[10] E. J. Lyon, I. P. Georgakaki, J. H. Reibenspies, M. Y. Darensbourg, *J. Am. Chem. Soc.* **2001**, *123*, 3268–3278.
[11] J. D. Lawrence, H. Li, T. B. Rauchfuss, M. Benard, M. M. Rohmer, *Angew. Chem. Int. Ed.* **2001**, *40*, 1768–1771.
[12] M. Razavet, S. C. Davies, D. L. Hughes, J. E. Barclay, D. J. Evans, S. A. Fairhurst, X. Liu, C. J. Pickett, *Dalton Trans.* **2003**, 586–595.
[13] R. C. Linck, T. B. Rauchfuss, *Bioorganometallics* **2006**, 403–435.
[14] H. Li, T. B. Rauchfuss, *J. Am. Chem. Soc.* **2002**, *124*, 726–727.

 © 2009 Wiley-VCH Verlag GmbH & Co. KGaA, Weinheim

[15] S. Ott, M. Kritikos, B. Åkermark, L. Sun, *Angew. Chem. Int. Ed.* **2003**, *42*, 3285–3288.
[16] C. Tard, X. Liu, S. K. Ibrahim, M. Bruschi, L. De Gioia, S. C. Davies, X. Yang, L.-S. Wang, G. Sawers, C. J. Pickett, *Nature* **2005**, *433*, 610–613.
[17] L.-C. Song, Z.-Y. Yang, H.-Z. Bian, Q.-M. Hu, *Organometallics* **2004**, *23*, 3082–3084.
[18] D. Seyferth, R. S. Henderson, L.-C. Song, *Organometallics* **1982**, *1*, 125–133.
[19] D. Seyferth, R. S. Henderson, L.-C. Song, *J. Organomet. Chem.* **1980**, *192*, C1.
[20] U. P. Apfel, Y. Halpin, H. Görls, J. G. Vos, B. Schweizer, G. Linti, W. Weigand, *Chem. Biodivers.* **2007**, *4*, 2138–2148.
[21] J. Windhager, R. A. Seidel, U. P. Apfel, H. Görls, G. Linti, W. Weigand, *Eur. J. Inorg. Chem.* **2008**, *10*, 2023–2041.
[22] J. Windhager, M. Rudolph, S. Bräutigam, H. Görls, W. Weigand, *Eur. J. Inorg. Chem.* **2007**, *18*, 2748–2760.
[23] J. Windhager, H. Görls, H. Petzold, G. Mloston, G. Linti, W. Weigand, *Eur. J. Inorg. Chem.* **2007**, *28*, 4462–4471.
[24] L.-C. Song, Z. Y. Yang, H. Z. Bian, Y. Liu, H. T. Wang, X. F. Liu, Q. M. Hu, *Organometallics* **2005**, *24*, 6126–6135.
[25] L.-C. Song, Z. Y. Yang, Y. J. Hua, H. T. Wang, Y. Liu, Q. M. Hu, *Organometallics* **2007**, *26*, 2106–2110.
[26] P. Li, M. Wang, C. He, G. Li, X. Liu, C. Chen, B. Akermark, L. Sun, *Eur. J. Inorg. Chem.* **2005**, 2506–2513.
[27] E. J. Lyon, I. P. Georgakaki, J. H. Reibenspies, M. Y. J. Darensbourg, *J. Am. Chem. Soc.* **2001**, *123*, 3268–3278.
[28] J. F. Capon, S. E. Hassnaoui, P. Schollhammer, J. Talarmin, *Organometallics* **2005**, *24*, 2020–2022.
[29] J. W. Tye, J. Lee, H. Wang, R. Mejia-Rodriguez, J. H. Reibenspies, M. B. Hall, M. Y. J. Darensbourg, *Inorg. Chem.* **2005**, *44*, 5550–5552.
[30] L. Duan, M. Wang, P. Li, Y. Na, N. Wang, L. Sun, *Dalton Trans.* **2007**, 1277–1283.
[31] W. Gao, J. Ekström, J. Liu, C. Chen, L. Eriksson, L. Weng, B. Akermark, L. Sun, *Inorg. Chem.* **2007**, *46*, 1981–1991.
[32] S. Ezzaher, J. F. Capon, F. Gloaguen, F. Y. Pétillon, P. Schollhammer, J. Talarmin, *Inorg. Chem.* **2007**, *46*, 3426–3428.
[33] S. Ezzaher, J. F. Capon, F. Gloaguen, F. Y. Pétillon, P. Schollhammer, J. Talarmin, *Inorg. Chem.* **2007**, *46*, 9863–9872.
[34] A. K. Justice, G. Zampella, L. D. Gioia, T. B. Rauchfuss, J. I. V. D. Vlugt, S. R. Wilson, *Inorg. Chem.* **2007**, *46*, 1655–1664.
[35] S. Ezzaher, J. F. Capon, F. Gloaguen, F. Y. Petillon, P. Schollhammer, J. Talarmin, *Inorg. Chem.* **2009**, *48*, 2–4.
[36] P. Y. Orain, J. F. Capon, N. Kervarec, F. Gloaguen, F. Y. Petillon, R. Pichon, P. Schollhammer, J. Talarmin, *Dalton Trans.* **2007**, 3745–3756; J.-F. Capon, F. Gloaguen, F. Y. Pétillon, P. Schollhammer, J. Talarmin, *Eur. J. Inorg. Chem.* **2008**, 4671–4681; S. Ezzaher, J.-F. Capon, N. Dumontet, F. Gloaguen, F. Y. Pétillon, P. Schollhammer, J. Talarmin, *J. Electroanal. Chem.* **2009**, *626*, 161–170.
[37] S. Gao, J. Fan, S. Sun, X. Peng, X. Zhao, J. Hou, *Dalton Trans.* **2008**, 2128–2135.
[38] M. K. Harb, T. Niksch, J. Windhager, H. Görls, R. Holze, L. T. Lockett, N. Okumura, D. H. Evans, R. S. Glass, D. L. Lichtenberger, M. El-khateeb, W. Weigand, *Organometallics* **2009**, *28*, 1039–1048.
[39] U. P. Apfel, Y. Halpin, M. Gottschaldt, H. Görls, J. G. Vos, W. Weigand, *Eur. J. Inorg. Chem.* **2008**, 5112–5118.
[40] L.-C. Song, B. Gai, H. T. Wang, Q. M. Hu, *J. Inorg. Biochem.*, accepted; DOI: 10.1016/j.jinorgbio.2009.02.002.
[41] J. L. Stanley, Z. M. Heiden, T. B. Rauchfuss, S. R. Wilson, *Organometallics* **2008**, *27*, 119–125.
[42] G. A. N. Felton, C. A. Mebi, B. J. Petro, A. K. Vannucci, D. H. Evans, R. S. Glass, D. L. Lichtenberger, *J. Organomet. Chem.*, accepted, DOI:10.1016/j.jorganchem.2009.03.017.
[43] R. C. Burns, M. J. Collins, R. J. Gillespie, G. J. Schrobilgen, *Inorg. Chem.* **1986**, *25*, 4465–4469.
[44] B. V. Nonius, *COLLECT, Data Collection Software*, The Netherlands, **1998**.
[45] Z. Otwinowski, W. Minor, "Processing of X-ray Diffraction Data Collected in Oscillation Mode" in *Methods in Enzymology*, vol. 276 (*Macromolecular Crystallography, Part A*), Academic Press, San Diego, **1997**, pp. 307–326.
[46] G. M. Sheldrick, *Acta Crystallogr., Sect. A* **1990**, *46*, 467–473.
[47] G. M. Sheldrick, *SHELXL-97 (Release 97-2)*, University of Göttingen, Germany, **1997**.
[48] N. A. Macías-Ruvalcaba, D. H. Evans, *J. Phys. Chem. B* **2005**, *109*, 14642–14647.

Received: March 17, 2009
Published Online: June 30, 2009

 © 2009 Wiley-VCH Verlag GmbH & Co. KGaA, Weinheim

2.3 [MK3] Substitution Reactions at [FeFe]-Hydrogenase Models Containing [2Fe3S] Cluster by Phosphine or Phosphite Ligands.

A. Q. Daraosheh, M. K. Harb, J. Windhager, H. Görls, M. El-khateeb, W. Weigand.

Organometallics **2009, *28*, 6275-6280.**

ORGANOMETALLICS
Article

Organometallics **2009,** *28,* 6275–6280 6275
DOI: 10.1021/om9005752

Substitution Reactions at [FeFe] Hydrogenase Models Containing [2Fe3S] Assembly by Phosphine or Phosphite Ligands

Ahmad Q. Daraosheh,[†] Mohammad K. Harb,[†] Jochen Windhager,[†] Helmar Görls,[†] Mohammad El-khateeb,*[,‡] and Wolfgang Weigand*[,†]

[†]*Institut für Anorganische und Analytische Chemie, Friedrich-Schiller-Universität Jena, August-Bebel-Strasse 2, 07743 Jena, Germany, and* [‡]*Chemistry Department, Jordan University of Science and Technology, 22110 Irbid, Jordan*

Received July 3, 2009

In order to elucidate the role of the "on−off" coordination mode of the thioether group in the [2Fe3S] complex **1**, which is related to the active site of [FeFe] hydrogenases, substitution studies of CO ligands by phosphite and phosphine ligands at compound $Fe_2(\mu\text{-}S_2(C_3H_6)_2S\text{-}\mu)(CO)_5$ (**1**) have been investigated. The reaction of **1** with 1 equiv of trimethylphosphite gave the kinetically controlled product $Fe_2(\mu\text{-}S_2(C_3H_6)_2S)(CO)_5P(OMe)_3$ (**2**) or the thermodynamically controlled product $Fe_2(\mu\text{-}S_2(C_3H_6)_2S\text{-}\mu)(CO)_4P(OMe)_3$ (**3**) depending on the reaction conditions. Moreover, $Fe_2(\mu\text{-}S_2(C_3H_6)_2S)(CO)_4[P(OMe)_3]_2$ (**4**) and $Fe_2(\mu\text{-}S_2(C_3H_6)_2S)(CO)_4(PMe_3)_2$ (**5**) were obtained from the reactions of **1** with excess $P(OMe)_3$ and excess PMe_3, respectively. These novel complexes have been characterized by IR, ^1H, $^{13}C\{^1H\}$, and $^{31}P\{^1H\}$ NMR spectroscopy, mass spectrometry, elemental analysis, and X-ray single-crystal structure analysis.

Introduction

In an earlier communication we reported our investigation on the reactions of 1,2,4-trithiolane, 1,2,5-trithiepane, 1,2,5-trithiocane, and 1,2,6-trithionane with nonacarbonyldiiron.[1] In that study, we found that the ring size in these different heterocycles influenced the constitutional structures of the resultant complexes. The reaction of nonacarbonyldiiron with the 1,2,6-trithionane provided $Fe_2(\mu\text{-}S_2(C_3H_6)_2S\text{-}\mu)(CO)_5$ (**1**), which can be envisioned as a model complex for the [2Fe3S] subsite of the H-cluster. In this compound the thioether sulfur atom acts as an additional S-donor by intramolecular substitution of one carbonyl group (Scheme 1).[1]

During the last several years, the research groups of Pickett,[2,3] Rauchfuss,[4] Song,[5] and Chen[6] reported the syntheses of various models for the [2Fe3S] subunit of the [FeFe] hydrogenases' active site (Scheme 2). It is generally accepted that the role of the proximal [4Fe4S] unit in the H-cluster is to shuttle electrons in and out the [2Fe2S] subunit via a cysteinato ligand.[7]

Pickett described the effect of the thioether sulfur atom on the substitution of CO ligands at the complex $[Fe_2(CO)_5\{MeSCH_2C(Me)(CH_2S)_2\}]$ and its benzyl thioether analogue by cyanide. The mechanism and the kintetics of these reactions have been extensively studied. However the proposed intermediate $[Fe_2(CO)_5(CN)\{RSCH_2C(Me)(CH_2S\text{-}\mu)_2\}]^-$ in the reaction mechanism has never been isolated.[3,8−11] Therefore, it would be of particular interest to isolate and characterize analogous intermediates that would support and verify the suggested mechanism. In the course of our present study, we investigated the substitution reactions of the carbonyl ligands at [2Fe3S] complex **1** with trimethylphosphite $[P(OMe)_3]$ and trimentylphosphine (PMe_3).

Results and Discussion

Reaction of 1 with 1 equiv of $P(OMe)_3$. Treatment of [2Fe3S] complex **1** with 1 equiv of $P(OMe)_3$ in THF at room temperature gave the first-formed kinetically controlled product $Fe_2(\mu\text{-}S_2(C_3H_6)_2S)(CO)_5P(OMe)_3$ (**2**), which upon standing at room temperature for 90 min converted to $Fe_2(\mu\text{-}S_2(C_3H_6)_2S\text{-}\mu)(CO)_4P(OMe)_3$ (**3**), the thermodynamic product. In contrast, under reflux conditions, **1** reacts with $P(OMe)_3$ to give exclusively complex **3** as the thermodynamically controlled product (Scheme 3).

*Corresponding authors. E-mail: c8wewo@uni-jena.de.

(1) Windhager, J.; Rudolph, M.; Bräutigam, S.; Görls, H.; Weigand, W. *Eur. J. Inorg. Chem.* **2007**, 2748–2760. Windhager, J.; Görls, H.; Petzold, H.; Mloston, G.; Linti, G.; Weigand, W. *Eur. J. Inorg. Chem.* **2007**, 4462–4471.
(2) Razavet, M.; Davies, S. C.; Hughes, D. L.; Pickett, C. J. *Chem. Commun.* **2001**, 847–848.
(3) Razavet, M.; Davies, S. C.; Hughes, D. L.; Barclay, J. E.; Evans, D. J.; Fairhurst, S. A.; Liu, X.; Pickett, C. J. *Dalton Trans.* **2003**, 586–595.
(4) Lawrence, J. D.; Li, H.; Rauchfuss, T. B. *Chem. Commun.* **2001**, *16*, 1482–1483.
(5) Song, L.-C.; Yang, Z.-Y.; Bian, H.-Z.; Hu, Q.-M. *Organometallics* **2004**, *23*, 3082–3084.
(6) Hu, M.-Q.; Ma, C.-B.; Si, Y.-T.; Chen, C.-N.; Liu, Q.-T. *J. Inorg. Biochem.* **2007**, *101*, 1370–1375.
(7) Capon, J.-F.; Gloaguen, F.; Pétillon, F. Y.; Schollhammer, P.; Talarmin, J. *Eur. J. Inorg. Chem.* **2008**, 4671–4681. Tard, C.; Pickett, C. *J. Chem. Rev.* **2009**, *109*, 2245–2274.
(8) Zampella, G.; Bruschi, M.; Fantucci, P.; Razavet, M.; Pickett, C. J.; Gioia, L. D. *Chem. Eur. J.* **2005**, *11*, 509–520.
(9) George, S. J.; Cui, Z.; Razavet, M.; Pickett, C. J. *Chem. Eur. J.* **2002**, *8*, 4037–4046.
(10) Liu, X.; Ibrahim, S. K.; Tard, C.; Pickett, C. J. *Coord. Chem. Rev.* **2005**, *249*, 1641–1652.
(11) Evans, D. J.; Pickett, C. J. *Chem. Soc. Rev.* **2003**, *32*, 268–275.

© 2009 American Chemical Society
Published on Web 10/16/2009

Scheme 1

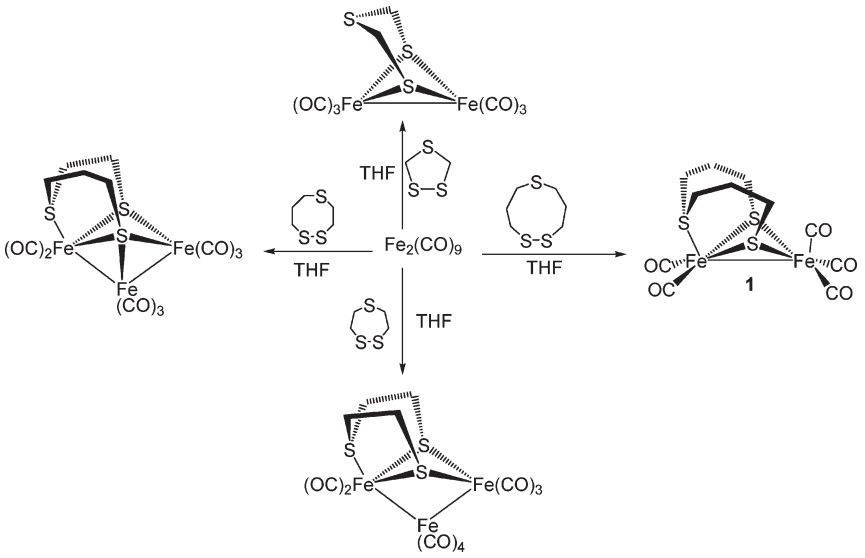

Scheme 2

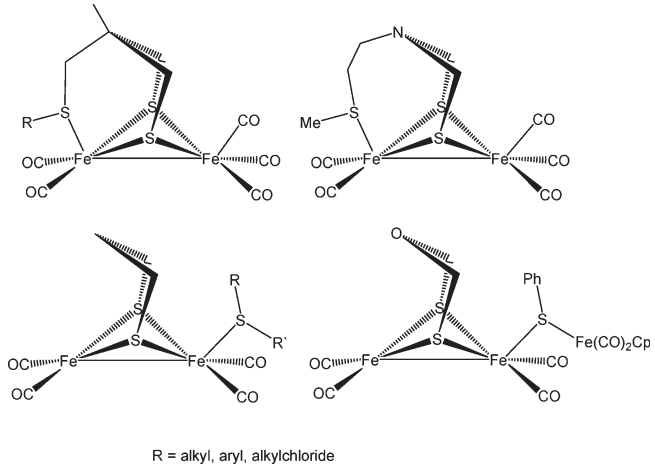

Scheme 3

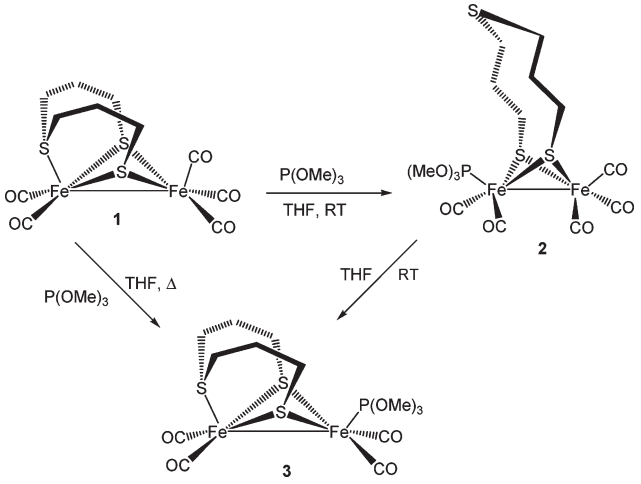

Complexes **2** and **3** are stable in the solid state for several days. In solution, the [2Fe3S] complex **3** is stable for several hours, while **2** is unstable due to fast conversion to **3**. Compounds **2** and **3** were characterized by IR, NMR spectroscopy, mass spectrometry, elemental analysis, and X-ray crystallography. It is noteworthy that the ^{1}H and $^{13}C\{^{1}H\}$ NMR spectra of **2** always contain resonance signals of **3**. The ^{1}H and $^{13}C\{^{1}H\}$ NMR spectra of **3** exhibit a singlet at 3.74 ppm and at 52.0 ppm, respectively, corresponding to the $P(OMe)_3$ group. $^{1}H,^{1}H$ COSY, $^{1}H,^{13}C$ HSQC, and $^{1}H,^{13}C$ HMBC NMR analysis substantiated the assignments of the proton and carbon signals of the $S(CH_2)_3S(CH_2)_3S$ moiety. These resonances are in the same range as those observed for **1**.[1] The $^{31}P\{^{1}H\}$ spectrum of **3** displays two singlets at 180.1 and 183.1 ppm, indicating the presence of the basal and apical isomers in solution. The mass spectra of **2** and **3** show the molecular ion peaks followed by the fragmentation of five CO groups in **2** and four in **3**.

The X-ray diffraction analysis reveals the proposed structures of **2** and **3** as shown in Figures 1 and 2, respectively. The central [2Fe2S] moieties of these complexes are in the butterfly conformation, and the geometry around the iron atoms is distorted square pyramidal, as observed from the bond angles. This is rather similar to that of **1**[1] and to those of other analogues reported in the literature.[3,12−22] The Fe−Fe distances of **2** and **3** are 2.5049(7) and 2.5400(6) Å, respectively. The Fe−Fe bond length of **2** is comparable to that observed for the nonsubstituted complex **1**,[1] also bearing five

(12) Zhao, X.; Georgakaki, I. P.; Miller, M. L.; Yarbrough, J. C.; Darensbourg, M. Y. *J. Am. Chem. Soc.* **2001**, *123*, 9710–9711.
(13) Zhao, X.; Chiang, C.-Y.; Miller, M. L.; Rampersad, M. V.; Darensbourg, M. Y. *J. Am. Chem. Soc.* **2003**, *125*, 518–524.
(14) Gloaguen, F.; Lawrence, J. D.; Schmidt, M.; Wilson, S. R.; Rauchfuss, T. B. *J. Am. Chem. Soc.* **2001**, *123*, 12518–12527.
(15) Lyon, E. J.; Georgakaki, I. P.; Reibenspies, J. H.; Darensbourg, M. Y. *J. Am. Chem. Soc.* **2001**, *123*, 3268–3278.
(16) Lawrence, J. D.; Li, H.; Rauchfuss, T. B.; Benard, M.; Rohmer, M.-M. *Angew. Chem., Int. Ed.* **2001**, *40*, 1768–1771.
(17) Li, H.; Rauchfuss, T. B. *J. Am. Chem. Soc.* **2002**, *124*, 726–727.
(18) Ott, S.; Kritikos, M.; Åkermark, B.; Sun, L. *Angew. Chem., Int. Ed.* **2003**, *42*, 3285–3288.
(19) Li, P.; Wang, M.; He, C.; Li, G.; Liu, X.; Chen, C.; Åkermark, B.; Sun, L. *Eur. J. Inorg. Chem.* **2005**, 2506–2513.
(20) Tard, C.; Liu, X.; Ibrahim, S. K.; Bruschi, M.; Gioia, L. D.; Davies, S. C.; Yang, X.; Wang, L.-S.; Sawers, G.; Pickett, C. J. *Nature* **2005**, *433*, 610–613.
(21) Ezzaher, S.; Capon, J.-F.; Gloaguen, F.; Petillon, F. Y.; Schollhammer, P.; Talarmin, J. *Inorg. Chem.* **2009**, *48*, 2–4.
(22) Apfel, U.-P.; Halpin, Y.; Görls, H.; Vos, J. G.; Schweizer, B.; Linti, G.; Weigand, W. *Chem. Biodiversity* **2007**, *4*, 2138–2148.

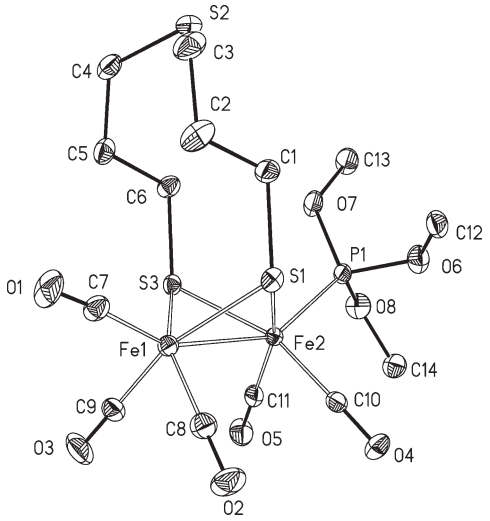

Figure 1. ORTEP drawing of $Fe_2(\mu\text{-}S_2(C_3H_6)_2S)(CO)_5P(OMe)_3$ (**2**) with thermal ellipsoids set at the 50% probability level (hydrogen atoms were omitted for clarity). Selected distances [Å] and angles [deg]: Fe1−Fe2 2.5049(7), Fe1−S1 2.2819(11), Fe1−S3 2.2849(10), Fe2−S1 2.2836(10), Fe2−S3 2.2814(10), Fe1−S1−Fe2 66.55(3), Fe1−S3−Fe2 66.54(3).

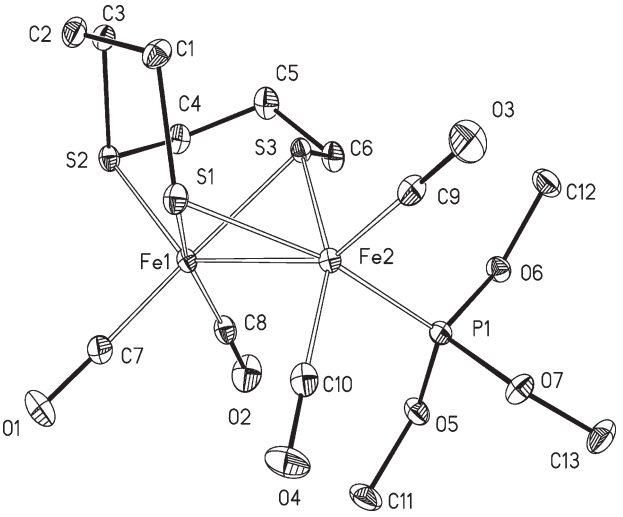

Figure 2. ORTEP drawing of $Fe_2(\mu\text{-}S_2(C_3H_6)_2S\text{-}\mu)(CO)_4P(OMe)_3$ (**3**) with thermal ellipsoids set at the 50% probability level (hydrogen atoms were omitted for clarity). Selected distances [Å] and angles [deg]: Fe1−Fe2 2.5400(6), Fe1−S1 2.2546(9), Fe1−S3 2.2554(8), Fe2−S1 2.3055(8), Fe2−S3 2.2426(8), Fe1−S2 2.2504(8), Fe1−S1−Fe2 67.69(3), Fe1−S3−Fe2 68.76(2).

CO ligands. The Fe−Fe bond length of **3** is significantly longer than that of **1**[1] due to replacement of a CO group by $P(OMe)_3$, and it is slightly longer than that observed for $[Et_4N][Fe_2\{MeSCH_2C(Me)(CH_2S)_2\}(CN)(CO)_4]$.[3] The significant increase in the Fe−Fe bond lengths of **3** compared to that in **2** could be attributed to the replacement of a carbonyl group by the thioether sulfur atom. The Fe−S (thioether sulfur atom) distance of **3** [2.2504(8) Å] is comparable to those observed for complex **1**[1] and $[Et_4N][Fe_2\{MeSCH_2C(Me)(CH_2S)_2\}(CN)(CO)_4]$.[3] The iron−

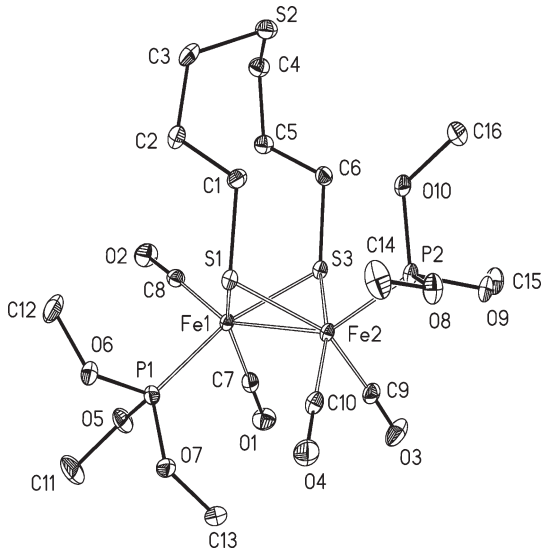

Figure 3. ORTEP drawing of $Fe_2(\mu\text{-}S_2(C_3H_6)_2S)(CO)_4[P(OMe)_3]_2$ (**4**) with thermal ellipsoids set at the 50% probability level (hydrogen atoms were omitted for clarity). Selected distances [Å] and angles [deg]: Fe1−Fe2 2.5431(5), Fe1−S1 2.2716(7), Fe1−S3 2.2845(7), Fe2−S1 2.2779(7), Fe2−S3 2.2950(7), Fe1−S1−Fe2 67.97(2), Fe1−S3−Fe2 67.47(2).

thiolato bond lengths in **2** and **3** are in the same range reported for analogous complexes.[1−3,23−39]

Reaction of 1 with Excess $P(OMe)_3$ or PMe_3. The reaction of **1** with excess $P(OMe)_3$ under reflux gave the disubstituted complex $Fe_2(\mu\text{-}S_2(C_3H_6)_2S)(CO)_4[P(OMe)_3]_2$ (**4**) in 85% yield (Scheme 4). Moreover, stirring of **1** with excess PMe_3

(23) Windhager, J.; Görls, H.; Petzold, H.; Mloston, G.; Linti, G.; Weigand, W. *Eur. J. Inorg. Chem.* **2007**, 4462–4471.
(24) Windhager, J.; Seidel, R. A.; Apfel, U.-P.; Görls, H.; Linti, G.; Weigand, W. *Chem. Biodiversity* **2008**, *10*, 2023–2041.
(25) Song, L.-C.; Yang, Z.-Y.; Bian, H.-Z.; Liu, Y.; Wang, H.-T.; Liu, X.-F.; Hu, Q.-M. *Organometallics* **2005**, *24*, 6126–6135.
(26) Heinekey, D. M. *J. Organomet. Chem.* **2009**, in press (doi: 10.1016/j.jorganchem.2009.03.047).
(27) Ezzaher, S.; Capon, J.-F.; Gloaguen, F.; Pétillon, F. Y.; Schollhammer, P.; Talarmin, J. *Inorg. Chem.* **2007**, *46*, 9863–9872.
(28) Orain, P.-Y.; Capon, J.-F.; Kervarec, N.; Gloaguen, F.; Pétillon, F.; Pichon, R.; Schollhammer, P.; Talarmin, J. *Dalton Trans.* **2007**, 3754–3756.
(29) Zhang, T.-T.; Wang, M.; Wang, N.; Li, P.; Liu, Z.-Y.; Sun, L.-C. *Polyhedron* **2009**, *28*, 1138–1144.
(30) Morvan, D.; Capon, J.-F.; Gloaguen, F.; Pétillon, F. Y.; Schollhammer, P.; Talarmin, J.; Yaouanc, J.-J.; Michaud, F.; Kervarec, N. *J. Organomet. Chem.* **2009**, in press (doi: 10.1016/j.jorganchem.2009.01.018).
(31) Song, L.-C.; Luo, X.; Wang, Y.-Z.; Gai, B.; Hu, Q.-M. *J. Organomet. Chem.* **2009**, *694*, 103–112.
(32) Gao, W.; Ekström, J.; Liu, J.; Chen, C.; Eriksson, L.; Weng, L.; Åkermark, B.; Sun, L. *Inorg. Chem.* **2007**, *46*, 1981–1991.
(33) Ezzaher, S.; Capon, J.-F.; Gloaguen, F.; Pétillon, F. Y.; Schollhammer, P.; Talarmin, J. *Inorg. Chem.* **2007**, *46*, 3426–3428.
(34) Justice, A. K.; Zampella, G.; Gioia, L. D.; Rauchfuss, T. B.; Vlugt, J. I. V. D.; Wilson, S. R. *Inorg. Chem.* **2007**, *46*, 1655–1664.
(35) Ezzaher, S.; Capon, J.-F; Gloaguen, F.; Kervarec, N.; Pétillon, F. Y.; Pichon, R.; Schollhammer, P.; Talarmin, J. *C. R. Chim.* **2008**, *11*, 906–914.
(36) Wang, Z.; Liu, J.-H.; He, C.-J.; Jiang, S.; Åkermark, B.; Sun, L.-C. *J. Organomet. Chem.* **2007**, *692*, 5501–5507.
(37) Zhao, X.; Georgakaki, I. P.; Miller, M. L.; Mejia-Rodriguez, R.; Chiang, C.-Y.; Darensbourg, M. Y. *Inorg. Chem.* **2002**, *41*, 3917–3928.
(38) Ibrahim, S. K.; Liu, X.; Tard, C.; Pickett, C. J. *Chem Commun.* **2007**, 1535–1537.
(39) Boyke, C. A.; Rauchfuss, T. B.; Wilson, S. R.; Rohmer, M.-M.; Benard, M. *J. Am. Chem. Soc.* **2004**, *126*, 15151–15160.

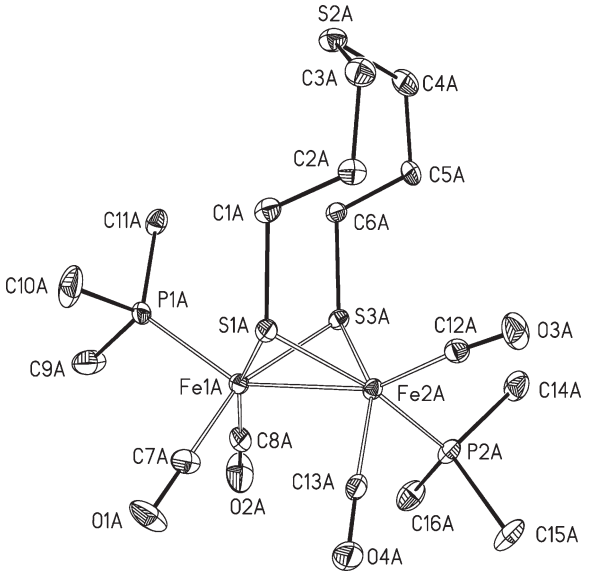

Figure 4. ORTEP drawing of $Fe_2(\mu\text{-}S_2(C_3H_6)_2S)(CO)_4[PMe_3]_2$ (**5**) with thermal ellipsoids set at the 50% probability level (hydrogen atoms were omitted for clarity). Selected distances [Å] and angles [deg]: Fe1−Fe2 2.5372(9), Fe1−S1 2.2977(13), Fe1−S3 2.2764(13), Fe2−S1 2.2829(12), Fe2−S3 2.2709(12), Fe1−S1−Fe2 67.27(4), Fe1−S3−Fe2 67.83(4).

afforded the analogous disubstituted complex $Fe_2(\mu\text{-}S_2(C_3H_6)_2S)(CO)_4(PMe_3)_2$ (**5**) (Scheme 4). Compounds **4** and **5**, which are stable in the solid state and for several hours in solution, were characterized by IR, NMR spectroscopy, mass spectrometry, elemental analysis, and X-ray crystallography. The mass spectra of **4** and **5** show the molecular ion peaks followed by stepwise loss of CO groups.

The ^{1}H NMR spectra of **4** and **5** exhibit three signals at 1.83, 2.41, 2.60 ppm (**4**) and 1.98, 2.42, 2.62 ppm (**5**), corresponding to SCH_2CH_2, SCH_2CH_2, and CH_2SCH_2 moieties, respectively. Their ^{1}H,^{1}H COSY and ^{1}H,^{13}C HSQC analysis verified the assignments of the ^{13}C resonances at 26.9, 31.9, 32.6 ppm (**4**) and 28.2, 32.1, 32.4 ppm (**5**). In addition, the ^{13}C resonances for of the methyl groups of **4** (51.8 ppm), **5** (20.3 ppm) and the carbonyl groups were observed as expected. The $^{31}P\{^1H\}$ NMR spectrum of **4** displays one broad resonance at δ 180.6 ppm at 25 °C, indicative of the two phosphite ligands, which are in fast exchange on the NMR time scale. Upon cooling the sample to −40 °C, this signal splits into an AB spin system (180.6 and 183.7 ppm) with coupling constant $J_{P,P}$ = 38.9 Hz, due to the apical and basal positions of the two phosphite ligands. The $^{31}P\{^1H\}$ NMR spectrum of **5** consists of a broad singlet at δ 29.2 ppm, which upon cooling to −40 °C splits into two broad signals at 22.9 and 37.2 ppm, indicating the presence of the basal and apical isomers, too.

The geometries around the Fe cores of **4** and **5** are rather similar to those observed for **2** and **3**. The Fe−Fe bond lengths of **4** (2.5431(5) Å) and **5** (2.5372(9) Å) are longer than those observed for **1** and **2** and comparable to that of **3**. These observations show that the Fe−Fe bond lengths in our model complexes depend on the number of CO ligands around the Fe atoms, which increases as the CO number decreases. The Fe−S bond lengths of **4** and **5** are within the range observed for **2** and **3**.

The IR spectra of complexes **1**−**5** (KBr disk) show three strong absorption bands at ν = 1906, 1952, 2040 cm^{-1} (**1**),[1] 1942, 1986, 2046 cm^{-1} (**2**), 1930, 1962, 2003 cm^{-1} (**3**), 1925, 1963, 2004 cm^{-1} (**4**), and 1901, 1937, 1979 cm^{-1} (**5**). The increase in the CO stretching frequencies from **1** to **2** could be attributed to the better π-acceptor property of $P(OMe)_3$ compared to that of the thioether sulfur atom. The values of ν(CO) in complexes **3**−**5** are as expected for the well-known electronic properties of the P-donor ligands.

Scheme 4

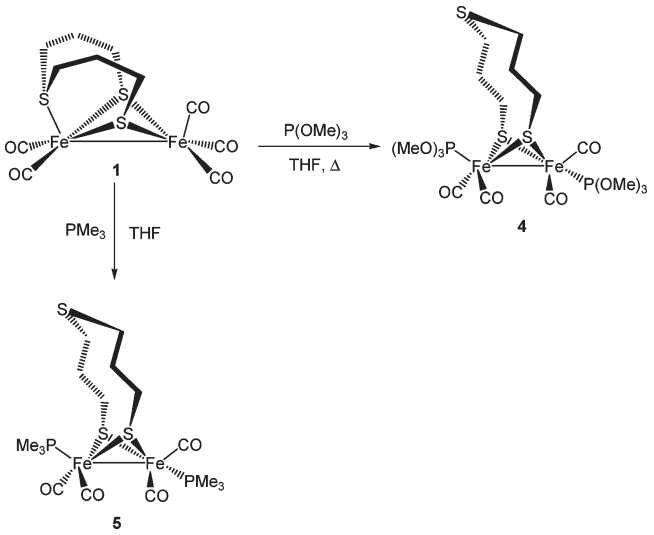

Conclusion

Substitution reactions of CO by $P(OMe)_3$ in complex **1** gave complexes **2**−**4**, as a result of the on−off coordination of a thioether ligand bound at the iron atom. These complexes were characterized by spectroscopic techniques and X-ray structure determination. Moreover, we were able to isolate and characterize the structure of complex **2**, which is believed to be the intermediate of the reaction pathway. This result could be seen as an important contribution to corroborate the mechanism for the cyanation reaction of [2Fe3S] cluster.[3,8,9] In addition, treatment of **1** with PMe_3 produced the disubstituted product **5** in a fast reaction, and the monosubstituted complex was not observed.

Experimental Section

All reactions were performed using standard Schlenk techniques under an inert atmosphere. The NMR spectra were recorded at room temperature on either a Bruker AVANCE 200 or 400 MHz spectrometer using the solvent residual peak as reference. Mass spectra were recorded on a Finnigan MAT SSQ 710 instrument. IR spectra were measured on a Perkin-Elmer System 2000 FT-IR spectrometer. Elemental analyses were performed with a LECO CHNS-932 apparatus. Silica gel 60 (0.015−0.040 mm) was used for column chromatography; TLC was done using Merck TLC aluminum sheets (silica gel 60 F_{254}). All solvents were dried and distilled prior to use according to the standard methods. $Fe_3(CO)_{12}$ was purchased from Aldrich, solvents were from Fisher Scientific, and other chemicals were from Acros; all were used without further purification. $Fe_2(\mu\text{-}S_2(C_3H_6)_2S\text{-}\mu)(CO)_5$ (**1**) was prepared according to a literature protocol.[1]

Preparation of $Fe_2(\mu\text{-}S_2(C_3H_6)_2S)(CO)_5P(OMe)_3$ (2). Trimethylphosphite (11.5 mg, 0.093 mmol) was added to a solution of **1** (40 mg, 0.093 mmol) in THF (30 mL) under argon. The reaction mixture turned immediately from brown-red to bright red and was stirred for an additional 3 min at room temperature.

Table 1. Crystal Data and Refinement Details for the X-ray Structure Determinations of Compounds 2, 3, 4, and 5

	2	**3**	**4**	**5**
formula	$C_{14}H_{21}Fe_2O_8PS_3$	$C_{13}H_{21}Fe_2O_7PS_3$	$C_{16}H_{30}Fe_2O_{10}P_2S_3$	$C_{16}H_{30}Fe_2O_4P_2S_3$
fw/g·mol^{-1}	556.16	528.15	652.22	556.22
T/°C	−90(2)	−90(2)	−90(2)	−90(2)
cryst syst	monoclinic	orthorhombic	triclinic	monoclinic
space group	$P2_1/n$	$P2_12_12_1$	$P\bar{1}$	$P2_1/c$
a/Å	9.3441(4)	9.4103(2)	9.4048(4)	13.2992(5)
b/Å	13.8053(3)	12.1233(3)	11.4370(5)	17.6628(7)
c/Å	17.3332(6)	17.5501(5)	13.3328(4)	20.6173(6)
α/deg	90	90	74.714(2)	90
β/deg	102.167(2)	90	84.777(2)	93.677(2)
γ/deg	90	90	72.652(2)	90
V/Å^3	2185.72(13)	2002.18(9)	1320.33(9)	4833.1(3)
Z	4	4	2	8
ρ/g·cm^{-3}	1.690	1.752	1.641	1.529
μ/cm^{-1}	17.24	18.73	15.03	16.1
measd data	15 390	14 338	9342	32 414
data with $I > 2\sigma(I)$	3676	4155	4947	6034
unique data/R_{int}	4995/0.0558	4548/0.0429	5934/0.0382	10981/0.1303
wR_2 (all data, on F^2)[a]	0.1227	0.0560	0.0971	0.1022
R_1 ($I > 2\sigma(I)$)[a]	0.0455	0.0260	0.0388	0.0556
S[b]	1.020	0.856	1.022	0.957
res dens/e·Å^{-3}	1.800/−0.482	0.382/−0.284	0.556/−0.477	0.528/−0.449
absorpt method	NONE	NONE	NONE	NONE
CCDC no.	727151	727152	727153	727154

[a] Definition of the R indices: $R_1 = (\sum||F_o| - |F_c||)/\sum|F_o|$; $wR_2 = \{\sum[w(F_o^2 - F_c^2)^2]/\sum[w(F_o^2)^2]\}^{1/2}$ $w^{-1} = \sigma^2(F_o^2) + (aP)^2 + bP$; $P = [2F_c^2 + \mathrm{Max}(F_o^2]/3$. [b] $S = \{\sum[w(F_o^2 - F_c^2)^2]/(N_o - N_p)\}^{1/2}$.

Volatiles were removed under vacuum. The bright red solid **2** was recrystallized from a mixture of CH_2Cl_2/pentane at −25 °C. Yield 48 mg (93%). Anal. Calcd for $C_{14}H_{21}Fe_2O_8S_3P$: C, 30.23; H, 3.81; S, 17.3. Found: C, 30.35; H, 3.87; S, 17.5. IR (KBr disk): $\nu_{C\equiv O}$ 2046 (s), 1986 (vs), 1944 (vs) cm^{-1}. DEI-MS (m/z): 557 [M$^+$], 528 [M$^+$ − CO], 500 [M$^+$ − 2CO], 472 [M$^+$ − 3CO], 444 [M$^+$ − 4CO], 416 [M$^+$ − 5CO].

Preparation of $Fe_2(\mu\text{-}S_2(C_3H_6)_2S\text{-}\mu)(CO)_4P(OMe)_3$ (3). Trimethylphosphite (16 mg, 0.13 mmol) was added to a brown-red solution containing **1** (56 mg, 0.13 mmol) in THF (30 mL). The reaction mixture first turned bright red then darkened to brown-red. After 90 min stirring at room temperature examination by TLC showed complete conversion to **3**. The solvent was removed under reduced pressure, and the crude product was purified by column chromatography with diethyl ether. Crystals suitable for X-ray diffraction analysis were obtained from a solution of CH_2Cl_2/pentane at −25 °C. Yield: 53 mg (77%). Anal. Calcd for $C_{13}H_{21}Fe_2O_7S_3P\cdot 1/4\ C_5H_{12}$: C, 31.34; H, 4.43; S, 17.61. Found: C, 31.07; H, 4.13; S, 17.56. ^{1}H NMR (400 MHz, $CDCl_3$): δ 1.76, 2.83 (m, 4H, $FeSCH_2$), 2.00−2.30 (m, 4H, SCH_2CH_2), 2.63, 2.92 (m, 4H, CH_2SCH_2), 3.74 (s, 9H, $P(OMe)_3$) ppm. $^{13}C\{^1H\}$ NMR (50 MHz, $CDCl_3$): δ 29.5, 27.5 (SCH_2CH_2), 32.2, 38.0 (CH_2SCH_2), 30.9, 36.5 ($FeSCH_2$), 52.0 ($P(OMe)_3$), 213.1 (CO) ppm. $^{31}P\{^1H\}$ NMR (200 MHz, $CDCl_3$): δ 180.1, 183.1 ($P(OMe)_3$) ppm. IR (KBr disk): $\nu_{C\equiv O}$ 2003 (s), 1962 (vs), 1930 (vs) cm^{-1}. DEI-MS (m/z): 528 [M$^+$], 500 [M$^+$ − CO], 472 [M$^+$ − 2CO], 444 [M$^+$ − 3CO], 416 [M$^+$ − 4CO].

Preparation of $Fe_2(\mu\text{-}S_2(C_3H_6)_2S)(CO)_4[P(OMe)_3]_2$ (4). Trimethylphosphite (49.6 mg, 0.4 mmol) was added to a solution of **1** (45 mg, 0.1 mmol) in THF (30 mL). The reaction mixture was heated at reflux for 30 min, and the solvent was removed under reduced pressure. The crude product was purified by column chromatography using diethyl ether as eluent. The orange-red fraction was collected and the solvent removed under reduced pressure. The resultant orange-red solid was recrystallized from pentane at −25 °C. Yield: 55 mg (85%). Anal. Calcd for $C_{16}H_{30}Fe_2O_{10}P_2S_2$: C, 29.46; H, 4.64; S, 14.75. Found: C, 29.46; H, 4.97; S, 15.3. ^{1}H NMR (400 MHz, $CDCl_3$, 25 °C): δ 1.83 (m, 4H, SCH_2CH_2), 2.41 (m, 4H, $FeSCH_2$), 2.60 (m, 4H, CH_2SCH_2), 3.74 (d, $^3J_{H,P}$ = 11.2 Hz, 18H, $P(OMe)_3$) ppm. $^{13}C\{^1H\}$ NMR (50 MHz, $CDCl_3$): δ 26.9 ($FeSCH_2$), 31.9 (CH_2SCH_2), 32.6 (SCH_2CH_2), 51.8 ($P(OMe)_3$), 213.7 (CO) ppm. $^{31}P\{^1H\}$ NMR (200 MHz, $CDCl_3$): δ 180.6 (s, br, 2P-$(OMe)_3$) ppm. $^{31}P\{^1H\}$ NMR (200 MHz, 223 K, $CDCl_3$): δ 180.6 (d, $J_{P,P}$ = 38.9 Hz, $P(OMe)_3$), 183.7 (d, $J_{P,P}$ = 38.9 Hz, $P(OMe)_3$) ppm. IR (KBr disk): $\nu_{C\equiv O}$ 2004 (s), 1963 (vs), 1925 (vs) cm^{-1}. DEI-MS (m/z): 652 [M$^+$], 624 [M$^+$ − CO], 596 [M$^+$ − 2CO], 568 [M$^+$ − 3CO], 540 [M$^+$ − 4CO].

Preparation of $Fe_2(\mu\text{-}S_2(C_3H_6)_2S)(CO)_4(PMe_3)_2$ (5). Trimethylphosphine (30.4 mg, 0.4 mmol) was added to a solution of **1** (35 mg, 0.08 mmol) in THF (30 mL) at 0 °C. The reaction mixture was allowed to warm to room temperature and stirred for 30 min. The resulting dark red solution was evaporated to dryness under vacuum, and the product was purified by column chromatography with diethyl ether as eluent. A dark red fraction was collected and dried. Crystals suitable for X-ray diffraction analysis were obtained from a solution of pentane at −25 °C. Yield: 35 mg (78%). Anal. Calcd for $C_{16}H_{30}Fe_2O_4S_3P_2$: C, 34.55; H, 5.44; S, 17.29. Found: C, 34.54; H, 5.64; S, 17.35. ^{1}H NMR (400 MHz, $CDCl_3$): δ 1.51 (d, $^2J_{H,P}$ = 7.6 Hz, 18H, $P(Me)_3$), 1.98 (m, 4H, SCH_2CH_2), 2.42 (m, 4H, $FeSCH_2$), 2.62 (m, 4H, CH_2SCH_2) ppm. $^{13}C\{^1H\}$ NMR (50 MHz, $CDCl_3$): δ 20.3 (PMe_3), 28.2 ($FeSCH_2$), 32.1 (CH_2SCH_2), 32.4 (SCH_2CH_2), 215.8 (CO) ppm. $^{31}P\{^1H\}$ NMR (200 MHz, $CDCl_3$): δ 29.2, (s br, 2PMe_3) ppm. $^{31}P\{^1H\}$ NMR (200 MHz, 253 K, $CDCl_3$): δ 22.9, (s br, PMe_3), 37.2(s br, PMe_3) ppm. IR (KBr disk): $\nu_{C\equiv O}$ 1979 (s), 1937 (vs), 1901 (vs) cm^{-1}. DEI-MS (m/z): 557 [M$^+$], 528 [M$^+$ − CO], 472 [M$^+$ − 3CO], 444 [M$^+$ − 4CO].

Crystal Structure Determination. The intensity data for the compounds were collected on a Nonius KappaCCD diffractometer, using graphite-monochromated Mo Kα radiation. Data were corrected for Lorentz and polarization effects, but not for absorption effects.[40,41] Crystallographic data as well as structure solution and refinement details are summarized in Table 1. The structures were solved by direct methods (SHELXS)[42] and refined by full-matrix least-squares techniques against F_o^2 (SHELXL-97).[42] All hydrogen atoms were included at calculated

(40) *COLLECT, Data Collection Software*; Nonius, B. V.: The Netherlands, 1998.

(41) Otwinowski, Z.; Minor, W. Processing of X-Ray Diffraction Data Collected in Oscillation Mode. In *Methods in Enzymology*; Vol. 276, *Macromolecular Crystallography, Part A*; Carter, C. W.; Sweet, R. M., Eds.; **1997**; pp 307−326.

(42) Sheldrick, G. M. *Acta Crystallogr., Sect. A* **2008**, *64*, 112.

positions with fixed thermal parameters. All non-hydrogen atoms were refined anisotropically.[42] XP (SIEMENS Analytical X-ray Instruments, Inc.) was used for structure representations.

Crystallographic data (excluding structure factors) have been deposited with the Cambridge Crystallographic Data Centre as supplementary publication CCDC-727151 for **2**, CCDC-727152 for **3**, CCDC-727153 for **4**, and CCDC-727154 for **5**. Copies of the data can be obtained free of charge on application to CCDC, 12 Union Road, Cambridge CB2 1EZ, UK [e-mail: deposit@ccdc.cam.ac.uk].

2.4 [MK4] Preparation and Characterization of Homologous Diiron Dithiolato, Diselenato, and Ditellurato Complexes: [FeFe]-Hydrogenase Models.

M. K. Harb, U.-P. Apfel, J. Kübel, H. Görls, G. A. N. Felton, T. Sakamoto, D. H. Evans, R. S. Glass, D. L. Lichtenberger, M. El-khateeb, W. Weigand.

***Organometallics* 2009, *28*, 6666-6675.**

6666 *Organometallics* **2009,** *28,* 6666–6675
DOI: 10.1021/om900675q

ORGANOMETALLICS
Article

Preparation and Characterization of Homologous Diiron Dithiolato, Diselenato, and Ditellurato Complexes: [FeFe]-Hydrogenase Models

Mohammad K. Harb,[†] Ulf-Peter Apfel,[†] Joachim Kübel,[†] Helmar Görls,[†] Greg A. N. Felton,[‡] Taka Sakamoto,[‡] Dennis H. Evans,*[,‡] Richard S. Glass,*[,‡] Dennis L. Lichtenberger,*[,‡] Mohammad El-khateeb,[§] and Wolfgang Weigand*[,†]

[†]*Institut für Anorganische und Analytische Chemie, Friedrich-Schiller-Universität Jena, August-Bebel-Strasse 2, 07743 Jena, Germany,* [‡]*Department of Chemistry and Biochemistry, The University of Arizona, Tucson, Arizona 85721, and* [§]*Chemistry Department, Jordan University of Science and Technology, 22110 Irbid, Jordan*

Received July 30, 2009

In order to elucidate the influence of the bridging chalcogen atoms in hydrogenase model complexes, diiron dithiolato, diselenolato, and ditellurolato complexes have been prepared and characterized. Treatment of $Fe_3(CO)_{12}$ with 3,3-bis(thiocyanatomethyl)oxetane (**1**) or a mixture of 2-oxa-6,7-dithiaspiro[3.4]octane (**2a**) and 2-oxa-6,7,8-trithiaspiro[3.5]nonane (**2b**) in toluene at reflux afforded the model compound $Fe_2(\mu\text{-}S_2C_5H_8O)(CO)_6$ (**3**). The analogous diselenolato and ditellurolato complexes, $Fe_2(\mu\text{-}Se_2C_5H_8O)(CO)_6$ (**4**) and $Fe_2(\mu\text{-}Te_2C_5H_8O)(CO)_6$ (**5**), were obtained from the reaction of $Fe_3(CO)_{12}$ with 2-oxa-6,7-diselenaspiro[3.4]octane (**6**) and 2-oxa-6,7-ditelluraspiro-[3.4]octane (**7**), respectively. Compounds **3**−**5** were characterized by spectroscopic techniques (NMR, IR, photoelectron spectroscopy), mass spectrometry, single-crystal X-ray analysis, and computational modeling. The electrochemical properties for the new compounds have been studied to assess their ability to catalyze electrochemical reduction of protons to give dihydrogen, and the catalytic rate is found to decrease on going from the sulfur to selenium to tellurium compounds. In the series **3**−**5** the reorganization energy on going to the corresponding cation decreased from **3** to **4** to **5**. Spectroscopic and computational analysis suggests that the increasing size of the chalcogen atoms from S to Se to Te increases the Fe−Fe distance and decreases the ability of the complex to form the structure with a rotated $Fe(CO)_3$ group that has a bridging carbonyl ligand and a vacant coordination site for protonation. This effect is mirrored on reduction of **3**−**5** in that the rotated structure with a bridging carbonyl, which creates a vacant coordination site for protonation, is disfavored on going from the S to Se to Te complexes.

Introduction

The natural energy resources predominantly used today are diminishing, and their continued use has become more harmful for the environment. Therefore, efforts to develop alternative energy resources and fuels have become major goals for the scientific community. Dihydrogen is one of the future fuels that causes no deleterious products for the environment.[1−5] Efficient production of dihydrogen in good yield has become a challenge, and there has been much research aimed at overcoming this challenge.[6−12] Biomimetic catalysts, shown in Scheme 1a,[13−29] are based on the active site of [FeFe]-hydrogenases[5,30−34] (the identity of X in the enzyme is still unclear).[34−41] Recently, diiron complexes containing diselenolato ligands have been prepared and

*Corresponding authors. E-mail: dhevans@email.arizona.edu; rglass@u.arizona.edu; dlichten@email.arizona.edu; c8wewo@uni-jena.de.

(1) Melis, A.; Zhang, L.; Forestier, M.; Ghirardi, M. L.; Seibert, M. *Plant Physiol.* **2000**, *122*, 127.
(2) Cammack, R.; Frey, M.; Robson, R. *Hydrogen as a Fuel: Learning from Nature*; Taylor & Francis: London, 2001.
(3) Woodward, J.; Orr, M.; Cordray, K.; Greenbaum, E. *Nature* **2000**, *405*, 1014.
(4) Coontz, R.; Hanson, B. *Science* **2004**, *305*, 957.
(5) Shima, S.; Pilak, O.; Vogt, S.; Schick, M.; Stagni, M. S.; Meyer-Klaucke, W.; Warkentin, E.; Thauer, R. K.; Ermler, U. *Science* **2008**, *321*, 572.
(6) Zhang, Y. H. P.; Evans, B. R.; Mielenz, J. R.; Hopkins, R. C.; Adams, M. W. W. *PLoS ONE* **2007**, *2*, e456.
(7) Antal, M. J.; Allen, S. G.; Schulman, D.; Xu, X.; Divilio, R. J. *Ind. Eng. Chem. Res.* **2000**, *39*, 4040.
(8) Hallenbeck, P. C.; Benemann, J. R. *Int. J. Hydrogen Energy* **2002**, *27*, 1185.
(9) Cortright, R. D.; Davda, R. R.; Dumesic, J. A. *Nature* **2002**, *418*, 964.
(10) Huber, G. W.; Shabaker, J. W.; Dumesic, J. A. *Science* **2003**, *300*, 2075.
(11) Deluga, G. A.; Salge, J. R.; Schmidt, L. D.; Verykios, X. E. *Science* **2004**, *303*, 993.
(12) Adams, M. W. W.; Stiefel, E. I. *Science* **1998**, *282*, 1842.
(13) Zhao, X.; Georgakaki, I. P.; Miller, M. L.; Yarbrough, J. C.; Darensbourg, M. Y. *J. Am. Chem. Soc.* **2001**, *123*, 9710.
(14) Zhao, X.; Chiang, C.; Miller, M. L.; Rampersad, M. V.; Darensbourg, M. Y. *J. Am. Chem. Soc.* **2003**, *125*, 518.
(15) Gloaguen, F.; Lawrence, J. D.; Rauchfuss, T. B. *J. Am. Chem. Soc.* **2001**, *123*, 9476.
(16) Lyon, E. J.; Georgakaki, I. P.; Reibenspies, J. H.; Darensbourg, M. Y. *J. Am. Chem. Soc.* **2001**, *123*, 3268.

 Published on Web 11/11/2009 © 2009 American Chemical Society

Scheme 1

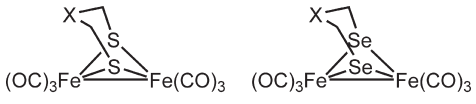

a) X = CH_2, O, NH, S b) X = NPh, CH_2, Se, CHO(Sugar)

characterized (Scheme 1b), and their ability to catalyze H_2 production from acids was evaluated.[42−45]

Photoelectron spectroscopy and theoretical calculations revealed that the reorganization energy of $Fe_2(\mu\text{-}Se_2C_3H_5CH_3)(CO)_6$ is substantially lower than that for analogous complexes with Fe_2S_2 cores.[44] This effect, which may lead to faster electron transfer with complexes containing Fe_2Se_2 rather than Fe_2S_2 cores, has not yet been investigated in detail. On the basis of these observations, we have now extended our studies also to the preparation of complexes containing ditellurolato ligands. In the present publication, the preparation of oxetane-containing dithiolato, diselenolato, and ditellurolato diiron complexes is reported (Scheme 2). The ability of these complexes to catalyze the formation of molecular hydrogen from weak acids is presented and compared with related systems. To compare S, Se, and Te analogues, it is important to have the same substitution pattern except for the chalcogen in each complex. This was achieved by synthesizing the homologous series **3**−**5** shown in Scheme 2. The oxetane ring allows the five-membered ring to which it is attached to be stable for all three 1,2-dichalcogenolanes. These precursors to the desired complexes do not polymerize, as is readily seen with the unsubstituted compounds.

Scheme 2

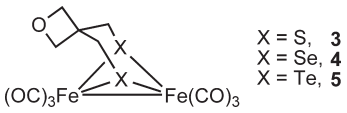

Experimental Section

General Comments. All reactions were carried out under an argon atmosphere with standard Schlenk techniques. THF, toluene, and hexane were dried and distilled prior to use according to standard methods. The ^1H, $^{13}C\{^1H\}$, $^{77}Se\{^1H\}$, and 2D NMR (^1H,^1H COSY, ^1H,^{13}C HSQC, ^1H,^{77}Se HMBC) spectra were recorded on either a Bruker AVANCE 200 or 400 MHz spectrometer using the solvent residual peak or a concentrated solution of SeO_2 in D_2O as reference. The ^{77}Se chemical shifts are reported relative to neat Me_2Se [$\delta(Me_2Se) = \delta(SeO_2) + 1302.6$ ppm].[46] The ^{125}Te chemical shift was measured versus external PhTeTePh and converted to that versus Me_2Te.[47] Mass spectra were recorded on a Finnigan MAT SSQ 710 instrument. IR spectra were measured as KBr disks on a Perkin-Elmer System 2000 FT-IR spectrometer and in Nujol on a Thermo Nicolet Avatar ESP 380 FT-IR spectrometer utilizing the OMNIC version 6.1 software. Elemental analyses were performed with a LECO CHNS-932 apparatus. Silica gel 60 (0.015−0.040 mm) was used for column chromatography, and TLC was done using Merck TLC aluminum sheets (silica gel 60 F254). 3,3-Bis(thiocyanatomethyl)oxetane[48] (**1**), a 2-oxa-6,7-dithiaspiro[3.4]octane (**2a**) and 2-oxa-6,7,8-trithiaspiro[3.5]-nonane (**2b**) mixture,[48] 2-oxa-6,7-disellenaspiro[3.4]octane[49] (**6**), and 2-oxa-6,7-ditelluraspiro[3.4]octane[50] (**7**) were prepared according to literature protocols. $Fe_3(CO)_{12}$ purchased from Aldrich, solvents from Fisher Scientific, and other chemicals from Acros were used without further purification. Yield calculations were based on substoichiometric utilized chemicals or on $Fe_3(CO)_{12}$ for the diiron complexes.

Synthesis of $Fe_2(\mu\text{-}S_2C_5H_8O)(CO)_6$ (3). Method A. A solution of $Fe_3(CO)_{12}$ (140 mg, 0.28 mmol) and **1** (56 mg, 0.28 mmol) in toluene (25 mL) was heated under reflux for one hour. The resulting dark red mixture was evaporated to dryness under reduced pressure. The obtained solid was redissolved in a

(17) Lawrence, J. D.; Li, H.; Rauchfuss, T. B.; Benard, M.; Rohmer, M. *Angew. Chem., Int. Ed.* **2001**, *40*, 1768.
(18) Razavet, M.; Davies, S. C.; Hughes, D. L.; Barclay, J. E.; Evans, D. J.; Fairhurst, S. A.; Liu, X.; Pickett, C. J. *J. Chem. Soc., Dalton Trans.* **2003**, 586.
(19) Linck, R. C.; Rauchfuss, T. B. In *Synthetic models for bioorganometallic reaction centers*; Bioorganometallics; Wiley-VCH Verlag GmbH & Co.: Weinheim, Germany, 2006; p 403.
(20) Li, H.; Rauchfuss, T. B. *J. Am. Chem. Soc.* **2002**, *124*, 726.
(21) Tard, C.; Liu, X.; Ibrahim, S. K.; Bruschi, M.; De Gioia, L.; Davies, S. C.; Yang, X.; Wang, L.; Sawers, G.; Pickett, C. J. *Nature* **2005**, *433*, 610.
(22) Song, L.-C.; Yang, Z. Y.; Bian, H. Z.; Hu, Q. M. *Organometallics* **2004**, *23*, 3082.
(23) Seyferth, D.; Henderson, R. S.; Song, L.-C. *Organometallics* **1982**, *1*, 125.
(24) Windhager, J.; Rudolph, M.; Bräutigam, S.; Görls, H.; Weigand, W. *Eur. J. Inorg. Chem.* **2007**, 2748.
(25) Windhager, J.; Goerls, H.; Petzold, H.; Mloston, G.; Linti, G.; Weigand, W. *Eur. J. Inorg. Chem.* **2007**, 4462.
(26) Song, L.-C.; Yang, Z. Y.; Bian, H. Z.; Liu, Y.; Wang, H. T.; Liu, X. F.; Hu, Q. M. *Organometallics* **2005**, *24*, 6126.
(27) Tard, C.; Pickett, C. *J. Chem. Rev.* **2009**, *109*, 2245.
(28) Windhager, J.; Seidel, R. A.; Apfel, U.; Görls, H.; Linti, G.; Weigand, W. *Chem. Biodiversity* **2008**, *5*, 2023.
(29) Ott, S.; Kritikos, M.; Åkermark, B.; Sun, L. *Angew. Chem., Int. Ed.* **2003**, *42*, 3285.
(30) Albracht, S. P. J. *Biochim. Biophys. Acta, Bioenerg.* **1994**, *1188*, 167.
(31) Graf, E.; Thauer, R. K. *FEBS Lett.* **1981**, *136*, 165.
(32) Cammack, R.; Patil, D.; Aguirre, R.; Hatchikian, E. C. *FEBS Lett.* **1982**, *142*, 289.
(33) Wang, G.; Benecky, M.; Huynh, B.; Cline, J.; Adams, M.; Mortenson, L.; Hoffman, B.; Munck, E. *J. Biol. Chem.* **1984**, *259*, 14328.
(34) Adams, M. W.; Mortenson, L. E. *J. Biol. Chem.* **1984**, *259*, 7045.
(35) Chen, J.; Mortenson, L. E. *Biochim. Biophys. Acta, Protein Struct.* **1974**, *371*, 283.
(36) Chen, J.; Blanchard, D. K. *Biochem. Biophys. Res. Commun.* **1978**, *84*, 1144.
(37) Glick, B. R.; Martin, W. G.; Martin, S. M. *Can. J. Microbiol.* **1980**, *26*, 1214.
(38) Adams, M. W. W.; Mortenson, L. E. *Biochim. Biophys. Acta, Bioenerg.* **1984**, *766*, 51.
(39) Fauque, G.; Peck, H. D.Jr.; Moura, J. J. G.; Huynh, B. H.; Berlier, Y.; DerVartanian, D. V.; Teixeira, M.; Przybyla, A. E.; Lespinat, P. A. *FEMS Microbiol. Rev.* **1988**, *54*, 299.
(40) Adams, M. W. *Biochim. Biophys. Acta* **1990**, *1020*, 115.
(41) Hatchikian, E. C.; Forget, N.; Fernandez, V. M.; Williams, R.; Cammack, R. *Eur. J. Biochem.* **1992**, *209*, 357.
(42) Gao, S.; Fan, J.; Sun, S.; Peng, X.; Zhao, X.; Hou, J. *Dalton Trans.* **2008**, 2128.
(43) (a) Song, L.-C.; Gai, B.; Wang, H.; Hu, Q. *J. Inorg. Biochem.* **2009**, *103*, 805. (b) Song, L.-C.; Gao, W.; Feng, C.-P.; Wang, D.-F.; Hu, Q.-M. *Organometallics* **2009**, *28*, 6121.
(44) Harb, M. K.; Niksch, T.; Windhager, J.; Görls, H.; Holze, R.; Lockett, L. T.; Okumura, N.; Evans, D. H.; Glass, R. S.; Lichtenberger, D. L.; El-khateeb, M.; Weigand, W. *Organometallics* **2009**, *28*, 1039.
(45) Apfel, U.; Halpin, Y.; Gottschaldt, M.; Görls, H.; Vos, J. G.; Weigand, W. *Eur. J. Inorg. Chem.* **2008**, *2008*, 5112.
(46) Burns, R. C.; Collins, M. J.; Gillespie, R. J.; Schrobilgen, G. J. *Inorg. Chem.* **1986**, *25*, 4465.
(47) Granger, P.; Chapelle, S.; McWhinnie, W. R.; Al-Rubaie, A. *J. Organomet. Chem.* **1981**, *220*, 149.
(48) Campbell, T. W. *J. Org. Chem.* **1957**, *22*, 1029.
(49) Günther, W. H.; Salzman, M. N. *Ann. N.Y. Acad. Sci.* **1972**, *192*, 25.
(50) Lakshmikantham, M. V.; Cava, M. P.; Gunther, W. H. H.; Nugara, P. N.; Belmore, K. A.; Atwood, J. L.; Craig, P. *J. Am. Chem. Soc.* **1993**, *115*, 885.

minimum amount of CH_2Cl_2 and column chromatographed. From the major red fraction, which was eluted with THF/hexane (1:3), **3** was obtained as a red solid (56 mg, 47%).

Method B. Twenty-five milligrams of the 2-oxa-6,7-dithiaspiro[3.4]octane and 2-oxa-6,7,8-trithiaspiro[3.5]nonane mixture (**2a** and **2b**) and $Fe_3(CO)_{12}$ (85 mg, 0.169 mmol) were dissolved in 20 mL of toluene and heated under reflux for 1.5 h. Evaporation and column chromatography (THF/hexane, 1:3) gave 36 mg (50%) of the red crystalline product **3**. Anal. Calcd for $C_{11}H_8Fe_2O_7S_2 \cdot 1$hexane: C, 32.34; H, 2.29, S, 14.56. Found: C, 32.27; H, 2.31, S, 14.16. IR $\nu_{C\equiv O}$ cm^{-1}: (KBr disk) 2076 (vs), 2033 (vs), 1997 (vs, sh), (Nujol) 2077 (s), 2036 (vs), 2008 (s), 1993 (s), 1982 (m). ^1H NMR (200 MHz, $CDCl_3$): δ 4.28 (s, 4H, $(CH_2)_2O$), 2.48 (s, 4H, $2SCH_2$). ^1H NMR (200 MHz, −50 °C, $CDCl_3$): δ 4.28 (s, 4H, $(CH_2)_2O$), 3.07 (d, $^2J_{H,H}$ = 8.8 Hz, 2H, SCH_AH_B and SCH_CH_D), 1.81 (d, $^2J_{H,H}$ = 8.8 Hz, 2H, SCH_AH_B and SCH_CH_D). ^{13}C NMR (50 MHz, $CDCl_3$): δ 207.1 (CO), 82.2 ($(CH_2)_2O$), 42.2 (C_q), 30.3 ($2SCH_2$). DEI-MS (*m*/*z*): 428 (M^+), 400 ($M^+ - CO$), 372 ($M^+ - 2CO$), 344 ($M^+ - 3CO$), 316 ($M^+ - 4CO$), 288 ($M^+ - 5CO$), 260 ($M^+ - 6CO$).

Synthesis of $Fe_2(\mu\text{-}Se_2C_5H_8O)(CO)_6$ (4). A solution of $Fe_3(CO)_{12}$ (101 mg, 0.2 mmol) and **5** (49 mg, 0.2 mmol) in THF (50 mL) was heated at reflux for one hour. The resulting mixture was evaporated to dryness in vacuo. The obtained solid was suspended in a minimum amount of hexane and chromatographed on silica gel, eluting with CH_2Cl_2/hexane (1:3). From the major red fraction, **4** was obtained as a red solid (73 mg, 70%). Single crystals were obtained from hexane solution. Mp: 169−170 °C. Anal. Calcd for $C_{11}H_8Fe_2O_7Se_2$: C, 25.32; H, 1.55. Found: C, 25.14; H, 1.66. IR $\nu_{C\equiv O}$ cm^{-1}: (KBr disk) 2068 (vs), 2025 (vs), 1988 (vs) cm^{-1}, (Nujol) 2070 (s), 2029 (vs), 2000 (s), 1989 (s), 1977 (m). ^1H NMR (200 MHz, $CDCl_3$): δ 4.26 (s, 4H, $(CH_2)_2O$), 2.52 (s, 4H, 2SeCH2). ^1H NMR (200 MHz, −50 °C, $CDCl_3$): δ 4.26 (s, 4H, $(CH_2)_2O$), 3.15 (d, $^2J_{H,H}$ = 10.2 Hz, 2H, $SeCH_AH_B$ and $SeCH_CH_D$), 1.89 (d, $^2J_{H,H}$ = 10.2 Hz, 2H, $SeCH_AH_B$ and $SeCH_CH_D$). ^{13}C NMR (50 MHz, $CDCl_3$): δ 208.2 (CO), 81.8 ($(CH_2)_2O$), 42.2 (C_q), 21.5 ($2SeCH_2$). $^{77}Se\{^1H\}$ NMR (76 MHz, $CDCl_3$): δ 107 ppm. DEI-MS (*m*/*z*): 524 (M^+), 496 ($M^+ - CO$), 468 ($M^+ - 2CO$), 440 ($M^+ - 3CO$), 411 ($M^+ - 4CO$), 384 ($M^+ - 5CO$), 356 ($M^+ - 6CO$).

Synthesis of $Fe_2(\mu\text{-}Te_2C_5H_8O)(CO)_6$ (5). Complex **5** was prepared, separated, and recrystallized by a procedure similar to that of **4**. The reaction of $Fe_3(CO)_{12}$ (101 mg, 0.2 mmol) with **6** (68 mg, 0.2 mmol) was carried out in THF. Yield: 82 mg (66%). Mp: 175−176 °C. Anal. Calcd for $C_{11}H_8Fe_2O_7Te_2 \cdot 0.25$hexane: C, 23.44; H, 1.81. Found: C, 23.24; H, 1.99. IR $\nu_{C\equiv O}$ cm^{-1}: (KBr disk) 2055 (s), 2012 (vs), 1971 (vs) cm^{-1}, (Nujol) 2058 (s), 2020 (vs), 1990 (s), 1982 (s), 1969 (m). ^1H NMR (200 MHz, $CDCl_3$): δ 4.23 (s, 4H, $(CH_2)_2O$), 2.66 (s, 4H, $2TeCH_2$). ^1H NMR (200 MHz, −50 °C, $CDCl_3$): δ 4.48 (s, 2H, $CH_{2A}O$), 4.04 (s, 2H, $CH_{2B}O$) 3.22 (s, 2H, $TeCH_AH_B$ and $TeCH_CH_D$), 2.12 (s, 2H, $TeCH_AH_B$ and $TeCH_CH_D$). ^{13}C NMR (50 MHz, $CDCl_3$): δ 210 (CO), 80.2 ($(CH_2)_2O$), 42.3 (C_q), 4.2 ($2TeCH_2$). ^{125}Te NMR (158 MHz, $CDCl_3$): δ 197. DEI-MS (*m*/*z*): 620 (M^+), 496, 564 ($M^+ - 2CO$), 508 ($M^+ - 4CO$), 452 ($M^+ - 6CO$).

Crystal Structure Determination. The intensity data for the compounds were collected on a Nonius KappaCCD diffractometer, using graphite-monochromated Mo Kα radiation. Data were corrected for Lorentz and polarization effects, but not for absorption effects.[51,52] The structures were solved by direct methods (SHELXS)[53] and refined by full-matrix least-squares techniques against F_o^2 (SHELXL-97).[54] All hydrogen atoms were included at calculated positions with fixed thermal parameters. All non-hydrogen atoms were refined anisotropically. XP (SIEMENS Analytical X-ray Instruments, Inc.) was used for structure representations.

Electrochemical Measurements. Instrumentation and the source and treatment of solvent and supporting electrolyte have been reported earlier.[55] All potentials are reported versus the potential of the ferrocenium/ferrocene (Fc^+/Fc) couple measured in acetonitrile. The voltammetric experiments were conducted at 298 K, using ∼1.0 mM of each compound in acetonitrile containing 0.10 M Bu_4NPF_6 on a glassy carbon working electrode (GCE), under an Ar atmosphere. The area of the GCE was determined to be 0.0707 cm^2 from cyclic voltammetric studies of the oxidation of ferrocene in acetonitrile using 2.5×10^{-5} cm^2/s as its diffusion coefficient.[55]

Photoelectron Spectroscopy. Photoelectron spectra were recorded using an instrument that features a 36 cm radius hemispherical analyzer (McPherson),[56] with custom-designed photon source, sample cells, detection and control electronics, calibration, and data analysis as described previously.[57] In the figures of the photoelectron spectra, the spectra obtained with the He I source photons are represented by the solid black lines, and the spectra obtained with the He II source photons are represented with the red dashed lines. The He II spectra are scaled to match the low ionization energy intensities in the He I spectra for visual comparison of the change in relative intensity at higher ionization energies. All samples sublimed cleanly, with no visible changes in the spectra during data collection after initial observation of ionizations from the diiron complex. The sublimation temperatures for the compounds (in °C, at 10^{-5} Torr) were as follows: complex **3**, 90−110; **4**, 100−110; **5**, 110−120.

Density Functional Theory (DFT) Calculations. Computational methods have been developed previously for this class of diiron hexacarbonyl systems with S and Se heteroatoms in the bridging positions and validated by their ability to account for structures, adiabatic ionization energies, carbonyl stretching frequencies, pK_a values, oxidation and reduction potentials, and other electrochemical parameters, as well as metal−metal and pertinent metal−ligand bond energies.[44,58−60] Density functional theory calculations were carried out with the Amsterdam density functional (ADF2006.01d) package.[61,62] Geometry optimizations and frequency calculations (with no imaginary frequencies in the final geometries) were carried out using the VWN functional with the Stoll correction implemented.[63] All electronic energies were obtained with the OPBE functional.[64] Comparison of the OPBE functional to other common functionals found it to be the best for the prediction of nuclear

(51) Nonius, B. V. *COLLECT, Data Collection Software*, **1998**.
(52) Otwinowski, Z.; Minor, W. In *Processing of X-ray diffraction data collected in oscillation mode*; Carter, C. W., Jr., Ed.; Methods in Enzymology; Academic Press: New York, 1997; Vol. *276*, pp 307−326.
(53) Sheldrick, G. M. *Acta Crystallogr., Sect. A* **1990**, *46*, 467.
(54) Sheldrick,G. M. *SHELXL-97* (*Release 97-2*); **1997**.
(55) Macías-Ruvalcaba, N. A.; Evans, D. H. *J. Phys. Chem. B* **2005**, *109*, 14642.
(56) Siegbahn, K.; Nordling, C.; Fahlman, A.; Nordberg, R.; Hamrin, K.; Hedman, J.; Johansson, G.; Bergmark, T.; Karlsson, S. E.; Lindgren, I.; Lindberg, B. *Nova Acta Regiae Societatis Scientiarum Upsaliensis* **1967**, *20*, 282.
(57) Cranswick, M. A.; Dawson, A.; Cooney, J. J. A.; Gruhn, N. E.; Lichtenberger, D. L.; Enemark, J. H. *Inorg. Chem.* **2007**, *46*, 10639.
(58) Felton, G. A. N.; Vannucci, A. K.; Chen, J.; Lockett, L. T.; Okumura, N.; Petro, B. J.; Zakai, U. I.; Evans, D. H.; Glass, R. S.; Lichtenberger, D. L. *J. Am. Chem. Soc.* **2007**, *129*, 12521.
(59) Petro, B. J.; Vannucci, A. K.; Lockett, L. T.; Mebi, C.; Kottani, R.; Gruhn, N. E.; Nichol, G. S.; Goodyer, P. A. J.; Evans, D. H.; Glass, R. S.; Lichtenberger, D. L. *J. Mol. Struct.* **2008**, *890*, 281.
(60) Felton, G. A. N.; Vannucci, A. K.; Okumura, N.; Lockett, L. T.; Evans, D. H.; Glass, R. S.; Lichtenberger, D. L. *Organometallics* **2008**, *27*, 4671.
(61) Te Velde, G.; Bickelhaupt, F. M.; Baerends, E. J.; Fonseca Guerra, C.; Van Gisbergen, S. J. A.; Snijders, J. G.; Ziegler, T. *J. Comput. Chem.* **2001**, *22*, 931.
(62) *ADF2006.01d, SCM*, Theoretical Chemistry, Vrije Universiteit: Amsterdam, The Netherlands, 2006.
(63) Stoll, H.; Pavlidou, C. M. E.; Preuss, H. *Theor. Chim. Acta* **1978**, *49*, 143.
(64) Swart, M.; Ehlers, A. W.; Lammertsma, K. *Mol. Phys.* **2004**, *102*, 2467.

Scheme 3

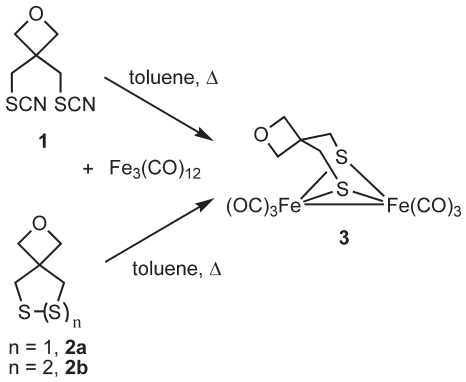

Scheme 4

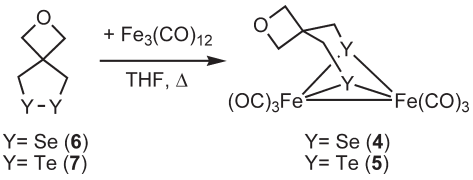

magnetic constants[65] and the only functional to correctly predict the spin states of seven different iron complexes.[64] All calculations utilized a triple-ζ Slater-type orbital (STO) basis set with one polarization function (TZP) for H, C, O, Fe, S, and Se and two polarization functions (TZ2P) for Te. Relativistic effects by the zero-order regular approximation (ZORA)[66,67] were also applied during all calculations. The frozen core approximation was used for the inner core of all atoms. The theoretical stretching frequencies and IR absorption intensities for all species were calculated analytically with the same computing method as described above and scaled by a factor of 1.002. For the simulated IR spectra in the figure the linewidths are adjusted by a constant factor to approximate the linewidths in the experimental spectra. Figures of the optimized geometries and molecular orbital plots were created with Molekel.[68]

Results and Discussion

Treatment of $Fe_3(CO)_{12}$ with bisthiocyanate **1** in toluene under reflux for one hour afforded the diiron dithiolato complex $Fe_2(\mu\text{-}S_2C_5H_8O)(CO)_6$ (**3**). Moreover, complex **3** also was prepared from the reaction of $Fe_3(CO)_{12}$ with an inseparable 1:1 mixture of **2a** and **2b**[48] in toluene under reflux conditions for one and a half hour in 50% yield (Scheme 3).

The analogous diselenolato and ditellurolato complexes $Fe_2(\mu\text{-}Se_2C_5H_8O)(CO)_6$ (**4**) and $Fe_2(\mu\text{-}Te_2C_5H_8O)(CO)_6$ (**5**) were synthesized from the reaction of $Fe_3(CO)_{12}$ with 2-oxa-6,7-diselenaspiro[3.4]octane (**6**) or 2-oxa-6,7-ditelluraspiro-[3.4]octane (**7**), respectively. These reactions were carried out in THF (Scheme 4).

Compounds **3**−**5** are air-stable in the solid state and for several hours in solution. These products were characterized by IR spectroscopy, multinuclear NMR spectroscopy, mass spectrometry, elemental analysis, X-ray crystallography, and photoelectron spectroscopy.

The room-temperature ^{1}H NMR spectra of **3**−**5** display two singlets at 2.48 and 4.28 (**3**), 2.52 and 4.26 (**4**), and 2.66 and 4.23 (**5**) ppm for the two different methylene groups YCH_2 (Y = S, Se, Te) and CH_2O, respectively. Upon cooling to −50 °C, the resonance signals of the more shielded methylene groups in **3** and **4** split into AB spin systems, since ring flipping of the three-carbon bridge is frozen out and the hydrogen atoms of YCH_2 (Y = S, Se) are now nonequivalent. The low-temperature (−50 °C) ^{1}H NMR spectrum of **5** displays two unresolved signals of an AB spin system corresponding to the diastereotopic protons at $TeCH_2$, as well as two broad singlets for the CH_2OCH_2 group. The $^{13}C\{^1H\}$ NMR spectra of **3**−**5** exhibit three resonances at 82.2, 42.2, and 30.3 (**3**), 81.8, 42.2, and 21.5 (**4**), and 80.2, 42.3, and 4.2 (**5**) for CH_2O, C_q, and YCH_2 (Y = S, Se, Te). The ^{13}C resonance of $TeCH_2$ in **5** is significantly shifted to high field ($\Delta\delta$(S,Te) = 26.1, $\Delta\delta$(Se,Te) = 17.3), which could be attributed to the "heavy atom" effect.[69] One signal is observed at 107 ppm in the ^{1}H,^{77}Se HMBC NMR spectrum of **4**, indicating equivalent Se atoms. This resonance is shifted to higher field compared to that of the propanediselenolato (PDS) model complex (145 ppm).[43,44] The mass spectra of **3**−**5** showed the molecular ion peaks and the elimination of six CO ligands sequentially.

The IR spectra of complexes **3**−**5** (KBr disk) exhibit three strong absorption bands in the regions 1997−2076 for **3**, 1988−2068 for **4**, and 1971−2055 cm^{-1} for **5**. When comparing the spectra, it can be seen that the CO absorption bands are shifted to lower frequencies from **3** to **5**, which can be explained by the increasing back-donation to CO caused by rising donor ability from S to Te. These data are within the same ranges as those observed for propanedithiolato (PDT),[70] PDS,[43,44] and propaneditellurolato (PDTe)[71] complexes.

The X-ray diffraction analyses reveal the proposed structures of **3**−**5** as shown in Figures 1−3 and Table 1. The central 2Fe2Y (Y = S, Se, Te) moieties of **3**−**5** are in the butterfly conformation and the geometry around the iron atoms is similar to that reported for PDT, PDS, and PDTe complexes.[43,44,70,71] The Fe−Fe bond distances in **3**−**5** are 2.4923(3), 2.5367(19), and 2.6322(11) Å, respectively, a trend attributed to the increase of atomic sizes from S to Te. The Fe−S, Fe−Se, and Fe−Te bond lengths are comparable to those reported for PDT, PDS, and PDTe complexes.[43,44,70,71] Moreover an increase of the bonding angle X−C1−C2 (X = S, Se, Te) is visible (**3**: 117.76(12)°, **4**: 118.2(6)°, **5**: 118.5(4)°). These values are unexpectedly high in comparison to a regular sp^3-hybridized atom (109.5°). An explanation for this is given in the literature and can be described by the rule of Bent.[72,73]

It is noteworthy that the Fe−CO bond lengths {average lengths: 1.800 Å (**3**), 1.793 Å (**4**), 1.785 Å (**5**)} are slightly decreasing from **3** to **5** due to the increasing electron density at the Fe atoms caused by more back-donation ability from S

(65) Zhang, Y.; Lin, H.; Truhlar, D. G. *J. Chem. Theory Comput.* **2007**, *3*, 1378.
(66) van Lenthe, E.; Ehlers, A.; Baerends, E. *J. Chem. Phys.* **1999**, *110*, 8943.
(67) van Lenthe, E.; Baerends, E. J.; Snijders, J. G. *J. Chem. Phys.* **1993**, *99*, 4597.
(68) Portmann, S.; Luthi, H. P. *Chimia* **2000**, *54*, 766.
(69) Kalabin, G. A.; Bzhezovskii, V. M.; Kushnarev, D. F.; Proidakov, A. G. *Zh. Org. Khim* **1981**, *17*, 1143.
(70) Lyon, E. J.; Georgakaki, I. P.; Rabenspies, J. H.; Darensbourg, M. Y. *Angew. Chem., Int. Ed.* **1999**, *38*, 3178.
(71) Shieh, M.; Shieh, M. H. *Organometallics* **1994**, *13*, 920.
(72) Apfel, U.; Halpin, Y.; Görls, H.; Vos, J. G.; Schweizer, B.; Linti, G.; Weigand, W. *Chem. Biodiversity* **2007**, *4*, 2138.
(73) Bent, H. A. *Chem. Rev.* **1961**, *61*, 275.

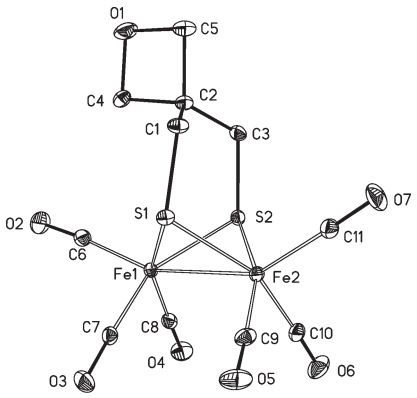

Figure 1. ORTEP drawing of $Fe_2(\mu\text{-}S_2C_5H_8O)(CO)_6$ (**3**) with thermal ellipsoids set at the 50% probability level (hydrogen atoms were omitted for clarity). Selected distances [Å] and angles [deg]: Fe1−Fe2 2.4923(3), Fe1−S1 2.2682(5), Fe1−S2 2.2676(5), Fe2−S1 2.2578(5), Fe2−S2 2.2600(5), Fe1−S1−Fe2 66.826(14), Fe1−S2−Fe2 66.799(14), S1−Fe1−S2 84.279(17), S1−Fe2−S2 84.690(17).

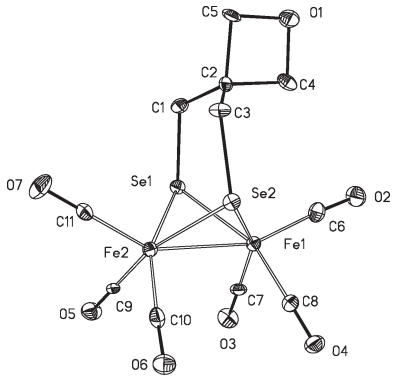

Figure 2. ORTEP drawing of $Fe_2(\mu\text{-}Se_2C_5H_8O)(CO)_6$ (**4**) with thermal ellipsoids set at the 50% probability level (hydrogen atoms were omitted for clarity). Selected distances [Å] and angles [deg]: Fe1−Fe2 2.5367(19), Fe1−Se1 2.3813(15), Fe1−Se2 2.3824(14), Fe2−Se1 2.3753(16), Fe2−Se2 2.3823(17), Fe1−Se1−Fe2 64.46(5), Fe1−Se2−Fe2 64.34(5), Se1−Fe1−Se2 85.61(5), Se1−Fe2−Se2 85.74(6).

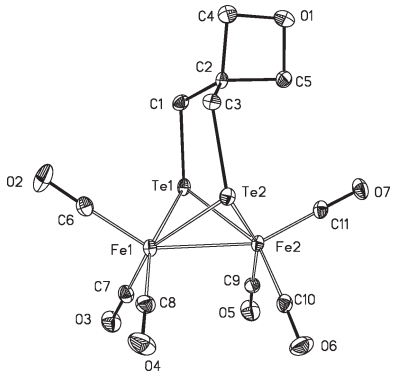

Figure 3. ORTEP drawing of $Fe_2(\mu\text{-}Te_2C_5H_8O)(CO)_6$ (**5**) with thermal ellipsoids set at the 50% probability level (hydrogen atoms were omitted for clarity). Selected distances [Å] and angles [deg]: Fe1−Fe2 2.6322(11), Fe1−Te1 2.5435(8), Fe1−Te2 2.5344(8), Fe2−Te1 2.5317(8), Fe2−Te2 2.5384(7), Fe1−Te1−Fe2 62.48(3), Fe1−Te2−Fe2 62.52(2), Te1−Fe1−Te2 86.92(3), Te1−Fe2−Te2 87.09(2).

Table 1. Crystal Data and Refinement Details for the X-Ray Structure Determinations of the Compounds 3, 4, and 5

	3	**4**	**5**
formula	$C_{11}H_8Fe_2O_7S_2$	$C_{11}H_8Fe_2O_7Se_2$	$C_{11}H_8Fe_2O_7Te_2$
fw	427.99	521.79	619.07
T/°C	−90(2)	−90(2)	−90(2)
cryst syst	triclinic	triclinic	triclinic
space group	$P\bar{1}$	$P\bar{1}$	$P\bar{1}$
a/Å	8.7511(3)	8.7942(7)	7.7877(4)
b/Å	9.3583(4)	9.4877(11)	9.0734(4)
c/Å	10.2267(3)	10.3124(13)	12.6096(6)
α/deg	100.509(2)	100.635(7)	101.493(2)
β/deg	91.881(2)	92.451(7)	95.493(2)
γ/deg	110.795(2)	110.565(7)	110.171(3)
V/Å^3	765.48(5)	786.33(15)	806.39(7)
Z	2	2	2
ρ/g·cm^{-3}	1.857	2.204	2.550
μ/cm^{-1}	21.95	65.01	53.72
measd data	5538	5339	5678
data with $I > 2\sigma(I)$	3198	1946	2893
unique data/R_{int}	3484/0.0231	3540/0.0868	3644/0.0364
wR_2 (all data, on F^2)[a]	0.0636	0.1352	0.0860
R_1 ($I > 2\sigma(I)$)[a]	0.0246	0.0655	0.0378
s[b]	1.021	1.004	1.046
res dens/e·Å^{-3}	0.420/−0.414	0.989/−1.183	0.785/−1.366
absorpt method	none	none	none
CCDC no.	723576	723577	723578

[a] $R_1 = (\sum||F_o|-|F_c||)/\sum|F_o|$, $wR_2 = \{\sum[w(F_o^2 - F_c^2)^2]/\sum[w(F_o^2)^2]\}^{1/2}$ with $w^{-1} = \sigma^2(F_o^2) + (\alpha P)^2$. [b] $s = \{\sum[w(F_o^2 - F_c^2)^2]/(N_o - N_p)\}^{1/2}$.

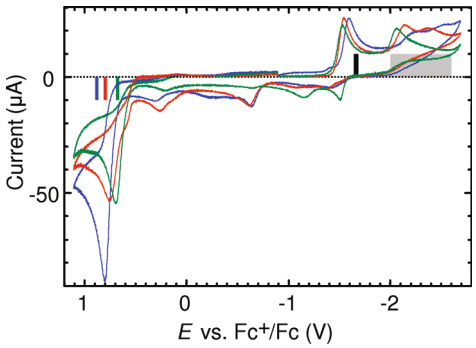

Figure 4. Background-corrected voltammograms of 1.01 mM **3** (blue), 1.00 mM **4** (red), and 1.00 mM **5** (green) in acetonitrile with 0.10 M tetrabutylammonium hexafluorophosphate at glassy carbon (0.10 V/s; scan segments: −0.9 to −2.7 V; −2.7 to +1.1 V; +1.1 to −0.9 V; argon purged). The bars on the zero current axis represent the oxidation and reduction potentials obtained from DFT computations. The colored bars are the calculated oxidation potentials for each respective molecule, the black bar is the range of calculated first reduction potentials for all three molecules, and the gray bar represents the range of calculated second reduction potentials for a variety of final geometries.

to Te. This observation is consistent with the CO band shifts to lower frequencies from **3** to **5** in their IR spectra.

Electrochemical Investigations. Cyclic voltammograms (CV) of **3**−**5** were recorded in order to observe the electrochemically induced reduction and oxidation properties of this family of compounds and to assess their ability to catalyze the reduction of weak acids to form dihydrogen. Comparison of a wide potential range of CV data, Figure 4, for all three compounds shows some broadly similar processes.

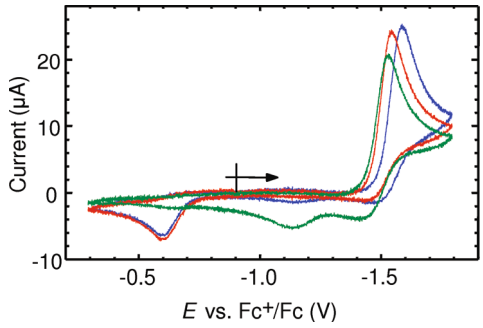

Figure 5. Background-corrected voltammograms of 1.01 mM **3** (blue), 1.00 mM **4** (red), and 1.00 mM **5** (green) in acetonitrile with 0.10 M tetrabutylammonium hexafluorophosphate at glassy carbon (0.10 V/s; scan segments: −0.9 to −1.8 V; −1.8 to −0.3 V; −0.3 to −0.9 V; argon purged).

A primary one-electron reduction with a peak potential around −1.55 V is observed followed by a less distinct second reduction feature at least a further 600 mV more negative. The conclusion that the reduction peak corresponds to a one-electron process is based on comparison of the peak height with that of other known one-electron processes, such as the oxidation of ferrocene, measured under the same conditions. For information about the electronic structure of the one-electron reduction product, see section "Electronic Structure and Observed Properties" below. Strong irreversible oxidation peaks are seen between 0.70 and 0.80 V. Small oxidation peaks are observed for compounds **3** and **4** at −0.60 V but only following an initial scan through the primary reduction peak (see SI-1 and SI-4), suggesting that this feature is due to the oxidation of a species formed upon reduction of the initial compound (this feature is largest at slow scan rates, suggesting that it is due to a species formed in a slow reaction following the initial reduction, SI-2 and SI-5). All three compounds have a degree of chemical reversibility to the primary reduction feature at the larger scan rates (see SI-2, SI-5, and SI-8). At 0.1 V/s, as in Figures 4 and 5, only the Te compound, **5**, shows distinct reversibility. There is a small positive shift, ∼70 mV, in the primary reduction peak potential as S is changed to Se and to Te (from Figure 5: $E_{p,red}$ = −1.602 V (**3**), −1.551 V (**4**), and −1.535 V (**5**)). The second more negative reduction peak is chemically irreversible for all three compounds. The anodic peak potentials span a range of ∼100 mV, with the Te compound being the most easily oxidized and S most difficult (from Figure 4: $E_{p,ox}$ = 0.810 V (**3**), 0.778 V (**4**), and 0.708 V (**5**)). The finding that the Te compound, **5**, is both the easiest to reduce and the easiest to oxidize is surprising, although the magnitudes of the shifts are fairly small. The oxidation peak is chemically irreversible for all three compounds.

Catalysis of the reduction of weak acids by compounds **3**−**5** was tested with additions of acetic acid to acetonitrile solutions (see Figures 6, 7, SI-3, SI-6, SI-9, and SI-10). The response with a 5-fold excess of acid shows some catalysis, indicated by enhanced current in a region where neither the catalyst nor the acid alone are reduced.[58] There is evidence of modest catalysis in this region, most strongly for **3**, with enhanced current around −2.0 V. The feature is broad and not well-defined, so that determination of the overpotential is imprecise but can be considered to be at least 0.5 V (using the standard potential for reduction of acetic acid,

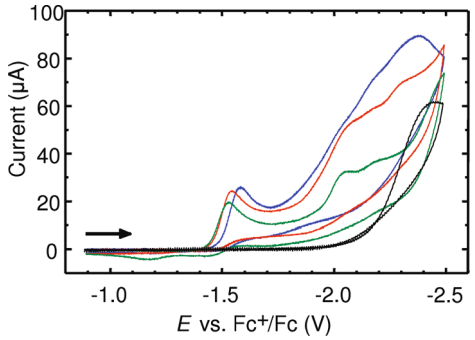

Figure 6. Background-corrected voltammograms of 1.01 mM **3** + 5 mM acetic acid (blue), 1.00 mM **4** + 5 mM acetic acid (red), 1.00 mM **5** + 5 mM acetic acid (green), and 5 mM acetic acid only (black) in acetonitrile with 0.10 M tetrabutylammonium hexafluorophosphate at glassy carbon (0.10 V/s, argon purged); scan: −0.9 to −2.5 V and return to −0.9 V.

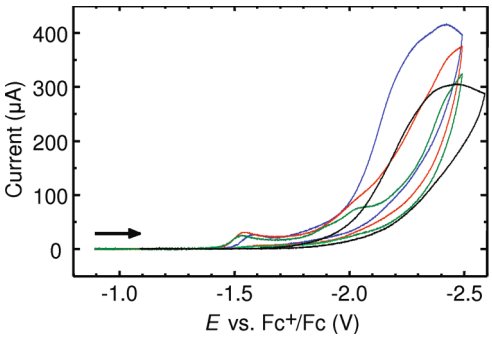

Figure 7. Background-corrected voltammograms of 1.01 mM **3** + 50 mM acetic acid (blue), 1.00 mM **4** + 50 mM acetic acid (red), 1.00 mM **5** + 50 mM acetic acid (green), and 50 mM acetic acid only (black) in acetonitrile with 0.10 M tetrabutylammonium hexafluorophosphate at glassy carbon (0.10 V/s, argon purged); scan: −0.9 to −2.5 V and return to −0.9 V.

−1.46 V).[74] There is little enhancement for **5**, where most of the extra current with 5 mM acid is likely due to the direct reduction of acetic acid on glassy carbon. Compound **4** (Se) represents a case intermediate between compounds **3** (S) and **5** (Te). Figure 7 shows the response with a much larger acid excess, 50:1, wherein any catalytic current is mostly swamped by direct reduction. The addition of acetic acid to these compounds does not lead to growth in the height of the primary reduction peak; such growth was not expected, as this would represent an extremely low overpotential of ∼0.10 V. due to the direct reduction of acetic acid on glassy carbon. Compound **4** (Se) represents a case intermediate between compounds **3** (S) and **5** (Te). Figure 7 shows the response with a much larger acid excess, 50:1, wherein any catalytic current is mostly swamped by direct reduction.

Photoelectron Spectroscopy. The He I and He II gas-phase ultraviolet photoelectron spectra of the molecules containing chalcogens S through Te are shown in Figure 8. The general assignment of the ionizations is based on previously reported analogous compounds.[44] The displayed spectrum contains ionizations from the Fe-based metal 3d-orbitals,

(74) Felton, G. A. N.; Glass, R. S.; Lichtenberger, D. L.; Evans, D. H. *Inorg. Chem.* **2006**, *45*, 9181. Corrections: Felton, G. A. N.; Glass, R. S.; Lichtenberger, D. L.; Evans, D. H. *Inorg. Chem.* **2007**, *46*, 5126. Felton, G. A. N.; Glass, R. S.; Lichtenberger, D. L.; Evans, D. H. *Inorg. Chem.* **2007**, *46*, 8098.

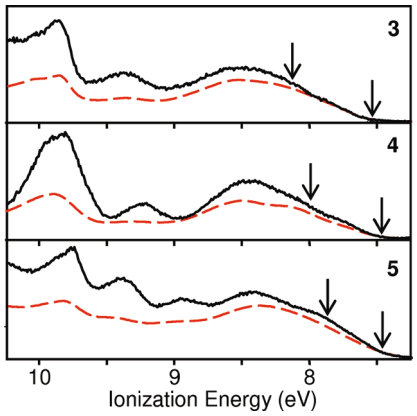

Figure 8. He I (black solid line) and He II (red dashed line) photoelectron spectra of oxetane molecules. The arrows around 7.5 eV indicate the DFT-calculated adiabatic ionization energy for each molecule. The arrows around 8 eV indicate the DFT-calculated vertical ionization energy for each molecule.

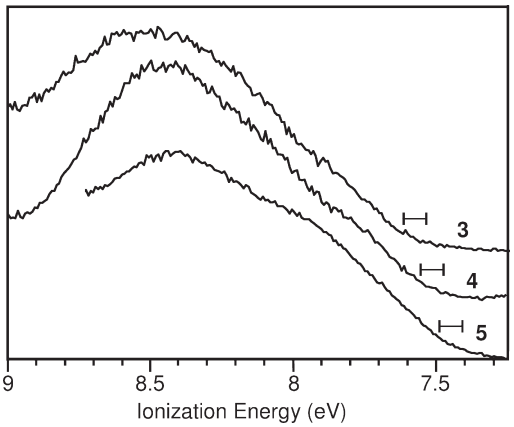

Figure 9. First ionization bands of molecules **3**−**5** in the He I photoelectron spectra. The brackets indicate the region of onset of ionization intensity, which approximates the adiabatic ionization energy for the molecules.

chalcogen-based valence p-orbitals, and O-based 2p-orbitals. The metal d-based ionizations include a formal metal−metal bond of the diiron center and the three occupied d-orbitals of each Fe center that are involved in back-bonding to the carbonyl ligands. The chalcogen-based and O-based valence p-orbital ionizations are expected to be observed in the high ionization energy side of this region based on previously reported photoelectron spectra of chalcogen-[75−77] and oxetane-[78,79]containing organometallic compounds.

The first broad ionization profile, shown in more detail in Figure 9, contains the predominantly Fe d-based ionizations and ranges up to about 9 eV for the S- and Se-containing molecules and up to about 8.7 eV for the Te-containing molecule. This band has a weak shoulder on the low ionization energy side corresponding to ionization from the HOMO of the molecule, calculated to be predominantly the Fe−Fe σ-bond (vide infra), with an adiabatic ionization energy approximately in the region indicated by the onset of ionization intensity around 7.5 eV. The estimated shift of the adiabatic ionization energy from molecule **3** to molecule **5** based on these spectra is 0.1 eV, which is the same as the observed shift in oxidation potentials reported above.

The second and third distinct ionization bands (shown in Figure 8), ranging from about 9.0 to 9.5 eV, are chalcogen based, and above 10.0 eV are O p-based ionizations. The additional identifiable band in this region of the spectrum of **5** is most likely the consequence of spin−orbit effects for the heavy tellurium atom. Compared to the ionizations observed in the He I spectra, these chalcogen-based ionizations exhibit substantially decreased intensity relative to the Fe d-based ionizations when the higher-energy He II excitation was used. The probability of ionization from a chalcogen p-orbital falls by an average factor of 10 from He I to He II excitation, while the probability of O p-orbital and Fe d-orbital ionizations increases by almost a factor of 2 based on theoretical partial photoionization cross-sections of the atoms.[80] However, the relative intensity changes observed in the photoelectron spectra are much less in magnitude than the theoretical values predicted for pure atomic orbital ionizations. This suggests substantial mixing of chalcogen character with iron d orbital and oxygen p orbital character. The energies of these ionizations visibly decrease with substitution from S to Se to Te, as expected from the decreasing electronegativity of the atoms and the decreasing inherent stability of the atomic orbitals.

Electronic Structure and Observed Properties. Density functional theory calculations of these oxetane compounds have been carried out to provide further information on how the electronic structure and properties of the molecules are altered as the chalcogen is changed from S to Se to Te. A computational methodology has been developed previously for [FeFe]-hydrogenase mimics that shows good agreement between calculated and experimental results.[44,58−60] This is the first test of the computational model to account for the properties of a mimic with tellurium atoms in the bridging positions. Optimized geometries and comparisons with the crystal structures are provided in the Supporting Information. For the S- and Se-containing molecules **3** and **4** the calculated Fe−Fe and Fe−chalcogen bond distances are within 0.025 Å of those obtained from crystal structures (see SI). For the Te-containing molecule **5** the optimized Fe−Fe distance is 0.05 Å shorter than the crystal structure distance, and the Fe−Te distance is about 0.07 Å longer than the crystal structure distance. There was some concern about additional relativistic effects or other limitations of the basis set or model for the heavy tellurium atoms, but this was not found to be an issue for the electron distribution or the spectroscopic and thermodynamic properties of the molecule, as evidenced by agreement with the carbonyl stretching frequencies, molecular ionization energies, and oxidation and reduction potentials. It was noted that geometry optimization was much more difficult for the Te-containing molecule because of a fairly flat potential energy surface, perhaps due to the larger and softer tellurium atoms, leading to larger differences in the calculated distances from

(75) Guillemin, J. C.; Bajor, G.; Riague, E.; Khater, B.; Veszpremi, T. *Organometallics* **2007**, *26*, 2507.
(76) Cozzolino, A. F.; Gruhn, N. E.; Lichtenberger, D. L.; Vargas-Baca, I. *Inorg. Chem.* **2008**, *47*, 6220.
(77) Cranswick, M. A.; Gruhn, N. E.; Oorhles-Steele, O.; Ruddick, K. R.; Burzlaff, N.; Schenk, W. A.; Lichtenberger, D. L. *Inorg. Chim. Acta* **2008**, *361*, 1122.
(78) Roszak, S.; Kaufman, J. J.; Koski, W. S.; Barreto, R. D.; Fehlner, T. P.; Balasubramanian, K. *J. Phys. Chem.* **1992**, *96*, 7226.
(79) Mollere, P. D. *Tetrahedron Lett.* **1973**, *14*, 2791.
(80) Yeh, J. J.; Lindau, I. *At. Data Nucl. Data Tables* **1985**, *32*, 1.

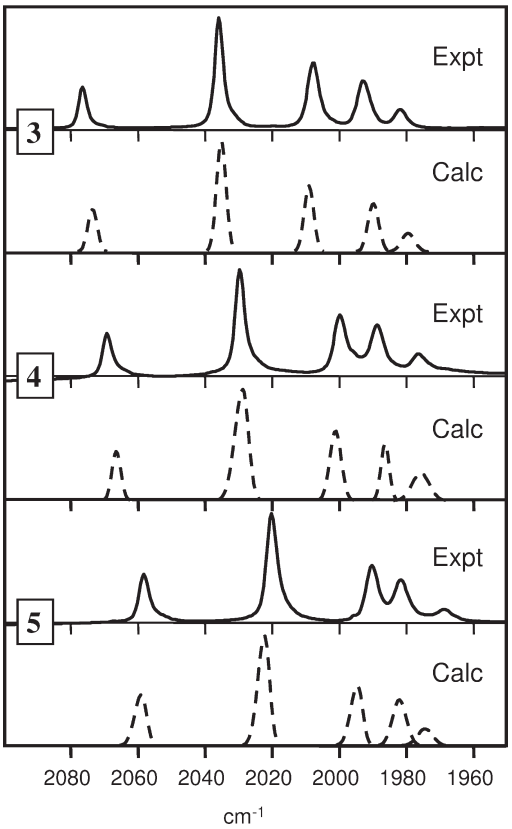

Figure 10. Comparison of the experimental IR spectra (in Nujol) in the carbonyl stretching region (solid lines) with calculated IR spectra (dashed lines) for each of the oxetane molecules.

experiment, but not to significantly larger differences in the calculated energy quantities.

The carbonyl stretching frequencies are an energy measure sensitive to the electron distribution in the molecules, and the intensities of the normal mode absorptions are sensitive to the molecular geometry and carbonyl coupling. The calculated and observed spectra are compared in Figure 10. The average difference in the calculated and experimental frequencies is less that 0.2%, and the relative absorption intensities are in good agreement. As mentioned previously, the decrease in carbonyl stretching frequencies from **3** to **4** to **5** indicates an increase of electron richness at the diiron core of the molecule from S to Se to Te. The trend is as expected considering the changes in electronegativity from S to Se to Te. The increasing donor ability from S to Se to Te is evidenced by the increasing positive charge on these atoms. Based on Voronoi deformation densities, which are less sensitive to basis sets than Mulliken population analysis,[81] the electron density in the vicinity of the chalcogen decreases by 0.06 e^- from S to Se and another 0.09 e^- from Se to Te. Much of the charge is transferred to the carbonyls, and the corresponding increases in electron density in the vicinity of the Fe atoms are 0.02 and 0.04 e^-.

The agreement of the calculations with the experimental ionization energies is also very good. The arrows in Figure 8 indicate the adiabatic and vertical ionization energies as calculated by the ΔSCF energy between the neutral molecule

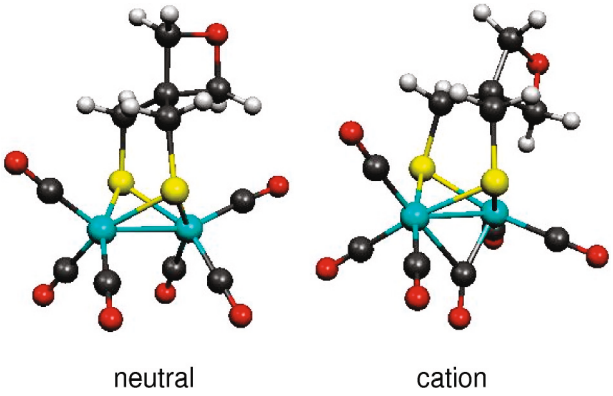

Figure 11. Calculated neutral and cation structures of **3**.

and the positive ion. The calculated first vertical ionization energies, for which the structures of the positive ions are constrained to the optimized structures of the neutral molecules, are able to account for the shift of the primary ionization band intensity to lower energy from S to Se to Te substitution. Calculated adiabatic ionization energies, for which the structures of the positive ions are optimized to their global minima, are close to the experimental onset energies of the first ionization bands, indicated by the arrows near 7.5 eV in Figure 8. In each case the global minimum structure of the cation in the gas phase has a semibridging carbonyl ligand, as shown in Figure 11. This general arrangement of the carbonyl ligands, which has been has been the subject of much attention,[59,82−87] has been termed the "rotated" structure because it can be viewed as an approximate 60° rotation of one $Fe(CO)_3$ group. This rotated structure creates a vacant axial coordination site on the Fe center analogous to the active site of [FeFe]-hydrogenase.[19,21,23,88,89]

The cation reorganization energy for each molecule was calculated as the energy difference of the optimized semibridged rotated structure of the cation shown in Figure 11 (corresponding to the adiabatic ionization energy) from the energy of the cation calculated with the nonbridged frozen structure of the neutral molecule (corresponding to the vertical ionization energy). Reorganization energies are calculated to be 0.59 eV for **3**, 0.53 eV for **4**, and 0.42 eV for **5**. Substantial reduction of reorganization energy was calculated with increasing atomic radii of the chalcogen, favoring increasing electron transfer rates from S- to Te-containing molecule. The decrease in the reorganization energy was not as great as observed from S to Se in $[\mu\text{-Se}(CH_2)_2\text{-}CHCH_3Se][Fe(CO)_3]_2$, where the energies decreased from 0.65 to 0.45 eV.[44] Interestingly, although the vertical ionizations shift significantly to lower energy with the heavier chalcogens, reflecting their greater donor ability, the reorganization energies also decrease down the series, and the

(81) Guerra, C. F.; Handgraaf, J. W.; Baerends, E. J.; Bickelhaupt, F. M. *J. Comput. Chem.* **2004**, *25*, 189.
(82) van der Vlugt, J. I.; Rauchfuss, T. B.; Whaley, C. M.; Wilson, S. R. *J. Am. Chem. Soc.* **2005**, *127*, 16012.
(83) Justice, A. K.; Zampella, G.; DeGioia, L.; Rauchfuss, T. B.; vanderVlugt, J. I.; Wilson, S. R. *Inorg. Chem.* **2007**, *46*, 1655.
(84) Justice, A. K.; Zampella, G.; Gioia, L. D.; Rauchfuss, T. B. *Chem. Commun.* **2007**, 2019.
(85) Justice, A. K.; Rauchfuss, T. B.; Wilson, S. R. *Angew. Chem., Int. Ed.* **2007**, *46*, 6152.
(86) Liu, T.; Darensbourg, M. Y. *J. Am. Chem. Soc.* **2007**, *129*, 7008.
(87) Thomas, C. M.; Darensbourg, M. Y.; Hall, M. B. *J. Inorg. Biochem.* **2007**, *101*, 1752.
(88) Peters, J. W. *Curr. Opin. Struct. Biol.* **1999**, *9*, 670.
(89) Nicolet, Y.; Piras, C.; Legrand, P.; Hatchikian, C.; Fontecilla-Camps, J. C. *Struct. Fold Des.* **1999**, *7*, 13.

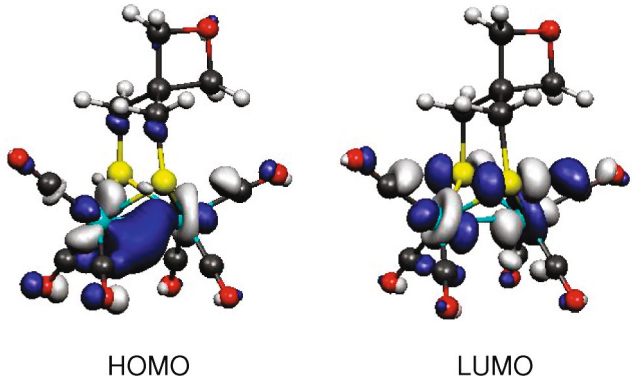

Figure 12. Highest occupied and lowest unoccupied orbitals of **3**.

consequence of the combination of these effects is that there is little shift, only about 0.1 eV overall, in the adiabatic ionization energies, as also seen in the oxidation potentials.

The trend in ionization energies and reorganization energies shows that as the bridging atoms change from S to Se to Te, the cations gain less stabilization in forming the "rotated" structures with the bridging carbonyls. This is counter to the usual expectation that as electron richness at the metal center increases, as shown by the carbonyl stretching frequencies for these molecules, the bridging carbonyl should become more favored because of its greater ability to withdraw and stabilize the electron density. The other important factor in these molecules is that as the chalcogen atoms become larger down the series, there is a corresponding increase in the Fe−Fe distance, such that the bridging carbonyl becomes less effective at favoring the rotated structure. The relative stability of the rotated structure is important to the reduction chemistry and catalysis discussed below.

From plots of the Kohn−Sham orbitals of the HOMO and LUMO, shown in Figure 12, the HOMO is primarily the metal−metal bonding interaction with delocalization of electron density to the carbonyl ligands. The tilt of the oxetane imparts some asymmetry to the HOMO. The LUMO consists mainly of the metal−metal antibonding interaction with some metal−chalcogen antibonding interaction of chalcogen p-orbitals.

The Kohn−Sham orbitals corresponding to the ionizations from 9.0 to 9.5 eV (see SI for orbital plots) were found to contain substantial chalcogen p-orbital character (HOMO−8 to HOMO−10). This is in agreement with the relative intensity of the ionizations observed in He I/He II photoelectron spectra. Also, the orbital (HOMO−11) above 9.5 eV is calculated to contain O 2p character. In addition to the above, mixing of chalcogen orbital characters with Fe and O orbital characters is consistent with the mixing suggested by the He I/He II photoelectron data.

The calculated oxidation and reduction potentials are displayed with the observed cyclic voltammograms in Figure 4. The calculated oxidation potentials that are shown correspond to cation structures without a bridging carbonyl ligand, similar to the neutral molecule. The good agreement between calculated and observed oxidation potentials and their trends suggests that the structures without bridging carbonyl ligands are favored in acetonitrile solution on the time scale of these experiments. Calculated oxidation potentials with a bridging carbonyl ligand in the cation structure gave oxidation potentials in the range 0.51−0.67 V, which agreed less well with experiment, although such structures cannot be ruled out with confidence on this basis.

Various structures also were explored for the anions of these molecules obtained by reduction. For the sulfur-containing molecule **3** the free energy of the structure with the rotated iron center and semibridging carbonyl is calculated to be the same (within 0.01 eV) as the free energy of the structure with the unrotated iron center. For the selenium-containing molecule **4** the free energy of the rotated structure is calculated to be 0.1 eV higher than the unrotated structure, and for the tellurium-containing molecule **5** the difference in free energy between these structures increases again to 0.2 eV. The global minimum structure for the dianions of all three molecules has a bridging carbonyl, along with one broken Fe−chalcogen bond, as found in the study of the corresponding benzenedithiolato[58] and ethanedithiolato[90] complexes. The decreasing favorability of the rotated structures in the anions from S to Se to Te parallels the observed increase in reversibility of the reduction of the Te molecule and the decrease in the rate of reduction of protons to hydrogen observed down this series. Previously, the rate of rotation of the $Fe(CO)_3$ unit has been correlated with the rate of cyanide substitution for carbonyl by an associative mechanism.[28,91] Similarly, these observations strongly indicate that the catalytic reduction of protons by these molecules is promoted by transformation to the rotated structure with the bridging carbonyl to open up the site for protonation and subsequent production of hydrogen.

Conclusion

Diiron dithiolato, diselenolato, and ditellurolato compounds containing an oxetane ring have been prepared in good yields as [FeFe]-hydrogenase models. The oxetane ring remarkably stabilizes the cyclic diselenium and ditellurium precursor compounds, which provides the opportunity to synthesize the homologous S, Se, and Te series **3**−**5**. The objective of this paper was to determine the basis for the difference in reorganization energy of 2Fe2Y (Y = S, Se, and Te) cores. Overall the electronic effects of substitution from S to Se to Te are small. The increasing donor ability of these bridge atoms, as reflected in both the decreasing carbonyl stretching frequencies and the decreasing vertical ionization energies, is compensated by the decreasing reorganization energies such that the adiabatic ionization energies and the electrochemical oxidation potentials occur within narrow energy ranges. The first reduction potentials occur in a similarly small range. However, despite these small changes in potentials, the rate of catalytic reduction of protons to hydrogen is substantially diminished from S to Se to Te. Also diminished is the calculated favorability of the anions to adopt the rotated structures with a bridging carbonyl ligand, which creates an open coordination site on an iron atom for protonation. The increasing size of the chalcogen atoms and the corresponding increasing distance between the iron atoms are likely factors in disfavoring the bridging carbonyl structures.

(90) Felton, G. A. N.; Petro, B. J.; Glass, R. S.; Lichtenberger, D. L.; Evans, D. H. *J. Am. Chem. Soc.* **2009**, *131*, 11290.
(91) Darensbourg, M. Y.; Lyon, E. J.; Zhao, X.; Georgakaki, I. P. *Proc. Natl. Acad. Sci. U.S.A.* **2003**, *100*, 3683.

Acknowledgment. Financial support for this work was provided by the DAAD (Ph.D. grant to M.H.), by the Studienstiftung des Deutschen Volkes (U.-P. Apfel), and by the National Science Foundation through the Collaborative Research in Chemistry program, Grant No. CHE 0527003 (D.H.E., R.S.G., and D.L.L.).

Supporting Information Available: Crystallographic data (excluding structure factors) have been deposited with the Cambridge Crystallographic Data Centre as supplementary publication CCDC-723576 for $Fe_2(\mu\text{-}S_2C_5H_8O)(CO)_6$ (**3**), CCDC-723577 for $Fe_2(\mu\text{-}Se_2C_5H_8O)(CO)_6$ (**4**), and CCDC-723578 for $Fe_2(\mu\text{-}Te_2C_5H_8O)(CO)_6$ (**5**). Copies of the data can be obtained free of charge on application to CCDC, 12 Union Road, Cambridge CB2 1EZ, UK [e-mail: deposit@ccdc.cam.ac.uk]. Supporting Information contains sample input files for calculations, optimized Cartesian coordinates and total energies for all structures, pictures of molecular structures and frontier orbitals, comparison of experimental and calculated geometries, calculated oxidation and reduction potentials, and CV diagrams. This material is available free of charge via the Internet at http://pubs.acs.org.

3.5 [MK5] Synthesis and Characterization of [FeFe]-Hydrogenases Models with Bridging Moieties Containing (S, Se) and (S, Te).

M. K. Harb, H. Görls, L. T. Lockett, G. A. N. Felton, D. H. Evans, R. S. Glass, D. L. Lichtenberger, M. El-khateeb, W. Weigand.

***Eur. J. Inorg. Chem.* 2010, Accepted.**

Job/Unit: I10278 /KAP1 Date: 18-06-10 11:01:49 Pages: 11

DOI: 10.1002/ejic.201000278

Synthesis and Characterization of [FeFe]-Hydrogenase Models with Bridging Moieties Containing (S, Se) and (S, Te)

Mohammad K. Harb,[a] Helmar Görls,[a] Taka Sakamoto,[b] Greg A. N. Felton,[c] Dennis H. Evans,*[d] Richard S. Glass,*[b] Dennis L. Lichtenberger,*[b] Mohammad El-khateeb,[e] and Wolfgang Weigand*[a]

Dedicated to Prof. Reinhold Tacke on the occasion of his 60th birthday.

Keywords: Iron / Hydrogenases / Tellurium / Selenium / Sulfur / Electrocatalysis

[FeFe]-hydrogenase-active-site models containing larger chalcogens such as Se or Te have exhibited greater electron richness at the metal centers and smaller gas-phase ionization energies and reorganization energies relative to molecules containing S atoms. Diiron complexes related to the much-studied molecule $[Fe_2(\mu\text{-}SC_3H_6S)(CO)_6]$ (**1**) have been prepared with one S atom replaced either by one Se atom to give $[Fe_2(\mu\text{-}SC_3H_6Se)(CO)_6]$ (**2**) or by one Te atom to give $[Fe_2(\mu\text{-}SC_3H_6Te)(CO)_6]$ (**3**). The molecules have been characterized by use of mass spectrometry and $^{13}C\{^1H\}$ NMR, $^{77}Se\{^1H\}$ NMR, IR, and photoelectron spectroscopic techniques along with structure determination with single-crystal X-ray diffraction, electrochemical measurements, and DFT calculations. He I photoelectron spectra and DFT computations of **2** and **3** show a lowering of ionization energies relative to those of the all-sulfur complex **1**, indicating increased electron richness at the metal centers that favors electrocatalytic reduction of protons from weak acids to produce H_2. However, chalcogen substitution from S to Se or Te also causes an increase in the Fe–Fe bond length, which disfavors the formation of a carbonyl-bridged "rotated" structure, as also shown by the photoelectron spectra and computations. This "rotated" structure is believed to be important in the mechanism of H_2 production. As a consequence of the competing influences of increased electron richness at the metals with less favorable "rotated" structures, the catalytic efficiency of the Se and Te molecules **2** and **3** is found to be comparable to that of molecule **1**.

Introduction

The importance of developing clean renewable energy sources and fuels is rising with the increasing depletion of global fossil fuel reserves and the increasing demand to reduce our carbon footprint. One potential alternative for fuel and energy storage is hydrogen gas. [FeFe]-hydrogenase is one of the enzymes that produce H_2 in nature,[1–3] and H_2 is one of cleanest renewable fuels available today.[4–11] Several [FeFe]-hydrogenase-active-site biomimetic compounds[12–32] containing dithiolato,[12–33] diselenolato,[33–38] or ditellurolato[33,39–41] bridging ligands have been prepared, characterized, and evaluated for the electrocatalytic production of H_2 from weak acids.

Recent spectroscopic and computational studies have revealed that substitution of S by Se or Te in the $Fe_2S_2(CO)_6$ core of [FeFe]-hydrogenase models results in lower ionization and reorganization energies for the Se or Te compounds,[35,39–42] which may lead to faster electron transfer rates and more active catalysts. However, the rate of catalytic reduction was found to be substantially diminished as the size of chalcogen increased,[39–41] which was the in contrast to one previous finding.[35] Hence, further study on complexes containing heavier chalcogens rather than a S atom is warranted.

In this paper we elucidate the influence of the chalcogen on the electrocatalytic production of H_2 from [FeFe]-hydrogenase model complexes by utilizing mixed dichalcogenolato ligands. As a continuation of our previous studies in this area,[23–25,35,36,43] a series of homologous compounds **1** through **3** (Scheme 1) was prepared and evaluated with use of electrochemistry, photoelectron spectroscopy (PES), and density functional theory (DFT) calculations. Compounds

[a] Institut für Anorganische und Analytische Chemie, Friedrich-Schiller-Universität Jena, August-Bebel-Straße 2, 07743 Jena, Germany
[b] Department of Chemistry and Biochemistry, The University of Arizona, Tucson, AZ, 85721, USA
[c] Department of Chemistry, Oakland University, Rochester, MI, 48309, USA
[d] Department of Chemistry, Purdue University, West Lafayette, IN, 47907, USA
[e] Chemistry Department, Jordan University of Science and Technology, 22110 Irbid, Jordan
Supporting information for this article is available on the WWW under http://dx.doi.org/10.1002/ejic.201000278.

 © 0000 Wiley-VCH Verlag GmbH & Co. KGaA, Weinheim

2 and **3** allow direct comparison with dithiolato compound **1**, extensively studied for its ability to catalyze the formation of H_2 from weak acids.

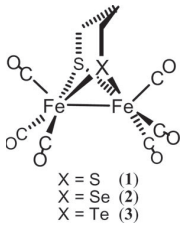

Scheme 1. Mixed dichalcogen [FeFe]-hydrogenase model compounds.

Results and Discussion

Reaction of 1,2-Thiaselenolane (4) and 1,2-Thiatellurolane (5) with $Fe_3(CO)_{12}$

Treatment of $Fe_3(CO)_{12}$ with 1,2-thiaselenolane (**4**) or 1,2-thiatellurolane (**5**) in THF under reflux resulted in the formation of diiron complexes $[Fe_2(\mu\text{-}SC_3H_6Se)(CO)_6]$ (**2**) or $[Fe_2(\mu\text{-}SC_3H_6Te)(CO)_6]$ (**3**), respectively (Scheme 2). Compounds **2** and **3** are air-stable in the solid state and for several hours in solution. These compounds have been characterized by IR, multinuclear NMR spectroscopy, mass spectrometry, and elemental analysis, as well as by X-ray crystallography. The ^1H NMR spectra of **2** and **3** exhibit three signals for the three different CH_2 moieties at 1.73 (CH_2), 2.11 (SCH_2), and 2.12 ($SeCH_2$) ppm for **2** and 1.46 (CH_2), 2.01 (SCH_2), and 2.29 ($TeCH_2$) ppm for **3**. The ^1H NMR resonances of the SCH_2 group in **2** and **3** are shifted upfield relative to that reported for the propanedithiolate (PDT) complex **1** (2.26 ppm).[21,32] The $SeCH_2$ and $TeCH_2$ proton resonances in **2** and **3** are also shifted to higher field relative to those reported for propanediselenolato (PDSe) (2.19 ppm)[36] and propaneditellurolato (PDTe) (2.3 ppm)[44] complexes. The $^{13}C\{^1H\}$ NMR spectra of **2** and **3** display three resonances at 13.1 ($SeCH_2$), 24.7 (SCH_2), and 30.3 ppm ($SeCH_2CH_2$) for **2** and at –9.4 ($TeCH_2$), 30.2 (SCH_2), 31.9 ($TeCH_2CH_2$) ppm for **3**. The ^{13}C resonance of $TeCH_2$ in **3** is significantly shifted to higher field relative to the respective resonances of SCH_2 and $SeCH_2$, which could be attributed to the "heavy atom" effect.[45] In addition, the expected resonances for the carbonyl groups were observed in the spectra. One signal was observed at δ = 132.9 ppm in the $^1H^{77}Se$ HMBC NMR spectrum of **2**, which was shifted upfield relative to those reported for PDSe (145 ppm).[36] The ^{125}Te NMR spectrum of **3** exhibits a signal at δ = 177 ppm. The mass spectra of **2** and **3** show the molecular ion peaks followed by several peaks obtained by loss of CO groups.

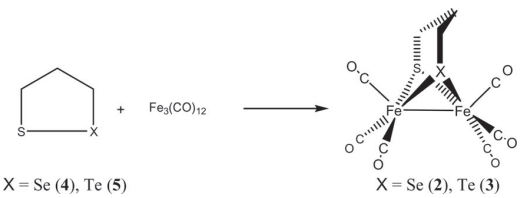

Scheme 2. The reaction of 1,2-thiaselenolane (**4**) and 1,2-thiatellurolane (**5**) with $Fe_3(CO)_{12}$ in THF.

The X-ray crystallographic structure analyses reveal the proposed structures of **2** and **3** as shown in Figures 1 and 2, and details of the crystal data are presented in Table 1. The central [2FeSX] (X = Se, Te) moieties of **2** and **3** are in the butterfly conformation, and the coordination geometry around the iron cores is rather similar to those reported for **1** and for the PDSe and PDTe complexes.[22,36,44] These Fe–Fe distances increase according to the trend **1** < **2** < PDSe < **3** < PDTe [with values of 2.5103(11) < 2.5373(9) < 2.5610(8) < 2.5736(10) < 2.633(1) Å, respectively], which is attributed to the increase in the atom size from S through Se to Te.[22,36,44] As observed in **1**, PDSe, and PDTe, the C2 methylene group of **2** and **3** is disordered over two positions with 50% probability.[22,36,44] Disorder also is likely between the location of the chalcogen atoms, especially in the case of the S and Se atoms of molecule **2**, where the Fe–Se and

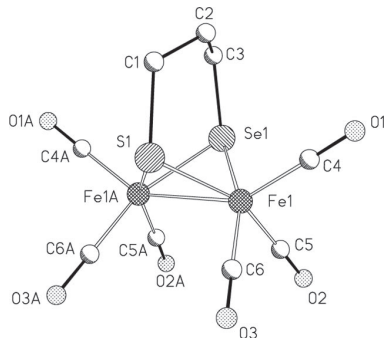

Figure 1. ORTEP drawing of $[Fe_2(\mu\text{-}SC_3H_6Se\text{-}\mu)(CO)_6]$ (**2**) at the 50% probability level (hydrogen atoms and the disordered C2 are omitted for clarity). Selected distances (Å) and angles (°): Fe1–Fe1A 2.5374(9), Fe1–S1 2.28(2), Fe1–Se1 2.332(4), Fe1–S1–Fe1A 67.7(7), Fe1–Se1–Fe1A 65.91(11).

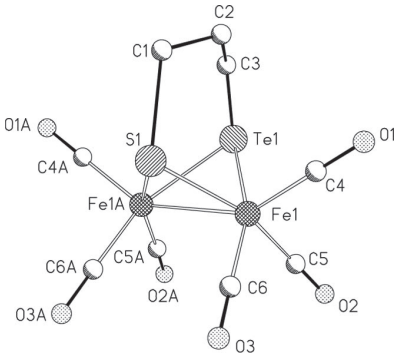

Figure 2. ORTEP drawing of $[Fe_2(\mu\text{-}SC_3H_6Te\text{-}\mu)(CO)_6]$ (**3**) at the 50% probability level (hydrogen atoms and the disordered C2 are omitted for clarity). Selected distances (Å) and angles (°): Fe1–Fe1A 2.574(1), Fe1–S1 2.256(7), Fe1–Te1 2.5074(9), Fe1–S1–Fe1A 69.5(3), Fe1–Te2–Fe1A 61.76(3).

 © 0000 Wiley-VCH Verlag GmbH & Co. KGaA, Weinheim

Fe–S distances from the structure determination differ by only 0.01 Å despite the difference in the sizes of the Se and S atoms. The covalent radius of Se is 0.15 Å greater than that of S,[46] and the computations that are discussed later optimize the Fe–Se distance at a value 0.15 Å longer than the Fe–S distance; the Fe–chalcogen distance from the crystal structure determination is intermediate between the values optimized in the computations.

Table 1. Crystal data and refinement details for the X-ray structure determinations of compounds **2** and **3**.

Compound	**2**	**3**
Formula	$C_9H_6Fe_2O_6SSe$	$>C_9H_6Fe_2O_6STe$
Fw (g mol^{-1})	432.86	481.50
T (°C)	–90(2)	–90(2)
Crystal system	Monoclinic	Monoclinic
Space group	$P2_1/m$	$P2_1/m$
a (Å)	6.8382(4)	6.9666(4)
b (Å)	13.3846(8)	13.3599(8)
c (Å)	7.9201(3)	8.0803(3)
β (°)	108.323(3)	109.792(3)
Z	2	2
ρ (g cm^{-3})	2.089	2.260
μ (cm^{-1})	49.19	42.32
Measured data	5614	4544
Data with $I>2\sigma(I)$	1487	1402
Unique data/R_{int}	1636/0.0632	1676/0.0336
wR_2 (all data, on F^2)[a]	0.1327	0.0889
R_1 [$I>2\sigma(I)$][a]	0.0477	0.0304
s[b]	1.043	1.018
Res. dens. (e Å^{-3})	1.360/–1.691	0.637/–0.913
Absorpt. method	NONE	NONE
CCDC No.	726555	726556

[a] Definition of the R indices: $R_1 = (\Sigma||F_o| - |F_c||)/\Sigma|F_o|$; $wR_2 = \{\Sigma[w(F_o^2-F_c^2)^2]/\Sigma[w(F_o^2)^2]\}^{1/2}$ with $w^{-1} = \sigma^2(F_o^2) + (aP)^2 + bP$; $P = [2F_c^2 + \mathrm{Max}(F_o)^2]/3$. [b] $s = \{\Sigma[w(F_o^2 - F_c^2)^2]/(N_o - N_p)\}^{1/2}$.

The IR spectra of complexes **2** and **3** exhibit three strong absorption bands with a KBr disk and four strong absorption bands in Nujol in the range 2071–1988 cm^{-1} for **2** and 2065–1983 cm^{-1} for **3**. These data are in the typical range of such model complexes.[16,17,20,22,24,36,47–49] For comparison, the carbonyl stretching frequencies of the all-sulfur PDT molecule **1** measured under the same conditions are in the range 2074–1990 cm^{-1}. The down-shifting of the CO absorption bands to lower frequencies from **1** through **2** to **3** is an indication of the increased π back-donation between the diiron center and the CO ligand caused by the rising donor ability of the chalcogen from S through Se to Te. The shifts are about half that observed when both S atoms are replaced by heavier chalcogens in other [FeFe]-hydrogenase model compounds.[39–41]

Electrochemical Investigations

The electrochemical behavior of compounds **1**–**3** has been investigated along with the ability of these complexes to catalyze the reduction of the weak acid acetic acid to form dihydrogen and acetate. Figure 3 presents two voltammograms for each compound, one with an initial negative-going sweep (right) to investigate cathodic processes, and one with an initial positive-going sweep (left) to explore anodic reactions.

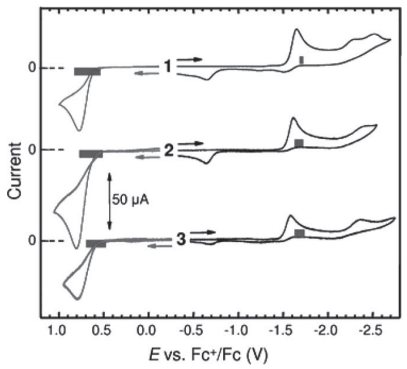

Figure 3. Voltammograms of ca. 1 mM **1**–**3** obtained in acetonitrile containing 0.10 M tetra-*n*-butylammonium hexafluorophosphate by using a glassy carbon working electrode (0.100 V/s). The gray bars represent the range of DFT-calculated oxidation and reduction potentials.

All three compounds show one principal cathodic peak near –1.6 V vs. Fc^+/Fc, whose height corresponds to slightly more than an overall one-electron reduction. The peak potentials are –1.652, –1.618, and –1.585 V for **1**, **2**, and **3**, respectively. The reduction is irreversible for **2** and **3** except at larger scan rates (1–5 V/s), where some chemical reversibility is observed and where the peak current function ($i_{p,c}/v^{1/2}$) decreases slightly, probably approaching the one-electron level as recently noted for μ-(1,2-ethanedithiolato)-diironhexacarbonyl (EDT).[50] Compound **1** shows some chemical reversibility even at 0.10 V/s (Figure 3). For all three compounds, additional cathodic processes are detected at potentials past –2 V.

On the return sweep of these voltammograms, an anodic peak is seen near –0.6 to –0.7 V, which is due to oxidation of a product formed at the first reduction peak. This peak is present, though smaller, in voltammograms where the scan is reversed just past the first cathodic peak.

Scans initiated in the positive direction (Figure 3) show an irreversible anodic peak whose height varies among the three compounds. The peak potentials are similar, +0.773, +0.802, and +0.791 for **1**, **2**, and **3**, respectively. Clearly, substitution of one of the sulfur atoms of **1** by selenium (**2**) or tellurium (**3**) has only a minor effect on the ease of oxidation of the complexes, as discussed with the photoelectron spectra and electronic structure of these molecules.

As noted above, however, there is a modest but significant increase in the ease of reduction along the series **1**–**3**, cathodic peak potentials moving to less negative values by about 67 mV. Almost exactly the same shift in potential was observed for a series of oxetane-containing dichalcogenolato $Fe_2(CO)_6$ complexes shown in Scheme 3, [(μ-$S_2C_5H_8O$){$Fe(CO)_3$}$_2$] (OxDT), [(μ-$Se_2C_5H_8O$){$Fe(CO)_3$}$_2$] (OxDSe), and [(μ-$Te_2C_5H_8O$){$Fe(CO)_3$}$_2$] (OxDTe), in which, however, both chalcogens were changed.[33]

 © 0000 Wiley-VCH Verlag GmbH & Co. KGaA, Weinheim

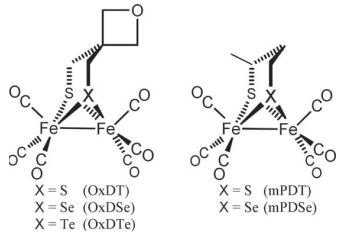

Scheme 3. $[(\mu\text{-}X_2C_5H_8O)\{Fe(CO)_3\}_2]$ (X = S, Se, Te) and $[\{\mu\text{-}S(CH_2)_2CHCH_3S\}\{Fe(CO)_3\}_2]$ (X = S, Se).

Catalysis of the Reduction of a Weak Acid

Complexes similar to **1**–**3** are known to catalyze the reduction of acids.[51] A typical acid for the evaluation of catalytic efficiency is acetic acid (pK_a = 22.3 in acetonitrile[52]) and a typical observation for such a weak acid is that catalytic reduction does not take place at the reduction peak of the catalyst but at a rather more negative potential. Such is the case for all three of these complexes. As acid is added, the reduction peak of the catalyst is hardly affected, but there appears a new peak in the range –1.8 to –2.5 V, which grows in height more or less linearly with the concentration of acid. Results for 1 mM catalyst and 50 mM acetic acid are shown in Figure 4. For all complexes, the catalytic peak is rather drawn-out along the potential axis, and for compound **1** there is evidence for resolution of the catalytic peak into two or three separate processes (Figure 4).

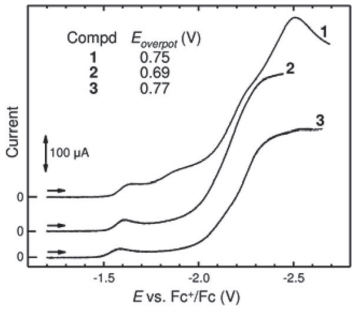

Figure 4. Voltammograms of ca. 1 mM **1**–**3** in the presence of 50 mM acetic acid. Other conditions as in Figure 3. Return scans are omitted for clarity. The overpotential, $E_{overpot}$, is the difference between the potential at which the catalytic current is half its maximum value and the standard potential for the reduction of acetic acid, –1.46 V.

It is difficult to evaluate the catalytic efficiency of these complexes, because considerable direct reduction of acetic acid occurs at the glassy carbon working electrode. The current obtained with 50 mM acetic acid alone (no catalyst) reaches 300 µA at –2.4 V.[53] However, the currents obtained for 50 mM acetic acid and 1 mM **1**–**3** greatly exceed this amount, so these complexes can be described as moderately good catalysts.

Another measure of efficiency is the overpotential, defined in this case as the difference between the potential at which the catalytic current is half its maximum value and the standard potential for the reduction of acetic acid in acetonitrile, –1.46 V. The overpotential, $E_{overpot}$, (shown in Figure 4) ranges from 0.69 to 0.77 V, not unlike other similar complexes.[51]

Photoelectron Spectroscopy

Photoelectron spectroscopy provides an experimental measure of the electron energies and molecular reorganization energies of the molecules and helps to quantify the trends in electronic structure in this series of molecules. The ionization energies also are well-defined energy quantities for validation of the electron energies from computational methods and provide a foundation for modeling the electrochemistry and chemical behavior (vide infra). The valence photoelectron spectra of these molecules are compared in Figure 5.

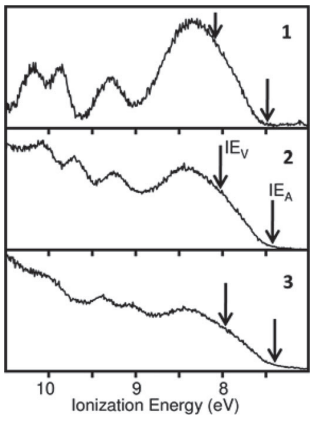

Figure 5. He I photoelectron spectra of **1**–**3**. The arrows near 7.5 eV are the DFT-calculated adiabatic ionization energies, IE_A, and the arrows near 8 eV are the DFT-calculated vertical ionization energies, IE_V. The energy difference between IE_V and IE_A for each molecule is the reorganization energy to the optimum geometry of the cation.

The general assignments of the ionizations are based on previously reported analogous compounds.[33,36,54] The energy region displayed in the spectra contains the valence ionizations from the Fe-based 3d orbitals and the chalcogen-based p orbitals. The first broad ionization profile of each molecule, from about 7.5 to 8.8 eV ionization energy, arises predominantly from combinations of the Fe d-based orbitals with a weak shoulder on the low-ionization-energy side corresponding to ionization from the HOMO of the molecule. The chalcogen-based valence p-orbital ionizations, S through Te, are expected to be observed in the higher-energy-ionization side of this region, on the basis of previously reported photoelectron spectra of chalcogen-containing [FeFe]-hydrogenase model compounds.[33,36,54] The second and third distinct ionization bands, above 9.0 eV, are assigned as having a mixture of chalcogen character and Fe d orbitals from previous studies.[33,36,54] These ionization energies decrease substantially with substitution from S through Se to Te, as expected from the decreasing

 © 0000 Wiley-VCH Verlag GmbH & Co. KGaA, Weinheim

electronegativity of the atoms and the decreasing inherent stability of the atomic orbitals.

However, the leading ionization band changes very little with chalcogen substitution, except for the difference in the instrument's baseline scatter for the different data collections. A close examination of the band profile (Figure S2 in the Supporting Information) shows that the onsets of the ionization bands shift by only about 0.1 eV from molecule **1** (ca. 7.5 eV) to molecule **3** (ca. 7.4 eV). The onset of the ionization band typically approximates the adiabatic ionization energy for removal of an electron from the HOMO, in which the molecule has relaxed to the optimum geometry of the positive molecule ion. The spectra suggest that the expected lowering of the adiabatic ionization due to the increased electron richness at the metals from **1** through **2** to **3**, as evidenced by the decrease in carbonyl stretching frequencies, is counterbalanced somewhat by a decrease in the molecular reorganization energies. This suggestion is consistent with previous studies[33,36,54] and is examined further in the following section.

Computational Results

Electronic structure calculations can provide additional understanding of the electronic structure and chemical properties of a chemical system, provided the calculations are appropriately validated against experimental structures, spectroscopic observations, electrochemical measurements, and thermodynamic properties. The DFT computational methodology utilized in this study has previously been shown to give good quantitative agreement with the structures, carbonyl stretching frequencies, oxidation potentials, reduction potentials, bond energies, and p*K*a values of a variety of [FeFe]-hydrogenase model compounds.[33,36,54–56] It is important to re-examine the validity of a method for each new class of molecules.

For the particular case of the substitutions of S, Se, and Te atoms in the molecules of this study, the optimized geometries from the computations agree very well with the crystal structure determinations. Key structural parameters are compared in Table S1 in the Supporting Information. For molecule **1**, the largest deviations in bond lengths are about 0.02 Å, and angles are well within a degree, except for the averaged angles in the experimental structure of the propane linkage between the S atoms, which is 50% disordered between two conformations in the crystal, as noted earlier. Most important is the Fe–Fe distance, which agrees within 0.01 Å. Molecule **2** shows evidence of additional disorder through interchange of the S and Se atoms in the crystal, as discussed earlier. However, this disorder does not seriously affect the determination of the Fe–Fe distance, which the computations match within 0.001 Å. Similar disorder may be present for molecule **3**, and a relatively flat potential energy surface for bonding to Te has been noted earlier, but the calculated Fe–Fe distance still agrees with the experimental value within 0.02 Å. Both experimental results and computations show an increasing Fe–Fe distance from **1** through **2** to **3**.

Agreement between the experimental and optimized structures does not necessarily mean that the computations yield sufficiently reasonable electron distributions and energies. The carbonyl stretching frequencies are one measure that is sensitive to the electron richness at the metal center. The frequencies are obtained computationally from the multidimensional potential well about the equilibrium geometry of the molecule, and thus reflect the energy of small geometric distortions. Furthermore, the electronic coupling and interaction force constants between the carbonyl vibrations are reflected in both the splitting and the intensities of the IR absorptions. Simulation of carbonyl stretching frequencies has become an important contribution to the understanding of hydrogenase active sites and hydrogenase mimics.[57,58] Figure S1 in the Supporting Information shows the good agreement between the observed and simulated IR absorption frequencies and intensities, and most particularly the shift of the vibrations to lower frequency from **1** through **2** to **3** with increasing donor ability from S through Se to Te. The increased electron-donor ability of heavier chalcogens is also evidenced in the computations by the increasing positive charge on these atoms. The Voronoi deformation electron densities[59] in the vicinity of the chalcogens decreased by 0.06 e^- from S to Se and by 0.10 e^- from Se to Te.

The computations also agree with the observations in the photoelectron spectra. The HOMO is calculated to be predominantly the Fe–Fe σ bond, as shown in Figure 6 for molecule **2**. This orbital is followed closely by six orbitals composed predominantly of the $3d^6$ electrons of the two Fe centers with some mixing of chalcogen p character, all clustered within an energy range of less than 1 eV. The orbitals with primary chalcogen character are found after a gap of approximately 0.5 eV, similar to the pattern observed in the photoelectron ionizations. Figures of these orbitals for all molecules are provided in the Supporting Information. The calculated first vertical ionization energies (IE_V, obtained by the ΔSCF difference in energy from the neutral molecule to the positive ion without change in geometry) and adiabatic ionization energies (IE_A, obtained by the ΔSCF method with full geometry optimization of the positive ion to its global minimum) are indicated by the arrows in Figure 5. The vertical ionization energies (calculated at 8.08 eV for **1**, 8.02 eV for **2**, and 7.97 eV for **3**) are difficult to define experimentally, because of the large number of broad overlapping ionizations in this region, but

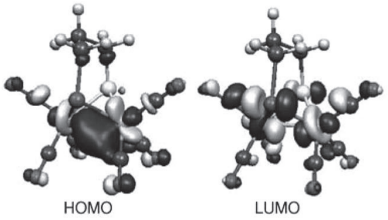

Figure 6. Highest-occupied and lowest-unoccupied molecular orbitals of **2**.

 © 0000 Wiley-VCH Verlag GmbH & Co. KGaA, Weinheim

the agreement between the calculated adiabatic ionization energies (7.48 eV for **1**, 7.43 eV for **2**, and 7.40 eV for **3**) and the onset of ionization band intensity in each spectrum illustrates the success of the computational model for these molecules.

On the basis of the Fe–Fe bonding character in the HOMO of the neutral molecule, one might expect the primary geometry relaxation in the positive ion to be a lengthening of the Fe–Fe distance, and indeed this is found when geometry optimization of the positive ion begins with the structure of the neutral molecule. However, a wider search of the potential energy surface finds a structure with a semibridging carbonyl group to be the global minimum. The optimized structure of the cation in the gas phase, shown in Figure 7, may be viewed as a rotation by approximately 60° of one $Fe(CO)_3$ group, which creates a vacant axial coordination site at the iron center.[60–64] This structure has been observed before and has been termed the "rotated" structure.[54,65–70] The stabilization energy from the nonbridged "unrotated" structure to the rotated structure is 0.28 eV for **1**, 0.25 eV for **2**, and 0.21 eV for **3**. The decrease in stabilization energy to the semibridged structure through the series may be related to both the increasing Fe–Fe distance and the greater electron richness at the metal centers.

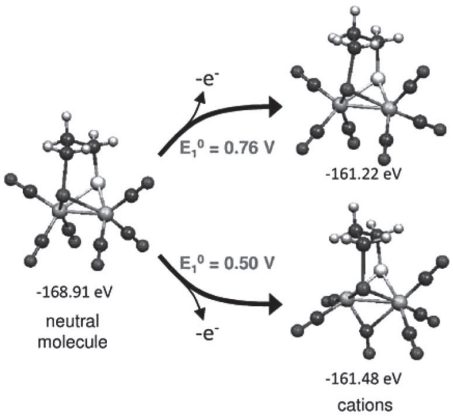

Figure 7. Calculated neutral and cation structures of molecule **2**. The cation structure without a bridging carbonyl group is at the top right, and the "rotated" cation structure with a semibridging carbonyl group is at the bottom right. The numbers in black are the gas-phase electronic energies, and the numbers in gray are the calculated solution oxidation potentials.

The total cation reorganization energy (ΔE_r) is the energy difference between the vertical ionization energy, IE_V, and the adiabatic ionization energy, IE_A. The ΔE_r energies are calculated to be 0.60 eV for **1**,[54] 0.58 eV for **2**, and 0.57 eV for **3**. The decrease in reorganization energies is visually apparent in Figure 5, where the energy separation between IE_V and IE_A decreases down the series. Also apparent in Figure 5 is the decrease in the vertical ionization energies, which follows the increase in electron richness at the metal centers from molecules **1** to **3**, but the decreasing reorganization energies reduces the shift (ca. 0.1 eV experimental, 0.08 eV calculated) of the adiabatic ionization energies through this series. The balance between these factors is important to the relative behavior of these molecules.

The largest contribution to the calculation of the electrochemical oxidation potentials is the adiabatic ionization energy, followed by differences in solvation energies and thermal contributions to the free energies of the neutral and ionized molecules. The calculated oxidation potentials of molecule **2** to the unrotated and rotated cation structures discussed above are shown in Figure 7 and compared with the cyclic voltammograms in Figure 3. An exact determination of the standard oxidation potential by cyclic voltammetry (CV) is not possible, because the process is not chemically reversible, and the rate of transformation to the rotated structure (with the lower oxidation potential) is not known, but the calculated oxidation potentials agree well with the region of oxidation processes in the voltammogram. Note also from Figure 7 that the 0.26 eV stabilization of the rotated structure relative to the unrotated structure of the cation is directly reflected in the difference of oxidation potentials to the two structures.

The calculated reduction potentials of molecule **2** are shown in Figure 8 and also compared with the cyclic voltammograms in Figure 3. The LUMO for accepting the electron consists mainly of the metal–metal antibonding interaction with some metal–chalcogen antibonding interaction of the chalcogen p orbitals, as shown in Figure 6. Similar to the removal of an electron from the HOMO, adding an electron into the LUMO also initiates geometric change. Various structures were explored for the anions of these molecules obtained by reduction, and the results suggest a complex thermodynamic and kinetic combination of reduction events. Reduction to the unrotated structure with an elongated metal–metal bond is favored initially, reduction to the rotated structure occurring at a more negative potential (more negative by 0.27 V for **1**, 0.21 V for **2**, and 0.18 V for **3**). The trend does not change if the conformation of the propane linker between the two chalcogens is changed from bending over the rotated iron, as shown in Figure 8, to bending over the unrotated iron. Reduction of the unrotated anion to the dianion at potentials more negative than –2 V leads directly to a structure with an extremely elongated metal–metal distance. However, the global minimum structure of the dianion has a bridging carbonyl ligand with one broken Fe–chalcogen bond, and reduction to this structure requires less negative potential than the first reduction of the neutral molecule to the anion. This is termed potential inversion and is similar to the process observed for the related molecule with a benzenedithiolato ligand.[55] Formation of the bridging carbonyl structure requires a substantial structural rearrangement of the nonbridging anion, such that kinetic factors become relevant on the CV time scale. Previously, **1** exhibited a greater-than-one-electron reduction under significantly slow CV scan rates.[71] Furthermore, the formation of the bridging dianion from a nonbridging anion through an energetically stable intermediate structure, becoming a two-electron reduction processes with decreased CV scan rates, was reported for EDT ■■ ((<=Author: Is this

 © 0000 Wiley-VCH Verlag GmbH & Co. KGaA, Weinheim

change ok?)) ■■ .[50] The reductions are not chemically reversible, and the calculations indicate potential inversion with the second reduction, so it is difficult to compare directly the calculated potentials with the observed CV results. However, as Figure 3 shows, the calculated reduction potentials are in the region of reduction events, perhaps slightly too negative, and confirm that there is little shift in potential between the molecules. This occurs again, because of the decreasing reorganization energies with change in charge. Because of the complexity of these reduction processes, we do not attempt further modeling of the reductions in the presence of acids in this contribution.

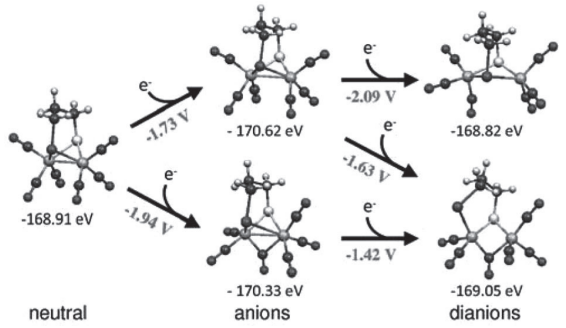

Figure 8. Calculated anion and dianion structures of molecule **2** with gas-phase electronic energies (black) and calculated solution reduction potentials (gray).

Conclusions

Synthesis and characterization of the mixed dichalcogenolato [FeFe]-hydrogenase model compounds related to the much-studied molecule $[Fe_2(\mu\text{-}SC_3H_6S)(CO)_6]$, where one sulfur atom is replaced by either a selenium atom or a tellurium atom, were successful. Combinations of experimental and computational analyses have provided useful insight into the electronic perturbations resulting from single chalcogen substitutions at the diiron core of the molecules. The crystal structures show the slight increase in the Fe–Fe distance with increasing size of the chalcogen atom. The increasing donor ability of chalcogens down the group and the corresponding greater electron richness at the iron centers in the molecules is evidenced spectroscopically by the lower carbonyl stretching frequencies and lower ionization energies for the molecules with heavier chalcogens. However, the influence of these electronic perturbations is muted for thermodynamic processes that involve a gain or loss of electrons from the molecules, such that the adiabatic ionization energies and initial oxidation and reduction potentials vary only slightly with chalcogen substitution. The reason is that the reorganization energy, ΔE_r, with electron transfer also decreases with substitution down the series, which counterbalances the influence of increasing electron richness at the metals. The longer Fe–Fe distances in the neutral molecules and the decreasing stabilization energies from the unrotated structure to the rotated structure with a semibridging carbonyl ligand in the ions are important factors in these trends. The computations agree well with these observations.

Reduction processes both with and without weak acid are studied to –2.7 V. Computations find that a number of structural transformations are possible for the anions and dianions that are formed in this range. A dianion structure with a bridging carbonyl and broken iron–chalcogen bond is found to be most stable in solution, suggesting an inversion of potential with the first reduction and the possibility for a greater-than-one-electron transfer in the first reduction peak, depending on the rate of transformation to the rotated structure with the broken iron–chalcogen bond. A slightly greater-than-one-electron process is observed in the first reduction peak for molecule **1** at the scan rate of this study, where the kinetic transformation may be favored over the heavier chalcogens by the shorter Fe–Fe distance and the greater reorganization energy. The thermodynamic and kinetic complexity of the reductions obviates a detailed structural and mechanistic modeling of the reduction of protons to H_2. Experimentally, the catalytic efficiency for the reduction of protons is found to be similar for the three molecules, with overall similar overpotentials and catalytic peak currents. This similarity is consistent with the balance between electronic structure and energy factors discussed above.

Experimental Section

General Comments: All reactions were performed by using standard Schlenk and vacuum-line techniques under an argon atmosphere. All solvents were purchased from Fisher Scientific and dried and distilled prior to use according to standard methods. $Fe_3(CO)_{12}$ (purchased from Aldrich) and other chemicals (purchased from Acros) were used without further purification. The ^1H, $^{13}C\{^1H\}$, $^{77}Se\{^1H\}$, and 2D NMR (^1H,^1H COSY, ^1H,^{13}C HSQC, ^1H,^{77}Se HMBC) spectra were recorded with a Bruker AVANCE 200 or 400 MHz spectrometer by using the solvent residual peak (^1H, $^{13}C\{^1H\}$ NMR) or a concentrated solution of SeO_2 in D_2O as reference. The ^{77}Se chemical shifts are reported relative to neat Me_2Se [$\delta(Me_2Se) = \delta(SeO_2) + 1302.6$ ppm].[72] The ^{125}Te chemical shift was measured vs. external PhTeTePh and converted to that of Me_2Te. Mass spectra were recorded with a FINNIGAN MAT SSQ 710 instrument. IR spectra were measured with a Perkin–Elmer System 2000 FTIR spectrometer and in Nujol with a Thermo Nicolet Avatar ESP 380 FTIR spectrometer utilizing the OMNIC version 6.1 software. Elemental analyses were performed with a LECO CHNS-932 apparatus. Silica gel 60 (0.015-0.040 mm) was used for column chromatography, TLC was done with Merck TLC aluminum sheets (Silica gel 60 F_{254}). Bis(bromomethyl)selenide,[73] bis(bromomethyl)sulfide,[53] 1,2-thiaselenolane (**4**),[74] and 1,2-thiatellurolane (**5**)[74] were prepared according to literature protocols. Yield calculations were based on the substoichiometric utilized chemicals or on $Fe_3(CO)_{12}$ for the diiron complexes.

$[Fe_2(\mu\text{-}SC_3H_6Se)(CO)_6]$ (2): Triirondodecacarbonyl (0.10 g, 0.20 mmol) and **4** (0.03 g, 0.20 mmol) were heated at reflux in THF (30 mL) for one hour. The solvent was removed from the resulting brown-red mixture under reduced pressure. The obtained solid was dissolved in a minimum amount of hexane and column chromatographed (SiO_2/hexane). From the major red fraction, **2** was ob-

 © 0000 Wiley-VCH Verlag GmbH & Co. KGaA, Weinheim

tained as a red solid (0.06 g, 69%). $C_9H_6Fe_2O_6SSe$ (433.77): calcd. C 24.97, H 1.40, S 7.41; found: C 25.09, H 1.36, S 7.23. IR (KBr disk): $\tilde{\nu}_{C\equiv O}$ = 2070 (s), 2030 (vs), 1993 (s), (Nujol) 2071 (s), 2031 (vs), 2000 (s), 1988 (s), 1977 (m) cm^{-1}. ^1H NMR (400 MHz, $CDCl_3$): δ = 1.73 (m, 2 H, $SeCH_2CH_2$), 2.11 (m, SCH_2), 2.12 (m, $SeCH_2$) ppm. $^{13}C\{^1H\}$ NMR (100 MHz, $CDCl_3$): δ = 13.1 ($SeCH_2$), 24.7 (SCH_2), 30.3 ($SeCH_2CH_2$), 208.2 (CO) ppm. ^1H ^{77}Se HMBC NMR (76 MHz, $CDCl_3$): δ = 132.9 ppm. DEI-MS: *m/z* = 434 $[M]^+$, 406 $[M - CO]^+$, 350 $[M - 3CO]^+$, 294 $[M - 5CO]^+$, 366 $[M - 6CO]^+$.

[Fe_2(μ-$STeC_3H_6Te$)$(CO)_6$] (3): Triirondodecacarbonyl (0.10 g, 0.20 mmol) and **5** (0.04 g, 0.2 mmol) in THF (30 mL) were heated at reflux. After one hour, the green solution became red-brown, and it was then allowed to cool to room temperature. The THF solvent was removed, and the obtained solid was dissolved in a minimum amount of hexane and column chromatographed (SiO_2/hexane). The red fraction containing complex **3** (0.03 g, 31%) was collected, and the hexane was removed. $C_9H_6Fe_2O_6STe{\cdot}0.67$hexane (540.84): calcd. C 28.97, H 2.87, S 5.95; found: C 28.83, H 2.43, S 6.34. IR (KBr disk): $\tilde{\nu}_{C\equiv O}$ = 2063 (s), 2024 (vs), 1989 (vs), (Nujol) 2065 (s), 2026 (vs), 1996 (s), 1983 (s), 1971 (m) cm^{-1}. ^1H NMR (400 MHz, $CDCl_3$): δ = 1.46 (m, 2 H, $TeCH_2CH_2$), 2.01 (m, 2 H, SCH_2), 2.29 (m, 2 H, $TeCH_2$) ppm. $^{13}C\{^1H\}$ NMR (100 MHz, $CDCl_3$): δ = –9.4 ($TeCH_2$), 30.2 (SCH_2), 31.9 ($TeCH_2CH_2$), 209.1 (CO) ppm. ^{125}Te NMR (158 MHz, $CDCl_3$): δ = 177 ppm. DEI-MS: *m/z* = 482 $[M]^+$, 454 $[M - CO]^+$, 426 $[M - 2CO]^+$, 398 $[M - 3CO]^+$, 368 $[M - 4CO]^+$, 342 $[M - 5CO]^+$, 314 $[M - 6CO]^+$.

Crystal Structure Determination: The intensity data for the compounds were collected with a Nonius KappaCCD diffractometer, by using graphite-monochromated Mo-K_α radiation. Data were corrected for Lorentz and polarization effects, but not for absorption effects.[75,76] The structures were solved by direct methods (SHELXS)[77] and refined by full-matrix least-squares techniques against F_o^2 (SHELXL-97).[78] All hydrogen atoms were included at calculated positions with fixed thermal parameters. All non-hydrogen atoms were refined anisotropically.[77] The (S, Se) and (S, Te) positions in **2** and **3** are superimposed. Crystallographic data (excluding structure factors) has been deposited with the Cambridge Crystallographic Data Centre. CCDC-726555 (for **2**) and -726556 (for **3**) contain the supplementary data for this paper. These data can be obtained free of charge from The Cambridge Crystallographic Data Centre via www.ccdc.cam.ac.uk/data_request/cif.

Electrochemical Measurements: Instrumentation and the source and treatment of solvent and supporting electrolyte have been reported earlier.[79] All potentials are reported vs. the potential of the ferrocenium/ferrocene (Fc^+/Fc) couple measured in acetonitrile. Voltammetric experiments were conducted at 298 K, by using approximately 1.0 mM of each compound in acetonitrile containing 0.10 M Bu_4NPF_6 on a Glassy Carbon working Electrode (GCE), under an Ar atmosphere. The area of the GCE was determined to be 0.0707 cm^2 from cyclic voltammetric studies of the oxidation of ferrocene in acetonitrile by using 2.5×10^{-5} cm^2/s as its diffusion coefficient.[79]

Photoelectron Spectroscopy: Photoelectron spectra were recorded by using an instrument that features a 36 cm radius hemispherical analyzer (McPherson),[80] with a custom-designed photon source, sample cells, detection, and control electronics. Calibration and data analysis were described previously.[81] In the figures of the photoelectron spectra, the spectra obtained with the He I source photons are represented by solid black lines. Both samples sublimed cleanly, with no visible changes in the spectra during data collection after initial observation of ionizations from the diiron complexes. The sublimation temperatures (at 10^{-5} Torr) were 37–39 and 40–44 °C for complexes **2** and **3**, respectively.

Density Functional Theory (DFT) Calculations: Computational methods have been developed previously for this class of diiron hexacarbonyl systems with S and Se heteroatoms in the bridging positions and validated by their ability to account for geometric structures, adiabatic ionization energies, carbonyl stretching frequencies, pK_a values, oxidation and reduction potentials, and other electrochemical parameters, as well as metal–metal and pertinent metal–ligand bond energies.[36,54–56] DFT calculations were carried out with the Amsterdam density functional (ADF2009.01b) package.[82,83] Geometry optimizations and frequency calculations (with no imaginary frequencies in the final geometries) were carried out by using the VWN functional with the Stoll correction implemented.[84] All electronic energies were obtained with the OPBE functional.[85] Comparison of the OPBE functional to other common functionals found it to be the best for the prediction of nuclear magnetic constants[86] and the only functional to correctly predict the spin states of seven different iron complexes.[85] All calculations utilized a triple-ζ Slater type orbital (STO) basis set with one polarization function (TZP) for H, C, O, Fe, S, Se, and Te. Relativistic effects by the zero-order regular approximation (ZORA)[87,88] were also applied during all calculations. The frozen-core approximation was used for the inner core of all heavy atoms. The theoretical stretching frequencies and IR absorption intensities for all species were calculated analytically with the same computing method as for the geometry optimizations and scaled by a factor of 1.002. For the simulated IR spectra in Figure S1, the linewidths are adjusted by a constant factor to approximate the linewidths in the experimental spectra. Figures of the optimized geometries and molecular orbital plots were created with the program Molekel.[89]

Supporting Information (see footnote on the first page of this article): Comparison of the experimental IR spectra (in Nujol) in the carbonyl stretching region (solid lines) with calculated IR spectra (dashed lines) for each of **1**–**3** (Figure S1); He I photoelectron spectra of the first ionization bands of molecules **1** (blue), **2** (green), and **3** (red) (Figure S2); calculated neutral and cation structures of **1** (Figure S3); highest occupied and lowest unoccupied orbitals, calculated structures (Figures S4–S13); calculated geometries (Tables S1–S11).

Acknowledgments

Financial support for this work was provided for M. K. H. by the Deutscher Akademischer Austausch Dienst (DAAD) and by the National Science Foundation through the Collaborative Research in Chemistry program, Grant No. CHE 0527003, (D. H. E., R. S. G. and D. L. L.).

[1] M. Frey, *ChemBioChem* **2002**, *3*, 153–160.
[2] P. M. Vignais, B. Billoud, *Chem. Rev.* **2007**, *107*, 4206–4272.
[3] A. L. De Lacey, V. M. Fernandez, M. Rousset, R. Cammack, *Chem. Rev.* **2007**, *107*, 4304–4330.
[4] Y. Nicolet, C. Cavazza, J. C. Fontecilla-Camps, *J. Inorg. Biochem.* **2002**, *91*, 1-8.
[5] S. Shima, O. Pilak, S. Vogt, M. Schick, M. S. Stagni, W. Meyer-Klaucke, E. Warkentin, R. K. Thauer, U. Ermler, *Science* **2008**, *321*, 572–575.
[6] R. Cammack, M. Frey, R. Robson, *Hydrogen as a Fuel: Learning from Nature*, Taylor & Francis, London, **2001**.
[7] R. Coontz, B. Hanson, *Science* **2004**, *305*, 957–975.
[8] A. Melis, L. Zhang, M. Forestier, M. L. Ghirardi, M. Seibert, *Plant Physiol.* **2000**, *122*, 127–136.

 © 0000 Wiley-VCH Verlag GmbH & Co. KGaA, Weinheim

[9] P. C. Hallenbeck, J. R. Benemann, *Int. J. Hydrogen Energy* **2002**, *27*, 1185–1193.
[10] P. Tamagnini, R. Axelsson, P. Lindberg, F. Oxelfelt, R. Wunschiers, P. Lindblad, *Microbiol. Mol. Biol. Rev.* **2002**, *66*, 1–20.
[11] T. Happe, A. Hemschemeier, M. Winkler, A. Kaminski, *Trends Plant Sci.* **2002**, *7*, 246–250.
[12] a) X. Zhao, I. P. Georgakaki, M. L. Miller, J. C. Yarbrough, M. Y. Darensbourg, *J. Am. Chem. Soc.* **2001**, *123*, 9710–9711; b) M. Y. Darensbourg, E. J. Lyon, J. J. Smee, *Coord. Chem. Rev.* **2000**, *206–207*, 533–561; c) D. J. Evans, C. J. Pickett, *Chem. Soc. Rev.* **2003**, *32*, 268–275; d) W. Lubitz, B. Tumas, *Chem. Rev.* **2007**, *107*, 3900–3903; e) L.-C. Song, *Acc. Chem. Res.* **2005**, *38*, 21–28; f) X. Liu, S. K. Ibrahim, C. Tard, C. J. Pickett, *Coord. Chem. Rev.* **2005**, *249*, 1641–1652; g) J.-F. Capon, F. Gloaguen, P. Schollhammer, J. Talarmin, *Coord. Chem. Rev.* **2005**, *249*, 1664–1676; h) J.-C. Fontecilla-Camps, A. Volbeda, C. Cavazza, Y. Nicolet, *Chem. Rev.* **2007**, *107*, 4273–4303; i) D. M. Heinekey, *J. Organomet. Chem.* **2009**, *694*, 2671–2680.
[13] X. Zhao, C. Chiang, M. L. Miller, M. V. Rampersad, M. Y. Darensbourg, *J. Am. Chem. Soc.* **2003**, *125*, 518–524.
[14] F. Gloaguen, J. D. Lawrence, M. Schmidt, S. R. Wilson, T. B. Rauchfuss, *J. Am. Chem. Soc.* **2001**, *123*, 12518–12527.
[15] J. D. Lawrence, H. Li, T. B. Rauchfuss, M. Benard, M. Rohmer, *Angew. Chem. Int. Ed.* **2001**, *40*, 1768–1771.
[16] H. Li, T. B. Rauchfuss, *J. Am. Chem. Soc.* **2002**, *124*, 726–727.
[17] S. Ott, M. Kritikos, B. Åkermark, L. Sun, *Angew. Chem. Int. Ed.* **2003**, *42*, 3285–3288.
[18] M. Razavet, S. C. Davies, D. L. Hughes, J. E. Barclay, D. J. Evans, S. A. Fairhurst, X. Liu, C. J. Pickett, *Dalton Trans.* **2003**, 586–595.
[19] C. Tard, X. Liu, S. K. Ibrahim, M. Bruschi, L. De Gioia, S. C. Davies, X. Yang, L.-S. Wang, G. Sawers, C. J. Pickett, *Nature* **2005**, *433*, 610–613.
[20] L.-C. Song, Z.-Y. Yang, H.-Z. Bian, Q.-M. Hu, *Organometallics* **2004**, *23*, 3082–3084.
[21] S. Ezzaher, J.-F. Capon, F. Gloaguen, F. Y. Pelìtillon, P. Schollhammer, J. Talarmin, N. Kervarec, *Inorg. Chem.* **2009**, *48*, 2-4.
[22] D. Seyferth, G. B. Womack, M. K. Gallagher, *Organometallics* **1987**, *6*, 283–294.
[23] U.-P. Apfel, Y. Halpin, H. Görls, J. G. Vos, B. Schweizer, G. Linti, W. Weigand, *Chem. Biodivers.* **2007**, *4*, 2138–2148.
[24] J. Windhager, M. Rudolph, S. Bräutigam, H. Görls, W. Weigand, *Eur. J. Inorg. Chem.* **2007**, 2748–2760.
[25] J. Windhager, H. Goerls, H. Petzold, G. Mloston, G. Linti, W. Weigand, *Eur. J. Inorg. Chem.* **2007**, 4462–4471.
[26] L.-C. Song, Z.-Y. Yang, H.-Z. Bian, Y. Liu, H.-T. Wang, X.-F. Liu, Q.-M. Hu, *Organometallics* **2005**, *24*, 6126–6135.
[27] S. Ezzaher, J.-F. Capon, F. Gloaguen, F. Y. Petillon, P. Schollhammer, J. Talarmin, *Inorg. Chem.* **2007**, *46*, 3426–3428.
[28] P. Orain, J.-F. Capon, N. Kervarec, F. Gloaguen, F. Petillon, R. Pichon, P. Schollhammer, J. Talarmin, *Dalton Trans.* **2007**, 3754–3756.
[29] T.-T. Zhang, M. Wang, N. Wang, P. Li, Z.-Y. Liu, L.-C. Sun, *Polyhedron* **2009**, *28*, 1138–1144.
[30] D. Morvan, J.-F. Capon, F. Gloaguen, F. Y. Pétillon, P. Schollhammer, J. Talarmin, J. Yaouanc, F. Michaud, N. Kervarec, *J. Organomet. Chem.* **2009**, *694*, 2801–2807.
[31] L.-C. Song, X. Luo, Y.-Z. Wang, B. Gai, Q.-M. Hu, *J. Organomet. Chem.* **2009**, *694*, 103–112.
[32] E. J. Lyon, I. P. Georgakaki, J. H. Rabenspies, M. Y. Darensbourg, *Angew. Chem. Int. Ed.* **1999**, *38*, 3178–3180.
[33] M. K. Harb, U.-P. Apfel, J. Kübel, H. Görls, G. A. N. Felton, T. Sakamoto, D. H. Evans, R. S. Glass, D. L. Lichtenberger, M. El-khateeb, W. Weigand, *Organometallics* **2009**, *28*, 6666–6675.
[34] S. Gao, J. Fan, S. Sun, X. Peng, X. Zhao, J. Hou, *Dalton Trans.* **2008**, 2128–2135.
[35] U.-P. Apfel, Y. Halpin, M. Gottschaldt, H. Görls, J. G. Vos, W. Weigand, *Eur. J. Inorg. Chem.* **2008**, 5112–5118.
[36] M. K. Harb, T. Niksch, J. Windhager, H. Görls, R. Holze, L. T. Lockett, N. Okumura, D. H. Evans, R. S. Glass, D. L. Lichtenberger, M. El-khateeb, W. Weigand, *Organometallics* **2009**, *28*, 1039–1048.
[37] L.-C. Song, B. Gai, H.-T. Wang, Q.-M. Hu, *J. Inorg. Biochem.* **2009**, *103*, 805–812.
[38] M. K. Harb, J. Windhager, A. Daraosheh, H. Görls, L. T. Lockett, N. Okumura, D. H. Evans, R. S. Glass, D. L. Lichtenberger, M. El-khateeb, W. Weigand, *Eur. J. Inorg. Chem.* **2009**, 3414–3420.
[39] J. C. Guillemin, G. Bajor, E. Riague, B. Khater, T. Veszpremi, *Organometallics* **2007**, *26*, 2507–2518.
[40] A. F. Cozzolino, N. E. Gruhn, D. L. Lichtenberger, I. Vargas-Baca, *Inorg. Chem.* **2008**, *47*, 6220–6226.
[41] M. A. Cranswick, N. E. Gruhn, O. Oorhles-Steele, K. R. Ruddick, N. Burzlaff, W. A. Schenk, D. L. Lichtenberger, *Inorg. Chim. Acta* **2008**, *361*, 1122–1133.
[42] L.-C. Song, B. Gai, H.-T. Wang, Q.-M. Hu, *J. Inorg. Biochem.* **2009**, *103*, 805–812.
[43] J. Windhager, R. A. Seidel, U.-P. Apfel, H. Görls, G. Linti, W. Weigand, *Chem. Biodivers.* **2008**, *5*, 2023–2041.
[44] M. Shieh, M. H. Shieh, *Organometallics* **1994**, *13*, 920–924.
[45] G. A. Kalabin, V. M. Bzhezovskii, D. F. Kushnarev, A. G. Proidakov, *Zh. Org. Khim.* **1981**, *17*, 1143.
[46] B. Cordero, V. Gomez, A. E. Platero-Prats, M. Reves, J. Echeverria, E. Cremades, F. Barragan, S. Alvarez, *Dalton Trans.* **2008**, 2832–2838.
[47] J. D. Lawrence, T. B. Rauchfuss, S. R. Wilson, *Inorg. Chem.* **2002**, *41*, 6193–6195.
[48] L.-C. Song, B.-S. Yin, Y.-L. Li, L.-Q. Zhao, J.-H. Ge, Z.-Y. Yang, Q.-M. Hu, *Organometallics* **2007**, *26*, 4921–4929.
[49] L.-C. Song, Z.-Y. Yang, Y.-J. Hua, H.-T. Wang, Y. Liu, Q.-M. Hu, *Organometallics* **2007**, *26*, 2106–2110.
[50] G. A. N. Felton, B. J. Petro, R. S. Glass, D. L. Lichtenberger, D. H. Evans, *J. Am. Chem. Soc.* **2009**, *131*, 11290–11291.
[51] G. A. N. Felton, C. A. Mebi, B. J. Petro, A. K. Vannucci, D. H. Evans, R. S. Glass, D. L. Lichtenberger, *J. Organomet. Chem.* **2009**, *694*, 2681–2699.
[52] K. Izutsu in *Acid-Base Dissociation Constants in Dipolar Aprotic Solvents*, Blackwell Scientific Publishers, Oxford, UK, **1990**.
[53] E. Weissflog, M. Schmidt, *Z. Anorg. Allg. Chem.* **1977**, *437*, 146–148.
[54] B. J. Petro, A. K. Vannucci, L. T. Lockett, C. Mebi, R. Kottani, N. E. Gruhn, G. S. Nichol, P. A. J. Goodyer, D. H. Evans, R. S. Glass, D. L. Lichtenberger, *J. Mol. Struct.* **2008**, *890*, 281–288.
[55] G. A. N. Felton, A. K. Vannucci, J. Chen, L. T. Lockett, N. Okumura, B. J. Petro, U. I. Zakai, D. H. Evans, R. S. Glass, D. L. Lichtenberger, *J. Am. Chem. Soc.* **2007**, *129*, 12521–12530.
[56] G. A. N. Felton, A. K. Vannucci, N. Okumura, L. T. Lockett, D. H. Evans, R. S. Glass, D. L. Lichtenberger, *Organometallics* **2008**, *27*, 4671–4679.
[57] J. W. Tye, M. Y. Darensbourg, M. B. Hall, *J. Comput. Chem.* **2006**, *27*, 1454–1462.
[58] J. W. Tye, M. Y. Darensbourg, M. B. Hall, *Inorg. Chem.* **2008**, *47*, 2380–2388.
[59] C. F. Guerra, J. W. Handgraaf, E. J. Baerends, F. M. Bickelhaupt, *J. Comput. Chem.* **2004**, *25*, 189–210.
[60] J. W. Peters, *Curr. Opin. Struct. Biol.* **1999**, *9*, 670–676.
[61] Y. Nicolet, C. Piras, P. Legrand, C. Hatchikian, J. C. Fontecilla-Camps, *Struct. Fold. Des.* **1999**, *7*, 13–23.
[62] M. W. Adams, *Biochim. Biophys. Acta* **1990**, *1020*, 115–145.
[63] M. W. W. Adams, L. E. Mortenson, *Biochim. Biophys. Acta Bioenerg.* **1984**, *766*, 51–61.
[64] J. Chen, D. K. Blanchard, *Biochem. Biophys. Res. Commun.* **1978**, *84*, 1144–1150.
[65] J. I. van der Vlugt, T. B. Rauchfuss, C. M. Whaley, S. R. Wilson, *J. Am. Chem. Soc.* **2005**, *127*, 16012–16013.
[66] A. K. Justice, G. Zampella, L. De Gioia, T. B. Rauchfuss, J. I. van der Vlugt, S. R. Wilson, *Inorg. Chem.* **2007**, *46*, 1655–1664.

 © 0000 Wiley-VCH Verlag GmbH & Co. KGaA, Weinheim

[67] A. K. Justice, G. Zampella, L. De Gioia, T. B. Rauchfuss, *Chem. Commun.* **2007**, 2019–2021.
[68] A. K. Justice, T. B. Rauchfuss, S. R. Wilson, *Angew. Chem. Int. Ed.* **2007**, *46*, 6152–6154.
[69] T. Liu, M. Y. Darensbourg, *J. Am. Chem. Soc.* **2007**, *129*, 7008–7009.
[70] C. M. Thomas, M. Y. Darensbourg, M. B. Hall, *J. Inorg. Biochem.* **2007**, *101*, 1752–1757.
[71] S. J. Borg, T. Behrsing, S. P. Best, M. Razavet, X. Liu, C. J. Pickett, *J. Am. Chem. Soc.* **2004**, *126*, 16988–16999.
[72] R. C. Burns, M. J. Collins, R. J. Gillespie, G. J. Schrobilgen, *Inorg. Chem.* **1986**, *25*, 4465–4469.
[73] E. Weissflog, *Phosphorus Sulfur Silicon Relat. Elem.* **1980**, *8*, 87–88.
[74] E. Block, E. V. Dikarev, R. S. Glass, J. Jin, B. Li, X. Li, S. Zhang, *J. Am. Chem. Soc.* **2006**, *128*, 14949–14961.
[75] B. V. Nonius, *COLLECT, Data Collection Software*, **1998**.
[76] Z. Otwinowski, W. Minor, "Processing of X-ray Diffraction Data Collected in Oscillation Mode" in *Methods in Enzymology, Vol. 276* (Ed.: C. W. Carter Jr.,), Elsevier, New York, **1997**, pp. 307–326 ■■ ((<=Author: Is this change ok?)) ■■ .
[77] G. M. Sheldrick, *Acta Crystallogr., Sect. A* **1990**, *46*, 467–473.
[78] G. M. Sheldrick, *SHELXL-97 (Release 97-2)*, University of Göttingen, Germany, **1997**.
[79] N. A. Macías-Ruvalcaba, D. H. Evans, *J. Phys. Chem. B* **2005**, *109*, 14642–14647.
[80] K. Siegbahn, C. Nordling, A. Fahlman, R. Nordberg, K. Hamrin, J. Hedman, G. Johansson, T. Bergmark, S. E. Karlsson, I. Lindgren, B. Lindberg, *Nova Acta Regiae Societatis Scientiarum Upsaliensis* **1967**, *20*, 282.
[81] M. A. Cranswick, A. Dawson, J. J. A. Cooney, N. E. Gruhn, D. L. Lichtenberger, J. H. Enemark, *Inorg. Chem.* **2007**, *46*, 10639–10646.
[82] G. Te Velde, F. M. Bickelhaupt, E. J. Baerends, C. Fonseca Guerra, S. J. A. Van Gisbergen, J. G. Snijders, T. Ziegler, *J. Comput. Chem.* **2001**, *22*, 931–967.
[83] ADF2009.01b, **2009**.
[84] H. Stoll, C. M. E. Pavlidou, H. Preuss, *Theor. Chim. Acta* **1978**, *49*, 143–149.
[85] M. Swart, A. W. Ehlers, K. Lammertsma, *Mol. Phys.* **2004**, *102*, 2467.
[86] Y. Zhang, H. Lin, D. G. Truhlar, *J. Chem. Theory Comput.* **2007**, *3*, 1378–1398.
[87] E. van Lenthe, A. Ehlers, E. Baerends, *J. Chem. Phys.* **1999**, *110*, 8943–8953.
[88] E. van Lenthe, E. J. Baerends, J. G. Snijders, *J. Chem. Phys.* **1993**, *99*, 4597–4610.
[89] S. Portmann, H. P. Luthi, *Chimia* **2000**, *54*, 766–769.

Received: March 11, 2010

 © 0000 Wiley-VCH Verlag GmbH & Co. KGaA, Weinheim

3.6 [MK6] [FeFe]-Hydrogenase Models Containing Different Length Diselenolato Bridging Moieties.

M. K. Harb, A. Daraosheh, H. Görls, R. S. Glass, D. L. Lichtenberger, M. El-khateeb, W. Weigand.

In Preparation.

DOI: 10.1002/ejic.200

[FeFe] Hydrogenase Models Containing Different Length Diselenolato Bridging Moieties

Mohammad K. Harb,[a] Ahmad Daraosheh,[a] Helmar Görls,[a] Dennis H. Evans,*[b] Richard S. Glass,*[c] Dennis L. Lichtenberger,*[c] Mohammad El-khateeb[d] and Wolfgang Weigand*[a]

Keywords: Iron / Selenium ligands / Hydrogenase / Bridging moieties / Electrocatalysis

Models of [FeFe]-hydrogenases containing diselenolato ligands with different length bridging moieties have been prepared. Treatment of $Fe_3(CO)_{12}$ with one equivalent of $NCSe(CH_2)_4SeCN$ (**1**) in thf at reflux afforded $Fe_2(\mu\text{-}Se(CH_2)_4Se\text{-}\mu)(CO)_6$ (**2**). However, treatment of $Fe_3(CO)_{12}$ with one equivalent of $NCSe(CH_2)_5SeCN$ (**3**) in thf at reflux afforded a mixture of diiron compound $Fe_2(\mu\text{-}Se(CH_2)_5Se\text{-}\mu)(CO)_6$ (**4**) and tetrairon complex $[Fe_2(\mu\text{-}Se(CH_2)_5Se\text{-}\mu)(CO)_6]_2$ (**5**). The analogues hexyl diiron $Fe_2(\mu\text{-}Se(CH_2)_6Se\text{-}\mu)(CO)_6$ (**6**) and tetrairon $[Fe_2(\mu\text{-}Se(CH_2)_6Se\text{-}\mu)(CO)_6]_2$ (**7**) complexes were also obtained from the reaction of $Fe_3(CO)_{12}$ with $NCSe(CH_2)_6SeCN$ (**8**). Compounds **2** and **4-7** were characterized by spectroscopic techniques including NMR, IR, mass spectrometry, elemental analysis and X-ray crystal structure analysis. The electrochemical investigation of complexes **2**, **4** and **6** under work, in order to prove to be good catalysts for proton reduction of the weak acid to give hydrogen.
(© WILEY-VCH Verlag GmbH & Co. KGaA, 69451 Weinheim, Germany, 2007)

[a] Institut für Anorganische und Analytische Chemie, Friedrich-Schiller-Universität Jena, August-Bebel-Straße 2, 07743 Jena, GERMANY
[b] Department of Chemistry, Purdue University, 560 Oval Drive, West Lafayette, IN, 47907, U.S.A
[c] Department of Chemistry, The University of Arizona, Tucson, AZ, 85721, U.S.A
[d] Chemistry Department, Jordan University of Science and Technology, 22110 Irbid, JORDAN

Introduction

Hydrogenase is a group of enzyme, which is capable of catalyzing the reversible reaction of hydrogen production from water ($2H^+ + 2e^- \Leftrightarrow H_2$).[1-5] [FeFe]-, [FeNi]- and [Fe]-hydrogenases are the main three kinds of hydrogenase.[6-8] Nowadays, these enzymes became very important because of diminution of fossil fuel recourses and their injurious to the environment. [FeFe]-hydrogenases have received more attention in biomimetic studies, due to their ability to hydrogen production.[9] Therefore, several models of [FeFe]-hydrogenases containing either [2Fe2S][10-26] or [2Fe3S][26-30] subcluster units have been reported (some examples of minimal models are shown in Scheme 1a). Recently, selenium homologues of [FeFe]-hydrogenases showing the [2Fe2Se] subunit were prepared (Scheme 1b).[31-35] The ability of these dithiolato and diselenolato complexes to catalyze the reversible hydrogenation process from week acids has been investigated.

Diiron ($Fe_2(\mu\text{-}S(CH_2)_4S)(CO)_6$[36] and tetrairon $[Fe_2(\mu\text{-}S(CH_2)_5S)(CO)_6]_2$[37] complexes have been reported. Darensbourg and co-workers[38] have carried out an optimization study of geometry of rotated and unrotated forms of ($Fe_2(\mu\text{-}S(CH_2)_xS)(CO)_6$, x = 2-5) to determine the role of the length of the dithiolato linker in the stabilization or destabilization energy of these systems. In this report, we launched a study to prepare diiron and tetrairon model complexes containing diselenolato ligands with different length bridging moieties, in order to elucidate the influence of the length of the bridging moieties on the properties of the target compounds.

Results and Discussion

Reaction of 1,4-diselenocyanatobutane (1) with $Fe_3(CO)_{12}$ Treatment of $Fe_3(CO)_{12}$ with $NCSe(CH_2)_4SeCN$ (**1**) under reflux in thf resulted in the formation of the diiron diselenolato complex $Fe_2(\mu\text{-}Se(CH_2)_4Se\text{-}\mu)(CO)_6$ (**2**) in 67% yield (Scheme 2). Complex **2**, which has been characterized by IR, multinuclear NMR spectroscopy, mass spectrometry, elemental analysis, as well as by X-ray crystallography, is air-stable in the solid state and for several hours in hexane solution. The ^1H NMR spectrum of **2** exhibits two signals in a 1:1 ratio for the two different CH_2 moieties at 1.75 ($2SeCH_2CH_2$) and 2.61 ($2SeCH_2$) ppm. These resonances are shifted highfield compared to that observed for propane diselenolato complex (PDS)[32] and downfield compared to the analogous sulfur containing complex $Fe_2(\mu\text{-}S(CH_2)_4S\text{-}\mu)(CO)_6$.[36] Its $^{13}C\{^1H\}$ NMR spectrum displays two resonances at 21.2 ($2SeCH_2$) and 25.5 ($2SeCH_2CH_2$) ppm. These resonances are comparable to those reported for PDS.[32] One signal was observed at 284 ppm in $^1H^{77}Se$ HMBC NMR spectrum of **2** indicating equivalent Se atoms. This value is shifted to higher field compared to that of PDS.[32]

The structure of **2** was examined by X-ray diffraction analysis (Figure 1). The central 2Fe2Se moiety of **2** shows butterfly conformation and the geometry around the iron atoms is distorted octahedral, as those observed for sulfur analogues and PDS.[32,34,36] The Fe-Fe bond distance in **2** was determined as 2.5370(10) Å, which is longer than those reported in the sulfur containing complexes.[36] The elongation of the Fe-Fe bond could be attributed the larger size of selenium atoms, while it is shorter than that reported for the PDS complex [2.5610(10) Å].[32] The Fe-Se bond lengths are comparable to those found for PDS and $Fe_2(\mu\text{-}SeCH_2CH_2Se)(CO)_6$.[32,34,39]

Reaction of 1,5-Diselenocyanatopentane (3) with $Fe_3(CO)_{12}$ The reaction of $Fe_3(CO)_{12}$ with $NCSe(CH_2)_5SeCN$ (**3**) in thf afforded the diiron diselenolato $Fe_2(\mu\text{-}Se(CH_2)_6Se\text{-}\mu)(CO)_6$ (**4**) and tetrairon $[Fe_2(\mu\text{-}Se(CH_2)_5Se\text{-}\mu)(CO)_6]_2$ (**5**) complexes (Scheme 3). Compounds **4** and **5** are air-stable in the solid state and for several hours in hexane solution. These products were characterized by IR, multinuclear NMR spectroscopy, mass spectrometry, elemental analysis and X-ray crystallography. The ^1H NMR spectra of **4** and **5** displays resonances at 1.62 ($SeCH_2CH_2CH_2CH_2$) and 2.84 ($2SeCH_2$) (**4**), and 1.36, 1.83 ($SeCH_2CH_2$), 2.02 ($SeCH_2CH_2CH_2$) and 2.25, 2.71 ($SeCH_2$) (**5**). These resonances are comparable to that observed for **2**. The $^{13}C\{^1H\}$ NMR spectrum of **4** exhibits three resonances at 20.5, 28.4 ($SeCH_2CH_2CH_2CH_2$) and 22.8 ($SeCH_2$) ppm, while five resonances are observed for **5** at 14.1, 31.9 ($SeCH_2$), 27.5 ($SeCH_2CH_2CH_2$) and 30.1, 32.5 ($SeCH_2CH_2$). In addition, the expected resonances for the carbonyl groups were observed (**4**: 208.5, **5**: 209.6). The $^1H^{77}Se$ HMBC NMR spectrum of **2** shows a singlet at 186 ppm indicating equivalent Se atoms. While two signals are obtained in the $^{77}Se\{^1H\}$ NMR spectrum of **5** due to the presence of two different Se atoms.

The X-ray diffraction analysis reveals the structure of **4** and **5** as shown in Figure 2 and 3, respectively. The Fe-Fe bond distance in **4** and **5** are 2.5431(11) Å (**4**), 2.5423(17) Å, 2.5606(13) Å (**5**). These distances are slightly longer than that observed for **2**, and shorter than that in PDS. The Fe-Se bond distances are comparable to those observed for **2**.

Reaction of 1,6-Diselenocyanatohexane (8) with $Fe_3(CO)_{12}$ Treatment of $Fe_3(CO)_{12}$ with $NCSe(CH_2)_6SeCN$ (**8**) in thf under reflux conditions for one hour afforded the diiron $Fe_2(\mu\text{-}Se(CH_2)_5Se\text{-}\mu)(CO)_6$ (**6**) and tetrairon $[Fe_2(\mu\text{-}Se(CH_2)_6Se\text{-}\mu)(CO)_6]_2$ (**7**) complexes (Scheme 4). The stability of **6** and **7** are comparable to those of **4** and **5** in solution and in the solid state. $^1H,^1H$ COSY, $^1H,^{13}C$ HSQC and $^1H,^{13}C$ HMBC NMR spectra of **6** and **7** reveal three groups of ^1HNMR resonances in a 1:1:1 ratio as well as three ^{13}C signals at 22.2, 26.0 and 30.2 ppm for (**6**) and 14.0, 29.8 and 32.6 ppm for (**7**). These resonances are comparable to those observed for pentyl analogues **4** and **5**. The $^1H^{77}Se$ HMBC NMR spectra of **6** and **7** show one singlet each at 244 and 188 ppm, respectively.

The X-ray crystallographic study confirmed the molecular structures of **6** and **7,** (Figure 4) and (Figure 5) respectively. The Fe-Fe bond lengths of **6** (2.5550(15) Å) and **7** (2.5681(7) Å) are longer that those reported for **2** and **4**. On the bases of these information, we conclude that the Fe-Fe bond lengths of $Fe_2(\mu\text{-}Se(CH_2)_nSe\text{-}\mu)(CO)_6$ (n = 4, 5, 6) complexes are in direct proportions with n. This trend is also acceptable for the tetrairon model complexes **5** and **7**. The Fe-Se bond lengths of **6** and **7** are close to the corresponding bond lengths found in **2**, **4**, **5** and other reported diiron diselenolato model compounds.[31,32,34]

It is noteworthy that the iron atoms in **7** are equivalent due to the similarity distributed of the two diselenolato linker between the four iron atoms. While in **5** this symmetry is demolish, which revels the disorder arrangement of the two diselenolato linkers between the iron atoms. This has been proved by NMR spectroscopy and X-ray crystallography (Figures 3 and 5).

The mass spectra of **2** and **4**-**7** show the molecular ion peaks followed by the fragmentation of six CO groups in **2**, **4** and **6**, and twelve in **5** and **7**. The IR spectra of complexes **2** and **4**-**7** (KBr disk) show three strong absorption bands in the regions of 1984-1989, 2017-2028 and 2062-2065 cm^{-1}. These data are within the same ranges as those observed for sulfur and selenium analogues.[30-33]

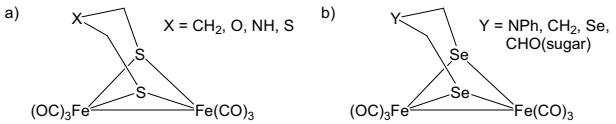

Scheme 1. a) Models of [FeFe] hydrogenases contain dithiolato ligands. b) Models of [FeFe] hydrogenases contain diselenolato ligands.

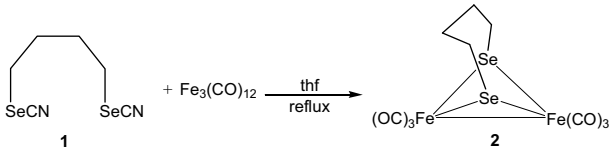

Scheme 2. Model of [FeFe] hydrogenases containing butane diselenolato ligand (**2**) prepared in our lab.

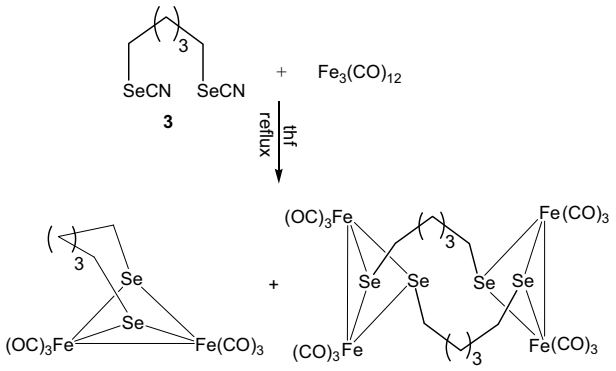

Scheme 3. Diiron (**4**) and tetrairon (**5**) models of [FeFe] hydrogenases containing pentane diselenolato ligand prepared in our lab.

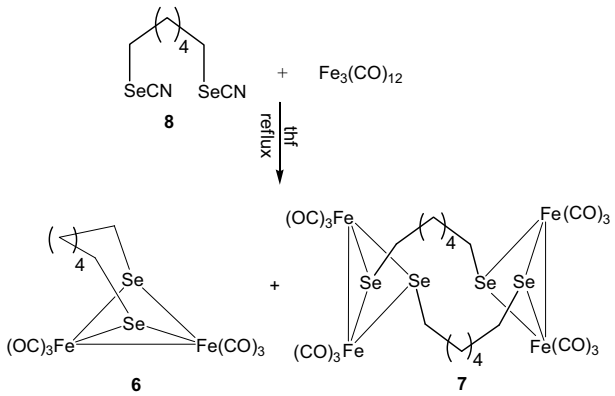

Scheme 4. Diiron (**6**) and tetrairon (**7**) models of [FeFe] hydrogenases containing hexane diselenolato ligand prepared in our lab.

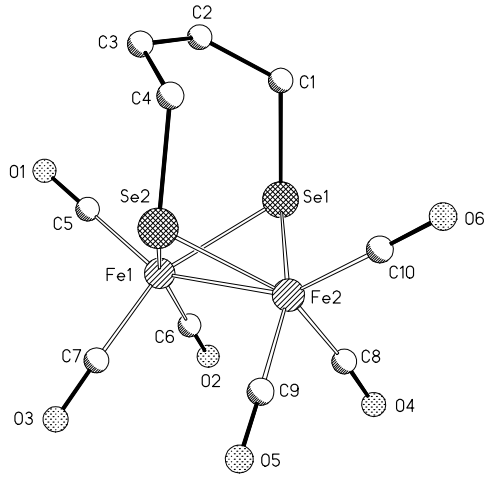

Figure 1. ORTEP drawing of $Fe_2(\mu\text{-}Se_2(CH_2)_4Se\text{-}\mu)(CO)_6$ (**2**). Selected distances [Å] and angles [°]: Fe1-Fe2 2.5370(10), Fe1-Se1 2.3758(9), Fe1-Se2 2.3793(9), Fe2-Se1 2.3720(9), Fe2-Se2 2.3780(9), Fe1-Se1-Fe2 64.60(3), Fe1-Se2-Fe2 64.46(3).

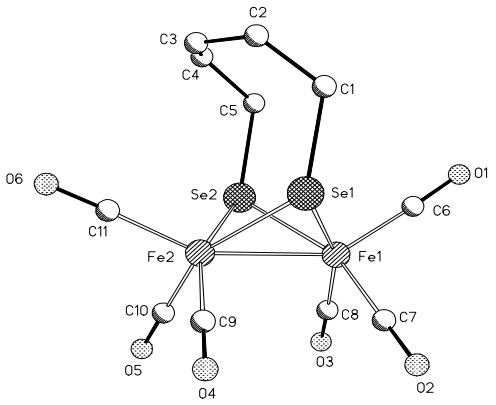

Figure 2. ORTEP drawing of $Fe_2(\mu\text{-}Se_2(CH_2)_5Se\text{-}\mu)(CO)_6$ (**5**). Selected distances [Å] and angles [°]: Fe1-Fe2 2.5431(11), Fe1-Se1 2.3805(10), Fe1-Se2 2.3810(10), Fe2-Se1 2.3808(10), Fe2-Se2 2.3761(10), Fe1-Se1-Fe2 64.57(3), Fe1-Se2-Fe2 64.60(3).

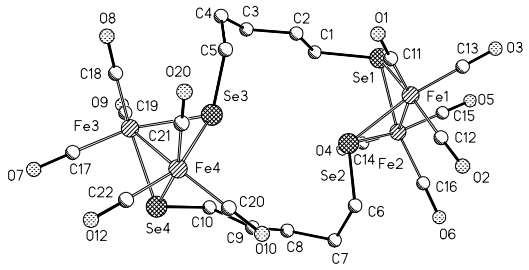

Figure 3. ORTEP drawing of $[Fe_2(\mu\text{-}Se_2(CH_2)_5Se\text{-}\mu)(CO)_6]_2$(**6**). Selected distances [Å] and angles [°]: Fe1-Fe2 2.5606(13), Fe3-Fe4 2.5423(17), Fe1-Se1 2.3874(13), Fe1-Se2 2.3658(12), Fe3-Se3 2.3737(14), Fe3-Se4 2.3812(14), Fe1-Se1-Fe2 64.83(4), Fe1-Se2-Fe2 65.42(4).

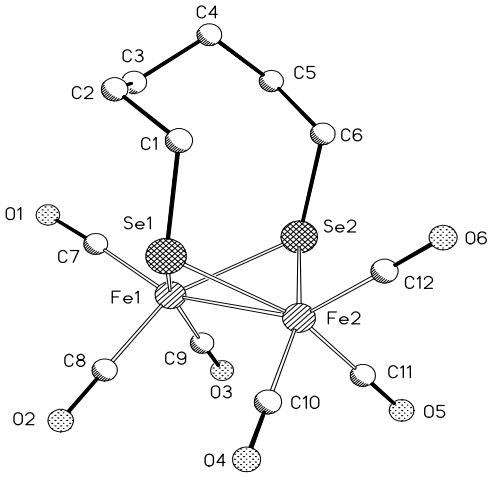

Figure 4. ORTEP drawing of $Fe_2(\mu\text{-}Se_2(CH_2)_6Se\text{-}\mu)(CO)_6$ (**6**). Selected distances [Å] and angles [°]: Fe1-Fe2 2.5550(15), Fe1-Se1 2.3832(12), Fe1-Se2 2.3894(14), Fe2-Se1 2.3872(13), Fe2-Se2 2.3899(13), Fe1-Se1-Fe2 64.77(4), Fe1-Se2-Fe2 64.63(4).

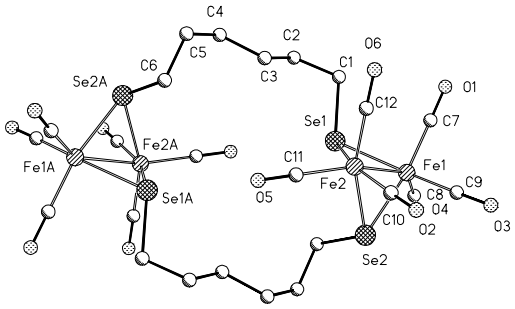

Figure 5. ORTEP drawing of $[Fe_2(\mu\text{-}Se_2(CH_2)_6Se\text{-}\mu)(CO)_6]_2$ (**7**). Selected distances [Å] and angles [°]: Fe1-Fe2 2.5681(7), Fe1-Se1 2.3686(6), Fe1-Se2 2.3864(6), Fe2-Se1 2.3768(6), Fe2-Se2 2.3832(6), Fe1-Se1-Fe2 65.526(18), Fe1-Se2-Fe2 65.153(19).

Table 1. Crystal data and structure refinement details for **2** and **4-7**.

Compound	**2**	**4**	**5**	**6**	**7**
formula	$C_{10}H_8Fe_2O_6Se_2$	$C_{11}H_{10}Fe_2O_6Se_2$	$C_{22}H_{20}Fe_4O_{12}Se_4$	$C_{12}H_{12}Fe_2O_6Se_2$	$C_{24}H_{24}Fe4O_{12}Se_4$
fw ($g \cdot mol^{-1}$)	493.78	507.81	1015.62	521.84	1043.67
T/°C	-90(2)	-90(2)	-90(2)	-90(2)	-90(2)
crystal system	monoclinic	monoclinic	triclinic	triclinic	monoclinic
space group	$P2_1/m$	P21/n	Pī	Pī	$P2_1/n$
a/ Å	9.0282(2)	7.7436(5)	7.8889(3)	7.7924(6)	10.8746(5)
b/ Å	22.6317(4)	16.6358(14)	9.9029(7)	10.4448(5)	10.8214(4)
c/ Å	14.8842(3)	12.5656(8)	21.2847(12)	11.0679(9)	15.1398(6)
α/°	90	90	96.953(3)	71.785(5)	90
β/°	97.741(1)	95.110(5)	94.918(3)	79.445(3)	110.150(2)
γ/°	90	90	96.862(3)	83.995(5)	90
V/Å^3	3013.5(1)	1612.3(2)	1630.3(2)	840.12(10)	1672.58(12)
Z	8	4	2	2	2
ρ ($g \cdot cm^{-3}$)	2.177	2.092	2.069	2.063	2.072
μ (cm^{-1})	67.74	63.33	62.63	60.8	61.08
measured data	21513	10682	11438	8525	11542
data with I > 2σ(I)	5012	2021	3814	2151	2772
unique data / R_{int}	7073/0.0828	3626/0.0796	7410/0.0575	3795/0.0989	3815/0.0524
wR_2 (all data, on F^2)[a)]	0.1171	0.1216	0.1239	0.1405	0.0674
R_1 ($I > 2\sigma(I)$)[a)]	0.0452	0.0505	0.0541	0.0593	0.0327
s[b)]	1.022	0.999	0.950	0.966	0.939
Res. dens./e·Å^{-3}	1.219/-0.722	0.702/-0.897	0.556/-0.477	0.776/-1.269	0.479/-0.670
absorpt method	NONE	NONE	NONE	NONE	NONE
CCDC No.	727693	727694	727695	727696	727697

Experimental Section

General Comments. All reactions were carried out under inert atmosphere with standard Schlenk techniques. thf and hexane were dried and distilled prior to use according to the standard methods. The ^{1}H, ^{13}C{^{1}H}, ^{77}Se{^{1}H} and 2D NMR (^{1}H,^{1}H COSY, ^{1}H,^{13}C HSQC, ^{1}H,^{77}Se HMBC) spectra were recorded on either a Bruker AVANCE 200 or 400 MHz spectrometer using solvent residual peak or a concentrated solution of SeO_2 in D_2O as reference. The ^{77}Se chemical shifts are reported relative to neat Me_2Se [$\delta(Me_2Se) = \delta(SeO_2) + 1302.6$ ppm].[40] Mass spectra were recorded on a FINNIGAN MAT SSQ 710 instrument. IR spectra were measured on a Perkin-Elmer System 2000 FT-IR spectrometer. Elemental analyses were performed with a LECO CHNS-932 apparatus. Silica gel 60 (0.015-0.040 mm) was used for column chromatography. TLC was done using Merck TLC aluminum sheets (Silica gel 60 F_{254}). $NCSe(CH_2)_4SeCN$ (**1**), $NCSe(CH_2)_5SeCN$ (**3**) and $NCSe(CH_2)_6SeCN$ (**8**) were prepared according to literature protocols.[41,42] $Fe_3(CO)_{12}$ was purchased from Aldrich, solvents from Fisher Scientific, and other chemicals from Acros, and were used without further purification. Yield calculations were based on substoichiometric utilized chemicals or on $Fe_3(CO)_{12}$ for the diiron complexes.

Synthesis of Fe_2(μ-Se(CH_2)$_4$Se-μ)(CO)$_6$ (2): A green solution of $Fe_3(CO)_{12}$ (150 mg, 0.30 mmol) in thf (50 mL) was treated with **1** (80 mg, 0.30 mmol) and heated at reflux for one hour. The resulting brown-red mixture was evaporated to dryness in vacuo. The obtained solid was suspended in a minimum amount of hexane and column chromatographed (SiO_2/hexane). From the major red fraction, **2** was obtained as a red solid (99 mg, 67%) and was recrystallized from hexane at 25 °C. $C_{10}H_8Fe_2O_6Se_2$ (493.78): calcd. C 24.32, H 1.63; found C 24.73, H 1.86. ^{1}H NMR (400 MHz, $CDCl_3$, 25 °C): δ = 1.75 (s, 4 H, $SeCH_2CH_2$), 2.61 (s, 4 H, $SeCH_2$) ppm. ^{13}C{^{1}H} NMR (50 MHz, $CDCl_3$): δ = 21.2 ($SeCH_2$), 25.5 ($SeCH_2CH_2$) 208.8 (CO) ppm. ^{77}Se{^{1}H}NMR (76 MHz, $CDCl_3$): δ = 284 ($SeCH_2$) ppm. FTIR (KBr): ν = 2064 (vs), 2022 (vs), 1985 (vs) cm^{-1}. MS (DEI = 70 eV): m/z (%) = 494 (23) [M^+], 466 (8) [M^+ – 28; CO], 438 (9) [M^+ – 56; 2CO], 410 (12) [M^+ – 84; 3CO], 382 (8) [M^+ – 112; 4CO], 354 (14) [M^+ – 140; 5CO], 326 (33) [M^+ – 168; 6CO].

Synthesis of Fe_2(μ-Se(CH_2)$_6$Se-μ)(CO)$_6$ (4), and [Fe_2(μ-Se(CH_2)$_5$Se-μ)(CO)$_6$]$_2$ (5): $Fe_3(CO)_{12}$ (150 mg, 0.30 mmol) and **3** (84 mg, 0.30 mmol) were refluxed in thf (50 mL) for one hour under argon. The color of the green solution changed to red-brown. The reaction mixture was cooled to room temperature and the solvent was removed under reduced pressure. The crude brown product was purified by column chromatography (SiO_2/hexane). The crude product was purified by chromatography on silica gel using hexane as eluent. Complex **4** was obtained from the first red fraction and recrystallized from hexane at –25 °C. A second red brownish band provided complex **5**, which was also recrystallized from hexane at –25 °C.

Fe_2(μ-Se(CH_2)$_6$Se-μ)(CO)$_6$ (**4**) Yield 61 mg (40%). $C_{11}H_{10}Fe_2O_6Se_2$ (507.8): calcd. C 26.02, H 1.98; found C 26.79, H 2.09. ^{1}H NMR (400 MHz, $CDCl_3$, 25 °C): δ = 1.62 (s, 6 H, $SeCH_2CH_2CH_2CH_2$), 2.84 (s, 4 H, $SeCH_2$) ppm. ^{13}C{^{1}H} NMR (50 MHz, $CDCl_3$): δ = 20.5, 28.4 ($SeCH_2CH_2CH_2CH_2$), 22.8 ($SeCH_2$), 208.5 (CO) ppm. ^{77}Se{^{1}H}NMR (76 MHz, $CDCl_3$): δ = 186 ($SeCH_2$) ppm. FTIR (KBr): ν = 2065 (vs), 2027 (vs), 1989 (vs) cm^{-1}. MS (DEI = 70 eV): m/z (%) = 508 (25) [M^+], 480 (10) [M^+ – 28; CO], 452 (17) [M^+ – 56; 2CO], 424 (17) [M^+ – 84; 3CO], 396 (17) [M^+ – 112; 4CO], 368 (20) [M^+ – 140; 5CO], 340 (48) [M^+ – 168; 6CO].

[Fe_2(μ-Se(CH_2)$_5$Se-μ)(CO)$_6$]$_2$ (**5**) Yield 71 mg (23%). $C_{22}H_{20}Fe_4O_{12}Se_4$ (1015.61): calcd. for $C_{22}H_{20}Fe_4O_{12}Se_4 \cdot 0.5$ hexane C 31.89, H 3.39; found C 31.47, H 3.52. ^{1}H NMR (400 MHz, $CDCl_3$, 25 °C): δ = 1.36 (m, 4 H, $SeCH_2CH_2$), 1.83 (m, 4 H, $SeCH_2CH_2$), 2.02 (m, 4 H, $SeCH_2CH_2CH_2$), 2.25 (t, $^3J_{H,H}$ = 8.0 Hz, 4 H, $SeCH_2$), 2.71 (t, $^3J_{H,H}$ = 5.4 Hz, 4 H, $SeCH_2$). ^{13}C{^{1}H} NMR (50 MHz, $CDCl_3$): δ = 14.1, 31.9 ($SeCH_2$), 27.5 ($SeCH_2CH_2CH_2$), 30.1, 32.5 ($SeCH_2CH_2$), 209.6 (CO) ppm. ^{77}Se{^{1}H}NMR (76 MHz, $CDCl_3$): δ = 163, 197 ($SeCH_2$) ppm. FTIR (KBr): ν = 2062 (s), 2028 (vs), 1986 (s) cm^{-1}. MS (DEI = 70 eV): m/z (%) = 1016 (35) [M^+], 932 (81) [M^+ – 84; 3CO], 904 (8) [M^+ – 112; 4CO], 876 (8) [M^+ – 140; 5CO], 848 (100) [M^+ – 168; 6CO], 820 (9) [M^+ – 196; 7CO], 792 (5) [M^+ – 224; 8CO], 764 (23) [M^+ – 252; 9CO], 736 (7) [M^+ – 280; 10CO], 708 (9) [M^+ – 308; 11CO], 680 (11) [M^+ – 336; 12CO].

Synthesis of Fe_2(μ-Se(CH_2)$_5$Se-μ)(CO)$_6$ (6) and [Fe_2(μ-Se(CH_2)$_6$Se-μ)(CO)$_6$]$_2$ (7): Complexes **6** and **7** were prepared, separated, and recrystallized by a procedure similar to those of **4**.and **5**. The reaction of $Fe_3(CO)_{12}$ (150 mg, 0.30 mmol) with **8** (88 mg, 0.30 mmol) was carried out in thf.

Fe_2(μ-Se(CH_2)$_5$Se-μ)(CO)$_6$ (**6**) Yield 26 mg (17%). $C_{12}H_{12}Fe_2O_6Se_2$ (521.83): calcd. for $C_{12}H_{12}Fe_2O_6Se_2 \cdot 0.4$ hexane C 31.09, H 3.19; found C 31.07, H 3.03. ^{1}H NMR (400 MHz, $CDCl_3$, 25 °C): δ = 1.43 (s, 4 H, $SeCH_2CH_2$), 1.57 (s, 4 H, $SeCH_2CH_2CH_2$), 2.56 (t, ^{3}J = 6.8 Hz, 4 H, $SeCH_2$) ppm. ^{13}C{^{1}H} NMR (50 MHz, $CDCl_3$): δ = 22.2 ($SeCH_2$), 26.0 ($SeCH_2CH_2$), 30.2 ($SeCH_2CH_2CH_2$), 208.5 (CO) ppm. ^{77}Se{^{1}H}NMR (76 MHz, $CDCl_3$): δ = 244 ($SeCH_2$) ppm. FTIR (KBr): ν = 2063 (vs), 2017 (vs), 1989 (vs, sh) cm^{-1}. MS (DEI = 70 eV): m/z (%) = 524 (3) [M^+], 496 (3) [M^+ – 28; CO], 468 (6) [M^+ – 56; 2CO], 440 (4) [M^+ – 84; 3CO], 412 (6) [M^+ – 112; 4CO], 384 (7) [M^+ – 140; 5CO], 354 (28) [M^+ – 168; 6CO].

[Fe_2(μ-Se(CH_2)$_6$Se-μ)(CO)$_6$]$_2$ (**7**) Yield 115 mg (37%). $C_{24}H_{24}Fe_4O_{12}Se_4$ (1043.66): calcd. for $C_{24}H_{24}Fe_4O_{12}Se_4 \cdot 0.5$ hexane C 31.89, H 3.39; found C

31.95, H 3.45. ^{1}H NMR (400 MHz, $CDCl_3$, 25 °C): δ = 1.65 (s, 8 H, $SeCH_2CH_2$), 2.34 (s, 8 H, $SeCH_2CH_2CH_2$), 2.63 (s, 8 H, $2SeCH_2$) ppm. $^{13}C\{^{1}H\}$ NMR (50 MHz, $CDCl_3$): δ = 14.0 ($SeCH_2CH_2CH_2$), 29.8 ($SeCH_2CH_2$), 32.6 (SeCH), 209.6 (CO) ppm. $^{77}Se\{^{1}H\}$NMR (76 MHz, $CDCl_3$): δ = 188 ($SeCH_2$) ppm. FTIR (KBr): ν = 2062 (vs), 2022 (vs), 1984 (vs) cm^{-1}. MS (DEI = 70 eV): m/z (%) = 1046 (8) [M^+], 1015 (2) [M^+ – 28; CO], 960 (12) [M^+ – 84; 3CO], 906 (7) [M^+ – 140; 5CO], 878 (10) [M^+ – 168; 6CO], 849 (3) [M^+ – 196; 7CO], 820 (7) [M^+ – 224; 8CO], 792 (17) [M^+ – 252; 9CO], 764 (4) [M^+ – 280; 10CO], 736 (9) [M^+ – 308; 11CO], 708 (11) [M^+ – 336; 12CO].

Crystal Structure Determination

The intensity data for the compounds were collected on a Nonius KappaCCD diffractometer, using graphite-monochromated Mo-K_α radiation. Data were corrected for Lorentz and polarization effects, but not for absorption effects.[43,44] Crystallographic data as well as structure solution and refinement details are summarized in Table 1. The structures were solved by direct methods (SHELXS)[45] and refined by full-matrix least squares techniques against F_o^2 (SHELXL-97)[46]. All hydrogen atoms were included at calculated positions with fixed thermal parameters. All nonhydrogen atoms were refined anisotropically.[46] XP (SIEMENS Analytical X-ray Instruments, Inc.) was used for structure representations.

Crystallographic data (excluding structure factors) has also been deposited with the Cambridge Crystallographic Data Centre as supplementary publication CCDC-727693 for **2**, CCDC-727694 for **4**, CCDC-727695 for **5**, CCDC-727696 for **6**, and CCDC-727697 for **7**. Copies of the data can be obtained free of charge on application to CCDC, 12 Union Road, Cambridge CB2 1EZ, UK [E-mail: deposit@ccdc.cam.ac.uk].

Acknowledgments

Financial support for this work was provided for Mohammad Harb by the Deutscher Akademischer Austausch Dienst (DAAD).

1. M. Frey, *Chembiochem*. **2002**, *3*, 153-160.
2. P. M. Vignais, B. Billoud, *Chem. Rev*. **2007**, *107*, 4206-4272.
3. A. L. De Lacey, V. M. Fernandez, M. Rousset, R. Cammack, *Chem. Rev*. **2007**, *107*, 4304-4330.
4. R. Cammack, *Nature* **1999**, *397*, 214-215.
5. M. W. W. Adams, E. I. Stiefel, *Science* **1998**, *282*, 1842–1843.
6. S. Shima, O. Pilak, S. Vogt, M. Schick, M. S. Stagni, W. Meyer-Klaucke, E. Warkentin, R. K. Thauer, U. Ermler, *Science* **2008**, *321*, 572-575.
7. M. Y. Darensbourg, E. J. Lyon, J. J. Smee, *Coord. Chem. Rev*. **2000**, *206*, 533-561.
8. D. J. Evans, C. J. Pickett, *Chem. Soc. Rev*. **2003**, *32*, 268–275.
9. J. Alper, *Science* **2003**, *299*, 1686-1687.
10. M. Razavet, S. C. Davies, D. L. Hughes, J. E. Barclay, D. J. Evans, S. A. Fairhurst, X. Liu, C. J. Pickett, *Dalton Trans*. **2003**, 586-595.
11. X. Zhao, I. P. Georgakaki, M. L. Miller, J. C. Yarbrough, M. Y. Darensbourg, *J. Am. Chem. Soc*. **2001**, *123*, 9710-9711.
12. X. Zhao, C.-Y. Chiang, M. L. Miller, M. V. Rampersad, M. Y. Darensbourg, *J. Am. Chem. Soc*. **2003**, *125*, 518-524
13. F. Gloaguen, J. D. Lawrence, M. Schmidt, S. R. Wilson, T. B. Rauchfuss, *J. Am. Chem. Soc*. **2001**, *123*, 12518-12527.
14. E. J. Lyon, I. P. Georgakaki, J. H. Reibenspies, M. Y. Darensbourg, *J. Am. Chem. Soc*. **2001**, *123*, 3268-3278.
15. J. D. Lawrence, H. Li, T. B. Rauchfuss, M. Benard, M. M. Rohmer, *Angew. Chem. Int. Ed*. **2001**, *40*, 1768-1771.
16. D. Seyferth, R. S. Henderson, L.-C. Song, *Organometallics* **1982**, *1*, 125–133.
17. P. Li, M. Wang, C. He, G. Li, X. Liu, C. Chen, B. Akermark, L. Sun, *Eur. J. Inorg. Chem*. **2005**, 2506-2513.
18. U.-P. Apfel, Y. Halpin, H. Görls, J. G. Vos, B. Schweizer, G. Linti, W. Weigand, *Chem. Biodiv*. **2007**, *4*, 2138-2148.
19. J. Windhager, R. A. Seidel, U.-P. Apfel, H. Görls, G. Linti, W. Weigand, *Chem. Biodiv*. **2008**, *10*, 2023-2041.
20. J. Windhager, H. Görls, H. Petzold, G. Mloston, G. Linti, W. Weigand, *Eur. J. Inorg. Chem*. **2007**, *28*, 4462-4471.
21. L.-C. Song, Z.-Y. Yang, H.-Z. Bian, Y. Liu, H.-T. Wang, X.-F. Liu, Q.-M. Hu, *Organometallics* **2005**, *24*, 6126-6135.
22. S. Ezzaher, J.-F. Capon, F. Gloaguen, F. Y. Petillon, P. Schollhammer, J. Talarmin, *Inorg. Chem*. **2009**, *48*, 2-4.
23. P. Y. Orain, J.-F. Capon, N. Kervarec, F. Gloaguen, F. Y. Petillon, R. Pichon, P. Schollhammer, J. Talarmin, *Dalton Trans*. **2007**, 3754-3756.
24. S. Ezzaher, J.-F. Capon, N. Dumontet, F. Gloaguen, F. Y. Pétillon, P. Schollhammer, J. Talarmin, *J. Electroanal. Chem*. **2009**, *626*, 161-170.
25. S. Ezzaher, J.-F. Capon, F. Gloaguen, F. Y. Pétillon, P. Schollhammer, J. Talarmin, *Inorg. Chem*. **2007**, *46*, 3426-3428.
26. J. Windhager, M. Rudolph, S. Bräutigam, H. Görls, W. Weigand, *Eur. J. Inorg. Chem*. **2007**, *18*, 2748-2760.
27. S. J. George, Z. Cui, M. Razavet, C. J. Pickett *Chem. Eur. J*. **2002**, *8*, 4037-4046.
28. G. Zampella, M. Bruschi, P. Fantucci, M. Razavet, C. J. Pickett, L. D. Gioia, *Chem. Eur. J*. **2005**, *11*, 509-520.
29. S. K. Ibrahim, X. Liu, C. Tard, C. J. Pickett, *ChemComm*. **2007**, 1535-1537.
30. C. A. Boyke, T. B. Rauchfuss, S. R. Wilson, M.-M. Rohmer, M. Benard, *J. Am. Chem. Soc*. **2004**, *126*, 15151-15160.
31. S. Gao, J. Fan, S. Sun, X. Peng, X. Zhao, J. Hou, *Dalton Trans*. **2008**, 2128-2135.
32. M. K. Harb, T. Niksch, J. Windhager, H. Görls, R. Holze, L. T. Lockett, N. Okumura, D. H. Evans, R. S. Glass, D. L. Lichtenberger, M. El-khateeb, W. Weigand, *Organometallics* **2009**, *28*, 1039-1048.
33. U.-P. Apfel, Y. Halpin, M. Gottschaldt, H. Görls, J. G. Vos, W. Weigand, *Eur. J. Inorg. Chem*. **2008**, 5112-5118.
34. L.-C. Song, B. Gai, H.-T. Wang, Q.-M. Hu, *J. Inorg. Biochem*. **2009**, accepted; DOI: 10.1016/j.jinorgbio.2009.02.002.
35. M. K. Harb, J. Windhager, A. Daraosheh, H. Görls, L. T. Lockett, N. Okumura, D. H. Evans, R. S. Glass, D. L. Lichtenberger, M. El-khateeb, W. Weigand, *Eur. J. Inorg. Chem*. **2009**, In press.
36. D. Seyferth, R. S. Henderson, L.-C. Song, *J. Organomet. Chem*. **1980**, *192*, C1-C5.
37. Y. Zhang, Y.-T. Si, M.-Q. Hu, C.-N. Chen, Q.-T. Liu, *Acta Cryst*. **2007**, *C63*, m499-m500.
38. J. W. Tye, M. Y. Darensbourg, M. B. Hall, *Inorg. Chem*. **2006**, *45*, 1552-1559.
39. P. Mathur, B. Manimaran, R. Trivedi, M. M. Hossain, M. Arabatti, *J. Organomet. Chem*. **1996**, *515*, 155-162.
40. R. C. Burns, M. J. Collins, R. J Gillespie, G. J. Schrobilgen, *Inorg. Chem*. **1986**, *25*, 4465-4469.
41. M. Clarembeau, A. Cravador, W. Dumont, L. Hevesi, A. Krief, J. Lucchetti, D. van Ende, *Tetrahedron* **1985**, *41*, 4793-4812.
42. A. Krief, C. Delmotte, W. Dumont, *Tetrahedron* **1997**, *53*, 12147-12158.
43. *COLLECT*, Data Collection Software; Nonius, B.V. Netherlands. **1998**.
44. Z. Otwinowski, W. Minor, "Processing of X-Ray Diffraction Data Collected in Oscillation Mode" in *Methods in Enzymology*, vol. 276, *Macromolecular Crystallography*, Part A, Academic press: San Diego **1997**, pp. 307-326.
45. G. M. Sheldrick, *Acta Crystallogr. Sect. A* **1990**, *46*, 467-473.
46. G. M. Sheldrick, SHELXL-97 (Release 97-2), University of Göttingen, Germany, **1997**.

3.7 [MK7] *Synthesis and Characterization of Novel [FeFe]-Hydrogenase Models Containing Mixed S and Se Bridging Moieties.*

M. K. Harb, A. Daraosheh, T. Niksch, *H. Görls, R. S. Glass, D. L. Lichtenberger, M. El-khateeb, W. Weigand.*

In Preparation

Synthesis and Characterization of [FeFe]-Hydrogenases Models with Bridging Moieties Containing S and Se atoms

Mohammad K. Harb,[a] Ahmed Q. Daraosheh,[a] Tobias Niksch,[a] Helmar Görls,[a] Tori L. Lockett,[b] Greg A. N. Felton,[b] Dennis H. Evans,[b] Richard S. Glass,[b] Dennis L. Lichtenberger,[b] Mohammad El-khateeb[c] and Wolfgang Weigand[a]*

Keywords: Iron / Hydrogenase / Selenide / Sulfide / Electrocatalysis

In order to elucidate the influence of the bridging unit on the structure and electrochemical ability of the hydrogenase model complexes, novel butterfly diiron complexes containing S and Se atoms have been prepared and characterized. The reaction of $Fe_3(CO)_{12}$ with bis(thiocyanatomethyl)selenide (**1**) gave a mixture of $Fe_2(\mu\text{-}SeCH_2S\text{-}\mu)(CO)_6$ (**2**) and $Fe_2(\mu\text{-}SCH_2SeCH_2S\text{-}\mu)(CO)_6$ (**3**). The compound $Fe_2(\mu\text{-}SeCH_2SCH_2Se\text{-}\mu)(CO)_6$ (**4**) was prepared from the reaction of $Fe_3(CO)_{12}$ with bis(selenocyanatomethyl)sulfide (**5**). The new compounds were characterized by IR, ^{1}H-, ^{13}C{^{1}H}-, ^{77}Se{^{1}H}-NMR spectroscopy, mass spectrometry, elemental analysis and X-ray single crystal structure analysis. Oxidation and reduction of **2** and **4** was studied by cyclic voltammetry and the results were compared to related complexes. The ability of **2** and **4** to catalyze the reduction of acetic acid to form dihydrogen was characterized and it was found that the complexes exhibit catalytic efficiencies on the high end of the weak category when compared to similar complexes.

[a] Institut für Anorganische und Analytische Chemie, Friedrich-Schiller-Universität Jena, August-Bebel-Straße 2, 07743 Jena, GERMANY
[b] Department of Chemistry, The University of Arizona, Tucson, AZ, 85721, U.S.A
[c] Chemistry Department, Jordan University of Science and Technology, 22110 Irbid, JORDAN

Crystallographic data (excluding structure factors) has been deposited with the Cambridge Crystallographic Data Centre as supplementary publication CCDC-726555 for **2**, CCDC-726556 for **3**, CCDC-726557 for **7**, and CCDC-726558 for **9**. Copies of the data can be obtained free of charge on application to CCDC, 12 Union Road, Cambridge CB2 1EZ, UK [E- mail: deposit@ccdc.cam.ac.uk].

Introduction

Hydrogen is one of the best alternative solution of the energy recourses.[1-8] [FeFe]-hydrogenases are one of the enzymes which are producing hydrogen in nature.[9-11] Therefore several butterfly diiron model compounds as biomimics for the active site of these enzymes have been prepared (Scheme 1).[12-40] Recently it was proved that the presence of selenium atoms in [FeFe]-hydrogenases model complexes leads to higher activity towards H_2 production which occurs at more negative potentials than the corresponding sulfur complexes.[35] Therefoe, we were prepared and charachtrized several new models of [FeFe]-hydrogenases containing Fe_2Se_2 core. The electrochemistry of these model complexes reveals catalytic production of H_2 from weak acids. The observed behavior is analogous to that found for related models with Fe_2S_2 cores. Photoelectron spectroscopy and theoretical calculations revealed that the reorganization energy of $Fe_2(\mu\text{-}Se_2C_3H_5CH_3)(CO)_6$ with an Fe_2Se_2 is substantially lower than that for analogous complexes with Fe_2S_2 cores.[36] This effect, which may lead to faster electron transfer with complexes containing Fe_2Se_2 rather than Fe_2S_2 cores, has not yet been investigated in detail. Moreover, we extended our work to preparation complex containing Te_2Fe_2 core as model of the active site of [FeFe]-hydrogenases.[41] In that study, diiron dithiolato, diselenolato, and ditellurolato compounds containing an oxetane ring have been prepared, in order to compare the S, Se and Te homologues to each other.[41] We concluded that the rate of catalytic reduction of protons to hydrogen is substantially diminished from S to Se to Te.[41] Very recently a series of the mixed dichalcogenolato [FeFe]-hydrogenase model compounds related to the much-studied molecule $Fe_2(\mu\text{-}SC_3H_6S)(CO)_6$, where one sulfur atom is replaced by either a selenium atom or a tellurium atom were prepared (Scheme 2) and evaluated with electrochemistry, photoelectron spectroscopy (PES) and density functional theory (DFT) calculations.[42] As an extension of our previous modeling studies in this area[24-27,35,36,38,39,40,41] and to elucidate the influence of the bridged iron cores containing mixed S and Se ligands on the structure of hydrogenase model complexes, we launched a study concerning the synthesis and characterization of novel diiron complexes containing mixed S and Se ligands (Scheme 3). The ability of these complexes to act as models of the [FeFe]-hydrogenases will be presented, too.

Results and Discussion

Reaction of Bis(thiocyanatomethyl)selenide (1) with $Fe_3(CO)_{12}$

The reaction of **1** with $Fe_3(CO)_{12}$ in THF gave a mixture of $Fe_2(\mu\text{-}SeCH_2S\text{-}\mu)(CO)_6$ (**2**) and $Fe_2(\mu\text{-}SCH_2SeCH_2S\text{-}\mu)(CO)_6$ (**3**) (Scheme 3). Compounds **2** and **3** are air-stable in the solid state and for several hours in solution. The methylene group in **2** gives a singlet at 4.24 ppm in its ^1H NMR spectrum, which is shifted upfield compared to the analogous sulfur containing complex $Fe_2(\mu\text{-}SCH_2S\text{-}\mu)(CO)_6$ (4.9 ppm),[43] and downfield compared to its selenium analogue $Fe_2(\mu\text{-}SeCH_2Se\text{-}\mu)(CO)_6$ (4.02 ppm).[44] Its $^{13}C\{^1H\}$ NMR spectrum displays one signal at 46.1 ppm, and the carbonyl resonance at 208.9 ppm. The $^1H^{77}Se$ HMBC NMR spectrum shows a signal at 0.8 ppm. This value is shifted to higher field compared to the $Fe_2(\mu\text{-}SeCH_2Se\text{-}\mu)(CO)_6$ complex (67.6 ppm).[44] One singlet was observed at 3.3 ppm in ^1H NMR spectrum of **3** indicating two equivalent CH_2 groups. This value is comparable to those reported for $Fe_2(\mu\text{-}SCH_2SCH_2S\text{-}\mu)(CO)_6$ and $Fe_2(\mu\text{-}SeCH_2SeCH_2Se\text{-}\mu)(CO)_6$.[25,36,45] The $^{13}C\{^1H\}$ NMR spectrum of **3** displayed two signals at 16.9 and 206.8 ppm for the CH_2 and CO groups, respectively. One resonance at 461.1 ppm attributed to its Se atom was observed in $^1H^{77}Se$ HMBC NMR spectrum. The mass spectra of **2** and **3** showed the molecular ion peaks and subsequent stepwise loss of six CO groups. The single crystal X-ray structure analysis reveals the proposed structure of **3** as shown in Figure 1. The Fe-Fe bond distance in **3** is 2.5177(17) Å, which is slightly longer than those observed in PDT analogue [2.5103(11) Å],[23] oxadithiolate (ODT) analogue [2.5113(13) Å],[21] sulfurdithiolate (SDT) analogue [2.5120(5) Å][25,45] and azadithiolate (ADT) analogue [2.4924(7) Å].[16-18] The elongation of the Fe-Fe bond could be due to the larger size of selenium atom. Its Fe-S1 and Fe-S2 bond lengths 2.2727(15) Å and 2.2976(15) Å are slightly longer than in the SDT analogue.[25,45] The S1-C1-Se1 and S2-C2-Se1 bond angles in **3** are 119.8(4)° and 120.6(4)°, respectively. These values are larger than that observed for SDT complex [118.83(16)°][25,43] and unexpectedly high in comparison to a regular sp^3 hybridized atom (109.5°). An explanation for this is given in the literature and can be explained by the Rule of Bent.[24,46] Moreover the C1-S1-C2 bond angle in **3** is 101.6(2)°, which is smaller than that in the sulfur analogue [102.18(14)°].[25,45]

Reaction of Bis(selenocyanatomethyl)sulfide (5) with $Fe_3(CO)_{12}$

Diiron diselenolato complex $Fe_2(\mu\text{-}SeCH_2SCH_2Se\text{-}\mu)(CO)_6$ **4** was obtained from the reaction of **5** with $Fe_3(CO)_{12}$ in THF in 70% yield (Eq. 2). Whereas the reaction of **1** with $Fe_3(CO)_{12}$ gave a mixture of two compounds **2** and **3** (Scheme 3) due to the fragmentation of **1** under reflux condition, the reaction with **5** yielded **4** as the single product. This observation could be attributed to the weaker C-Se bond in ligand **1** compared to the C-S bond in ligand **5**. Compound **4** is air stable in the solid state and in solution for several hours. The elongation of the Fe-Fe bond could be due to the larger size of selenium atoms. For compound **4**, the ^1H NMR spectrum reveals a singlet at 3.27 ppm for the two equivalent CH_2 moieties. This resonance is comparable to those observed for **3** and to those of SDT and $Fe_2(\mu\text{-}SeCH_2SeCH_2Se\text{-}\mu)(CO)_6$.[25,36,45] Its $^{13}C\{^1H\}$ NMR spectrum displays two resonances at 17.6 ppm for the CH_2 groups and at 207.9 ppm for the CO groups. The equivalent Se atoms show resonance at 124 ppm in $^1H^{77}Se$ HMBC NMR spectrum of **4**. This value is shifted to higher field compared to those reported for **3**, $Fe_2(\mu\text{-}SeCH_2SeCH_2Se\text{-}\mu)(CO)_6$ and PDS.[36] The mass spectrum reveals the molecular ion at m/z = 500 and a stepwise fragmentation of the loss of six CO groups. Furthermore, the molecular structure of **4** was confirmed by X-ray diffraction analysis (Figure 2). The Fe-Fe bond distance in **4** of 2.5581(9) Å, is slightly shorter than that of (PDS) analogue [2.5610(8) Å] and comparable to that observed for $Fe_2(\mu\text{-}SeCH_2SeCH_2Se\text{-}\mu)(CO)_6$ complex [2.5555(10) Å]. The Fe-Se bond distances are comparable to those reported for $Fe_2(\mu\text{-}SeCH_2SeCH_2Se\text{-}\mu)(CO)_6$ and PDS.[36] The coordination geometry around the iron atoms in **3** and **4** is distorted octahedral as observed from the bond angles. This is rather similar to those in its sulfur and selenium analogus.[16-18,21,23,25,36,45] The S1-C1-Se1 and S1-C2-Se2 bond angles in **4** are 120.2(2)° and 118.3(2)°, respectively and are comparable to those observed for **3**. The C1-Se1-C2 bond angle in **4** of 99.6(3)° is smaller than those found in **3** and its selenium analogue.[36] It is noteworthy that the Fe-CO bond lengths of **3** (average lengths 1.809 Å) are longer than those in **4** (average lengths 1.793 Å) due to the increasing electron density at the Fe atoms in **4** compared to its in **3**. The IR spectra of these complexes (KBr disk) show three strong absorption bands observed in the 2076-1997 for **3** and 2069-1993 cm^{-1} for **4**, which are in the typical range of such model complexes.[16-18,21,23,25,36,45]

Voltammetric study

The electrochemical behavior of compounds **2** and **4** has been investigated along with the ability of these complexes to catalyze the reduction of the weak acid, acetic acid, to form dihydrogen and acetate. In Figure 3 are presented two voltammograms for each compound, one with an initial negative-going sweep to investigate cathodic processes, and one with an initial positive-going sweep to explore anodic reactions. Both compounds show one principal cathodic peak around −1.5 to −1.6 V vs. Fc^+/Fc whose height corresponds to slightly more than an overall one-electron reduction. (Peak potentials are listed in Table 1). The reduction is irreversible except at larger scan rates (1-5 V/s) where some chemical reversibility is observed and where the peak current function ($i_{p,c}/v^{1/2}$) decreases slightly probably approaching the one-electron level as recently noted for μ-(1,2-ethanedithiolato)diironhexacarbonyl.[47] This is particularly true for **4** whose peak current function decreases by a third on going from 0.050 to 5.0 V/s. As can be seen in Figure 3, a poorly defined second reduction peak is seen in the range of −2 to −2.4 V. For these two compounds this peak is relatively larger at the slower scan rates suggesting that it may arise from a secondary product of the process occurring at the first cathodic peak. On the return sweep of these voltammograms, an anodic peak is seen near −0.5 to −0.6 V which is due to oxidation of a product formed at the first reduction peak. This peak is present, though smaller, in voltammograms where the scan is reversed just past the first cathodic peak. Scans initiated in the positive direction (Figure 3) show one main anodic peak for **4** and two anodic peaks for **2** whose height varies among the four compounds ranging from slightly larger than the main cathodic peak for **4**. Compound **4** invites comparison with the all-sulfur analog, μ-(2-thia-1,3-propanedithiolato)diironhexacarbonyl (**6**). The standard potential for reduction of **6** has been estimated[48] to be −1.46 V but the overall reversible reaction has been assigned as a two-electron reduction.[25] (See, however, reference 50 where the reduction is reported to be a one-electron process, a claim that is not consistent with the reported peak current). For compound **4**, the cathodic peak potential from is −1.488 ± 0.006 V, indicating that substitution of Se for S has little effect. The anodic peak potential is +0.78 V, almost identical to that of **6**, +0.77 V.[45] As mentioned above, the cathodic peak current for **4** corresponds to greater than a one-electron process, but definitely short of two electrons. The reduction is almost irreversible except at the higher scan rates, 1

and 5 V/s, where chemical reversibility is restored. We suggest that the irreversible decomposition of the reduction product, noted for **4** by Weigand et al., is faster with **6**.

Catalysis of the reduction of a weak acid. Complexes similar to **2** and **4** are known to catalyze the reduction of acids.[48] A typical acid for the evaluation of catalytic efficiency is acetic acid (pK_a = 22.3 in acetonitrile[49]) and what is typically observed for such a weak acid is that catalytic reduction does not take place at the reduction peak of the catalyst but at a rather more negative potential. Such is the case for these two complexes. As acid is added, the reduction peak of the catalyst is hardly affected but there appears a new peak in the range of −2.0 to −2.4 V that grows in height more or less linearly with acid concentration. Results for 1 mM catalyst and 50 mM acetic acid are shown in Figure 4. There is a hint of resolution into two peaks for **4**. The catalytic efficiency, *C.E.*, of defined by equation 3 where i_{cat} is the magnitude of the catalytic current, i_d is the peak current for reduction of the catalyst and C_{HA} and C_{cat} are the concentrations of acid and catalyst, respectively.[48] Values of *C.E.* for each complex are shown in Figure 4. Weak catalysis is indicated by $0 < C.E. < 0.25$ so the range of 0.20-0.25 for these complexes is in the high end of the weak category. Another measure of efficiency is the overpotential, defined in this case as the difference between the potential where the catalytic current is half its maximum value and the standard potential for reduction of acetic acid in acetonitrile, −1.46 V. The overpotential, $E_{overpot}$, (also shown in Figure 4) ranges from 0.5 to 0.8 V, not unlike complexes with a [2Fe2S] core.[48] The overpotential of 0.5 V for **2** is among the lowest of those reported for such complexes.[48]

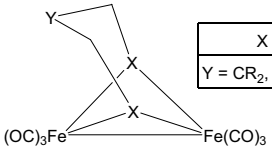

X = S	X = Se
Y = CR_2, O, NR, S	Y = CH_2, NPh, Se, CHO(Sugar)

Scheme 1. a) Models of [FeFe] hydrogenases contain dithiolato ligands (X = S) or diselenolato ligands (X = Se).

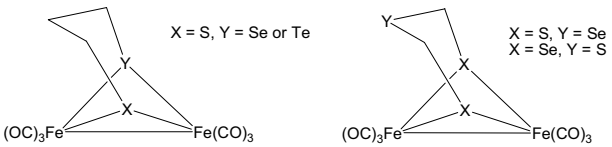

Scheme 2. Models of [FeFe] hydrogenases contain mixed dichalcogenolato ligands prepared in our lab.

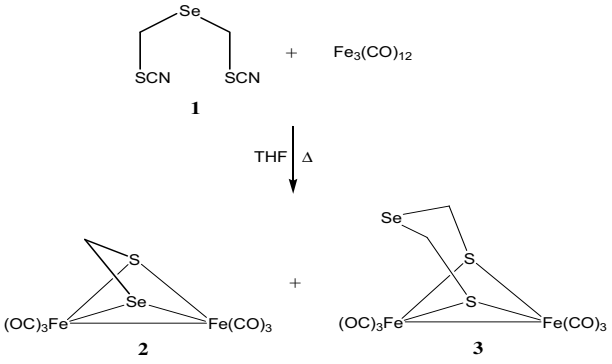

Scheme 3. The reaction of bis(thiocyanatomethyl)selenide (**1**) with $Fe_3(CO)_{12}$ in THF.

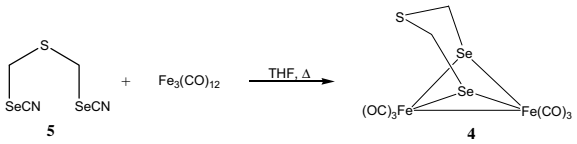

(1)

$$C.E. = \frac{i_{cat}/i_d}{C_{HA}/C_{cat}} \quad (2)$$

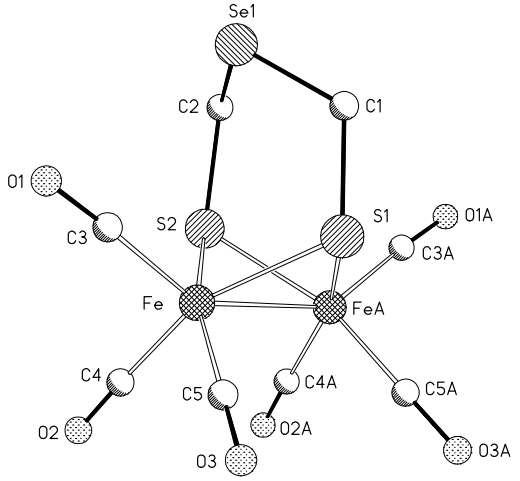

Figure 1. ORTEP drawing of $Fe_2(\mu\text{-}SCH_2SeCH_2S\text{-}\mu)(CO)_6$ (**3**) with thermal ellipsoids set at the 50% probability level (hydrogen atoms and the disordered Se1 were omitted for clarity). Selected distances [Å] and angles [°]: Fe-FeA 2.5177(17), Fe-S1 2.2727(15), Fe-S2 2.2976(15), Fe-S1-FeA 67.27(6), Fe-S2-FeA 66.45(6), S1-C1-Se1 119.8(4), S2-C2-Se1 120.6(4), C1-Se1-C2 99.6(3).

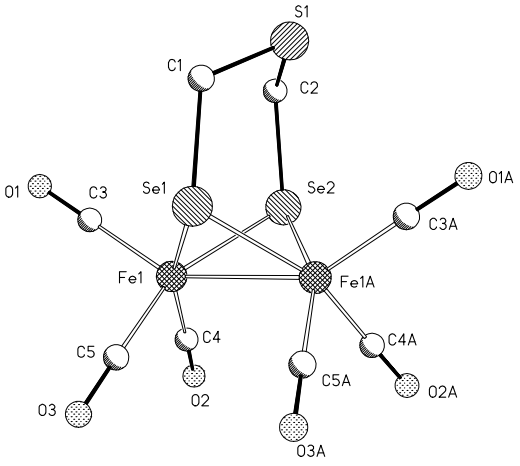

Figure 2. ORTEP drawing of $Fe_2(\mu\text{-}SeCH_2SCH_2Se\text{-}\mu)(CO)_6$ (**4**) with thermal ellipsoids set at the 50% probability level (hydrogen atoms and the disordered S1 were omitted for clarity). Selected distances [Å] and angles [°]: Fe1-Fe1A 2.5581(9), Fe1-Se1 2.3738(6), Fe1-Se2 2.3672(6), Fe1-Se1-Fe1A 65.20(3), Fe1-Se2-Fe1A 65.41(3), Se1-C1-S1 120.2(2), Se2-C2-S1 118.3(2), C1-S1-C2 101.6(2).

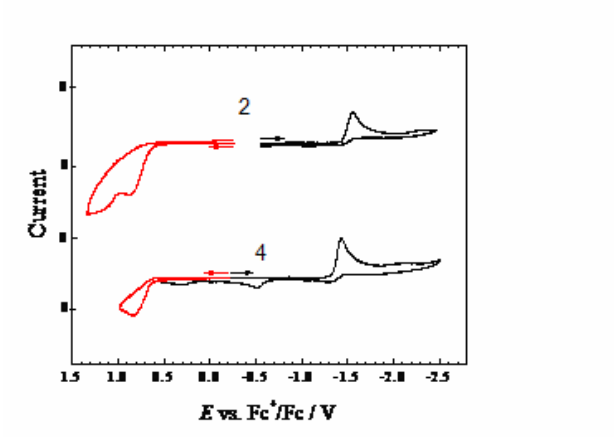

Figure 3. Voltammograms of ca. 1 mM **2** and **4** obtained in acetonitrile containing 0.10 M tetra-*n*-butylammonium hexafluorophosphate using a glassy carbon working electrode. 0.100 V/s.

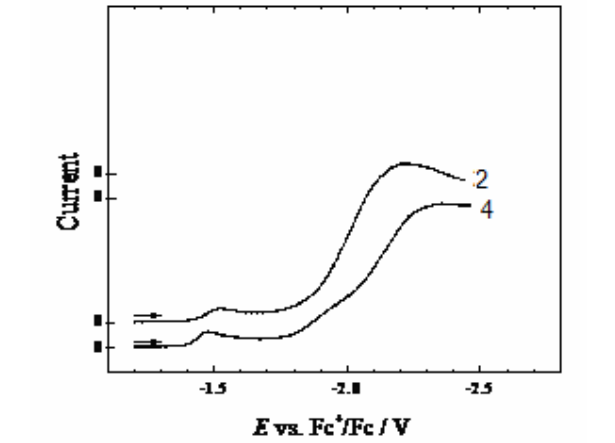

Figure 4. Voltammograms of ca. 1 mM **2** and **4** in the presence of 50 mM acetic acid. Other conditions as in Figure 3. Return scans omitted for clarity. *C.E.* is the catalytic efficiency as defined in equation 2. Overpotential, $E_{overpot}$, is the difference between the potential where the catalytic current is half its maximum value and the standard potential for reduction of acetic acid, −1.46 V.

Table 1. Peak potentials for compounds **2** and **4**.[a]

Compound	$E_{p,c}$ / V vs. Fc^+/Fc	$E_{p,a}$ / V vs. Fc^+/Fc
2	−1.540 ± 0.003	+0.892
4	−1.488 ± 0.005	+0.783

[a] From voltammograms like those in Figure 3.

Table 2: Crystal data and refinement details for the X-ray structure determinations of compounds **3** and **4**.

Compound	**3**	**4**
formula	$C_8H_4Fe_2O_6S_2Se$	$C_8H_4Fe_2O_6SSe_2$
fw ($g \cdot mol^{-1}$)	450.89	497.79
T/°C	-90(2)	-90(2)
crystal system	monoclinic	monoclinic
space group	$P2_1/m$	$P2_1/m$
a/ Å	6.8542(4)	6.9718(3)
b/ Å	13.3152(8)	13.2973(6)
c/ Å	8.0443(3)	8.0333(3)
β/°	107.750(3)	108.634(2)
V/Å^3	699.21(6)	705.70(5)
Z	2	2
ρ ($g \cdot cm^{-3}$)	2.142	2.343
μ (cm^{-1})	49.89	73.75
measured data	4847	7105
data with $I > 2\sigma(I)$	1368	1479
unique data / R_{int}	1649/0.0429	1685/0.0992
wR_2 (all data, on F^2)[a)]	0.1957	0.0941
R_1 ($I > 2\sigma(I)$)[a)]	0.0658	0.0362
s[b)]	1.070	1.073
Res. dens./$e \cdot Å^{-3}$	2.608/-1.082	0.756/-1.882
absorpt method	NONE	NONE
CCDC No.	726557	726558

[a] Definition of the R indices: $R_1 = (\Sigma \| |F_o| - |F_c| \|)/\Sigma |F_o|$; $wR_2 = \{\Sigma[w(F_o^2-F_c^2)^2]/\Sigma[w(F_o^2)^2]\}^{1/2}$ with $w^{-1} = \sigma^2(F_o^2) + (aP)^2+bP$; $P = [2F_c^2 + \mathrm{Max}(F_O^2]/3$; [b] $s = \{\Sigma[w(F_o^2-F_c^2)^2]/(N_o-N_p)\}^{1/2}$.

Conclusion

In the present work several diiron complexes containing mixed dichalcogenolato ligands (**2**, **3** and **4**) of the [FeFe] hydrogenase active site have been synthesized and characterized. The X-ray crystallographic study shows that the Fe-Fe distances are of **3** is longer than its of **4**, due to the larger atomic size of Se atom compared to the S. The electrochemistry of **2** and **4** reveal the ability of these complexes to be an electrocatalyst for reduction of acetic acid proton to dihydrogen.

Experimental Section

General Comments. All reactions were performed using standard Schlenk and vacuum-line techniques under argon atmosphere. All of the solvents used were dried and distilled prior to use according to the standard methods. The ^1H, $^{13}C\{^1H\}$, $^{77}Se\{^1H\}$ and 2D NMR ($^1H,^1H$ COSY, $^1H,^{13}C$ HSQC, $^1H,^{77}Se$ HMBC) spectra were recorded on either a Bruker AVANCE 200 or 400 MHz spectrometer using the solvent residual peak (^1H, $^{13}C\{^1H\}$ NMR) or a concentrated solution of SeO_2 in D_2O as reference. The ^{77}Se chemical shifts are reported relative to neat Me_2Se [$\delta(Me_2Se) = \delta(SeO_2) + 1302.6$ ppm].[50] Mass spectra were recorded on a FINNIGAN MAT SSQ 710 instrument. IR spectra were measured on a Perkin-Elmer System 2000 FT-IR spectrometer. Elemental analyses were performed with a LECO CHNS-932 apparatus. Silica gel 60 (0.015-0.040 mm) was used for column chromatography, TLC was done using Merck TLC aluminum sheets (Silica gel 60 F_{254}). $Fe_3(CO)_{12}$ was purchased from Aldrich, solvents from Fisher Scientific and other chemicals from Acros, and were used without further purification. Yield calculations were based on substoichiometric utilized chemicals or on $Fe_3(CO)_{12}$ for the diiron complexes.

Preparation of bis(thiocyanatomethyl)selenide (1).
Bis(bromomethyl)selenide (0.30 g, 1.12 mmol) and KSCN (0.22 g, 2.26 mmol) are heated under reflux for 5 hours in acetone and then filtrated to get rid of precipitated KBr. Removal of the solvent under reduce pressure provided **1** as yellow oil (0.25 g, 99%), which was used without further purification. IR (acetone): ν = 2157 (s) cm^{-1}. ^1H NMR (400 MHz, $CDCl_3$): δ = 4.25 (s with ^{77}Se satellites, $^2J_{H,Se}$ = 8.2 Hz, 4H, CH_2) ppm. $^{13}C\{^1H\}$ NMR (100 MHz, $CDCl_3$): δ = 25.4 (s with ^{77}Se satellites, $^1J_{C,Se}$ = 29.1 Hz, CH_2),

111.2 (CN) ppm. $^{1}H^{77}Se$ HMBC (76 MHz, $CDCl_3$): δ = 365.1 ppm. MS (DEI = 70 eV): *m/z* (%) = 224 (54) [M^+], 167 (21) [M^+ – 57; SCN], 73 (15) [M^+ – 151; SCN + $SeCH_2$].

Preparation of bis(selenocyanatomethyl)sulfide (5).
Coumpond **5** was prepared as described above for **1**. While Bis(bromomethyl)sulfide (0.30 g, 1.36 mmol) and KSeCN (0.39 g, 2.71 mmol) refluxed over night. Compound **5** was obtained as yellow oil (0.36 g, 98%) and was used without further purification. IR (acetone): ν = 2152 (s) cm^{-1}. ^{1}H NMR (400 MHz, $CDCl_3$): δ = 4.35 (s with ^{77}Se satellites, $^{2}J_{H,Se}$ = 8.3 Hz, 4H, CH_2) ppm. $^{13}C\{^{1}H\}$ NMR (100 MHz, $CDCl_3$): δ = 25.4 (s with ^{77}Se satellites, $^{1}J_{C,Se}$ = 29.1 Hz, CH_2), 101.5 (SeCN) ppm. $^{1}H^{77}Se$ HMBC (76 MHz, $CDCl_3$): δ = 264.6 (SeCN) ppm. MS (DEI = 70 eV): *m/z* (%) = 270 (48) [M^+], 167 (15) [M^+ – 103; SCN], 120 (44) [M^+ – 150; SeCN + SCH_2].

Preparation of $Fe_2(\mu\text{-}SeCH_2S\text{-}\mu)(CO)_6$ (2) and $Fe_2(\mu\text{-}SCH_2SeCH_2S\text{-}\mu)(CO)_6$ (3).
$Fe_3(CO)_{12}$ (0.20 g, 0.40 mmol) and **1** (0.09 g, 0.40 mmol) were refluxed in THF (40 mL) for one hour under argon. The color of the green solution changed to red-brown. The reaction mixture was cooled to room temperature and the solvent was removed under reduced pressure. The crude brown product was purified by column chromatography (SiO_2/hexane). Complex **2** (0.08 g, 49%) was obtained from the first main fraction, while the second red fraction gave **3** (0.02 g, 11%). Crystals of **3** suitable for X-ray diffraction analysis were obtained by slow evaporation of concentrated pentane solution at 0 °C.
$Fe_2(\mu\text{-}SeCH_2S\text{-}\mu)(CO)_6$ (2). $C_7H_2Fe_2O_6SSe$ (404.8): calcd. for $C_7H_2Fe_2O_6SSe{\cdot}0.25$ hexane C 23.95, H 1.30, S 7.52; found C 24.35, H 1.51, S 7.57. FTIR (KBr): ν = 2073 (s), 2030 (vs), 1992 (vs) cm^{-1}. ^{1}H NMR (400 MHz, $CDCl_3$): δ = 4.24 (s, 2H, CH_2). $^{13}C\{^{1}H\}$ NMR (100 MHz, $CDCl_3$): δ = 46.1 (CH_2), 208.9 (CO) ppm. $^{1}H^{77}Se$ HMBC NMR (76 MHz, $CDCl_3$): δ = 0.8 ($SeCH_2$) ppm. MS (DEI = 70 eV): *m/z* (%) = 406 (66) [M^+], 378 (25) [M^+ – 28; CO], 350 (21) [M^+ – 56; 2CO], 322 (18) [M^+ – 84; 3CO], 294 (29) [M^+ – 112; 4CO], 266 (17) [M^+ – 140; 5CO], 238 (49) [M^+ – 168; 6CO].
$Fe_2(\mu\text{-}SCH_2SeCH_2S\text{-}\mu)(CO)_6$ (3). $C_8H_4Fe_2O_6S_2Se$ (450.89): calcd. C 21.31, H 0.89, S 14.22; found C 20.85, H 1.04, S 14.92. FTIR (KBr): ν = 2076 (s), 2034 (vs), 1997 (vs) cm^{-1}. ^{1}H NMR (400 MHz, $CDCl_3$): δ = 3.30 (s, 4H, CH_2). $^{13}C\{^{1}H\}$ NMR (100 MHz, $CDCl_3$): δ = 16.9 (CH_2), 206.8 (CO) ppm. $^{1}H^{77}Se$ HMBC NMR (76 MHz, $CDCl_3$): δ = 461.1($SeCH_2$) ppm. MS (DEI = 70 eV): *m/z* (%) = 552 (27) [M^+], 424 (22) [M^+ – 28; CO], 396 (15) [M^+ – 56; 2CO], 368 (9) [M^+ – 84; 3CO], 340 (44) [M^+ – 112; 4CO], 312 (49) [M^+ – 140; 5CO], 284 (91) [M^+ – 168; 6CO].

Preparation of $Fe_2(\mu\text{-}SeCH_2SCH_2Se\text{-}\mu)(CO)_6$ (4).
To a green THF solution of $Fe_3(CO)_{12}$ (0.10 g, 0.20 mmol) compound **5** (0.06 g, 0.22 mmol) was added and the mixture was heated under reflux for 1 hour. The resulting dark red mixture was evaporated to dryness and the obtained solid was suspended in a minimum amount of hexane and introduced to column chromatography (SiO_2/hexane). From the major red fraction **4** (0.07 g, 70%) was obtained as red solid. Crystals suitable for X-ray diffraction analysis were obtained from pentane at 0 °C. $C_8H_4Fe_2O_6SSe_2$ (497.79): calcd. C 19.30, H 0.81, S 6.44; found C 19.79, H 0.88, S 6.44. FTIR (KBr): ν = 2069 (s), 2032 (vs), 1993 (s) cm^{-1}. ^{1}H NMR (200 MHz, $CDCl_3$): δ = 3.27 (s, 4H, CH_2) ppm. $^{13}C\{^{1}H\}$ NMR (100 MHz, $CDCl_3$): δ = 17.6 (CH_2), 207.9 (CO) ppm. $^{1}H^{77}Se$ HMBC NMR (76 MHz, $CDCl_3$): δ = 124 ($SeCH_2$) ppm. MS (DEI = 70 eV): *m/z* (%) = 500 (50) [M^+], 472 (21) [M^+ – 28; CO], 444 (11) [M^+ – 56; 2CO], 416 (10) [M^+ – 84; 3CO], 388 (18) [M^+ – 112; 4CO], 358 (22) [M^+ – 140; 5CO], 332 (44) [M^+ – 168; 6CO].

Crystal Structure Determination
The intensity data for the compounds were collected on a Nonius KappaCCD diffractometer, using graphite-monochromated Mo-K_α radiation. Data were corrected for Lorentz and polarization effects, but not for absorption effects.[51,52] Crystallographic data as well as structure solution and refinement details are summarized in Table 2. The structures were solved by direct methods (SHELXS)[53] and refined by full-matrix least squares techniques against F_o^2 (SHELXL-97).[54] All hydrogen atoms were included at calculated positions with fixed thermal parameters. All non-hydrogen atoms were refined anisotropically.[54]

Electrochemical measurements
Instrumentation and the source and treatment of solvent and supporting electrolyte have been reported earlier.[55] All potentials are reported vs. the potential of the ferrocenium/ferrocene (Fc^+/Fc) couple measured in acetonitrile. The voltammetric experiments were conducted at 298 K, using ~1.0 mM of each compound in acetonitrile containing 0.10 M Bu_4NPF_6 on a glassy carbon working electrode (GCE), under an Ar atmosphere. The area of the GCE was determined to be 0.0707 cm^2 from cyclic voltammetric studies of the oxidation of ferrocene in acetonitrile using 2.5 × 10-5 cm^2/s as its diffusion coefficient.[55]

Acknowledgment

Financial support for this work was provided for Mohammad Harb by the Deutscher Akademischer Austausch Dienst (DAAD).

1. Y. Nicolet, C. Cavazza, J. C. Fontecilla-Camps, *J. Inorg. Biochem*. **2002**, *91*, 1-8.
2. S. Shima, O. Pilak, S. Vogt, M. Schick, M. S. Stagni, W. M. Klaucke, E. Warkentin, R. K. Thauer, U. Ermler, *Science*. **2008**, *321*, 572-575.
3. R. Cammack, M. Frey, R. Robson, *Hydrogen as a Fuel: Learning from Nature*, Taylor & Francis, London, **2001**.
4. R. H. B. Coontz, *Science*. **2004**, *305*, 957-975.
5. A. Melis, L. Zhang, M. Forestier, M. L. Ghirardi, M. Seibert, *Plant Physiol*. **2000**, *122*, 127-136.
6. P. C. Hallenbeck, J. R. Benemann, *Int. J. Hydrogen Energy* **2002**, *27*, 1185-1193.
7. P. Tamagnini, R. Axelsson, P. Lindberg, F. Oxelfelt, R. Wünschiers, P. Lindblad, *Microbiol. Mol. Biol. Rev*. **2002**, *66*, 1-20.
8. T. Happe, A. Hemschemeier, M. Winkler, A. Kaminski, *Trends Plant Sci*. **2002**, *7*, 246-250.
9. M. Frey, *Chembiochem*. **2002**, *3*, 153-160.
10. P. M. Vignais, B. Billoud, *Chem. Rev*. **2007**, *107*, 4206-4272.
11. A. L. De Lacey, V. M. Fernandez, M. Rousset, R. Cammack, *Chem. Rev*. **2007**, *107*, 4304-4330.
12. X. Zhao, I. P. Georgakaki, M. L. Miller, J. C. Yarbrough, M. Y. Darensbourg, *J. Am. Chem. Soc*. **2001**, *123*, 9710–9711.
13. X. Zhao, C. Y. Chiang, M. L. Miller, M. V. Rampersad, M. Y. Darensbourg, *J. Am. Chem. Soc*. **2003**, *125*, 518–524
14. F. Gloaguen, J. D. Lawrence, M. Schmidt, S. R. Wilson, T. B. Rauchfuss, *J. Am. Chem. Soc*. **2001**, *123*, 12518–12527.
15. E. J. Lyon, I. P. Georgakaki, J. H. Reibenspies, M. Y. Darensbourg, *J. Am. Chem. Soc*. **2001**, *123*, 3268–3278.
16. J. D. Lawrence, H. Li, T. B. Rauchfuss, M. Benard, M. M. Rohmer, *Angew. Chem. Int. Ed*. **2001**, *40*, 1768–1771.
17. H. Li, T. B. Rauchfuss, *J. Am. Chem. Soc*. **2002**, *124*, 726–727
18. S. Ott, M. Kritikos, B. Åkermark, L. Sun, *Angew. Chem. Int. Ed*. **2003**, *42*, 3285–3288.
19. M. Razavet, S. C. Davies, D. L. Hughes, J. E. Barclay, D. J. Evans, S. A. Fairhurst, X. Liu, C. J. Pickett, *Dalton Trans*. **2003**, 586–595.
20. C. Tard, X. Liu, S. K. Ibrahim, M. Bruschi, L. De Gioia, S. C. Davies, X. Yang, L.-S. Wang, G. Sawers, C. J. Pickett, *Nature* **2005**, *433*, 610–613.
21. L.-C. Song, Z.-Y. Yang, H.-Z. Bian, Q.-M. Hu, *Organometallics* **2004**, *23*, 3082–3084.
22. S. Ezzaher, J.-F. Capon, F. Gloaguen, F. Y. Petillon, P. Schollhammer, J. Talarmin, *Inorg. Chem*. **2009**, *48*, 2-4.
23. D. Seyferth, G. B. Womack, M. K. Gallagher, M. Cowie, B. W. Hames, , J. P. Fackler, A. M. Mazany, *Organometallics* **1987**, *6*, 283-294.
24. U.-P. Apfel, Y. Halpin, H. Görls, J. G. Vos, B. Schweizer, G. Linti, W. Weigand, *Chem. Biodiv*. **2007**, *4*, 2138-2148.
25. J. Windhager, M. Rudolph, S. Bräutigam, H. Görls, W. Weigand, *Eur. J. Inorg. Chem*. **2007**, *18*, 2748-2760.
26. J. Windhager, H. Görls, H. Petzold, G. Mloston, G. Linti, W. Weigand, *Eur. J. Inorg. Chem*. **2007**, *28*, 4462-4471.
27. J. Windhager, R. A. Seidel, U.-P. Apfel, H. Görls, G. Linti, W. Weigand, *Eur. J. Inorg. Chem*. **2008**, *10*, 2023-2041.
28. L.-C. Song, Z.-Y. Yang, H.-Z. Bian, Y. Liu, H.-T. Wang, X.-F. Liu, Q.-M. Hu, *Organometallics* **2005**, *24*, 6126–6135.
29. S. Ezzaher, J.-F. Capon, F. Gloaguen, F. Y. Pétillon, P. Schollhammer, J. Talarmin, *Inorg. Chem*. **2007**, *46*, 9863-9872.

30. P.-Y. Orain, J.-F. Capon, N. Kervarec, F. Gloaguen, F. Y. Petillon, R. Pichon, P. Schollhammer, J. Talarmin, *Dalton Trans*. **2007**, 3754-3756.
31. T.-T. Zhang, M. Wang, N. Wang, P. Li, Z.-Y. Liu, L.-C. Sun, *Polyhedron* **2009**, *28*, 1138-1144.
32. D. Morvan, J.-F. Capon, F. Gloaguen, F. Y. Pétillon, P. Schollhammer, J. Talarmin, J.-J. Yaouanc, F. Michaud, N. Kervarec, *J. Organomet. Chem.* **2009**, *694*, 2801-2807.
33. L.-C. Song, X. Luo, Y.-Z. Wang, B. Gai, Q.-M. Hu, *J. Organomet. Chem.* **2009**, *694*, 103-112.
34. S. Gao, J. Fan, S. Sun, X. Peng, X. Zhao, J. Hou, *Dalton Trans*. **2008**, 2128-2135.
35. U.-P. Apfel, Y. Halpin, M. Gottschaldt, H. Görls, J. G. Vos, W. Weigand, *Eur. J. Inorg. Chem.* **2008**, 5112–5118.
36. M. K. Harb, T. Niksch, J. Windhager, H. Görls, R. Holze, L. T. Lockett, N. Okumura, D. H. Evans, R. S. Glass, D. L. Lichtenberger, M. El-khateeb, W. Weigand, *Organometallics* **2009**, *28*, 1039-1048.
37. L.-C. Song, B. Gai, H.-T. Wang, Q.-M. Hu, *J. Inorg. Biochem.* **2009**, *103*, 805-812.
38. M. K. Harb, J. Windhager, A. Daraosheh, H. Görls, L. T. Lockett, N. Okumura, D. H. Evans, R. S. Glass, D. L. Lichtenberger, M. El-khateeb, W. Weigand, *Eur. J. Inorg. Chem.* **2009**, 3414-3420.
39. A. Q. Daraosheh, M. K. Harb, J. Windhager, H. Görls, M. El-khateeb, W. Weigand, *Organometallics* **2009**, *28*, 6275-6280.
40. M. K. Harb, U.-P. Apfel, J. Kübel, H. Görls, G. A. N. Felton, T. Sakamoto, D. H. Evans, R. S. Glass, D. L. Lichtenberger, M. El-khateeb, W. Weigand, *Organometallics* **2009**, In press (doi: 10.1021/om900675q).
41. M. Shieh, M.-H. Shieh, *Organometallics* **1994**, *13*, 920-924.
42. G. A. Kalabin, V. M. Bzhezovskii, D. F. Kushnarev, A. G. Proidakov, *Zh. Org. Khim.* **1981**, *17*, 1143.
43. A. Shaver, P. J. Fitzpatrick, K. Steliou, I. S. Butler, *J. Am. Chem. Soc.* **1979**, *101*, 1313-1315.
44. P. Mathur, B. Manimaran, R. Trivedi, M. M. Hossain, M. Arabatti, *J. Organomet. Chem.* **1996**, *515*, 155-162.
45. L.-C. Song, Z.-Y. Yang, Y.-J. Hua, H.-T. Wang, Y. Liu, Q.-M. Hu, *Organometallics* **2007**, *26*, 2106-2110.
46. H. A. Bent, *Chem. Rev.* **1961**, *61*, 275–311.
47. G. A. N. Felton, B. J. Petro, R. S. Glass, D. L. Lichtenberger, D. H. Evans, *J. Am. Chem. Soc.* **2009**, *131*, 11290-11291.
48. G. A. N. Felton, C. A. Mebi, B. J. Petro, A. K. Vannucci, D. H. Evans, R. S. Glass, D. L. Lichtenberger, *J. Organomet. Chem.* **2009**, *694*, 2681-2699.
49. K. Izutsu, *Acid-Base Dissociation Constants in Dipolar Aprotic Solvents;* Blackwell Scientific Publishers: Oxford, UK, **1990**.
50. R. C. Burns, M. J. Collins, R. J. Gillespie, G. J. Schrobilgen, *Inorg. Chem.* **1986**, *25*, 4465-4469.
51. *COLLECT*, Data Collection Software; Nonius, B.V. Netherlands. **1998**.
52. Z. Otwinowski, W. Minor, "Processing of X-Ray Diffraction Data Collected in Oscillation Mode" in *Methods in Enzymology*, vol. 276, *Macromolecular Crystallography*, Part A, Academic press: San Diego **1997**, pp. 307-326.
53. G. M. Sheldrick, *Acta Crystallogr. Sect. A* **1990**, *46*, 467-473.
54. G. M. Sheldrick, SHELXL-97 (Release 97-2), University of Göttingen, Germany, **1997**.
55. N. A. Macías-Ruvalcaba, D. H. Evans, *J. Phys. Chem. B* **2005**, *109*, 14642-14647.

4 Documentation of Authorship

[MK1] M. K. Harb, T. Niksch, J. Windhager, H. Görls, R. Holze, L. T. Lockett, N. Okumura, D. H. Evans, R. S. Glass, D. L. Lichtenberger, M. El-khateeb, W. Weigand. ***Synthesis and Characterization of Diiron Diselenolato Complexes Including Iron Hydrogenase Models.*** *Organometallics* **2009**, *28*, 1039-1048.

- M. K. Harb: Synthesis and characterization of all complexes
  Preparation of manuscript
- T. Niksch: Synthesis of 3-methyl-1,2-diselenolane and
  1,3,5-triselenacyclohexane
- J. Windhager: Assistance in complex preparation
- H. Görls: X-Ray structures analyses
- R. Holze/D. Evans: Electrochemical investigations
- L. T. Lockett: Assistance in preparation of electrochemical investigations
- R. Glass: Preparation of DFT calculations and PES investigations
- D. Lichtenberger: Preparation of DFT calculations and PES investigations
- N. Okumura: Assistance in preparation of DFT calculations
- M. El-khateeb: Co-Adviser, Preparation of manuscript
- W. Weigand: Supervision, Preparation of manuscript

[MK2] M. K. Harb, J. Windhager, A. Daraosheh, H. Görls, L. T. Lockett, N. Okumura, D. H. Evans, R. S. Glass, D. L. Lichtenberger, M. El-khateeb, W. Weigand. ***Phosphane- and Phosphite-Substituted Diiron Diselenolato Complexes as Models for [FeFe]-Hydrogenases.*** *Eur. J. Inorg. Chem.* **2009**, 3414-3420.

- M. K. Harb: Synthesis and characterization of all complexes
  Preparation of manuscript
- J. Windhager: Assistance in manuscript preparation
- A. Q. Daraosheh: Assistance in complex preparation
- H. Görls: X-Ray structures analyses

- L. Lockett/N. Okumura: Assistance in preparation of electrochemical investigations
- D. H. Evans: Electrochemical investigations
- R. S. Glass: Electrochemical investigations
- D. L. Lichtenberger: Electrochemical investigations
- M. El-khateeb: Co-Adviser, Preparation of manuscript
- W. Weigand: Supervision, Preparation of manuscript

[MK3] A. Q. Daraosheh, M. K. Harb, J. Windhager, H. Görls, M. El-khateeb, W. Weigand. ***Substitution Reactions at [FeFe]-Hydrogenase Models Containing [2Fe3S] Cluster by Phosphine or Phosphite Ligands.*** *Organometallics* **2009**, *28*, 6275-6280.

- A. Q. Daraosheh: Synthesis and Characterization of all complexes
  Preparation of manuscript
- M. K. Harb: Assistance in complex preparation
  Assistance in manuscript preparation
- J. Windhager: Assistance in complex preparation
- H. Görls: X-Ray structures analyses
- M. El-khateeb: Co-Adviser, Preparation of manuscript
- W. Weigand: Supervision, Preparation of manuscript

[MK4] M. K. Harb, U.-P. Apfel, J. Kübel, H. Görls, G. A. N. Felton, T. Sakamoto, D. H. Evans, R. S. Glass, D. L. Lichtenberger, M. El-khateeb, W. Weigand. ***Preparation and Characterization of Homologous Diiron Dithiolato, Diselenato, and Ditellurato Complexes: [FeFe]-Hydrogenase Models.*** *Organometallics* **2009**, *28*, 6666-6675.

- M. K. Harb: Synthesis and Characterization of all complexes
  Preparation of manuscript
- U.-P. Apfel: Assistance in complex preparation
- J. Kübel: Assistance (undergraduate student)
- H. Görls: X-Ray structures analyses

- G. A. N. Felton: Assistance in preparation of DFT calculations
- T. Sakamoto: Assistance in preparation of electrochemical investigations
- D. H. Evans: Electrochemical and DFT calculations
- R. S. Glass: Electrochemical and DFT calculations
- D. L. Lichtenberger: Electrochemical and DFT calculations
- M. El-khateeb: Co-Adviser, Preparation of manuscript
- W. Weigand: Supervision, Preparation of manuscript

[MK5] M. K. Harb, H. Görls, T. Sakamoto, G. A. N. Felton, D. H. Evans, R. S. Glass, D. L. Lichtenberger, M. El-khateeb, W. Weigand. ***Synthesis and Characterization of [FeFe]-Hydrogenases Models with Bridging Moieties Containing (S, Se) and (S, Te).*** *Eur. J. Inorg. Chem.* **2010**, Accepted.

- M. K. Harb: Synthesis and characterization of all complexes
  Preparation of manuscript
- H. Görls: X-Ray structures analyses
- T. Sakamoto: Assistance in preparation of electrochemical investigations
- G. A. N. Felton: Assistance in preparation of DFT and PES calculations
- D. H. Evans: Electrochemical, DFT and PES calculations
- R. S. Glass: Electrochemical, DFT and PES calculations
- D. L. Lichtenberger: Electrochemical, DFT and PES calculations
- M. El-khateeb: Co-Adviser, Preparation of manuscript
- W. Weigand: Supervision, Preparation of manuscript

[MK6] M. K. Harb, A. Daraosheh, H. Görls, D. H. Evans, R. S. Glass, D. L. Lichtenberger, M. El-khateeb, W. Weigand. ***[FeFe]-Hydrogenase Models Containing Different Length Diselenolato Bridging Moieties.*** *In preparation*.

- M. K. Harb: Synthesis and Characterization of all complexes
  Preparation of manuscript

- A. Q. Daraosheh: Assistance in ligands preparation
- H. Görls: X-Ray structures analyses
- D. H. Evans: Electrochemical and DFT calculations
- D. L. Lichtenberger: Electrochemical and DFT calculations
- R. S. Glass: Electrochemical and DFT calculations
- M. El-khateeb: Co-Adviser, Preparation of manuscript
- W. Weigand: Supervision, Preparation of manuscript

[MK7] M. K. Harb, A. Daraosheh, T. Niksch, H. Görls, R. S. Glass, D. L. Lichtenberger, M. El-khateeb, W. Weigand. ***Synthesis and Characterization of Novel [FeFe]-Hydrogenase Models Containing Mixed S and Se Bridging Moieties.*** *In preparation*.

- M. K. Harb: Synthesis and Characterization of all complexes
  Preparation of manuscript
- A. Q. Daraosheh: Assistance in ligands preparation
- T. Niksch: Assistance in ligands preparation
- H. Görls: X-Ray structures analyses
- D. H. Evans: Preparation of DFT calculations
- D. L. Lichtenberger: Electrochemical investigations
- R. S. Glass: Assistance in manuscript preparatio
- M. El-khateeb: Co-Adviser, Preparation of manuscript
- W. Weigand: Supervision, Preparation of manuscript

5 Summary

This dissertation focused on the synthesis and characterization of novel model complexes of the [FeFe]-hydrogenase active site. The electrochemical properties for the newly prepared compounds have been studied to assess their ability to catalyze electrochemical reduction of protons to give dihydrogen. All attached articles [MK1]-[MK7] deal with the structural and electrochemical investigations of synthesized model complexes. Furthermore, [MK1], [MK3] and [MK5] payed attention to the photoelectron spectroscopy of some compounds. The electronic structure of these complexes is further analyzed with the aid of DFT computations. To give the reader a brief overview of the work, the articles are shortly summarized below.

[MK1]: The first article describes several diiron diselenolato complexes which have been prepared as models of the active site of [FeFe]-hydrogenase. The reactions of 1,3-diselenocyanatopropane, 3-methyl-1,2-diselenolane and 1,3,5-triselenacyclohexane with $Fe_3(CO)_{12}$ have been investigated. These reactions afforded the model compounds $Fe_2(\mu\text{-}Se_2C_3H_6)(CO)_6$, $Fe_2(\mu\text{-}Se_2C_3H_5CH_3)(CO)_6$ and a mixture of $Fe_2(\mu^2,\kappa\text{-}Se,C\text{-}SeCH_2SeCH_2)(CO)_6$, $Fe_2[(\mu\text{-}SeCH_2)_2Se](CO)_6$, $Fe_2(\mu\text{-}Se_2CH_2)(CO)_6$, respectively. The compounds were characterized by IR, ^1H, ^{13}C, ^{77}Se NMR spectroscopy, mass spectrometry, elemental analysis and X-ray single crystal structure analysis. The electrochemical properties for $Fe_2(\mu\text{-}Se_2C_3H_6)(CO)_6$ and $Fe_2(\mu\text{-}Se_2C_3H_5CH_3)(CO)_6$ have been also studied and proved their ability to catalyze electrochemical reduction of protons to give dihydrogen. Moreover, the photoelectron spectrum and theoretical calculations of $Fe_2(\mu\text{-}Se_2C_3H_5CH_3)(CO)_6$ were studied and revealed that the reorganization energy is substantially lower than that for sulfur analogous complexes. This observation could lead to faster electron transfer with complexes containing [2Fe2Se] rather than [2Fe2S] cores.

[MK2]: In this article the substitution of one or two carbonyl groups of $Fe_2(\mu\text{-}Se_2C_3H_5CH_3)(CO)_6$ by PPh_3, $P(OMe)_3$ or dppe were investigated and leads to syntheses of several [FeFe]-hydrogenase models containing [2Fe2Se] core. $Fe_2(\mu\text{-}Se_2C_3H_5CH_3)(CO)_5(PPh_3)$ has proved to be a catalyst for the electrochemical reduction of the weak acid, acetic acid, to give molecular hydrogen.

[MK3]: This paper investigated the substitution of CO at [2Fe3S] cluster complex $Fe_2(\mu\text{-}S_2(C_3H_6)_2S\text{-}\mu)(CO)_5$ with $P(OMe)_3$ and PMe_3. The newly prepared model complexes were characterized by spectroscopic techniques and X-ray structure determination.

[MK4]: In this article, we extended our effort to prepare complexes containing ditellurolato ligands. Accordingly, a series of oxetane-containing diiron dithiolato, diselenolato, and ditellurolato complexes have been prepared In order to elucidate the influence of the bridging chalcogen atoms on the hydrogenases model complexes and to compare the S, Se and Te homologues to each other. Treatment of $Fe_3(CO)_{12}$ with 3,3-bis(thiocyanatomethyl)oxetane afforded the model compound $Fe_2(\mu\text{-}S_2C_5H_8O)(CO)_6$. The analogous diselenolato and ditellurolato complexes, $Fe_2(\mu\text{-}Se_2C_5H_8O)(CO)_6$ and $Fe_2(\mu\text{-}Te_2C_5H_8O)(CO)_6$, were obtained from the reaction of $Fe_3(CO)_{12}$ with 2-oxa-6,7-diselenaspiro[3.4]octane and 2-oxa-6,7-ditelluraspiro[3.4]octane, respectively. The new compounds were characterized by IR, ^{1}H-, $^{13}C\{^1H\}$-, $^{77}Se\{^1H\}$-NMR spectroscopy, mass spectrometry, elemental analysis and X-ray single crystal structure analysis. On the bases of electrochemical investigations of S, Se and Te compounds, we concluded that the rate of catalytic reduction of protons to hydrogen is substantially diminished from S to Se to Te. The reorganization energy for the action of S, Se and Te compounds decreased on going from S to Te. In order to find out the ability of our complexes to form the structure with a rotated $Fe(CO)_3$ group that has a bridging carbonyl ligand and a vacant coordination site for protonation, spectroscopic and computational analysis were studied. We found that this ability is disfavoured on going from the S to Se to Te complexes, which clarify the decreasing in the catalytic reduction rate of protons to give H_2 on going from the sulfur to selenium to tellurium compounds.

[MK5]: Here, diiron model complexes containing (S, Se) or (S, Te) atoms have been prepared, characterized and evaluated with electrochemistry, photoelectron spectroscopy (PES) and density functional theory (DFT) calculations. Treatment of $Fe_3(CO)_{12}$ with 1,2-thiaselenolane or 1,2-thiatellurolane resulted in the formation of the diiron complexes $Fe_2(\mu\text{-}SC_3H_6Se\text{-}\mu)(CO)_6$ or $Fe_2(\mu\text{-}SC_3H_6Te\text{-}\mu)(CO)_6$, respectively.

These complexes with mixed dichalcogenolato ligands are analogous to the much-studied molecule $Fe_2(\mu\text{-}SC_3H_6S)(CO)_6$. The purposes that we launched such a study are:

(i) To prepare the first examples of diiron models containing mixed dichalcogenolato atoms.

(ii) To elucidate the influence of the bridged iron cores containing mixed dichalcogenolato ligands on the structure and activity of hydrogenase model complexes.

(iii) Direct comparison of our complexes with the extensively studied dithiolato compound for its ability to catalyze the formation of H_2 from weak acids.

The electrochemistry of these complexes was investigated and reveals their ability to be good catalysts for the reduction of acetic acid to dihydrogen. The catalytic efficiency of the Se and Te containing molecules found to be comparable to that of all-sulfur containing molecule. Combinations of experimental and computational analyses have provided useful insight into the electronic perturbations resulting from single chalcogen substitutions at the diiron core of the molecules. He I photoelectron spectra and DFT computations of my complexes show a lowering of ionization energies compared to those of the all-sulfur complex, indicating increased electron richness at the metal centers that favors electrocatalytic reduction of protons from weak acids to produce H_2. However, chalcogen substitution from S to Se or Te also causes an increase in the Fe–Fe bond distance, which disfavors the formation of a carbonyl-bridged "rotated" structure, as also shown by the photoelectron spectra and computations.

[MK6]: In the present publication, our goal is to prepare butterfly the diiron $Fe_2(\mu\text{-}Se(CH_2)_xSe\text{-}\mu)(CO)_6$ and the tetrairon $[Fe_2(\mu\text{-}Se(CH_2)_ySe\text{-}\mu)(CO)_6]_2$ model complexes containing selenolato ligands with different length linker (x = 5, 6; y = 4, 5, 6). We launched such a study in order to determine the role of the length of the diselenolato linker in the [FeFe] model complexes and to elucidate the influence of the length of the linker on the structure of hydrogenases model complexes. Compound $Fe_2(\mu$-

$Se(CH_2)_4Se$-μ)$(CO)_6$ has been proved to be good catalysts for proton reduction of the weak acid to give hydrogen under electrochemical conditions.

[MK7]: In this work, treatment of $Fe_3(CO)_{12}$ with bis(thiocyanatomethyl)selenide gave a mixture of Fe_2(μ-$SeCH_2S$-μ)$(CO)_6$ and Fe_2(μ-SCH_2SeCH_2S-μ)$(CO)_6$. Moreover, the compound Fe_2(μ-$SeCH_2SCH_2Se$-μ)$(CO)_6$ was prepared from the reaction of $Fe_3(CO)_{12}$ with bis(selenocyanatomethyl)sulfide. We lunched such a study in order to elucidate the influence of the bridging unit containing mixed S and Se atoms on the structure and electrochemical ability of the hydrogenase model complexes. The ability of these complexes to act as models of the [FeFe]-hydrogenase will be also studied.

Summary in German

Zusammenfassung

Meine Dissertation beschäftigt sich mit der Synthese und Charakterisierung von neuartigen Modellen des aktiven Zentrums der [FeFe]-Hydrogenase. Zur Evaluierung der katalytischen Eigenschaften dieser Komplexe, Wasserstoff aus Protonen zu generieren, wurden die elektrochemischen Eigenschaften in Anwesenheit von Säuren untersucht. Die beigefügten Artikel [MK1]-[MK7] beschreiben die elektrochemischen und strukturellen Eigenschaften der Modelverbindungen. Zusätzlich wurden die elektronischen Eigenschaften einiger dieser Substanzen durch Photoelektronenspektroskpopie (PES) aufgeklärt und durch DFT-Rechnungen weiterhin verifiziert. Um den Leser dieser Dissertation einen Einblick in meine Forschung zu gewähren, soll der Inhalt der Publikationen kurz wiedergegeben werden.

[MK1]: Der erste Artikel befaßt sich mit verschiedenen Dieisendiselenolato Komplexen, die als Modelle für das aktive Zentrum der [FeFe]-Hydrogenase hergestellt wurden. Dazu wurden die Reaktionen von 1,3-Diselenocyanatopropan, 3-Methyl-1,2-diselenolan und 1,3,5-Triselenacyclohexan mit $Fe_3(CO)_{12}$ untersucht, und es konnten $Fe_2(\mu\text{-}Se_2C_3H_6)(CO)_6$, $Fe_2(\mu\text{-}Se_2C_3H_5CH_3)(CO)_6$ sowie $Fe_2(\mu^2,\kappa\text{-Se,C-}SeCH_2SeCH_2)(CO)_6$ und $Fe_2[(\mu\text{-}SeCH_2)_2Se](CO)_6$, $Fe_2(\mu\text{-}Se_2CH_2)(CO)_6$, isoliert werden. Die Substanzen wurden vollständig durch IR, ^1H, ^{13}C, ^{77}Se NMR Spektroskopie, Massenspektroskopie als auch durch Elementaranalyse und Röntgenstrukturanalyse aufgeklärt werden. Zyklovoltammetrische Untersuchungen von $Fe_2(\mu\text{-}Se_2C_3H_6)(CO)_6$ und $Fe_2(\mu\text{-}Se_2C_3H_5CH_3)(CO)_6$ zeigten, dass die Komplexe in der Lage sind, Protonen elektrochemisch zu Wasserstoff zu reduzieren. Weiterhin wurde mittels PES sowie mit DFT-Rechnungen gezeigt, dass die Reorganisationsenergie der Selen-haltigen Komplexe beträchtlich niedriger war, als diese, die für die entsprechenden Schwefel-haltigen Komplexe gefunden wurde. Ein schnellerer Elektronentransfer sollte demzufolge allgemein für [2Fe2Se] Komplexe zu beobachten sein.

[MK2]: Die Substitution von einer oder zwei Carbonylgruppen in $Fe_2(\mu\text{-}Se_2C_3H_5CH_3)(CO)_6$ durch PPh_3, $P(OMe)_3$ oder dppe führten zu neuartigen [2Fe2Se]-Komplexen. Es zeigte sich dabei, dass $Fe_2(\mu\text{-}Se_2C_3H_5CH_3)(CO)_5(PPh_3)$ in der Lage ist, elektrochemisch Wasserstoff aus Essigsäure zu generieren.

[MK3]: Diese Publikation befaßt sich mit Subtitutionsreaktionen von CO durch $P(OMe)_3$ und PMe_3 in $Fe_2(\mu\text{-}S_2(C_3H_6)_2S\text{-}\mu)(CO)_5$, einem [2Fe3S]-Komplex. Die resultierenden Komplexe konnten sowohl durch NMR-Spektroskopie, als auch Röntgenbeugungsuntersuchungen und Elementaranalyse charakterisiert werden.

[MK4]: Die Synthese von homologen Dichalcogenolatokomplexen stand im Mittelpunkt dieser Veröffentlichung. Es wurde eine Serie von [2Fe2S], [2Fe2Se] und [2Fe2Te] Komplexen hergestellt, die einen Oxetanring enthalten, der die Stabilität der Komplexe besonders begünstigt. Es sollten dabei die Einflüsse der Chalkogenbrückenkopfatome auf die Eigenschaften der Komplexe getestet werden. Die Komplexe konnten durch Reaktion von $Fe_3(CO)_{12}$ mit den jeweiligen Chalkogenverbindungen (2-oxa-6,7-dichalkogenaspiro[3.4]octan) erhalten werden. Diese Komplexe wurden mittels IR, ^{1}H-, $^{13}C\{^{1}H\}$-, $^{77}Se\{^{1}H\}$-NMR-Spektroskopie, Massenspektrometrie und Einkristallstrukturanalyse charakterisiert. Zyklovoltammetrische Untersuchungen zeigten eine deutliche Verringerung der katalytischen Wasserstoffgenerierung von Schwefel- zu den höheren Selen- und Tellurkomplexen. Ebenfalls konnte eine Verringerung der Reorganisationsenergie von Schwefel zu Tellur festgestellt werden. Die Untersuchungen ergaben auch, dass die Fähigkeit der Komplexe, in einer rotated Form verbrückende Carbonylliganden und damit eine freie Koordinationsstelle auszubilden, in der Reihe S, Se und Te stark abnimmt und damit auch die katalytischen Eigenschaften, Protonen zu Wasserstoff zu reduzieren, geringer werden.

[MK5]: In dieser Publikation wird die Synthese von Dieisen-Komplexen, welche (S, Se) oder (S, Te) Atome besitzen, beschrieben. Die erhaltenen Verbindungen wurden spektroskopisch, elektrochemischer, mittels PES sowie mit DFT-Rechnungen vollständig

charakterisiert. Die Reaktionen von $Fe_3(CO)_{12}$ mit 1,2-Thiaselenolan bzw. 1,2-Thiatellurolan führen zur Bildung der Dieisen-Komplexe $Fe_2(\mu\text{-}SC_3H_6Se\text{-}\mu)(CO)_6$ bzw. $Fe_2(\mu\text{-}SC_3H_6Te\text{-}\mu)(CO)_6$. Diese Komplexe mit gemischten Dichalkogenato-Liganden sind Homologe des bereits sehr gut untersuchten $Fe_2(\mu\text{-}SC_3H_6S)(CO)_6$ Komplexes. Die Untersuchungen wurden hier aus folgenden Gründen vertieft:

(i) Synthese der ersten Beispiele für gemischte Dichalkogenato-Dieisen Komplexe

(ii) Bestimmung des Einflusses auf die Hydrogenase-Aktivität

(iii) Vergleich der strukturellen Ähnlichkeiten mit dem aktiven Zentrum der natürlichen [FeFe]-Hydrogenase

Die elektrochemischen Untersuchungen zeigen, dass die Komplexe die Reduktion von Protonen zu molekularem Wasserstoff katalysieren und vergleichbar mit den Aktivitäten der Dithiolato-Komplexe sind. Das He I PES-Spektrum und DFT Berechnungen belegen eine Erniedrigung der Ionisationsenergien im Vergleich zu den Dithiolato-Komplexen, was für eine Erhöhung der Elektronendichte an den Metallzentren spricht, an denen die Protonenreduktion zu Wasserstoff stattfindet. Die Chalkogensubstitution führt in der Reihe S → Se → Te zu einer Verlängerung der Fe-Fe Abstände, womit die Bildung der rotated Form immer unwahrscheinlicher wird, was PES und DFT-Berechnungen belegen.

[MK6]: Diese Publikation beschäftigt sich mit der Synthese des Dieisenkomplexes $Fe_2(\mu\text{-}Se(CH_2)_xSe\text{-}\mu)(CO)_6$ sowie des Tetraeisenkomplexes $[Fe_2(\mu\text{-}Se(CH_2)_ySe\text{-}\mu)(CO)_6]_2$ bei denen die Selenato-Liganden über unterschiedlich lange Linker verknüpft sind (x = 5, 6; y = 4, 5, 6). Insbesondere wurde der Einfluss des Linkers auf die Struktur der [FeFe]-Hydrogenase-Modelle untersucht. Weiterhin konnte gezeigt werden, dass der Komplex $Fe_2(\mu\text{-}Se(CH_2)_4Se\text{-}\mu)(CO)_6$ als guter Katalysator für die Protonenreduktion zu Wasserstoff in Anwesenheit von schwachen Säuren wirkt.

[MK7]: In dieser Arbeit wird die Reaktion von $Fe_3(CO)_{12}$ mit Bis(thiocyanatomethyl)selenid betrachtet, welche ein Gemisch aus $Fe_2(\mu\text{-}SeCH_2S\text{-}\mu)(CO)_6$ und $Fe_2(\mu\text{-}SCH_2SeCH_2S\text{-}\mu)(CO)_6$ ergab. Weiterhin konnte die Verbindung $Fe_2(\mu\text{-}SeCH_2SCH_2Se\text{-}\mu)(CO)_6$ durch die Reaktion von $Fe_3(CO)_{12}$ mit

Bis(selenocyanatomethyl)sulfid synthetisiert werden. Die Forschungen wurden hier vertieft, um den Einfluss der überbrückenden S- und Se-Atome auf die Struktur und die Hydrogenaseaktivität zu bewerten.

6. References

1. A. Melis, L. Zhang, M. Forestier, M. L. Ghirardi, M. Seibert, *Plant Physiol.* **2000**, *122*, 127.
2. R. Cammack, M. Frey, R. Robson, Hydrogen as a fuel: Learning from Nature, Taylor & Francis, London, **2001**, p. 267.
3. J. Woodward, M. Orr, K. Cordray, E. Greenbaum, *Nature* **2000**, *405*, 1014.
4. R. H. B. Coontz, *Science* **2004**, *305*, 957.
5. Y. Nicolet, C. Cavazza, J. C. Fontecilla-Camps, *J. Inorg. Biochem.* **2002**, *91*, 1.
6. M. Ball, M. Wietschel, *Int. J. Hydrogen Energy* **2009**, *34*, 615.
7. P. Tamagnini, R. Axelsson, P. Lindberg, F. Oxelfelt, R. Wünschiers, P. Lindblad, *Microbiol. Mol. Biol. Rev.* **2002**, *66*, 1.
8. T. Happe, A. Hemschemeier, M. Winkler, A. Kaminski, *Trends Plant Sci.* **2002**, *7*, 246.
9. V. Ananthachar, J. J. Duffy, *Solar Energy* **2005**, *78*, 686.
10. L. E. Macaskie, V. S. Baxter-Plant, N. J Creamer, A. C. Humphries, I. P. Mikheenko, P. M. Mikheenko, D. W. Penfold, P. Yong, *Biochem Soc Trans* **2005**, *33*, 76.
11. Y.-H. Zhang, B. R. Evans, J. R. Mielenz, R. C. Hopkins, M. W. W. Adams, *PLoS ONE* **2007**, *e456*, 1.
12. M. J. Antal, S. G. Allen, D. Schulman, X. Xu, R. J. Divilio, *Ind. Eng. Chem. Res.* **2000**, *39*, 4040.
13. P. C. Hallenbeck, J. R. Benemann, *Int. J. Hydrogen Energy* **2002**, *27*, 1185.
14. R.D. Cortright, R. R. Davda, J. A. Dumesic, *Nature* **2002**, *418*, 964.
15. G. W. Huber, J. W. Shabaker, J. A. Dumesic, *Science* **2003**, *300*, 2075.
16. G. A. Deluga, J. R. Salge, L. D. Schmidt, X. E. Verykios, *Science* **2004**, *303*, 993.
17. M. W. W. Adams, E. I. Stiefel, *Science* **1998**, *282*, 1842.
18. M. Winkler, A. Hemschemeier, C. Gotor, A. Melis,T. Happe, *Int. J. Hydrogen Energy* **2002**, *27*, 1431.
19. A. Melis, T. Happe, *Plant Physiol* **2001**, *127*, 740.
20. J. Yano, J. Kern, K. Sauer, M. J. Latimer, Y. Pushkar, J. Bieseadka, B. Loll, W. Saenger, J. Messinger, A. Zouni, V. K. Yachandra, *Science* **2006**, *314*, 821.

21. R. Nandi, S. Sengupta, *Critical Review Microbiology* **1998**, *24*, 1.
22. N. Kataoka, A. Miya, K. Kiriyama, *Water Science Technology* **1997**, *36*, 41.
23. A. Kumar, S. R. Jain, C. B. Sharma, A. P. Joshi, V. C. Kalia, *World journal of Microbiology and Biotechnology* **1995**, *11*, 156.
24. H. Yokoi, T. Tokushige, J. Hirose, S. Hayashi, Y. Takasaki, *Journal of Fermentation and Bioengineering* **1997**, *83*, 481.
25. E. Fascetti, O. Todini, *Applied Microbiology and Biotechnology* **1995**, *44*, 300.
26. A. S. Fedorov, A. A. Tsygankov, K. K. Rao, D. O. Hall, *Biotechnology Letters* **1998**, *20*, 1007.
27. S. A. Markov, P. F. Weaver, M. Seibert, *Applied Biochemistry and Biotechnology* **1997**, *63-65*, 577.
28. T. Akano, Y. Miura, K. Fukatsu, H. Miyasaka, Y. Ikuta, H. Matsumoto, A. Hamasaki, N. Shioji, T. Mizoguchi, K. Yagi, I. Maeda, *Applied Biochemistry and Biotechnology* **1996**, *57-58*, 677.
29. V. B. Borodin, A. A. Tsygankov, K. K. Rao, D. O. Hall, *Biotechnology and Bioengineering* **2000**, *69*, 478.
30. T. Matsunaga, T. Hatano, A. Yamada, *Biotechnology and Bioengineering* **2000**, *68*, 647.
31. A. Karlsson, L. Vallin, J. Ejlertsson, *Int. J. Hydrogen Energy* **2008**, *33*, 953.
32. F. R. Hawkes, H. Forsey, G. C. Premier, R. M. Dinsdale, D. L. Hawkes, A. J. Guwy, J. Maddy, S. Cherryman, J. Shine, D. Auty, *Bioresour Technol* **2008**, *99*, 5020.
33. K. Sasikala, C. V. Ramana, P. R. Rao, *Int. J. Hydrogen Energy* **1992**, *17*, 23.
34. G. Kars, U. Gündüz, M. Yücel, G. Rakhely, K. L. Kovacs, I. Eroğlu, *Int. J. Hydrogen Energy* **2009**, *34*, 2184.
35. M. Frey, *Chembiochem.* **2002**, *3*, 153.
36. P. M. Vignais, B. Billoud, *Chem. Rev.* **2007**, *107*, 4206.
37. A. L. De Lacey, V. M. Fernandez, M. Rousset, R. Cammack, *Chem. Rev.* **2007**, *107*, 4304.
38. P. M. Vignais, B. Billoud, J. Meyer, *FEMS Microbiol. Rev.* **2001**, *25*, 455.
39. L. H. Stickland, D. E. Green, *Nature* **1934**, *133*, 573.

40. L. H. Stickland, D. E. Green, *Biochem. J.* **1934**, *28*, 898.
41. M. Stephenson, L. H. Strickland, *Biochem. J.* **1931**, *25*, 205.
42. B. R. Glick, W. G. Martin, S. M. Martin, *Can. J. Microbiol.* **1980**, *26*, 1214.
43. E. C. Hatchikian, N. Forget, V. M. Fernandez, R. Williams, R. Cammack, *Eur. J. Biochem.* **1992**, *209*, 357.
44. X. Zhao, I. P. Georgakaki, M. L. Miller, J. C. Yarbrough, M. Y. Darensbourg, *J. Am. Chem. Soc.* **2001**, *123*, 9710.
45. M. Y. Darensbourg, E. J. Lyon, J. J. Smee, *Coord. Chem. Rev.* **2000**, *206*, 533.
46. D. J. Evans, C. J. Pickett, *Chem. Soc. Rev.* **2003**, *32*, 268.
47. a) S. Shima, R. K. Thauer, *Chem. Rec.* **2007**, *7*, 37. b) O. Pilak, B. Mamat, S. Vogt, C. H. Hagemeier, R. K. Thauer, S. Shima, C. Vonrhein, E. Warkentin, U. Ermler, *Journal of Molecular Biology* **2006**, *358*, 798.
48. W. Lubitz, E. Reijerse, M. van Gastel, *Chem. Rev.* **2007**, *107*, 4331.
49. P. E. M. Siegbahn, J. W. Tye, M. B. Hall, *Chem. Rev.* **2007**, *107*, 4414.
50. S. Shima, O. Pilak, S. Vogt, M. Schick, M. S. Stagni, W. Meyer-Klaucke, E. Warkentin, R. K. Thauer, U. Ermler, *Science* **2008**, *321*, 572.
51. S. P. J. Albracht, *Biochim. Biophys. Acta Bioenergetics* **1994**, *1188*, 167.
52. E.G. Graf, R. K. Thauer, *FEBS Lett.* **1981**, *136*, 165.
53. R. Cammack, D. Patil, R. Aguirre, E. C. Hatchikian, *FEBS Lett.* **1982**, *142*, 289.
54. M. W. W. Adams, L. E. Mortenson, *J. Biol. Chem.* **1984**, *259*, 7045.
55. G. Wang, M. J. Benecky, B. H. Huynh, J. F. Cline, M. W. W. Adams, L. E. Mortenson, B. M. Hoffman, E. Münck, *J. Biol. Chem.* **1984**, *259*, 14328.
56. C. Tard, C. J. Pickett, *Chem. Rev.* **2009**, 109, 2245.
57. F. Gloaguen, T. B. Rauchfuss, *Chem. Soc. Rev.* **2009**, *38*,100.
58. D. M. Heinekey, *Journal of Organometallic Chemistry* **2009**, 694, 2671.
59. E. Garcin, X. Vernede, E. C. Hatchikian, A. Volbeda, M. Frey, J. C. Fontecilla-Camps, *Structure* **1999**, *7*, 557.
60. Y. Higuchi, N. Yasuoka, Y. Kakudo, Y. Katsube, T. Yagi, H. Inokuchi, *J. Biol. Chem.* **1987**, *262*, 2823.
61. V. Niviere, E. C. Hatchikian, C. Cambillaud, M. Frey, *J. Mol. Biol.* **1987**, *195*, 969.

62. A. Volbeda, M. H. Charon, C. Piras, E. C. Hatchikian, M. Frey, J. C. Fontecilla-Camps, *Nature* **1995**, *373*, 580.
63. M. Frey, J. C. Fontecilla-Camps, A. Volbeda, Handbook of Metalloproteins; Messerschmidt **2001**, p 880.
64. A. Volbeda, E. Garcin, C. Piras, A. L. De Lacey, V. M. Fernandez, E. C. Hatchikian, M. Frey, J. C. Fontecilla-Camps, *J. Am. Chem. Soc.* **1996**, *118*, 12989.
65. A. Volbeda, L. Martin, C. Cavazza, M. Matho, B. W. Faber, W. Roseboom, S. P. J. Albracht, E. Garcin, M. Rousset, J. C. Fontecilla-Camps, *J. Biol. Inorg. Chem.* **2005**, *10*, 239.
66. Y. Higuchi, T. Yagi, N. Yasuoka, *Structure* **1997**, *5*, 1671.
67. Y. Higuchi, H. Ogata, K. Miki, N. Yasuoka, T. Yagi, *Structure* **1999**, *7*, 549.
68. H. Ogata, Y. Mizogushi, N. Mizuno, K. Miki, S. Adachi, N. Yasuoka, T. Yagi, O. Yamauchi, S. Hirota, Y. Higuchi, *J. Am. Chem. Soc.* **2002**, *124*, 11628.
69. H. Ogata, S. Hirota, A. Nakahara, H. Komori, N. Shibata, T. Kato, K. Kano, Y. Higuchi, *Structure* **2005**, *13*, 1635.
70. P. M. Matias, C. M. Soares, L. M. Saraiva, R. Coelho, J. Morais, J. LeGall, M. A. Carrando, *J. Biol. Inorg. Chem.* **2001**, *6*, 63.
71. Y. Montet, P. Amara, A. Volbeda, X. Vernede, E. C. Hatchikian, M. J. Field, M. Frey, J. C. Fontecilla-Camps, *Nat. Struct. Biol.* **1997**, *4*, 523.
72. A. Volbeda, Y. Montet, X. Vernede, E. C. Hatchikian, J. C. Fontecilla-Camps, *Int. J. Hydrogen Energy* **2002**, *27*, 1449.
73. R. P. Happe, W. Roseboom, A. J. Pierik, S. P. J. Albracht, K. A. Bagley, *Nature* **1997**, *385*, 126.
74. A. J. Pierik, W. Roseboom, R. P. Happe, K. A. Bagley, S. P. J. Albracht, *J. Biol. Chem.* **1999**, *274*, 3331.
75. D. S. Patil, *Methods Enzymol.* **1994**, *243*, 68.
76. A. Pardo, A. L. De Lacey, V. M. Fernandez, H. J. Fan, Y. Fan, M. B. Hall, *J. Biol. Inorg. Chem.* **2006**, *11*, 286.
77. J. S. Chen, L. E. Mortenson, *Biochim. Biophys. Acta* **1974**, *371*, 283.
78. M. W. W. Adams, *Biochim. Biophys. Acta* **1990**, *1020*, 115.

79. J. S. Chen, D. K. Blanchard, *Biochem. Biophys. Res. Commun.* **1978**, *84*, 1144.
80. M. W. W. Adams, L. E. Mortenson, *Biochim. Biophys. Acta* **1984**, *766*, 51.
81. C. van Dijk, C. Veeger, *Eur. J. Biochem.* **1981**, *114*, 209.
82. C. van Dijk, H. J. Grande, S. G. Mayhew, C. Veeger, *Eur. J. Biochem.* **1980**, *107*, 251.
83. C. van Dijk, S. G. Mayhew, H. J. Grande, C. Veeger, *Eur. J. Biochem.* **1979**, *102*, 317.
84. M. Filipiak, W. R. Hagen, C. Veeger, *Eur. J. Biochem.* **1989**, *185*, 547.
85. W. R. Hagen, A. van Berkel-Arts, K. M. Kruse-Wolters, G. Voordouw, C. Veeger, *FEBS Lett.* **1986**, *203*, 59.
86. H. M. van der Westen, S. G. Mayhew, C. Veeger, *FEBS Lett.* **1978**, *86*, 122.
87. H. J. Grande, W. R. Dunham, B. Averill, C. van Dijk, R. H. Sands, *Eur. J. Biochem.* **1983**, *136*, 201.
88. H. J. Grande, A. van Berkel-Arts, J. Bregh, K. van Dijk, C. Veeger, *Eur. J. Biochem.* **1983**, *131*, 81.
89. B. H. Huynh, M. H. Czechowski, H. J. Krüger, D. V. DerVartanian, H. D. Peck, J. LeGall, Proc. *Natl. Acad. Sci. U.S.A.* **1984**, *81*, 3728.
90. D. S. Patil, S. H. He, D. V. DerVartanian, J. LeGall, B. H. Huynh, H. D. Peck, *FEBS Lett.* **1988**, *228*, 85.
91. D. S. Patil, J. J. G. Moura, S. H. He, M. Teixeira, B. C. Prickril, D. V. DerVartanian, H. D. Peck, J. LeGall, B. H. Huynh, *J. Biol. Chem.* **1988**, *263*, 18732.
92. D. S. Patil, B. H. Huynh, S. H. He, H. D. Peck, D. V. DerVartanian, J. LeGall, *J. Am. Chem. Soc.* **1988**, *110*, 8533.
93. G. Fauque, H. D. Peck, J. J. G. Moura, B. H. Huynh, Y. Berlier, D. V. DerVartanian, M. Teixeira, A. E. Przybyla, P. A. Lespinat, I. Moura, J. LeGall, *FEMS Microbiol. ReV.* **1988**, *54*, 299.
94. J. W. Peters, W. N. Lanzilotta, B. J. Lemon, L. C. Seefeldt, *Science* **1998**, *282*, 1853.
95. Y. Nicolet, C. Piras, P. Legrand, C. E. Hatchikian, J. C. Fontecilla-Camps, *Structure* **1999**, *7*, 13.

96. A. J. Pierik, M. Hulstein, W. R. Hagen, S. P. J. Albracht, *Eur. J. Biochem.* **1998**, *258*, 572.

97. A. L. De Lacey, C. Stadler, C. Cavazza, E. C. Hatchikian, V. M. Fernandez, *J. Am. Chem. Soc.* **2000**, *122*, 11232.

98. a) Y. Nicolet, A. L. De Lacey, X. Vernede, V. M. Fernandez, E. C. Hatchikian, J. C. Fontecilla-Camps, *J. Am. Chem. Soc.* **2001**, *123*, 1596. b) X. Liu, S. K. Ibrahim, C. Tard, C. J. Pickett, *Coordination Chemistry Reviews* **2005**, *249*, 1641.

99. W. Roseboom, A. L. De Lacey, V. M. Fernandez, C. Hatchikian, S. P. J. Albracht, *J. Biol. Inorg. Chem.* **2006**, *11*, 102.

100. A. J. Pierik, W. R. Hagen, J. S. Redeker, R. B. G. Wolbert, M. Boersma, M. F. J. M. Verhagen, H. J. Grande, C. Veeger, P. H. A. Mutsaers, R. H. Sands, W. R. Dunham, *Eur. J. Biochem.* **1992**, *209*, 63.

101. J. W. Tye, M. B. Hall, M. Y. Darensbourg, *Proc. Natl. Acad. Sci. U.S.A.* **2005**, *102*, 16911.

102. F. A. Armstrong, P. J. Albracht, *Philos. Trans. R. Soc. London, A* **2005**, *363*, 937.

103. D. Seyferth, G. B. Womack, M. K. Gallagher, M. Cowie, B. W. Hames, J. P. Fackler, A. M. Mazany, *Organometallics* **1987**, *6*, 283.

104. D. Chong, I. P. Georgakaki, R. Mejia-Rodriguez, J. Sanabria-Chinchilla, M. P. Soriaga, M. Y. Darensbourg, *Dalton Trans.* **2003**, 4158.

105. S. J. Borg, M. I. Bondin, S. P. Best, M. Razavet, X. Liu, C. J. Pickett, *Biochem. Soc. Trans.* **2005**, *33*, 3.

106. C. Greco, G. Zampella, L. Bertini, M. Bruschi, P. Fantucci, L. De Gioia, *Inorg. Chem.* **2007**, *46*, 108.

107. Z.-P. Liu, P. Hu, *Journal of Chemical Physics* **2002**, *117*, 8177.

108. E. J. Lyon, I. P. Georgakaki, J. H. Reibenspies, M.Y. Darensbourg, *Angew. Chem., Int. Ed.* **1999**, *38*, 3178.

109. F. Gloaguen, J. D. Lawrence, M. Schmidt, S. R. Wilson, T. B. Rauchfuss, *J. Am. Chem. Soc.* **2001**, *123*, 12518.

110. M. Razavet, S. C. Davies, D. L. Hughes, J. E. Barclay, D. J. Evans, S. A. Fairhurst, X. Liu, C. J. Pickett, *Dalton Trans.* **2003**, 586.

111. H. Li, T. B. Rauchfuss, *J. Am. Chem. Soc.* **2002**, *124*, 726.
112. J. D. Lawrence, H. Li, T. B. Rauchfuss, M. Benard, M.-M. Rohmer, *Angew. Chem. Int. Ed.* **2001**, *40*, 1768.
113. S. Ott, M. Kritikos, B. Åkermark, L. Sun, *Angew. Chem. Int. Ed.* **2003**, *42*, 3285.
114. L.-C. Song, Z.-Y. Yang, H.-Z. Bian, Q.-M. Hu, *Organometallics* **2004**, *23*, 3082.
115. L.-C. Song, Z.-Y. Yang, H.-Z. Bian, Y. Liu, H.-T. Wang, X.-F. Liu, Q.-M. Hu, *Organometallics* **2005**, *24*, 6126.
116. J. Windhager, M. Rudolph, S. Bräutigam, H. Görls, W. Weigand, *Eur. J. Inorg. Chem.* **2007**, 2748.
117. P. I. Volkers, T. B. Rauchfuss, S. R. Wilson, *Eur. J. Inorg. Chem.* **2006**, 4793.
118. M. L. Singleton, R. M. Jenkins, C. L. Klemashevich, M. Y. Darensbourg, *C. R. Chim.* **2008**, *11*, 861.
119. L.-C. Song, C.-G. Li, J. Gao, B.-S. Yin, X. Luo, X.-G. Zhang, H.-L. Bao, Q.-M. Hu, *Inorganic Chemistry* **2008**, *47*, 4545.
120. S. Jiang, J. Liu L. Sun, *Inorganic Chemistry* **2006**, *9*, 290.
121. T. Liu, M. Wang, Z. Shi, H. Cui, W. Dong, J. Chen, B. kermark, L. Sun, *Chem. Eur. J.* **2004**, *10*, 4474.
122. L.-C Song, G.-H. Ge, X.-G. Zhang, Y. Liu, Q.-M. Hu, *Eur. J. Inorg. Chem.* **2006**, 3204.
123. L.-C. Song, L.-X Wang, B.-S. Yin, Y.-L. Li, X.-G. Zhang, Y.-W. Zhang, X. Luo, Q.-M. Hu, *Eur. J. Inorg. Chem.* **2008**, 291.
124. J. D. Lawrence, H. Li, T. B. Rauchfuss, *Chem. Commun.* **2001**, 1482.
125. W. Dong, M. Wang, X. Liu, K. Jin, G. Li, F. Wang, L. Sun, *Chem. Commun.* **2006**, 305.
126. S. Jiang, J. Liu, Y. Shi, Z. Wang, B. Akermark, L. Sun, *Dalton Trans.* **2007**, 896.
127. D. Seyferth, R. S. Henderson, L.-C. Song, *J. Organomet. Chem.* **1980**, *192*, C1.
128. J. W. Tye, M. Y. Darensbourg, M. B. Hall, *Inorg. Chem.* **2006**, *45*, 1552.
129. M. Mirza, M. M. Hasan, M. B. Hursthouse, S. E. Kabir, K. M. Abdul Malik, *Polyhedron* **2001**, *20*, 97.
130. P. Li, M. Wang, C. He, G. Li, X. Liu, C. Chen, B. Akermark, L. Sun, *Eur. J. Inorg. Chem.* **2005**, 2506.

131. P. Li, M. Wang, C. He, K. Jin, X. Liu, L. Sun, *Eur. J. Inorg. Chem.* **2007**, 3718.
132. D. Morvan, J.-F Capon, F. Gloaguen, P. Schollhammer, J. Talarmin, *Eur. J. Inorg. Chem.* **2007**, 5062.
133. Z. Wang, W. Jiang, J. Liu, W. Jiang, Y. Wang, B. Åkermark, L. Sun, *Journal of Organometallic Chemistry* **2008**, *693*, 2828.
134. L.-C. Song, C.-G Li, G.-H. Ge, Z.-Y Yang, H.-T. Wang, J. Zhang, Q.-M. Hu, *Journal of Inorganic Biochemistry* **2008**, *102*, 1973.
135. Y. Na, M. Wang, K. Jin, R. Zhang, L. Sun, *Journal of Organometallic Chemistry* **2006**, *691*, 5045.
136. J. L. Stanley, Z. M. Heiden, T. B. Rauchfuss, S. R. Wilson, L. D. Gioia, G. Zampella, *Organometallics* **2008**, *27*, 119.
137. W. Wang, J.-H. Liu, C.-J. He, S. Jiang, B. A. Akermark, L.-C. Sun, *Journal of Organometallic Chemistry* **2007**, *692*, 5501.
138. R. M. Rodriguez, D. Chong, J. H. Reibenspies, M. B. Soriaga, M. Y. Darensbourg, *J. Am. Chem. Soc.* **2004**, *126*, 12004.
139. L. Schwartz, G. Eilers, L. Eriksson, A. Gogoll, R. Lomoth, S. Ott, *Chem. Commun.* **2006**, 520.
140. G. Si, W. G. Wang, H. Y. Wang, C. H. Tung, L. Z. Wu, *Inorg. Chem.* **2008**, *47*, 8101.
141. J. I. van der Vlugt, T. B. Rauchfuss, S. R. Wilson, *Chem. Eur. J.* **2006**, *12*, 90.
142. F. Gloaguen, J. D. Lawrence, T. B. Rauchfuss, *J. Am. Chem. Soc.* **2001**, *123*, 9476.
143. F. Gloaguen, J. D. Lawrence, T. B. Rauchfuss, M. Benard, M. M. Rohmer, *Inorg. Chem.* **2002**, *41*, 6573.
144. X. Zhao, Y. M. Hsiao, C. H. Lai, J. H. Reibenspies, M. Y. Darensbourg, *Inorg. Chem.* **2002**, *41*, 699.
145. X. Zhao, I. P. Georgakaki, M. L. Miller, R. Mejia-Rodriguez, C. Y. Chiang, M. Y. Darensbourg, *Inorg. Chem.* **2002**, *41*, 3917.
146. J. I. van der Vlugt, T. B. Rauchfuss, C. M. Whaley, S. R. Wilson, *J. Am. Chem. Soc.* **2005**, *127*, 16012.

147. G. A. N. Felton, A. K. Vannucci, J. Z. Chen, L. T. Lockett, N. Okumura, B. J. Petro, U. I. Zakai, D. H. Evans, R. S. Glass, D. L. Lichtenberger, *J. Am. Chem. Soc.* **2007**, *129*, 12521.
148. S. Loscher, L. Schwartz, M. Stein, S. Ott, M. Haumann, *Inorg. Chem.* **2007**, *46*, 11094.
149. M. T. Olsen, M. Bruschi, L. De Gioia, T. B. Rauchfuss, S. R. Wilson, *J. Am. Chem. Soc.* **2008**, *130*, 12021.
150. L. Schwartz, P. S. Singh, L. Eriksson, R. Lomoth, S. Ott, *C. R. Chimie* **2008**, *11*, 875.
151. Y. T. Si, M. Q. Hu, C. N. Chen, *C. R. Chimie* **2008**, *11*, 932.
152. Z. Zhao, M. Wang, W. Dong, P. Li, Z. Yu, L. Sun, *Journal of Organometallic Chemistry* **2009**, *694*, 2309.
153. G. A. Felton, C. A. Mebi, P. J. Petro, A. K. Vannucci, D. H. Evans, R. S. Glass, D. L. Lichtenberger, *Journal of Organometallic Chemistry* **2009**, *694*, 2681.
154. T.-T. Zhang, M. Wang, N. Wang, P. Li, Z.-Y. Liu, L.-C. Sun, *Polyhedron* **2009**, *28*, 1138.
155. W. Gao, J. Ekström, J. Liu, C. Chen, L. Eriksson, L. Weng, B. Akermark, L. Sun, *Inorg. Chem.* **2007**, *46*, 1981.
156. S. Ezzaher, J. F. Capon, F. Gloaguen, F. Y. Pétillon, P. Schollhammer, J. Talarmin, *Inorg. Chem.* **2007**, *46*, 3426.
157. S. Ezzaher, J. F. Capon, F. Gloaguen, F. Y. Pétillon, P. Schollhammer, J. Talarmin, *Inorg. Chem.* **2007**, *46*, 9863.
158. A. K. Justice, G. Zampella, L. D. Gioia, T. B. Rauchfuss, J. I. V. D. Vlugt, S. R. Wilson, *Inorg. Chem.* **2007**, *46*, 1655.
159. S. Ezzaher, J. F. Capon, F. Gloaguen, F. Y. Petillon, P. Schollhammer, J. Talarmin, *Inorg. Chem.* **2009**, *48*, 2.
160. F. I. Adam, G. Hogarth, S. E. Kabir, I. Richards, *C. R. Chimie* **2008**, *11*, 890.
161. S. Ezzaher, J. F. Capon, F. Gloaguen, Kervarec, N.; F. Y. Pétillon, Pichon, R.; P. Schollhammer, J. Talarmin. *C. R. Chimie* **2008**, *11*, 906.
162. A. K. Justice, M. J. Nilges, T. B. Rauchfuss, S. R. Wilson, L. D. Luca De Gioia, G. Zampella, *J. Am. Chem. Soc.* **2008**, *130*, 5293.

163. A. K. Justice, L. D. Gioia, M. J. Nilges, T. B. Rauchfuss, S. R. Wilson, G. Zampella, *Inorganic Chemistry* **2008**, *47*, 7405.
164. B. E. Barton, T. B. Rauchfuss, *Inorganic Chemistry* **2008**, *47*, 2261.
165. A. K. Justice, T. B. Rauchfuss, S. R. Wilson, *Angew. Chem. Int. Ed.* **2007**, *46*, 6152.
166. N. Wang, M. Wang, T. Liu, P. Li, T. Zhang, M. Y. Darensbourg, L. Sun, *Inorganic Chemistry* **2008**, *47*, 6948.
167. P. Y. Orain, J.-F. Capon, N. Kervarec, F. Gloaguen, F. Y. Petillon, R. Pichon, P. Schollhammer, J. Talarmin, *Dalton Trans.* **2007**, 3745.
168. J.-F. Capon, F. Gloaguen, F. Y. Pétillon, P. Schollhammer, J. Talarmin, *Eur. J. Inorg. Chem.* **2008**, 4671.
169. S. Ezzaher, J.-F. Capon, N. Dumontet, F. Gloaguen, F. Y. Pétillon, P. Schollhammer, J. Talarmin, *J. Electroanal. Chem.* **2009**, *626*, 161.
170. M. Schmidt, S. M. Contakes, T. B. Rauchfuss, *J. Am. Chem. Soc.* **1999**, *121*, 9736.
171. A. L. Cloirec, S. P. Best, S. Borg, S. C. Davies, D. J. Evans, D. L. Hughes, C. J. Pickett, *Chem. Commun.* **1999**, 2285.
172. J. L. Nehring, D. M. Heinekey, *Inorg. Chem.* **2003**, *42*, 4288.
173. C. A. Boyke, T. B. Rauchfuss, S. R. Wilson, M.-M. Rohmer, M. Benard, J. *Am. Chem. Soc.* **2004**, *126*, 15151.
174. C. A. Boyke, J. I. Vlugt, T. B. Rauchfuss, S. R. Wilson, G. Zampella, L. D. Gioia, *J. Am. Chem. Soc.* **2005**, *127*, 11010.
175. J. Hou, X. Peng, J. Liu, Y. Gao, X. Zhao, S. Gao, K. Han, *Eur. J. Inorg. Chem.* **2006**, 4679.
176. E. J. Lyon, I. P. Georgakaki, J. H. Reibenspies, M. Y. J. Darensbourg, *J. Am. Chem. Soc.* **2001**, *123*, 3268.
177. F. Gloaguen, J. D. Lawrence, M. Schmidt, S. R. Wilson, T. B. Rauchfuss, *J. Am. Chem. Soc.* **2001**, *123*, 12518.
178. J. D. Lawrence, H. Li, T. B. Rauchfuss, M. BeÂnard, M.-M. Rohmer, *Angew. Chem. Int. Ed.* **2001**, *40*, 1768.
179. H. Li, T. B. Rauchfuss, *J. Am. Chem. Soc.* **2002**, *124*, 726.

180. J. D. Lawrence, T. B. Rauchfuss, S. R. Wilson, *Inorg. Chem.* **2002**, *41*, 6193.
181. L.-C. Song, Z.-Y. Yang, Y.-J. Hua, H.-T. Wang, Y. Liu, Q.-M. Hu, *Organometallics* **200**7, *26*, 2106.
182. J. Windhager, H. Görls, H. Petzold, G. Mloston, G. Linti, W. Weigand, *Eur. J. Inorg. Chem.* **2007**, *28*, 4462.
183. W. A. Herrmann, *Angew. Chem., Int. Ed.* **2002**, *41*, 1290.
184. Y. Canac, M. Soleilhavoup, S. Conejero, G. Bertrand, *J. Organomet. Chem.* **2004**, *689*, 3857.
185. E. Peris, R. H. Crabtree, *Coord. Chem. ReV.* **2004**, *248*, 2239.
186. N. M. Scott, S. P. Nolan, *Eur. J. Inorg. Chem.* **2005**, 1815.
187. L. Cavallo, A. Correa, C. Costabile, H. Jacobsen, *J. Organomet. Chem.* **2005**, *690*, 5407.
188. W. A. Herrmann, J. Schutz, G. D. Frey, E. Herdtweck, *Organometallics* **2006**, *25*, 2437.
189. H. Jacobsen, A. Correa, C. Costabile, L. Cavallo, *J. Organomet. Chem.* **2006**, *691*, 4350.
190. L. Mercs, G. Labat, A. Neels, A. Ehlers, M. Albrecht, *Organometallics* **2006**, *25*, 5648.
191. M. Viciano, E. Mas-Marza´, M. Sanau, E. Peris, *Organometallics* **2006**, *25*, 3063.
192. J.-F. Capon, S. El Hassnaoui, F. Gloaguen, P. Schollhammer, J. Talarmin, *Organometallics* **2005**, *24*, 2020.
193. D. Morvan, J.-F. Capon, F. Gloaguen, A. Goff, M. Marchivie, F. Michaud, P. Schollhammer, J. Talarmin, J.-J. Yaouanc, *Organometallics* **2007**, *26*, 2042.
194. T. Liu, M. Y. Darensbourg, *J. Am. Chem. Soc.* **2007**, *129*, 7008.
195. J. W. Tye, J. Lee, H.-W. Wang, R. Mejia-Rodriguez, J. H. Reibenspies, M. B. Hall, M. Y. Darensbourg, *Inorg. Chem.* **2005**, *44*, 5550.
196. L. Duan, M. Wang, P. Li, Y. Na, N. Wang, L. Sun, *Dalton Trans.* **2007**, 1277.
197. S. Jiang, J. Liu, Y. Shi, Z. Wang, B. Akermark, L. Sun, *Polyhedron* **2007**, *26*, 1499.
198. C. M. Thomas, T. Liu, M. B. Hall, M. Y. Darensbourg, *Inorg. Chem.* **2008**, *47*, 7009.

199. C. M. Thomas, T. Liu, M. B. Hall, M. Y. Darensbourg, *Chem. Commun.* **2008**, 1563.
200. C. M. Thomas, M. Y. Darensbourg, M. B. Hall, *Journal of Inorganic Biochemistry* **2007**, *101*, 1752.
201. G. Zampella, M. Bruschi, P. Fantucci, M. Razavet, C. J. Pickett, L. D. Gioia, *Chem. Eur. J.* **2005**, *11*, 509.
202. M. Razavet, S. C. Davies, D. L. Hughes, C. J. Pickett, *Chem. Commun.* **2001**, 847.
203. S. J. George, Z. Cui, M. Razavet, C. J. Pickett, *Chem. Eur. J.* **2002**, *8*, 4037.
204. S. K. Ibrahim, X. Liu, C. Tard, C. J. Pickett, *ChemComm.* **2007**, 1535.
205. C. Tard, X. Liu, D. L. Hughes, C. J. Pickett, *ChemComm.* **2005**, 133.
206. L.-C. Song, J. Cheng, J. Yan, H.-T. Wang, X.-F. Liu, Q.-M. Hu, *Organometallics* **2006**, *25*, 1544.
207. L.-C. Song, F.-H. Gong, T. Meng, J.-H. Ge, L.-N. Cui, Q.-M. Hu, *Organometallics* **2004**, *23*, 823.
208. W. Gao, J. Liu, B. Åkermark, L. Sun, *Inorg. Chem.* **2006**, *45*, 9169.
209. I. A. Carcer, A. DiPasquale, A. L. Rheingold, D. M. Heinekey, *Inorg. Chem.* **2006**, *45*, 8000.
210. Y. Zhang, Y.-T. Si, M.-Q. Hu, C.-N. Chen, Q.-T. Liu, *Acta Cryst.* **2007**, *C63*, m499.
211. J. Messelhauser, K. U. Gutensohn, I.-P. Lorenz, W. Hiller, *J. Organomet. Chem.* **1987**, *321*, 377.
212. J. Windhager, R. A. Seidel, U.-P. Apfel, H. Görls, G. Linti, W. Weigand. *Chem. Biodiv.* **2008**, *5*, 2023.
213. T. Liu, B. Li, M. L. Singleton, M. B. Hall, M. Y. Darensbourg, *J. Am. Chem. Soc.* **2009**, *131*, 8296.

6. Acknowledgements

First of all, praise and all thanks for Almighty Allah for his assistance and protection.

I would like to express my sincere appreciation to my supervisor Prof. Dr. Wolfgang Weigand and my co-advisor Prof. Dr. Mohammad El-khateeb for giving me the opportunity to work in this attractive and interesting field, I thank them especially for them superior supervision, encouragement, assistance, and continuous help. Special thanks for the examination committee members and for the staff of Institut für Anorganische und Analytische Chemie, Friedrich-Schiller-Universität Jena.

Appreciation also goes out to Prof. Dr. Richard S. Glass, Prof. Dr. Dennis H. Evans and Prof. Dr. Dennis L. Lichtenberger and their co-workers of the Department of Chemistry, The University of Arizona for measured and interpreted my model complexes electrochemically by cyclovoltammetry, and for calculated the Density Functional Theory (DFT) for these model complexes. And also many thanks for writing the electrochemistry and DFT parts in the publications.

I would also like to thank all my friends in AG. Weigand, particularly Ahmad Daraosheh, for our accepting debates and exchanges of knowledge during my graduate program, which helped enhance the skill and experience.

I thank all Technical assistants of the Institut für Anorganische und Analytische Chemie, namely NMR, MS, EA and X-Ray for analyses of the samples.

Thanks to the publisher Wiley-VCH Verlag GmbH & Co. KGaA, Weinheim as well as the American Chemical Society for the permission to publish [MK1-MK6] in this PhD Thesis.

I would like to express my greatest thankfulness to my father and my mother and to my brothers and sisters for the support; they provided me through my entire life. Moreover, I acknowledge my wife, without her encouragement and assistance, I would not have finished this thesis.

I dedicate this thesis for my daughter Rand and my lovely sun (Kamal).

Finally, I recognize that this work would not have been possible without the financial support of the German Academic Exchange Service (DAAD), and express my

Declaration of Authorship

I certify that the work presented here is, to the best of my knowledge and belief, original and the result of my own investigations, except as acknowledged, and has not been submitted, either in part or whole, for a degree at this or any other university.

_____

Mohammad Harb

Curriculum Vitae

Personal Information

Name: Mohammad Kamal Abbas Harb

Date and Place of Birth: 28/7/1980. Dair Abi Said, Jordan

Nationality: Jordanian

Marital Status: Married

Gender: Male

Education:

03/2007 – 12/2009 Friedrich-Schiller University Jena

- Dissertation
- PhD. Thesis- Novel Diiron Dichalcogenolato Complexes: Models for Active Site of [FeFe]-Hydrogenases.
- Scholarship of DAAD from 04/2008 till 08/2010

10/2002 – 03/2006 Jordan university of science and technology Irbid

- Master Thesis- Determination of Selected Heavy Metals in Air Samples from Northern Part of Jordan.
- Degree in analytical chemistry.

10/1998 – 06/2002 Jordan university of science and technology Irbid

- Bachelor degree in applied Chemistry.

07/1997 – 07/1998 Dair Abi Said secondary school Irbid

- High school, scientific stream.

Languages:

Arabic, English, and basic German.

Experiences:

- Lab tech. in Kemira Arab Potash Company Ltd. *17/11/2004 till 16/2/2007.*
- Teacher assistant (General Chemistry Lab, Analytical Chemistry Lab, and Inorganic Chemistry Lab) at the Department of Applied Chemical Science, Faculty of Science, Jordan University of Science and Technology, in the first, second, and summer of the year 2002/2003-2003/2004.
- Trainee in Dar Al Dawa Development and Investment CO.LTD (Quality Department). 1/7/2001 – 23/8/2001.

_____

Mohammad Harb